UNIVERSITY OF SOUTHAMPTON

FACULTY OF ENGINEERING, SCIENCE & MATHEMATICS

SCHOOL OF ENGINEERING SCIENCES

Damage Tolerance of Repaired Composite Sandwich Structures

by

Richard Simon Trask

Thesis for the degree of Doctor of Philosophy

December 2004

ABSTRACT

Advanced polymer composite sandwich structures are increasingly being used in a variety of primary, secondary and tertiary structures in all forms of engineering endeavour. Whilst the key benefits of composite materials are widely recognised, high strength-to-weight and stiffness-to-weight ratios, their limited industrial use stems from their poor delamination resistance when subjected to impact damage. Any form of delamination damage can cause severe reductions in stiffness and strength, and may lead to catastrophic failure of the structure. To overcome this perceived limitation various repair designs have evolved to ensure that the stiffness and strength of the original structure is restored in an economically viable way. These methods, often industry and component specific, have started to overcome the designer's fear of applying composite materials to primary engineering structures.

The work presented here describes investigations into the damage tolerance performance of repairs contained within an advanced polymer composite sandwich structures. The composite materials considered were representative of the materials used by the Royal National Lifeboat Institution (RNLI) in the manufacture of their high performance rescue craft. The impact damage tolerance of a standard 3-degree tapered scarf repair design, commonly employed in the marine and aerospace communities, was considered within this project.

A design methodology, incorporating a Fracture Mechanics Assessment, Strength Based Assessment and a Repair Structural Integrity Assessment has been developed to assess the damage tolerance performance of the repaired structure. Through the application of a failure mode, effect and criticality analysis (FMECA), critical defects at critical locations have been identified for further evaluation.

A detailed approach for the damage tolerance assessment of damage tapered scarf repairs is proposed through the application of flowcharts and damage tolerance tables. This detailed route map helps the end user to make an informed decision about the criticality of the defect, i.e. whether the defect is benign and hence can be considered damage tolerant.

TABLE OF CONTENTS

LIST OF FIGURES

LIST OF TABLES

ACKNOWLEDGMENTS

This present project could not have been completed without considerable assistance from many individuals and I would like to express my gratitude to my friends and colleagues in the Royal National Lifeboat Institution and the School of Engineering Sciences who helped me during me stay at the University of Southampton.

Firstly, I wish to express my gratitude to the Royal National Lifeboat Institution (RNLI) who funded this research project. It has been a pleasure and honour to be associated with a dynamic organisation that still invests money, time and effort in engineering research and development. It is through the Advanced Technology Partnership (ATP), a key initiative between the RNLI and the University of Southampton that this work has been pulled together.

Special thanks go to my supervisors Professor R.M Cripps and Professor R.A Shenoi. Firstly, thank you both for taking me out of 'industry' and starting me upon the path of academia. To Bob, I wanted to express my thanks for the opportunity to work alongside a dynamic and forwarding thinking organisations. I am also indebted to you for all the opportunities and blind alleys you allowed me to explore during my stay within the ATP. To Ajit, thank you for making me feel a welcomed member of the Ship Science department. Thank you as well for your supervision, guidance and patience throughout the development of this project and the preparation of this manuscript. My thanks also go to my very own special helpline within the RNLI, i.e. Steve Austen and Holly Phillips. Knowing that technical assistance and good humour was only a telephone call away helped me through the dark days. Mind you, Steve, you still owe me a beer!

I also wish to express my gratitude to Green Marine, Lymington, UK for all their assistance in the manufacture of the composite sandwich beams and fracture mechanics specimens, and to the staff at Qinetiq Farnborough who undertook the mixed-mode bending tests.

Thanks to the staff in the Faculty of Engineering Sciences who have helped directly and indirectly in this project, to Ken Yates in Civil Engineering and Dave Beckett in the School of Engineering Sciences for all their technical help, to the students who have contributed manpower and technical debate along the way (S.H, C.L-F, H.H. & C.O) and in particular the 'coffee and cake crew' of Steve Boyd, Jacqui Earl and David Grant. Without them all, this project would not have been the success that it is.

To my wife, Catherine, thank you for your help, patience and understanding during the last 3 years. Without you I would still be stumbling in the dark. Thanks to my darling children, Jacob and Jessica, without whom I would have finished this PhD a lot sooner!

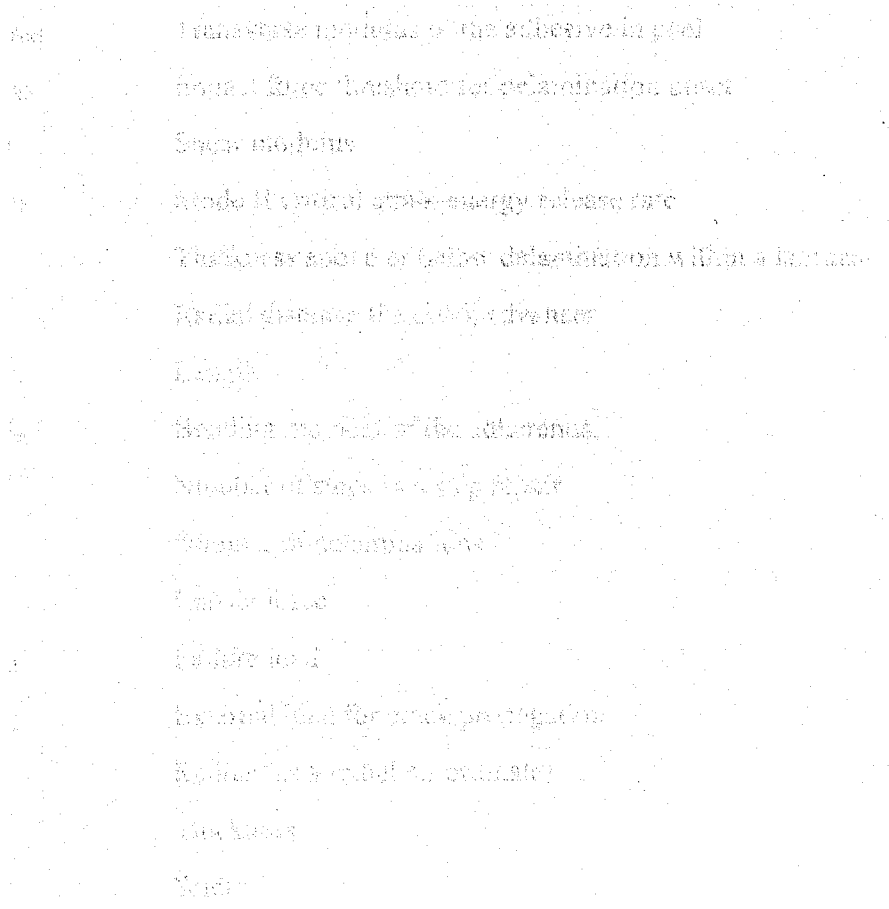

NOTATION

The following notation is used throughout this thesis. Subscripted versions are also used where appropriate and are described within the text as they occur.

Alphabetical symbols

a	Half-length of the interfacial crack
b	Sandwich beam width
c	Sandwich core thickness
d	Diameter of impactor
d	Distance from the patch edge to the point at which the stress is effectively zero
D	Bending stiffness of the adherends.
D_f	Effective plate stiffness
E	Elastic modulus
E_{Peel}	Transverse modulus of the adhesive in peel
F_{dth}	Impact force threshold for delamination onset
G	Shear modulus
G_{II}	Mode II critical strain energy release rate
h	Thickness above or below delamination within a laminate
l	Radial distance the crack advances
L	Length
M_e	Bending moment of the adherends,
N	Number of steps in a step repair
n	Number of delaminations
P	Impact force
P_d	Failure load
P_C	External load for crack propagation
r	Radius (as a radial co-ordinate)
t	Thickness
w	Width

Greek symbols

ε	Axial strain
γ	Fracture energy
γ_e	Elastic strain to yield
γ_p	Plastic strain to failure
η	Thickness of the adhesive
μstrain	Micro-strain (μm/ m)
ν	Possion's ratio
θ	Scarf angle
ρ_{cr}	Crush stress of the core
σ	Axial stress
σ_{Peel}	adhesive transverse tensile stress
τ	Shear stress
τ_p	Maximum shear strength of the adhesive

Abbreviations

BVID	Barely Visible Impact Damage
CAA	Civil Aviation Authority
CFRP	Carbon Fibre-Reinforced Plastics
CSM	Chopped Strand Mat
DCB	Double-cantilever beam
ELS	End-loaded split test
FAA	Federal Aviation Authority
FMECA	Failure Mode, Effects and Criticality Analysis
GFRP	Glass Fibre-Reinforced Plastics
GRP	Glass Reinforced Plastics
ILSS	Interlaminar Shear Stress
MCMV	Mine countermeasure vessel
MMB	Mixed-mode bending
NDT	Non-destructive techniques

PVC	Polyvinyl Chloride
PMI	Polymethacrylimide
RNLI	Royal National Lifeboat Institution
USL	Ultimate static load
WR	Woven roving

1 INTRODUCTION

Structural sandwich construction is one of the first forms of composite structures to have gained broad acceptance and usage within the different areas of engineering endeavour. Technical developments in composite processing and improved theoretical understanding have promoted light weight high performance composite sandwich structures for load bearing applications in military and commercial aerospace structures (e.g. airplanes and helicopters) and within military and commercial marine industry (e.g. mine counter measure vessels and lifeboats). Extensive reference material in the form of engineering text books [Zenkert, 1995; Allen, 1969; Vinson, 1999], design handbooks [Caprino & Teti, 1989; Schwan, 1998] and material property data sheets [SP Systems, Divinycell] have assisted the designer in the optimisation of sandwich structures for engineering applications. Whilst optimised design and analysis methods now exist, detailed knowledge of the long-term operational performance of composite sandwich structures is comparatively lacking.

In sandwich structures the question of damage resistance and damage tolerance is of critical concern since the inability of designers to predict the critical damage modes often leads to conservative designs with large factors-of-safety. Although the question of damage tolerance for composite laminates [Baker *et* al, 1985; Zhou, 1998; Tomblin *et* al, 1999; Irving, 2002] and sandwich structures [Burman & Zenkert, 1997; Shipsha, 2001] has started to be addressed, the question of whether a structural repair is as damage resistant and damage tolerant as the original structure has yet to be considered.

A repair scheme is generally designed and manufactured according to a repair manual, if one exists. If no manual exists a number of fundamental questions must be considered and addressed. In the case of sandwich structures the damage mode must be fully characterized and understood. For example, barely visible impact damage (BVID) may result in delaminations in the outer skin, a separation of the skin-core bonded interface or internal shear cracks in the core material. Which of these defects will initiate premature failure will depend upon the composite and the core materials,

the lay-up and the geometry. Once the defects have been correctly identified, it is imperative to understand whether they will propagate under typical structural loading, and therefore determine the nature of the repair required. Once the decision to repair the structure has been made, additional questions concerning the benefits and limitations of each repair technique, and the different methods of application must be addressed. This is a critical step if the repair is to meet the intended operational loads throughout the remaining life expectancy of the structure. Providing this design process is undertaken in a systematic way (validated against experimental and theoretical investigations) the best repair technique for each particular damage event will be derived.

Although the design methodology outlined above has been rigorously followed in the application of composite laminates with the introduction of standard repair designs, standard-manufacturing methods, and fully documented repair manuals, the same cannot be said of sandwich composite structures. Furthermore, whilst the composite laminate community have pursued a greater understanding of repair design, and the maximisation of load transfer across the repair joint, one fundamental area remains unconsidered for repairs of composite structures, namely the question of damage resistance and damage tolerance. This observation is pertinent to the users of both composite laminates and composite sandwich structures.

The motivation for this current research came from the Royal National Lifeboat Institution (RNLI). The RNLI is a UK based charity that exists to save lives at sea. The organisation operates two all-weather classes of lifeboats (illustrated in Figure 1.1) where the primary structure is manufactured from advanced composite sandwich materials (see Appendix A for further information concerning RNLI lifeboats, their design and manufacture).

(a) (b)

Figure 1.1: (a) Trent class all-weather lifeboat (b) Severn class all-weather lifeboat

Whilst on operational duty the hull of the lifeboat may be damaged, thus requiring a repair to be made to restore the structural efficiency of the sandwich structure.

The aim of the present thesis is to quantify and develop a damage tolerance methodology for the assessment of barely visible impact damage (BVID) to tapered scarf structural repairs in advanced polymer composite sandwich structures. The specific objectives are:

1. To understand how damage forms within a tapered scarf structural repair under an impact event.
2. To ascertain the residual strength response of the damaged specimens and to identify a fatigue damage threshold below which the structure is damage tolerant.
3. To devise a procedure that can be used to assess whether a repair is safe for operational use.

To address these objectives the thesis is structured into the following chapters. In Chapter 2, a literature review is undertaken to assess the current understanding of damage formation and damage propagation in operational structures and laboratory-based experiments. A review of the different repair techniques and their assessment is also made. Key findings and recommendations arising form the review are also presented. In Chapter 3, the project methodology is presented. A flowchart illustrates

the design methodology for the damage tolerance assessment of repaired composite sandwich structures.

The background information in support of the project methodology is contained in Chapter 4. This chapter describes the repair approach, the strength based and fracture mechanics based testing methods and the discusses and develops a failure mode, effects, and criticality analysis (FMECA) that examines and defines the exact nature of the problem, i.e. whether a tapered scarf repair is damage tolerant or not to BVID.

Chapter 5 considers the problem of damage formation within a 3° tapered scarf repair. The chapter characterises the influence of BVID impact damage on the original beams and at two locations on the tapered scarf repair, namely the tapered interface and at the end of the overlaminate. This chapter also assess the fracture mechanics performance of the parent laminate, the repair laminate and the repair-parent interface for varying fracture mechanics mixed-mode ratios.

The characterisation of the residual strength and the fatigue life of the impact damaged repair schemes are presented in Chapter 6. The strength-based assessment is undertaken using a four-point bend test. An assessment of impact damage on the performance of the pristine and repaired beams is undertaken.

The results from the fracture mechanics assessment and the strength based assessment and drawn together in Chapter 7 with supporting flowcharts to develop a procedure that can be used to assess whether a tapered scarf repair can be considered damage tolerant for a known damage size.

The thesis conclusions and suggestions for future work are detailed in Chapter 8.

2 LITERATURE REVIEW

2.1 Introduction

Repair of composite structures is a vast topic [see for example, Baker & Jones, 1988; Davies, 1994; Armstrong & Barrett, 1998]. Designers must understand the design and manufacture of the original component, they must be aware of non-destructive techniques that can be used to identify the types of damage and their limitations, they must understand the types and mechanisms involved in the failure sequence of a composite structure and whether a particular type of damage will grow under operational load. The designer must also understand the design of complex repair joints and the influence of stresses on the long-term durability of the repair scheme. They should also understand the advantages and limitations of adhesive bonding, and whether bondline defects will occur and what effect, if any, they will have on the fatigue life of the repair. Finally, the designer must devise a structural health-monitoring plan (i.e. during a routine or non-routine maintenance period) to confirm the structural integrity of the repair patch and surrounding structure for the duration of the components/structures operational life. In reality no single individual will have the depth of knowledge required for all these stages. Instead, they will turn to 'experts' in each specific discipline or consult a repair manual, if one exists.

2.2 Damage observed in aircraft, ships and other engineering sandwich structures

When considering the repair of a composite structure, it is imperative to correctly categorise the severity of the damage and the implication on the operational capability of the structure. Whilst on operational service a composite structure can be damaged in many ways, e.g. unexpected mechanical overload, fatigue loading at stress concentrations, heat/chemical attack or impact damage arising from collisions between moving objects. In general the damage mechanisms tend to occur due to mechanical loading or environmental conditions that are either unexpected or of low probability and hence were not allowed for in the original design.

The main cause of operational damage to composite structures is impact damage [Zhou, 1995]. Impact damage can be classified as either low or high velocity. Low

velocity impact events are often referred to impact events in the range 1 to 10 ms^{-1} where the contact period is such that the whole structure has time to respond to the loading [Pavier *et al*, 1995]. In a high velocity impact event a stress wave is generated which propagates through the material. The time frame in this event is so fast that the structure is unable to respond to the stress wave resulting in very localised damage. Marine craft are often subjected to repeated light docking collisions and collisions with floating debris and other vessels. Table 2.1 illustrates typical damage modes arising from operational collisions with floating debris. Aerospace structures suffer impact damage from runway debris and accidental impact damage during routine maintenance periods. These types of impact events can be considered as low velocity events.

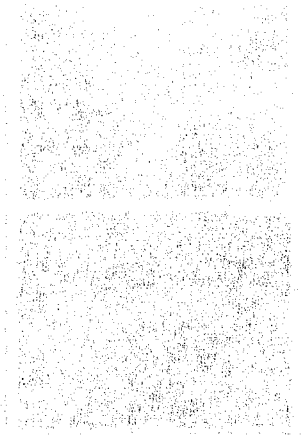

Defect Mechanism	Defect type	Defect illustration	Defect description
Local contact damage	Abrasion damage	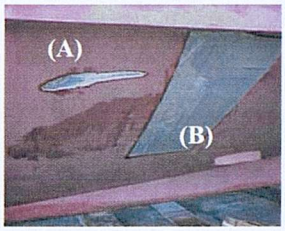	(A) The wearing away of a portion of the laminate by either natural (rain, wind, etc.) or man-made (over-blasting, slight collision). Confined to the outer skin surface.
	Face sheet damage and/or core crushing		(B) Localised surface indentation, damage confined to outer laminate skin. Matrix cracking, fibre breakage.
		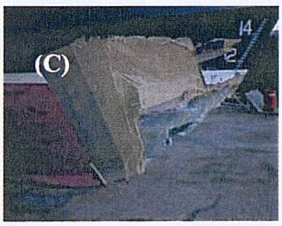	(C) Moderate impact damage greater than the damage initiation threshold for core crushing (permanent deformation) initiating debond in face/core interface
		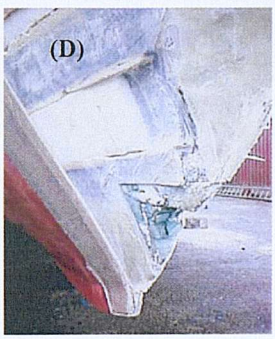	(D) Extended surface indentation resulting from significant impact damage, often associated with witness marks from the impactor and delamination damage. Penetration of outer skin, matrix cracking, delamination, fibre fracture, damage to core material and debond in face/core interface
Overload	Face fracture/ yielding		(E) External forces exceed the fibre tensile strength or the compressive strength of the matrix material resulting in the complete failure of the skin. Failure may have occurred from an impact penetration or overload of structure.

Table 2.1: Technical description and photographic evidence of operation impact damage to marine composite sandwich structures

2.2.1 Damage mode

In general, the disclosure of failure modes of operational structures within the open literature tends not to occur (i.e. organisations try to avoid bad publicity). However, Table 2.2 has been compiled with typical damage modes, i.e. examples of in-service damage, reported for composite sandwich structures in use within the air, sea or land environment.

Nature of damage mode		Damage examples from the open literature
In-service damage	Impact damage to the face sheet laminates	Surface gouge in the starboard keel of a lifeboat arising from collision, UK. [Chaplin & Austen, 2002] Surface gouge in main keel of a lifeboat, UK. [Austen, 2000a] Surface gouge in aft starboard hull quarter after collision, UK. [Austen 2001a] Delamination damage reported in lifeboat bottom shell panel, UK. [Austen 1999] Delamination damage in lifeboat bow, UK. [Austen 2001b] Delamination damage in helicopter rotor blades reported by MBB GmbH, Germany. [Hahn, 1986] Delamination damage in helicopter fuselage reported by Aérospatiale, France. [Torres & Plissonneau, 1986]
	Core crushing (due to indentation or impact)	Crushed bottom shell panel in lifeboat, UK. [Austen, 2000b] Crushed vertical stabiliser leading edge in military aircraft, Deutsche Aerospace AG, Germany. [Maier & Günther, 1995] Core crushed in military jet speed brake, Dornier GMBH, Germany. [Thiele, 1986] Core crushing in military aircraft fuselage skin, DSTO, Australian. [Whitehead *et al*, 2000]
	Impact induced skin/core debonding	Skin-core debonding in the wing closure panel of a UK commercial aircraft [Bristow & Goudie, 2002]
	Core shear cracks	Core shear cracks in the hull bottom forward of keel were reported in the W60 fleet in Whitbread race [COMPOSITES I, 1993]
	Fatigue & fracture at or near stress concentrations	Starboard hull fracture on a catamaran operated by Bruno Peyron [Decobert, 1994]

Table 2.2: Typical operational damage modes reported in the open literature

As indicated in Table 2.2 composite sandwich structures exhibit a wide range of different defect types. The majority of the damage reported in the open literature has arisen through impact or collisions with other vessels or stationary objects during the operational use of the sandwich structure. Whilst the references provide an overview

of the types of damage occurring within operational craft, the reports tend to omit the full extent of the impact damage.

The operational damage identified in Table 2.2 as the critical damage mode is impact damage to the face laminate. This form of damage would result in delamination damage within the laminate skin. The magnitude of the induced damage depends upon a multitude of factors including the outer skin lay-up configuration and thickness, core material and thickness, interface properties between the outer skin and the core, fabrication techniques, impact velocity and energy, indentor shape, temperature, boundary conditions, and environmental factors. Damage initiation thresholds as well as the damage size depend on the properties of the core material and the relationship between the properties of the core material to those of the facings.

2.2.2 Consequences of damage

Table 2.2 provides a generic snapshot of the critical damage types occurring in sandwich structures across the marine and aerospace industries. The criticality of each type of damage will depend upon the design and geometry of the sandwich structure, its intended purpose and the operational loading.

A damaged panel within a composite sandwich structure could result in the loss of the stiffness or strength based structural integrity, and the loss of structural stability and long-term durability. If the damage occurs within a critical part of the structure (i.e. a primary load bearing component), it could result in the complete loss of the vessel and the crew unless adequate structural redundancy has been built into the design.

In an effort to understand the consequences of damage researchers tend to examine the influence of damage at coupon or detail level (i.e. beams or panels) and not at semi-structural (i.e. skin/stringer) and full structural level (i.e. aircraft wing). The results from the coupon or detail level of the hierarchy will then be scaled-up and applied at structural level with additional factors of safety imposed upon the results.

The majority of the research directed at understanding the consequences of damage within sandwich structures has been undertaken on composite sandwich beams [Zenkert, 1995]. In this work [Zenkert, 1995], identified the common critical failure modes in sandwich beams when subjected to bending loads, shear loads, pure compression, compression and bending, and point load impact. He observed that these loading situations could induce the following failure modes – face yielding or fracture, core shear failure, face wrinkling (the skin indents the core or the skin 'pops' away from the core), general buckling, shear crimping, face dimpling (honeycomb cores only not foam cores), and local indentation.

During the service life of a composite sandwich composite structure the design has sought to eliminate all the potential failure modes that the expected (or predicted) loads may induce, i.e. the structure will be design against face fracture, core shear failure and global buckling. It is when the structure is subjected to an unexpected load, for example an impact event, that the structure may fail in an unpredicted manner. It is these unexpected, one-off events that necessitates the development of composite repair techniques.

2.3 Characterisation of damage in laboratory-based studies

2.3.1 Impact damage to composite laminates and composite sandwich structures

Foreign object impact to single skin laminates or sandwich construction composite structures can result in a drastic reduction in composite strength, elastic moduli, and structural durability and damage tolerance characteristics. The problem of impact damage to composite laminates has received the greater attention in the open literature [Choi *et al*, 1991; Davies *et al*, 1996; Dorey, ; Finn *et al*, 1993; Pavier *et al*, 1995; Richardson & Wisheart, 1996; Sutherland & Guedes Soares, 2003;] whilst understanding the effect of impact damage on the mechanical properties and residual strength of sandwich composite structures requires further development [Abrate, 1994; Mines *et al*, 1994; Wu & Sun, 1996].

Impact damage can be classified as either low or high velocity. Low velocity impact events are often referred to impact events in the range 1 to 10 ms^{-1} where the contact period is such that the whole structure has time to respond to the loading [Sutherland

& Guedes Soares, 2003]. In a high velocity impact event a stress wave is generated which propagates through the material. The timeframe in this event is so fast that structure is unable to respond to stress wave resulting in very localised damage. Marine craft are often subjected to repeated light docking collisions and collisions with floating debris and other vessels. These types of impact events can be considered as low velocity events.

Extensive research has been undertaken on the impact damage of both composite laminates and composite sandwich structures. The following paragraphs illustrate the range of this work. Although the impact research undertaken on composite laminates is not directly applicable to the work within this project, the inclusion of their research observations was considered prudent in identifying the best impact testing methodology for sandwich structures.

Richardson and Wishart [Richardson & Wishart, 1996] reported that four modes of failure where observed in composite laminates:

1. Matrix mode – cracking occurs parallel to the fibres due to tension, compression and shear;
2. Delamination mode – produced by interlaminar stresses;
3. Fibre mode – in-tension fibre breakage and in-compression fibre buckling; and
4. Penetration – the impactor completely perforates the impacted surface

Choi *et al* [Choi *et al*, 1991] reported that matrix cracking tends to lead to delamination damage once a threshold energy has been attained. Finn *et al* [Finn *et al*, 1993] identified that the threshold energy itself is dependent on the material properties, laminate stacking sequence and laminate thickness. Although impact damage consists of many fibre cracks and delaminations, only some of these will be active in the terms of controlling the residual strength of the structure [Pavier *et al*, 1995].

In the early impact work of composite laminates Dorey [Dorey, 1987] devised closed-form solutions to determine the energy levels needed to generate the delamination failure, fibre fracture and laminate penetration in 2mm thick CFRP. From the effects of geometry that delaminations are more likely with short spans, thick laminates or laminates with low interlaminar shear strengths. Back face fibre failure is more likely with large spans or thin skins and laminate penetration is most likely for small projectiles moving at a sufficiently high velocity that the laminate cannot respond quickly enough in flexure. In the work by Zhou [Zhou, 1995], it was shown that damage initiation in glass-reinforced laminates when dominated by delamination could be predicted using a simple ILSS analytical model. Davies *et al* [Davies *et* al, 1996] observed for thick E-glass woven fabric and polyester resin laminates that a strength-based criterion can be used to initiate a delamination but an energy release model is required to predict the subsequent growth and stability of that growth. Sutherland & Guedes Soares [Sutherland & Guedes Soares, 2003] reported that the specimen thickness, the dimensions of the impactor head, the clamp shape, and the application of clamp grip all had a significant effect on the maximum impact force, the absorbed energy and projected damage area at both high and low impact energy levels in laminates of E-glass woven roving fabric with polyester resin.

In sandwich structures, Abrate [Abrate, 1994] reported four different failure modes:

1. Delamination in the impacted face sheet
2. Matrix cracking and fibre breakage
3. Debond in the face/ core interface
4. Core crushing (permanent deformation) in the region of the impact

The extent of the damage within the sandwich structure will be dependent upon many factors including the impact damage tolerance performance of the skin and the core material. Mines *et al* [Mines *et al*, 1994] reported that different skin materials exhibited different failure mechanisms. In this work on chopped stand mat glass fibres, woven fabrics of glass, carbon, and aramid fibres in either an epoxy or polyester resin, it was observed that woven carbon, woven glass and CSM exhibited

upper skin compression (the skin compressive strength was lower than the tensile skin strength) whilst woven aramid skins exhibited upper skin crushing failure, which the authors attributed to the low compressive strength of aramid.

Thomson *et al* [Thomson *et al*, 1998] conducted 20J and 30J impact tests on GRP skins/PVC foam sandwich panels. The authors observed that the different impact energy had a strong influence on its residual shear properties. Following this work ,Mouritz & Thomson [Mouritz and Thomson, 1999] observed that the mechanical properties of the GFRP/PVC foam sandwich panels were highly sensitive to interfacial cracks and impact damage, but only when the load state causes a change in failure. To accurately predict the properties of a sandwich composite structure containing interfacial cracks and impact damage the complex interaction of material, structural geometry and damage parameters must be known.

Olsson [Olsson, 2002] noted that the inclusion of indentation and shear effects of the damaged sandwich beam was imperative for the successful prediction of impact damage threshold and damage length formation. In the work by Wu and Sun [Wu and Sun, 1996] the author's observed that impact event generated matrix cracking and delamination damage in the outer skin of a graphite/epoxy laminate face sheets (0.76mm thick) with local crushing of the Rohacell foam core (12.7mm thick). In an effort to characterise the location and extent of the delamination damage following a 2.2J (2.0 m/s) impact a virtual crack closure technique with total strain energy release rate was observed to be conservative.

This review of impact tests indicates that:

- Drop weight impact tests on composite laminates and sandwich structures are undertaken at low impact energies.
- To accurately predict impact damage the complex interaction of material, structural geometry and damage parameters must be known.
- Impact energy and tup profile will control the damage formation process.
- Low energy impact tests are not representative of damage experienced by operational structures (see Table 2.2).

- The formation of realistic impact damage (using realistic impact energy) is imperative for the generation of impact initiation thresholds.
- 2-dimensional and 3-dimensional impact damage tests undertaken within the laboratory setting are not representative of operational damage. Impact damage scaling will be required.
- 2-dimensional impact damage tests permit the evaluation of a range of impact variables and simplify the post-impact examination.

The points above indicate the pertinent issues in the design of an impact damage test. In this research, a 2-dimensional impact test procedure within impact energies ranging from 100J to 1000J is advocated. Through the application of this methodology and the design of a 'blunt-nosed' impactor, the evaluation of realistic damage observed in Table 2.2 can be achieved.

2.3.2 Theoretical treatment of impact damage initiation and propagation

An important aspect of any impact investigation is to be able to predict the damage initiation threshold and the magnitude of the damage arising from the impact event. Table 2.3 illustrates a selection of these theories. The majority of the theories within the table for both damage initiation threshold and damage size predictions have been developed specifically for composite laminates, with only the theories proposed by Olsson suitable for composite sandwich structures.

	Author	Formula	Observations
Damage initiation threshold predictions	[Dorey, 1987]	$Energy = \frac{2\tau^2 wL^3}{9E_f t}$	Proposed for composite laminates Requires knowledge of ILSS
	[Zhou, 1995]	$P = \frac{4\pi}{3}\tau t r$	Proposed for composite laminates Requires knowledge of ILSS
	[Davies *et al*, 1996]	$P_c^2 = \frac{8\pi^2 E(2h)^3}{9(1-\upsilon^2)} G_{IIC}$	Proposed for composite laminates Requires knowledge of mode II fracture toughness
	[Olsson, 2002]	$F_{dth} = \pi\sqrt{32 D_f G_{IIc}/3}$	Proposed for composite sandwich beams Requires knowledge of mode II fracture toughness
Damage size prediction	[Davies & Zhang, 1995]	$A = \frac{1}{\tau^2}\left(\frac{P}{t}\right)^2$	Proposed for composite laminates Requires knowledge of ILSS
	[Davies *et al*, 1996]	$P_c = \frac{4}{3}\left[\frac{2G_{IIC}Et^3}{(1-\nu^2)}\right]\frac{1}{(2R-l)l}$	Proposed for composite laminates Requires knowledge of mode II fracture toughness and initial defect size
	[Olsson, 2002]	$a_d = \sqrt{F_d \bar{a}_d^2 / \pi\rho_{cr}}$ $\bar{a}_d^2 = 2\left[1-(F_{dth}/F_d)^2 \times 3/(n+2)\right]$	Proposed for composite sandwich beams Requires knowledge of the number of delaminations and the crush stress of the core material

Table 2.3: Damage initiation and damage size predictions for composite laminates and composite sandwich structures

As Table 2.3 indicates the impact energy threshold predictions by [Dorey, 1987] and [Zhou, 1995] utilise the interlaminar shear strength (ILSS) properties of the individual materials whilst the predictions by [Davies *et al*, 1996] and [Olsson, 2002] require detailed knowledge of the mode II fracture toughness. A similar trend is observed with the damage size predictions where the ILSS and the mode II fracture toughness are required.

The impact investigations undertaken on polymer composite sandwich structures have indicated that the damage in these structures is often more local in nature than the equivalent impact damage in monolithic composite laminates. Although face sheet damage is local, damage resulting from a crushed core and a dented face sheet will lead to a loss of core stiffness and therefore lead to premature failure of the skin due to local skin buckling. A schematic illustration of how these individual failure modes manifest themselves in a sandwich panel after an impact event has been illustrated in Figure 2.1.

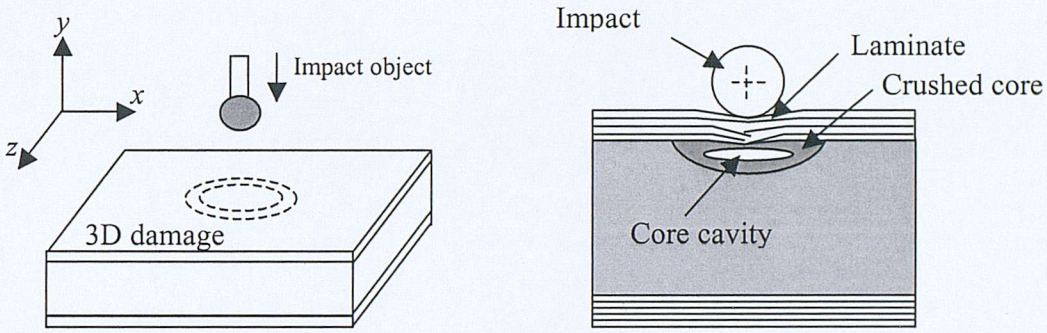

Figure 2.1: Typical impact damage in foam core sandwich structure [Abrate, 1994]

In Figure 2.1 the impact damage is composed of laminate fracture and crushing of the foam core resulting in a core cavity. Any fracture to the outside skin will be clearly visible and therefore instantly suggest that the structural integrity of the component has been compromised. However, due to the compliant nature of foam core materials the laminate skin may deform under the impact event but not fracture. In this particular case the damage within the core could go undetected, this damage is often referred as barely visible impact damage (BVID). BVID is a critical concern to designers and operators of composite sandwich structures.

2.3.3 Impact damage tolerance

A critical observation arising from the impact damage literature review is the need to address impact damage resistance (i.e. structural response and the damage caused by the impact), and impact damage tolerance, which considers the effect of the damage on strength and stability of the structure. Firstly, it should be recognised that

composite structures are neither impact damage resistant or impact damage tolerant [Christoforou, 2001; Baker *et al*, 1985; Zhou, 1998]. Secondly, to fully characterise and evaluate the damage resistance and damage tolerance of a composite structure, the precise nature and principal characteristics of the impact damage must be understood.

Baker *et al* [Baker *et al*, 1985] reported that damage tolerance as '*the ability of the structure to contain representative weakening defects under representative loading and environment without suffering reduction in residual strength, for some stipulated period of service*'. The authors observed that delaminations in composites in aircraft structures are a major concern under compressive loading since the delaminated region acts as a low modulus zone it may produce a loss in residual strength comparable of that produced by an unfilled hole of comparable area.

Zhou [Zhou, 1998] observed that damage tolerance is *'the ability of damaged composite structures to retain residual compressive strength in terms of a damage measure'*. In this work the author defines the damage measure as delamination area, surface indent, incident kinetic energy or impact force. The choice of this measure will greatly influence the test evaluation method, the data interpretation and the damage prediction method (whether it will be based on ILSS or fracture mechanics).

According to Irving [Irving, 2002] a good damage tolerance structural materials will have:

- Large window of slow predictable damage growth
- Large damage capability before catastrophic failure at limit load
- Robust quantitative models for damage growth
- Good detectability of damage
- Fail safe principles of construction – multiple load paths

To predict the response of the composite structure to adverse impact events it is imperative that the damage sources are correctly identified and that the critical

loading modes are established for developing the static and cyclic testing of structural elements and full-scale components [Tomblin *et al*, 1999].

At present the research into composite damage tolerance is still relatively new. In essence this is due to the extent of information required to generate a damage tolerance philosophy, i.e. the philosophy depends upon a comprehensive knowledge of the composite structure, the operational loads, knowledge of the starting defects and the defects formed during operation, identification of the critical defect types, the advantages and disadvantages of standard non-destructive techniques (NDT), the determination of NDT inspection frequencies and theoretical and experimental methods to predict damage growth rates.

In composite sandwich structures a number of defect types could be the critical defect, i.e. delamination within the outer skin, debonding within the skin and core interface, core-crushing arising from impact damage or core shear cracks due to fatigue. In theory, each of these defects could occur within the operational life of the composite sandwich structure, and therefore a damage tolerance philosophy would be required for each of these critical defect types.

In Table 2.2, delamination damage in the outer skin was identified as the most common defect occurring within operational sandwich structures after an impact event. If delamination damage in the outer skin is now assumed to be the critical defect type this permits a closer examination of the damage tolerance approach developed by [Baker *et al*, 1985] for delamination damage. This approach is outlined below:

1 Ability to predict reduction of residual strength or strain capacity by analytical/ experimental approaches accounting for:

- Damage nature, size, extent, location
- Laminate, matrix type/state, stacking sequence, ply drop offs, thickness
- Component, size, geometry, deformation geometry
- Stress-field, including interlaminar and residual stresses

- Environment, temperature, moisture
- Prior service history

2 Ability to predict rate and geometry of growth of damage, if any, accounting for:

- Above aspects
- Load spectrum
- Environmental cycling, thermal spikes, freeze/thaw

The approach proposed by [Baker *et al*, 1985] recommends a two-tier approach using residual strength and prediction of damage growth. The complex nature of this approach will necessitate an extensive evaluation programme. In reality, not many organisations can afford to undertake such a programme. It is therefore very likely that a damage tolerance philosophy will be restricted to a specific component operating under specific loading conditions with limited ability to transfer the results to different components manufactured from different composite materials operating within a different environment. In an effort to understand the extent of research undertaken on the problem of residual strength testing and the prediction of damage growth within composite sandwich structures and composite repairs Table 2.4 and Table 2.5 have been produced.

Authors	Materials	Structure/ Geometry	Impact variables	Damage mode	Assessment method	Experimental observations
[Burman and Zenkert, 1997]	E-Glass/ Vinyl ester 8084 HLU with H100 PVC foam. E-Glass Epoxy prepreg with WF51 foam	Sandwich beam	Simulated interface disband with Teflon film and butt-joint damage	(1) face/core interface damage (2) flawed butt-joint (mm to 10mm)	Static and fatigue testing in four-point bending	A simple model using notch factors obtained from static tests can be used to accurately predict the reduction in fatigue life due to the inflicted damages
[Thomson *et al*, 1998]	GRP skins/PVC foam	Sandwich beams	20J & 30J	Interfacial crack size and impact damage size	Static and fatigue testing in four-point bending	Abrupt decrease in the static shear strength and fatigue resistance when the interfacial crack length exceeded 20 to 30mm.
[Mouritz & Thomson, 1999]	E-Glass CSM & WR Vinyl ester 411-45 / HT-90 PVC foam	Sandwich panels and sandwich beams	25mm tup repeated impact of 20J & 30J to giving different impact damage lengths	Interfacial cracks of 20, 40, 70, 100 & 150mm. Impact damage lengths of 25, 58, 87 & 116 mm	Edge wise compression Four-point bend	Interaction of material, structural geometry and damage parameters must be known to predict the mechanical performance of a sandwich composite containing defects or damage
[Mines *et al*, 1994]	WR Carbon,/ polyester, CSM glass/ olyester, WR aramid/ polyester, WR glass/ polyester, WR + CSM glass/ polyester, WR glass/ epoxy prepreg with 13mm & 25mm honeycomb core	Sandwich beam	20mm tup with a maximum energy of 155J		Three-point bend. Impact damage loaded on compressive face.	Woven carbon, woven glass and CSM exhibited upper skin compression (the skin compressive strength was lower than the tensile skin strength) whilst woven aramid skins exhibited upper skin crushing failure, which the authors attributed to the low compressive strength of aramid fibres.

[Clark, 1997]	E-glass/Kevlar / epoxy and E-glass/ epoxy with H-100 PVC core	Sandwich beams	38mm diameter tup conducted on tensile face		Fatigue 10-point bend test	No fatigue property degradation, and no shift in failure mode for the Glass/Kevlar hybrid skins. 25% reduction of fatigue performance for the E-glass skins and shift of failure mode to skin tensile failure.
[Hansen, 1998]	E-glass/ epoxy with ECA 3.2-48 honeycomb core	Sandwich panels (300mm x 200mm)	Artificial Teflon debonds 15mm x 35mm between skin and core	Simulated debonds between skin and core	Edgewise compression test	
[Shipsha, 2003]	E-glass/ Vinyl ester with Rohacell WF51 foam core	Sandwich panels (270mm x 180mm)	7.8kg 25mm diameter tup 10J to 60J	10J = BVID impact damage, 60J = visible damage in the face laminate (18mm diameter)	Edgewise compression test	The impact damage was shown to cause a significant reduction in the compressive strength. Panels failed by local buckling provoked by the residual impact dent.

Table 2.4: Residual strength testing of composite sandwich structures

Authors	Materials	Loading conditions	Crack location	Assessment method	Model type	Experimental observations
[Ratcliffe & Cantwell, 2001]	E-glass/ polyester Al honeycomb, E-glass/ polyester balsa, E-glass mat/ polyester cross linked PVC, E-glass/ polyester linear PVC, E-glass/ polyester Nomex, Carbon fibre Nomex	Mode I with some mode mixity with crack length	Central crack in lower skin core interface	Centre notched flexure sandwich (CNFS) test method	Linear elastic fracture mechanics	The interfacial fracture energy for a glass fibre reinforced polyester/linear PVC system was found to be 170 J/m^2 and for Nomex honeycomb core the interfacial fracture energy was found to be 2750 J/m^2.
[Li & Carlsson , 1998]	H100 PVC foam core with glass/ polyester skin		Skin-core interface	Titled Debond Sandwich (TDS) test method		A tilt angle greater than 10° is required to ensure that interfacial debonding and not kinking occurs. However, the critical angle decreased with increased crack length indicating that the mode mixity depends on crack length
[Raizenne *et al*, 1994]	Aluminium face sheets/aluminium honeycomb core sandwich structure					Bonded repairs provided a 150 times improvement in the fatigue life under severe loading and environmental conditions compared to the un-repaired specimen.
[Noury *et al*, 1998]	Rigid PVC cellular foam	Mode-I, mode-II and mixed mode	Foam material	Compact-tension-shear test	Linear elastic fracture mechanics	Fatigue crack growth rate to be controlled by the mode I fracture toughness with some small contribution of mode II when mixed-mode testing was undertaken.
[Shipsha *et al*, 2000]	PVC Divinycell H100 and PMI Rohacell WF51	Mode I	Foam material	Compact tension specimen	LEFM and Paris' Law	Fatigue crack growth in PVC and PMI cellular foams can be analysed and expressed by Paris' Law.

[Romanko *et al*, 1984]						A comprehensive methodology using time-dependent fracture mechanics procedures and analytical methods for the lifetime predictions of structural lap joints.
[Krueger *et al*, 2000]		Mode I and mode II components	Bonded composite skin/stringer		Virtual Crack Closure Technique	The life prediction method determined delamination fatigue characterization
[Kinloch & Osiyemi, 1993]	Carbon fibre/ epoxy	Mode I	Bonded overlap region in a single-overlap joint	DCB specimen	Linear elastic fracture mechanics	Derived a relationship between the strain-energy release rate, G_{max}, and the length, a, of a crack propagating through a single overlap joint
[Attia *et al*, 2001]	Carbon fibre/ epoxy	Mode I	Bonded overlap region in a I-beam		Linear elastic fracture mechanics	Short-term fracture mechanics experimental data with finite-element analysis of the component to predict the number of cycles to failure of the composite I-beam
[Curley *et al*, 2000]	Mild-steel	Mode I	Single lap joint and a 'top-hat' box-beam joint	Tapered double-cantilever beam	Fracture mechanics and Paris' Law	Combination of the cyclic fracture mechanics data and the FE modelling studies the authors were able to predict the wet and dry cyclic-fatigue service-life
[Olsson *et al*, 1996]	Carbon fibre/ epoxy	Mode I, Mode II & mixed-mode	Composite laminates	Double-cantilever beam, Mixed-mode bending & Edge notched flexure	Irwin-Kies	The application of fracture mechanics to delaminations in fibre composites requires characterisation of the interlaminar toughness of angle ply interfaces in both pure and mixed mode conditions.

Table 2.5:Fracture mechanics testing of composite sandwich structures and bonded joint configurations

The first observation arising from Table 2.4 is the lack of experimental and theoretical residual strength investigations of composite repairs, whether to single skin laminates or sandwich structures. The second observation is the relatively limited amount of work that has been undertaken on composite sandwich structures. Since sandwich structures are highly sensitive to interfacial cracks and impact damage, the author had anticipated that more research would have been undertaken in this area.

In Table 2.5 the extent of fracture mechanics research on composite sandwich structures has been directed towards determining the interfacial properties of the skin-core interface or the fatigue crack growth properties of a defect within the core material. In terms of the fracture mechanics assessment of adhesive bondlines this has been directed towards the bonded joint between an external repair patch and the component, or the bonded joint between two structural components. A key observation arising from Table 2.5 is the success of the fracture mechanics test specimens at predicting the fatigue life of the semi-permanent repairs (i.e. external bonded patches) and structural components. The second observation concerns the lack of research into permanent repairs.

2.3.4 Experimental investigation of impact damage - areas of research opportunities

The extent of research undertaken on the problem of impact damage to single skin and sandwich skin composite structures is extensive. However, the one obvious area, which has yet to be investigated, is the impact response of the composite repair, whether to a single skin or a sandwich structure.

Once a better understanding of defect formation within structural repairs has been obtained, the question of repair damage tolerance can be considered. For example, although defects (manufacturing or operational) can now be tolerated within the structure (after rigorous development of a damage tolerance philosophy), at some point the defect will exceed the upper damage tolerance limit and therefore a structural repair will be required. After the completion of the repair the structure will then re-enter operational service. This raises a fundamental concern, i.e. is the repair as damage tolerant as the structure it has repaired? To assess whether this is the case, a thorough understanding of the residual strength and the prediction of damage growth within a

structural repair made to a composite sandwich structure must be understood. However, at this moment in time no such research has been undertaken.

In summary, operators of composite sandwich structures need to understand or have theoretical tools to predict:

1. How damage manifests itself within a structural repair to a sandwich structure,
2. Whether a repair is less damage resistant than the original structure, i.e. whether barely visible damage within a repair is more critical than in the original sandwich structure,
3. Whether a repair is less damage tolerant than the original structure, i.e. whether damage can propagate more easily at the same loads,
4. To predict the damage threshold and the damage growth within a composite repair,
5. How cracks or delaminations propagate within structural repairs, i.e. a fracture mechanics assessment of the tapered and stepped scarf repair is required,
6. The long-term response of sandwich structures subjected to adverse in-service impact events.

The lack of research in this area is very alarming since in real structures repairs are often undertaken in critical regions where there is a very high probability of a repeated impact event.

2.4 Repair of composite sandwich structures

2.4.1 Repair design guidelines

The design of any composite repair method depends greatly upon the particular component and the extent of the damaged incurred, e.g. a sandwich panel with one or both skins punctured. Since composite structures are employed in different industries with different design philosophies, current repair concepts include a wide range of approaches from highly refined and structurally efficient but expensive flush patch repairs to externally mechanically attached metal or composite patch [Schwan, 1998].

Although the exact nature of the repair, regardless of structure and operational role, will vary due to many factors, there are some basic guidelines that should be considered if a safe and effective repair is to be achieved [Cole, 1999]:

- Stiffness: The patch design should match the original laminate stiffness as closely as possible. If the stiffness of the repair is much greater, additional channelled load may exceed the strength limitations of the repair. A stiffness that is significantly less can lead to the over-stressing of the surrounding structure.
- Strength: Unless identical material and processes are employed for the repair, it is not often possible to match both the strength and stiffness of the original laminate. When this arises the primary methodology, depending upon the specific component, is to match the stiffness as closely as possible whilst ensuring that a strength margin of safety also exists.
- Stability: The global response of the repaired structure subjected to compressive loading is of critical concern to the design engineer. Precise design guidelines have been generated to ensure that the repair scarf angle and overlap length are limited to ensure that the strength and stiffness in compression is maintained at all times.
- Durability: The repair must be permanent, i.e. it lasts the lifetime of the structure being repaired. The durability should be designed into the original geometry, but if alternative materials have to be employed, they must at least match the operational environmental capabilities.
- Restoration of function requirements: The repair must restore functional requirements of the structure. In the marine environment, aspects like hydrodynamics and negligible weight penalty are important. Composite repairs tend to satisfy these considerations more easily than other repair methods.

The overall objective of the repair is to return the structure to its undamaged condition, such that it can support all design loads for the intended service life of the structure.

2.4.2 Repair design options

A wide range of repair designs has been considered for the cosmetic, temporary and structural repairs of composite structures. Repair geometries ranging from simplistic external patches to complex tapered scarfs have been considered and employed in most

industries. Typical examples of the different repair techniques has been illustrated in Figure 2.2 and Table 2.6.

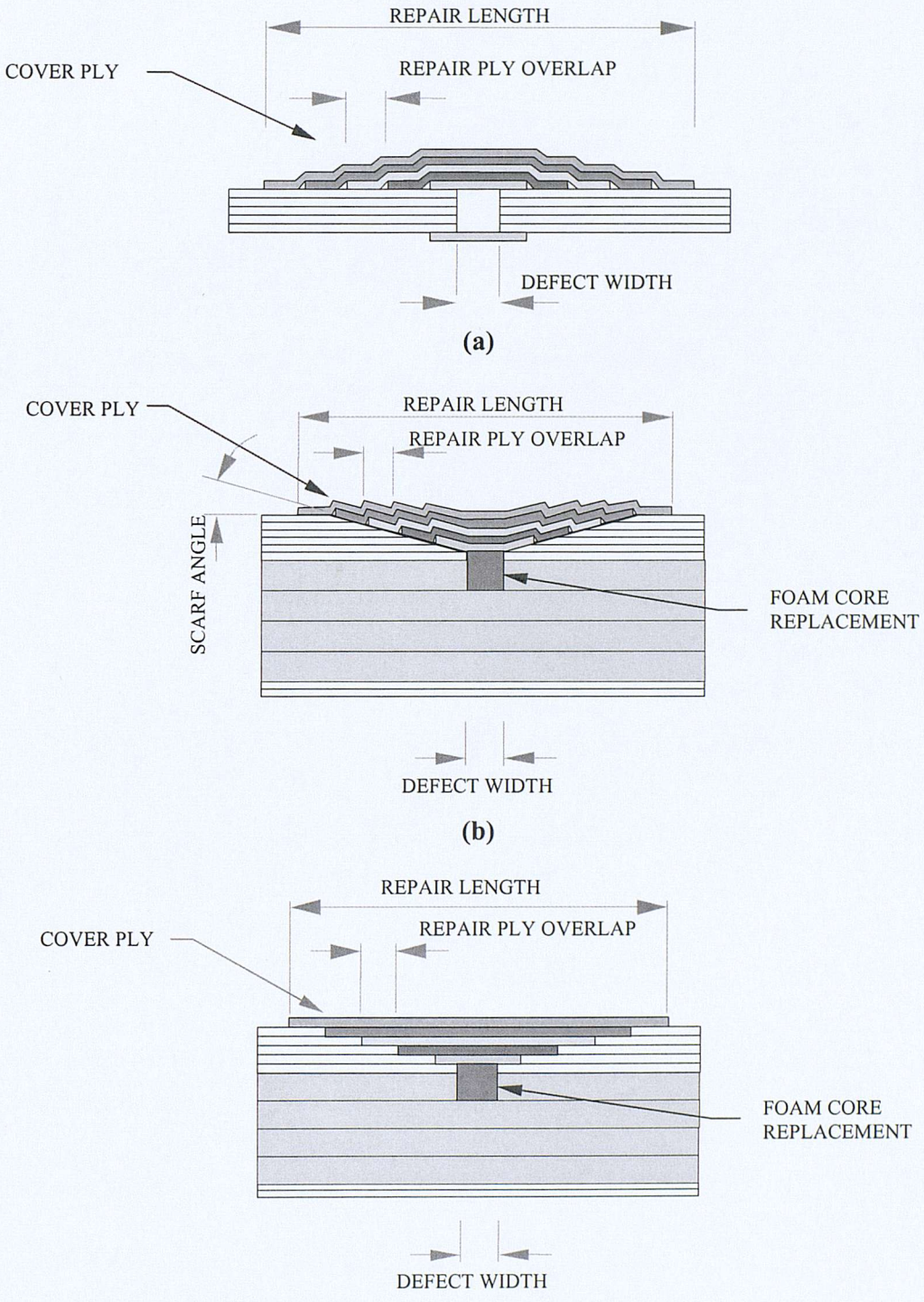

Figure 2.2: Repair design options (a) external patch [Davies & Bond, 1999], (b) tapered scarf repair [Hart-Smith, 1973a], and (c) stepped scarf repair [Fraisse & Schmit, 1992]

Design		Design criteria	Design equations
Cosmetic	Filler	Restoration of functional requirement	No design equations or recommendations
Semi-permanent	Bolted plate	Stiffness replacement Restoration of the design ultimate strain Durability	[Matthews, 1999; Cochran *et al*, 1986; Madenci *et al*, 1999; Ireman & Purin, 1999]
	Bonded patch	Strength replacement dependent upon substrate thickness and peel stresses Durability dependent upon minimisation of the transverse tensile stresses	[Hart-Smith, 1985; Hart-Smith, 1973a; Davies & Bond, 1999; Trabocco *et al*, ; Potter, 1979; Schwan,, 1998]
Permanent repairs	Tapered scarf	Stiffness and strength replacement Stability Durability Restoration of functional requirements	1. Foam core – no design equations or recommendations 2. Scarf angle $\theta < \frac{\tau_p}{E\varepsilon_u}$ for tensile load, or $\theta_{opt} \cong \tan^{-1}(0.816\tau_s/\sigma_{un})$ for compressive loads 3. External plies $d = \left(\frac{t_a}{G_a} \cdot \frac{E_p t_p}{(1+S)}\right)^{\frac{1}{2}}$ or $L_p = \frac{\sigma_{ULT} t_i}{2\tau_p}$ and $L_e = \frac{3}{\lambda}$ where $\lambda^2 = \frac{G}{\eta}\left(\frac{1}{E_i t_i} + \frac{1}{E_o t_o}\right)$ [Hart-Smith, 1973a; Soutis & Hu, 1997; Grosko, 1995; Lubkin, 1957; Webber, 1981]

	Stepped scarf	Stiffness and strength replacement Stability Durability Restoration of functional requirements	1. Foam core (as above in tapered scarf) 2. Step profile $P_C = B\sqrt{2EtG_{IIC}N}$ and $N_c = E\left(\frac{2\sigma_U t}{9EG_{IIC}}\right)$ 3. External plies (as above in tapered scarf) [Fraisse & Schmit, 1992; Hart-Smith, 1973a]

Table 2.6: Repair design options and supporting theory for cosmetic, semi-permanent and permanent repairs to sandwich structures

The repair design options identified in Table 2.6 for permanent tapered-scarf or permanent stepped-scarf repairs are based upon a few critical equations. These equations are widely employed by various military and commercial organisations in the repair of their composite structures (specific examples are given in Table 2.10). Although these equations were developed in the 1970s for the taper angle in scarf repair and in the 1980s for the design of the overlaminate there are still the principal design method when designers need to repair for composite structures.

2.4.3 Repair design considerations

In the design of permanent and semi-permanent repair schemes certain design variables have to be considered and optimised to ensure the maximum structural efficiency.

In the case of semi-permanent repairs to sandwich structures the length and application method of the bonded external plies, the taper at the end of the bonded patch, and adhesive properties such as thickness and stiffness. Consideration must also be given to whether the damage is left or filled.

For permanent repairs to sandwich structures, consideration needs to be given to the replacement of the foam core, the design of the foam replacement and the method of bonding the new core. For the reinstatement of the sandwich skin, a decision about the

scarf profile is required, the scarf angle or step length, the length and application method of external plies, different patch/parent lay-up (including stacking sequence), and adhesive properties such as thickness and stiffness must be optimised depending upon the requirements of the structure, the certifying authority and the operational environment. Key observations arising from the open literature include:

- Shallow scarf angles reduce the eccentricity of the loading path thereby minimising the tensile transverse stresses in the adhesive and the shear stress concentrations at the ends of the joint. This was noted by [Hart-Smith, 1973; Webber, 1981; Adkins & Pipes, 1988]
- Steep scarf angles can produce high strain concentration that initiate failure [Mahler, 1999]
- In tapered step repairs, the effect of step height, step modulus and non-uniform step length can significantly alter the repair performance [Tran-Cong & Heller, ; Fraisse & Schmit, 1992]
- Strain concentrations occur with a patch to parent mis-match in laminate stiffness. It is therefore recommended to balance the stiffness mismatch between the skin and the patch [Smith, 1995]
- Overlaminate plies protect scarf tip from damage and minimise stress concentration at the scarf tip end [Deaton, 1990; Smith, 1995]
- Load path eccentricity causes transverse tensile stresses at end of overlaminate patch [Deaton, 1990; PERA, 2000]
- Long overlaminate lengths are required to minimise transverse tensile stresses [Davies & Bond, 1999; Hart-Smith, 1973b]
- Apply a maximum of 5° taper to overlaminate edge to minimise transverse tensile stresses [Grosko, 1995; Trabocco, 1988]
- Avoid large bondline thickness since this increases stress in the adhesive and reduces strength [Grosko, 1995]
- Reduced adhesive stiffness, increases deformation, increase stress in adhesive.

To illustrate the number of design variables that would have to be considered for the permanent and semi-permanent repair of a sandwich structure Table 2.7 has been

generated. The table highlights the different philosophies employed by different researchers/ organisations

Operator	Materials	Design of repair
United States Coast Guard [Marine Composites,]	Polymer composite (no material definitions given)	Foam core - single replacement core, straight sided, bonded Tapered scarf - 5° taper scarf with the repair plies laid parallel to the scarf profile (i.e. the largest ply is laid first with each successive ply being slightly smaller). Overlaminate – single overlaminate ply extending beyond the end of the scarf tip
Swedish MCMV [Sjögren *et al*, 1984]	E-glass with polyester matrix and PVC foam core	Foam core - small individual blocks secured with screws/nails Tapered scarf – 1° taper scarf Overlaminate – no indication whether any overlaminate plies are used.
RAN: Bay Class Minesweeper [Thomson *et al*, 1998]	E-glass (CSM/WR/CSM with vinylester matrix) skins. PVC foam core	Foam core - single replacement core bonded with paste adhesive, vacuum consolidated with resin bleed holes Tapered scarf - 6° taper manufactured by abrading Overlaminate - vacuum consolidated. 40mm length per replacement layer plus one extra layer extending 100mm
Royal National Lifeboat Institution, UK [Austen, 1999]	E-glass and Kevlar hybrid with epoxy matrix. PVC foam core	Foam core - single replacement core bonded with epoxy paste adhesive Tapered scarf – 6° or 3° tapered scarf manufactured by abrading Overlaminate - vacuum consolidated. 50mm length for first replacement layer, 25mm length for next 3 replacement layers plus two extra layers each extending a further 50mm

Helicopter Division MBB GmbH, Germany. [Hahn, 1986]	Uni-directional E-glass. PVC foam core	Foam core - single replacement core bonded with epoxy paste adhesive Tapered scarf – elliptical 3° taper in longitudinal direction manufactured by grinding Overlaminate – no overlaminate to disturb air flow, all repair plies finish at the scraf repair edge
Helicopter Division Aérospatiale, France. [Torres & Plissonneau, 1986]	Carbon fibre epoxy matrix. Nomex honeycomb core	Nomex Honeycomb core – for major deterioration bonded single replacement core otherwise resin or microballoon filler Tapered scarf – 3° tapered scarf manufactured by abrading Overlaminate – pre-cured doubler bonded with cold-curing epoxy resin
Military Jet, Dornier GMBH, Germany. [Thiele, 1986]	E-glass epoxy matrix. Nomex honeycomb core	Foam core - single replacement core bonded with epoxy paste adhesive Tapered scarf – 3° tapered scarf manufactured by abrading Overlaminate – 15mm length per replacement ply
Military aircraft, Deutsche Aerospace AG, Germany. [Maier & Günther, 1995]	Uni-directional carbon fibre epoxy matrix. Aluminium alloy honeycomb core	Honeycomb core - single replacement core bonded with epoxy paste adhesive Tapered scarf – no scarf taper used Overlaminate – 10mm length per replacement ply. Pre-cured external doubler bonded with film adhesive
DSTO, Australian. [Whitehead *et al*, 2000]	Composite skin. Aluminium alloy honeycomb core	Honeycomb core - single replacement core bonded with film adhesive Tapered scarf – no scarf taper used Overlaminate – overlap lengths are specified depending upon the face thickness. Pre-cured external patch with tapering

Table 2.7: Design variables used within the repair of composite sandwich structures

Table 2.7 indicates the diverse repair design philosophies currently employed in the repair of sandwich panel construction. Each of the different organisations have independently developed design philosophies that embrace:

1) Different scarf angles ranging from 1° to 6°
2) The application, or not, of external plies
3) Replacement external plies range in length from 10mm to 50mm
4) The application of the largest or smallest repair ply first
5) Pre-cured patches or patches manufactured in-situ
6) The application of a vacuum to avoid air entrapment at the core bondline
7) The manufacture of vertical or horizontal core blocks
8) The manufacture of the repair on the component or the manufacture of a pre-cured repair that is bonded to the component as a secondary operation.

The precise benefits and limitations of these slight variations to the repair design of composite sandwich structures can only be speculated at. It is highly likely that a repair scheme having the smallest scarf angle possible with external plies extending beyond a critical length will obtain the greatest mechanical performance as well as maintaining the stability and durability requirements of the original structure. However, the precise benefit of applying the largest or smallest repair ply first, or whether vertical or horizontal replacement core blocks will enhance the long-term structural performance of the sandwich structure is questionable.

Finally, the selection of the manufacturing route will affect the mechanical performance and cost of the repair scheme. Ideally the repair should be made with the same manufacturing process as the parent laminate. However, this may not always be the case. If the structure has been made using pre-impregnated composite materials and the repair has to be made on the component, then a repair scheme manufactured by either hand lay-up or a dry fibre stack infused with a liquid resin are the two options. These two manufacturing options will not produce the same mechanical properties as the pre-impregnated composite materials. Vacuum consolidation of the hand lay-up repair and the application of heater mats to both repair schemes could enhance the mechanical performance further. However, even with these processing refinements the mechanical performance of the patch is still unlikely to match the parent laminate due to a higher void content and a lower volume fraction arsing from a lower consolidation pressure. If the mechanical performance of the patch must exactly match the original structure then a patch should be made using the same processing method and then bonded in place using a structural adhesive. To overcome the deficiencies of the manufacturing route

additional plies are added to the repair to match the stiffness requirements of the parent structure.

2.4.4 Repair of composite sandwich structures - areas of research opportunities

This review of repair designs for composite sandwich structures has indicated the importance of selecting the correct scarf angle and the overlaminate length. If either is incorrectly designed the repair joint will either fail below the static strength of the panel or have a reduced fatigue life performance through premature failure of overlaminate by load path eccentricity.

Although various repair schemes from external plies, to stepped scarf and tapered scarf could be evaluated, in this work, a tapered scarf repair with 3° taper, representative of the structural repair methods used in the repair of the RNLI rescue craft, will be evaluated. A standard RNLI overlaminate repair scheme will also be evaluated.

The design of the overlapping plies is critical if the joint efficiency is to be superior to the plain scarf joint [Deaton, 1990]. The role of the overlapping plies is twofold. Firstly, the overlapping plies protect the scarf tip and increase the load transfer area. Secondly, it enhances the strength and stiffness of the repair area. If the overlapping plies are correctly designed the locus of failure will remain outside of the scarf joint.

Whilst the role of the overlapping plies seems critical in the performance of the scarf joint, no design guidelines seem to exist for the number of replacement plies, their length or their lay-up. A critical question concerns whether the original laminate thickness should be used as a baseline for the overlap plies or whether a different fibre lay-up specific for the role of protecting the scarf tip should be employed. The only clear recommendation concerns the need to minimise the peel stresses at the end of the overlapping plies through the application of a taper. If the design guidelines employed for an external patch are considered, then a taper of 10 degrees should be used parallel to the load direction and a taper of 5 degrees should be used perpendicular to the load direction [Grosko, 1995].

Composite repairs are designed to restore the stiffness or strength requirements of the original structure, as well as the stability, durability and functional requirements. Whilst

the functional requirements of the repair will not be compromised by the inclusion of an internal defect, a concern exists about its influence on the stiffness, strength and durability. Since composite repairs are often manufactured outside of the ideal manufacturing environment it is possible that a manufacturing defect could be introduced and overlooked (e.g. the complex repair geometry, the changing thickness and the high void content will all cause significant problems for existing non-destructive techniques). In addition to manufacturing defects, composite repairs could also contain defects arising from operational use, i.e. if a repair is undertaken in a region of high impact probability then the same impact event could also occur during the lifetime of the repair scheme. Since both of these situations could occur it seems strange that no research has been undertaken to assess what defects could exist within a repair and what influence these defects would have on the repair's performance (whether stiffness, strength or durability). It therefore seems imperative that a damage resistance and damage tolerance assessment of defective repairs in composite sandwich structures is undertaken. The guidelines arising from this investigation could indicate whether composite repairs need to be designed for 'impact performance' as well as stiffness, strength and durability.

Finally, this review of composite repair methods has indicated the diverse range of repair techniques that can be used for composite sandwich structures. Whilst large organisations operating composite sandwich structures often have the technical capability and skills to design one-off repair schemes, it is the smaller operator who will have insufficient funds to correctly design a repair scheme. In this particular instance the operator may opt to design with a different material (i.e. aluminium), or use the wrong repair scheme thereby threatening the operational safety of the structure. Clearly, these two situations could be avoided if a generic repair manual for composite sandwich structures was made available to all users and operators. At present no such repair manual exists.

2.5 Assessment of composite repairs

2.5.1 Experimental research on composite repairs to composite sandwich structures

The majority of published work on composite repair is based around experimental approaches for aerospace laminates. This bias towards practical experimentation has

arisen because the aerospace design engineer has needed hard evidence on the operational performance of composite repairs to satisfy certification authorities (i.e. FAA and CAA). However, since composites by their very nature are complex, any experimental investigation would have to assess a wide variety of material and design parameters. Although thorough, this design methodology is expensive and time consuming and has therefore resulted in repair designs based on past experience or on similar structural damage.

Considerable experimental research has been undertaken on determining the tensile performance of repairs in composite laminates. Webber [Webber, 1981] tested scarf repairs in axial tension manufactured as a pre-cured or co-cured (wet lay-up) joint with increasing scarf angles. The scarf joints manufactured by wet lay-up (repair fibres in the same direction as the original material) had poor performance compared with joints manufactured within an autoclave environment (with fibres running parallel to the scarf angle). In a similar investigation Adkins and Pipes [Adkins and Pipes, 1988] examined the performance of co-cured scarf repairs loaded in tension with different scarf angles. It was found that scarf joints with 1.1° (i.e. 1/55) slopes were approximately twice as strong as 9.2° (i.e. 1/6) scarf joints. In an effort to characterise the influence of a uniform overlap and a tapered overlap compared with the plain scarf joint Deaton [Deaton, 1990] determined the tensile efficiency of the uniform overlap remained at 60% of the undamaged state where failure occurred by peeling of the extra plies. For the tapered overlap, which minimised the peel stress at the end of the overlap, the tensile efficiency increased from 60% to 90% of the undamaged state. Mahler [Mahler, 1999] assessed repairs subjected to tension and compression tests. In this research it was observed that steep scarf angles can produce high strain concentration that initiate failure and strain concentrations occur when a mis-match in laminate stiffness between the patch and parent. It was also noted that increased bondline thickness increases stress in adhesive and reduces strength whilst the inclusion of an overlaminate reduces strain level across laminate. Finally, the author noted that a reduced adhesive stiffness increases deformation in the repair thereby increasing the stress in adhesive.

Various researchers have also assessed the static and fatigue performance of repairs undertaken to composite sandwich structures. In the work by Clark [Clark, 1997]

different repair strategies were considered and assessed statically and in fatigue. For core sensitive beams the repair strategies did not affect the fatigue life compared to the undamaged beams. However, for skin sensitive beams, the failure load for many of the repair beams was significantly reduced by up to 20%. Thomson *et al* [Thomson *et al*, 1998] reported an abrupt decrease in the static shear strength and fatigue resistance in four point bend when the interfacial crack length between the skin and core exceeded 20-30 mm due to the failure mechanism changing from skin wrinkling of the GRP skins (woven roving 600 g/m^2 and chopped strand mat (CSM) 300 g/m^2) to shear cracking of the foam core (Divinycell HT90 PVC foam (90 kg/m^3)).

A static assessment in four-point bend of external patches bonded with cold curing epoxy adhesive over perforated sandwich panels has been undertaken by Torres and Plissonneau [Torres and Plissonneau, 1986]. Tests conducted at room temperature and aged for 750 hours at 70°C. Failure occurred outside the repaired area in all cases however the strength difference significantly dropped between the control and aged specimens. Whitehead *et al* [Whitehead *et al*, 2000] evaluated the problem of pre-cured external patches with overlap lengths specified depending upon the face thickness. External patch tapering 17t ± 3t. This review confirmed that adhesive degradation is a serious structural integrity issue for honeycomb sandwich panels and has highlighted a number of problems with damage limit specification and repair procedures for these panels. External hard patch repair of honeycomb structure using epoxy film adhesive has been evaluated by Maier and Günther [Maier and Günther, 1995]. Qualification of bonding the hard repair patch to the aircraft structure was undertaken through the simultaneous manufacture of a single lap shear specimen. The specimen was used to assess whether the repair had obtained the maximum shear stress target.

Fatigue assessment of single-sided and double-sided repairs to sandwich structures has been undertaken by Shah-Khan and Grabovac [Shah-Khan and Grabovac, 2000]. Single sided repairs had a greater fatigue life than the double-sided repairs. The authors attribute this reduction to the influence of material quality and manufacturing defects, suggesting a higher number of imperfections will exist in a double-sided repair compared to a single-skin repair.

In an effort to understand the mechanical performance of structural repairs to composite sandwich structures various mechanical test methods and loading conditions have been tried, i.e. tensile tests, flexural tests, compression tests and shear strength tests. In general these test methods tend to assess the static strength of the repair, although some researchers have considered the influence of fatigue loading [Shah-Khan & Grabovac, 2000; Clark, 1997].

2.5.2 Assessment of repairs - areas of research opportunities

The assessment of structural repairs to composite sandwich structures is not as comprehensive as the research on single skin laminates. The recommendations for scarf angle and overlaminate design arising research on composite laminates are equally applicable to the design of composite repairs to sandwich structures. It is therefore recommended that any experimental and theoretical investigation of sandwich structures should be preceded by an examination of the research on the repair of composite laminates.

Once again, an obvious limitation of the repair assessments that can be deduced from Table 2.11 is the lack of experimental and theoretical investigations into the influence of manufacturing defects or operational damage upon the static and fatigue performance of the repair method/repair bonded interface. These investigations could be strength-based or fracture mechanics based. It is therefore recommended for this research that:

1. A strength-based assessment is undertaken to determine the influence of operational damage on the pristine (as received materials) and the repaired beams.
2. A fracture mechanics assessment is used to evaluate the relative fracture toughness performance of the complete repair scheme, i.e. the different materials involved and the possible failure locations.

Finally, it is apparent after conducting this review of repair techniques to sandwich structures, there is an industry wide need to produce a detailed repair methodology providing precise guidance on the influence of manufacturing defects and operational damage on the design of permanent structural repairs and what influence, if any they will have on the integrity of the structure.

2.6 Literature review observations and conclusions

This extensive review of the open literature has illustrated the depth of knowledge required by a designer or engineer to undertake the repair of a composite sandwich structure.

The review has considered the influence impact damage on operational composite sandwich structures, the efforts undertaken by different researchers to duplicate and characterise impact behaviour within a controlled laboratory environment, and the theoretical techniques currently available to predict damage initiation and damage propagation.

Impact damage to composite sandwich structures can be classified by four different failure modes, namely:

- Delamination in the impacted face sheet
- Matrix cracking and fibre breakage
- Debond in the face/ core interface
- Core crushing (permanent deformation) in the region of the impact

Whilst considerable research effort has been undertaken in evaluating these different failure modes, there has been no equivalent effort to understand and determine the impact response of a structural or non-structural repair techniques contained within composite structures.

At present, there is no knowledge on how the damage forms within a repair to a sandwich structure, whether the damage type is critical or what effect it has on the structural integrity. With the increasing probability that damage is likely to occur on previously repaired structure it is imperative that this area is researched and understood.

The concept of damage tolerance for operational composite sandwich structures has been reviewed. In this review, a composite structure can be defined as damage tolerant if it has;

- Large window of slow predictable damage growth
- Large damage capability before catastrophic failure at limit load
- Robust quantitative models for damage growth
- Good detectability of damage
- Fail safe principles of construction – multiple load paths

Currently, there is no scientific or technical understanding for each of these five points for composite tapered scarf repairs. There is now a critical need to determine whether tapered scarf repairs can be used in existing damage tolerant sandwich structures without compromising the structural integrity of the vessel.

Residual strength assessments and the prediction of damage growth through fracture mechanics are critical components in the development of a damage tolerance methodology. Whilst a damage tolerance approach using current knowledge could be derived today for composite sandwich structures, there is no equivalent methodology for the damage tolerance assessment of composite repair schemes.

For this research programme it is therefore recommended that a damage tolerance methodology be generated for structural repair schemes to composite sandwich structures through the implementation of:

- Impact damage tolerance investigation of the tapered scarf repair
- Fracture and crack growth assessment within the parent laminate, the repair laminate and the repair-parent interface
- Strength based assessment of damaged structural repairs.

The repair of composite sandwich structures has been considered by examining the theoretical basis for the design of structural repairs (i.e. external patches, tapered scarf and stepped scarf joints), and through the examination of typical repair techniques employed by military and commercial organisations in the marine and aerospace communities. Key observations arising from the review of composite repair techniques are:

- The objective of a sandwich panel repair is to restore the damaged composite skins, replace the damaged core material and the bonding between the core and the skins, such that the mechanical and environmental resistance is returned to the required design levels.
- The experimental and analytical investigations that have been conducted over the last 20 years have identified generic guidelines for optimising the design of composite repairs to metallic and composite repairs. The optimisation of the design is usually specific to a particular material combination, or loading scenario, but these guidelines do help clarify the critical design parameters and thus help streamline any repair testing programme.
- The design of the repair is critical upon the loads which must be transferred; the region within which it must be accomplished; the geometry of the members to be joined; the environment within which the joint must operate; the weight/ cost efficiency of the joint; the reliability of the joint.
- Critical factors that govern the efficiency of the repair are the correct choice of the repair materials (fibres, resin system, fibre orientation and stacking sequence); load transfer across the joint (scarf angle, adhesive bonding, damage removal and surface preparation); and the protection the scarf edge with an external laminate (patch overlap length, patch stacking sequence, patch thickness, patch taper angle, patch edges feathered, adherent profiling)

Although the design guidelines identify all the critical elements of undertaking a tapered scarf repair, there is no consideration within the design for the inclusion of manufacturing or operational damage. A further alarming point concern the lack of acknowledgement that damage contained within repairs will have a significant bearing upon the efficiency of the tapered scarf repair. It is imperative that the efficiency of a damage structural repair is determined.

The prediction of operational performance of a composite repair depends upon the method of predicting the original fatigue life, the prediction of fatigue impact damage and the prediction of the interaction between the repair and the surrounding structure. The influence of low-velocity impact damage on the fatigue life and reliability of the

affected composite structure is still uncertain, even for a material for which the fatigue response in the undamaged state is well known. This problem is increasingly more difficult when the impact damage has occurred within a tapered interface (contained within a structural repair). Whether the damage will grow under the influence of an external load is uncertain and requires investigation.

Whilst considerable effort has been applied to the problem of repair design and repair manufacture, at present there is no scientific understanding or technical guidelines that can be used to assess the performance of a defective repair. There is a need to identify clear guidelines for the assessment of damaged structural repairs, i.e. a design tool is required to form the basis of an 'intelligent' interrogation system that skilled and unskilled workers can use to make an informed decision about a defects criticality.

The conclusions outlined above will provide the framework for the research undertaken within this thesis.

3 METHODOLOGY

The literature review in Chapter 2 highlighted three key areas that require further investigation:

1. The impact response of structural repair techniques contained within composite sandwich structures, i.e. how the damage forms within a repair, whether the damage is critical or what effect it has on the structural integrity.
2. The damage tolerance performance of the repair scheme is required, i.e. this will involve the characterisation of the impact damage tolerance, the initiation and propagation of critical defects, and the assessment of the residual strength.
3. The development of clear guidelines for the assessment of damaged structural repairs, i.e. a design tool is required to form the basis of an 'intelligent' interrogation system that skilled and unskilled workers can use to make an informed decision about a defects criticality.

The purpose of this chapter is to illustrate to the reader how these three key areas are drawn together to form a comprehensive methodology to address the question of 'Are structural repairs to composite sandwich structures damage tolerant?'

To evolve the methodology certain background information has been required, i.e.

1. What are the operational loads?
2. What is the environment?
3. What is the structure?
4. What is the repair geometry?
5. What are the material properties (strength, stiffness, toughness)?
6. How much energy is required to initiate critical defects?
7. What defects are critical?
8. Is defect location important?
9. What effect does the defect have on the repair/structure?
10. Will the defect grow under operational loading?
11. Can the rate and geometry of damage growth be predicted?

12. What residual strength reduction can be permitted?
13. How does the damage affect the static strength
14. How does the damage affect the fatigue life of the structure?

The interactions amongst these fundamental questions and how they are drawn together is critical in the development of this project's research methodology. Figure 3.1 helps to visualise these interactions.

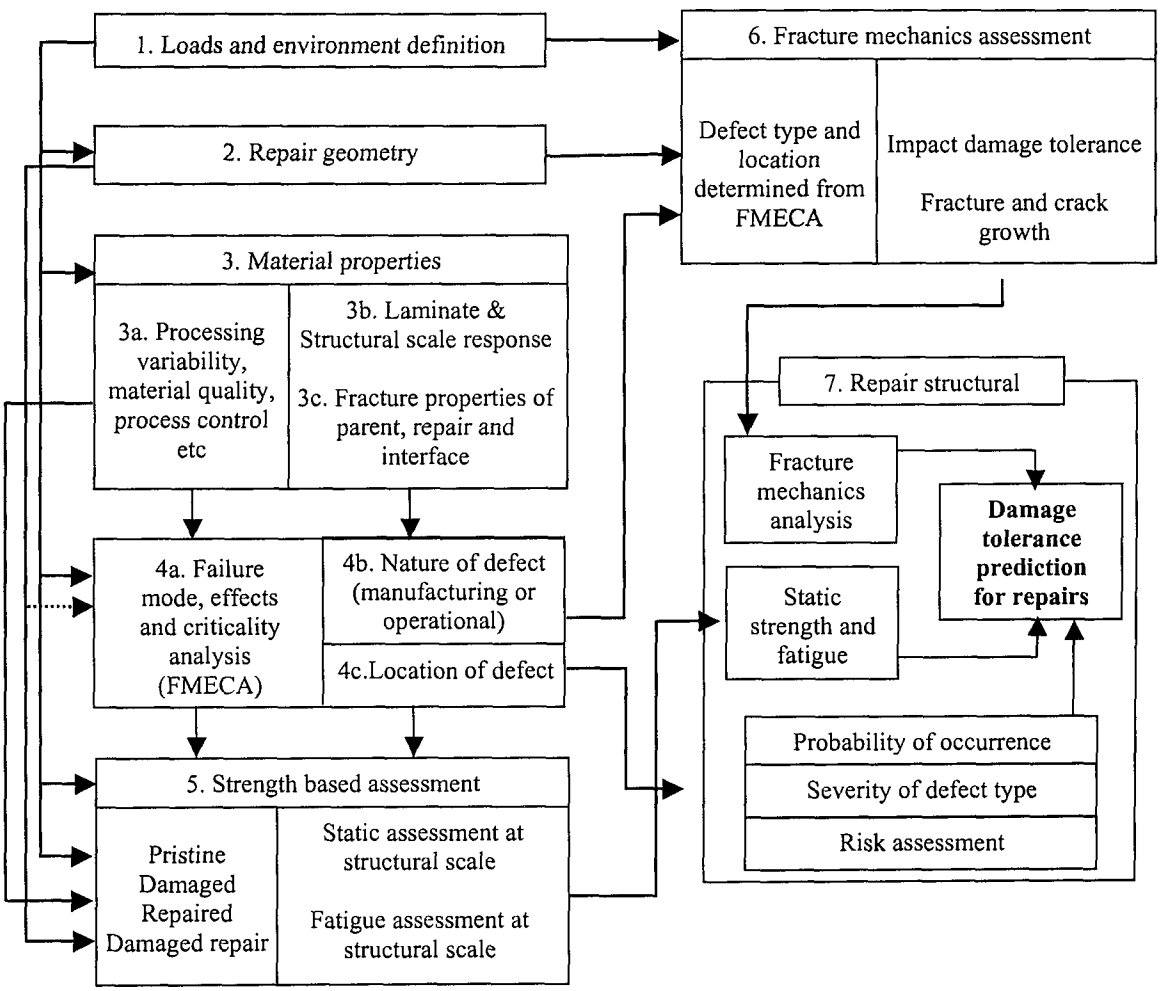

Figure 3.1: Design methodology for the damage tolerance assessment of repaired composite sandwich structures

Figure 3.1 illustrates the complex interaction between the composite structure, the defect type, the failure mode, the repair, and the damage tolerance assessment. The

design methodology within Figure 3.1 has been shown numerically and as a logic flowchart in Figure 3.2

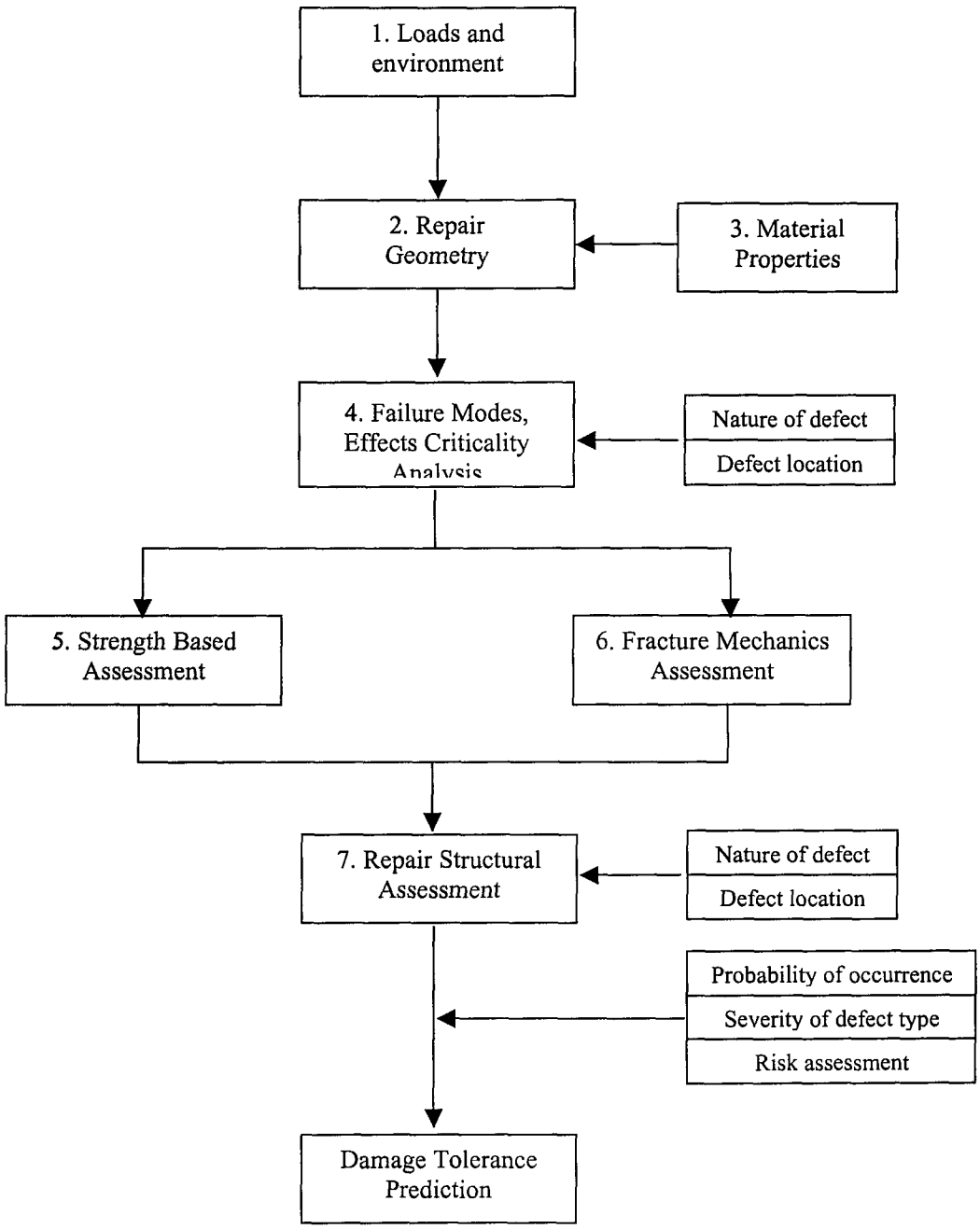

Figure 3.2: Step-by-step sequence for damage tolerance methodology

To correctly determine whether a tapered scarf repair is damage tolerant the flow chart in Figure 3.2 should be followed. The methodology outlined within this figure requires

a database of background knowledge about the environmental loads, the proposed repair geometry and key material properties before the strength based and fracture mechanics based assessments can be undertaken.

In the development of a damage tolerance methodology in this research project, some of the information in Figure 3.1 and 3.2 has been predefined (for example, the loads, the environment, the structure and the repair geometry) but the majority has had to be derived theoretically or experimentally. For example, the questions concerning defect criticality and location within structural repairs could potentially be a vast research topic requiring considerable resources. In this particular case, discussions with marine rescue craft operators and the application of a 'Failure Mode, Effects and Criticality Analysis' (FMECA) approach provided the structure and focus needed to concentrate the research in specific areas, i.e. the background information and the observations arising from the FMECA study determine the extent of the static and fatigue strength assessments and the damage tolerance assessment. The results from these studies determine the structural integrity of the damaged/defective repair and thus leading to a life prediction for a defect of known size. This information is presented in a series of tables and flowcharts and forms the basis of the 'intelligent' interrogation system that a skilled or unskilled worker can use to make an informed decision about a defects criticality.

4 METHODOLOGY IMPLEMENTATION

4.1 Introduction

The purpose of this chapter is to provide the background information to each of the critical steps within Figure 3.1, i.e.

- Loads and environment definition
- Repair geometry
- Material properties
- Failure mode, effects and criticality analysis (FMECA)
- Strength based assessment
- Fracture mechanics assessment
- Repair structural integrity

Each of these elements will be introduced and discussed in the remaining part of this chapter.

4.2 Loads and environment definition

Since the Royal National Lifeboat Institution sponsors this research programme the loads and environment definition are applicable to the operating environment experienced by the Severn and Trent class of all-weather class of lifeboat.

The sandwich structure within the lifeboat would typically be designed against a design pressure along the length of the hull of 620kPa (see [Hudson, 1993]). Whilst on operational duty, the individual sandwich panels (forming the hull) are likely to experience wave slamming (with accelerations up to 2-3g) and compression loading arising from equipment. In and around the waterline, wave slamming will induce mid-panel deflections of the order of 25mm. The sandwich structure is subjected to a vast range of harsh loading conditions, which it must survive throughout its operational life of 25 years. Whilst design calculations can be used to design the hull form for this environment, no such tool exists for the design of structural repairs.

4.3 Repair Geometry

The design of a structural repair to a composite sandwich structure can be based upon two elements. The first requirement is the design of the tapered scarf angle. The second requirement is for the design of the external overlaminate plies.

The design of the repair is critically dependent upon certain material properties. For example, Hart-Smith [Hart-Smith, 1973a] observed that the scarf angle is critically dependent upon the stiffness, strength and strain of the adherend, and the shear strength of the adhesive (see Table 2.9 for repair scarf angle design theory). Conversely, material properties for stiffness, strength and thickness of the adherend are needed whilst shear strength, shear modulus, Young's Modulus and thickness of the adhesive are required in the design of the overlaminate (see Table 2.9 for repair overlaminate design theory). Appendix A provides details concerning the material properties of these marine sandwich structures.

The research undertaken within this project was supported by the Royal National Lifeboat Institution and therefore the design of the structural repair schemes was dictated by proven marine practice. The RNLI have two different structural repair designs, namely a tapered scarf repair with a 3° angle and a tapered scarf repair with a 6° angle. The lay-up for a typical 20:1 scarf repair used in this research programme is indicated in Figure 4.1.

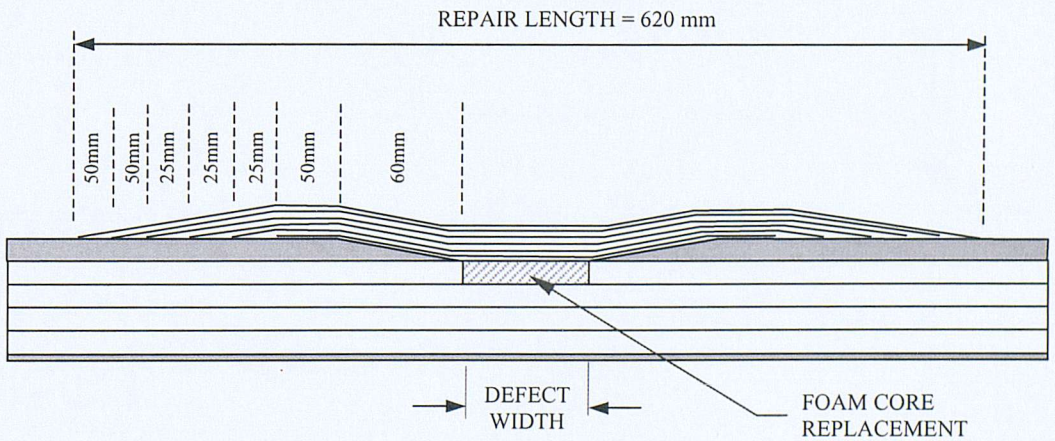

Figure 4.1: Overlap ply lengths in 3° tapered scarf repair

In the design of the repair schemes matching the parent and repair membrane stiffness has been shown to be important for scarf repairs hence the repair patches were made of five woven plies identical to the parent lay-up. Additional strengthening plies and an overlapping ply are used to enhance the strength of the repair and to protect the tip of the scarf from being damaged. Ideally repairs to the outer skin should be carried out using the original prepreg materials. However, in reality it has been very difficult to control and obtain the manufacture parameters needed for the processing of the prepreg materials. Instead the repair is manufactured with impregnation of dry reinforcement with a liquid epoxy resin. The repair is vacuum consolidated and cured according to the manufacturer's guidelines.

4.4 Material Properties and Manufacturing

In this research the sandwich structure comprises two skins of unequal thickness, a thicker outer skin and a thinner inner skin sandwiching a polymeric foam core. The outer skin is constructed of 3 layers of a quadriaxial E-glass/ Aramid fabric with a single light biaxial E-glass/ Aramid surface cloth. The matrix material is an epoxy resin, specifically Ampreg 75 manufactured by SP Systems, UK. The material is supplied as pre-impregnated lamina, which are stacked in sequence prior to consolidation with vacuum pressure and temperature. The core material is a closed-cell PVC core material manufactured by Divinycell with a density of 130kg/mm^2. Each layer is 25mm wide and four individual core sheets are bonded together to produce a core material with a total thickness of 100 mm. The inner skin is constructed of 2 layers of an E-glass quadriaxial fabric. The matrix material is an epoxy resin, specifically Ampreg 26 manufactured by SP Systems, UK. The composite laminate is manufactured by the hand lay-up process and then vacuum consolidated against the foam core. A schematic illustration of the four-point bend specimens indicating the fibre architecture is shown schematically in Figure 4.2.

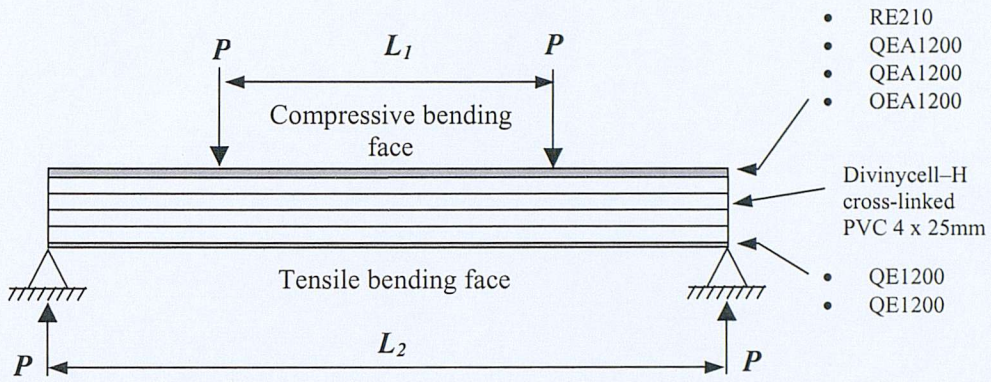

Figure 4.3: The four-point bend test specimen

The scarf repair is manufactured across the width of the beam, with an assumed defect width of 50mm in the centre. This width was selected to ensure that no stress or strain influences could exist between the two scarf tips and that the repair remained isolated from the loading points of the four-point bend test.

Throughout the thesis the composite sandwich beams are defined as:

1. Pristine beams, i.e. as received from the manufacturer.
2. Repair beams, i.e. sandwich beam containing a standard RNLI 3° tapered scarf repair, as detailed in Figure 4.1.
3. Damaged pristine beams, i.e. a pristine beam containing BVID.
4. Damaged repair beams, i.e. repair beam containing BVID.

Typical mechanical properties for the skins and core material are given in Table 4.1.

Material Type	Designation	Ply thickness	Nominal thickness	Fibre volume fraction	Young's modulus (E)	Tensile strength (σ_T)	Shear modulus (G)	Shear strength (τ)
Outer skin	3 * QEA 1200 and RE 210	1.07 mm	3.38mm	0.52	21.3 GPa	319 MPa	3.6 GPa	43 MPa
Inner Skin	2 * QE 1200	0.99 mm	1.98 mm	0.48	18.4 GPa	276 MPa	3.2 GPa	38 MPa
Foam core	Divinycell H130 (Density = 130kg/m^3)	-	100 mm	-	140 MPa	4.2 MPa	52 MPa	2.0 MPa

Lay-up code: E E-glass, A Aramid, R reinforced balanced 0/90 woven roving

Q balanced quadriaxial 0°/90°/+45°/-45° woven roving

No. e.g. 1200, weight of cloth per unit area (g/m^2)

Table 4.1: Summary of mechanical properties for face sheets and core material

Whilst the majority of the material properties have been defined by the material supplier or determined by the RNLI through independent testing, at present there is no baseline properties or understanding about the fracture toughness of E-glass/Kevlar fibre hybrid laminates reinforced with epoxy resins. To characterise the damage tolerance performance of a repaired composite sandwich structure this information will have to be derived.

4.5 Failure Mode, Effects and Criticality Analysis (FMECA)

4.5.1 Introduction

In the preceding two sections, the material configuration and repair geometry used within this research programme exactly matched the design specification of the project sponsor and therefore governed that element of the experimental approach.

The third element of the design methodology in Figure 3.1, namely the failure mode and effects criticality analysis (FMECA), permits the examination and definition of the

problem, i.e. within this research programme, the examination of whether a structural repair is damage tolerant or not.

The FMECA is an analysis which documents all probable failures within a system within specified ground rules, determines by failure mode analysis the effect of each failure on system operation, identifies single failure points, and ranks each failure according to a severity classification of failure effect. This procedure is the result of two steps, namely;

1. Failure mode and effects analysis (FMEA)
2. Criticality analysis (CA)

In general, the FMEA would be initiated within the design process. However, in this instance the FMEA will be used to:

1. Identify all potential failure modes within the repair zone and define their effect on the immediate function of the repair and the surrounding structure.
2. Evaluate each failure mode in terms of the worst potential consequences and assign a severity classification (ranging from catastrophic to minor).
3. Identify corrective design or other actions required to eliminate the failure or control the risk.

The severity classifications are used to provide a qualitative measure of the worst potential consequence resulting from design error or item failure. The severity classification used within this project follows the guidelines in MIL-STD-1629A 'Procedures for performing a failure mode, effects and criticality analysis', and are defined as:

- Category I – Catastrophic – A failure which may cause injury or death
- Category II – Critical – A failure which cause severe injury, major property damage, major system damage which will result in major downtime

- Category III – Marginal – A failure which may cause minor injury, minor property damage, or minor systems damage resulting in loss of system availability or degradation
- Category IV – Minor – A failure not serious enough to cause injury, property damage, or system damage, but which will result in unscheduled maintenance.

In this project the severity classification is concerned with the loss of structural capability. Although the loss of a composite repair would have significant consequences to the operational capability of a marine craft it is not expected that it would cause loss of life. This may not be the case for a composite repair to an aircraft structure.

The criticality assessment considers the probability of the defect occurrence (see Table 4.2) and its severity classification outlined above.

Description	Probability	Definition
Frequent	10^{-1}	Likely to occur frequently
Probable	10^{-2}	Likely to occur several times in the life of an item
Occasional	10^{-3}	Likely to occur sometime in the life of an item
Remote	10^{-4}	Unlikely to occur but possible
Improbable	10^{-5}	So unlikely that occurrence may not be experienced
Incredible	10^{-6}	Never occur within operational life

Table 4.2: Probability assessment [MIL-STD-1629A]

The combination of these variables will yield a risk assessment matrix that can be used to establish the probability and severity of manufacturing or operational defects. Table 4.3 contains the risk assessment with the lowest risk (indicated blue) starting in the bottom right hand corner, moving diagonally up to the top right hand corner where the risk (indicated red) is the highest.

Probability	Severity			
	Category I	Category II	Category III	Category IV
Frequent	A	A	A	B
Probable	A	A	B	C
Occasional	A	B	C	C
Remote	B	C	C	D
Improbable	C	C	D	D
Incredible	D	D	D	D

Table 4.3: Risk assessment matrix [MIL-STD-1629A]

The FMECA approach outlined above will be followed for the remaining part of this chapter.

4.5.2 Failure Mode analysis

In Chapter 2 the different types of defects that can occur in composite materials and bonded joints were introduced. Whilst local in nature, manufacturing defects such as surface contamination, debonded regions, and variations in bondline thickness can promote operational intralaminar (matrix cracking and fibre fracture) or interlaminar damage mechanism (delaminations) in the composite laminate, or they can attack the integrity of the repair patch-parent laminate interface or the skin-core bonded interface.

Table 2.2 identified that a range of critical defects exist, which could significantly impair the performance of composite sandwich structures. These include:

- Manufacturing flaws
  - Face/core interface debonds
  - Core/ core adhesive debonds
  - Face sheet laminate dry zones
- In-service damage
  - Impact damage to face sheets
  - Core crushing
  - Impact induced skin/core debonding

- Core shear cracks
- Fatigue and fracture at or near stress concentrations

The list above captures the typical damage modes experienced by composite sandwich structures. However, in this research, the question of damage location within the repair geometry has to be addressed.

In section 4.3, the repair geometry was first introduced. In the case of a tapered scarf repair used on foam core sandwich structures manufacturing or operational defects could occur in the following locations:

1. At the interface of the replacement foam core and the original foam core
2. At the interface between the replacement foam core and the repair
3. Along the tapered interface between the repair plies and the parent structure
4. Along the interface between the repair plies and the parent structure
5. In the repair plies
6. In the parent laminate plies
7. End of the overlaminate
8. External tip of scarf repair taper
9. Internal tip of scarf repair taper

The location of the defect is very important in understanding its influence on the failure mode of the repair and the sandwich structure. For example, a small debond or variation of bondline thickness located between the replacement foam core and the original foam core may not propagate under fatigue loading and therefore not influence the global performance of the repaired structure. However, a small debond or variation of bondline thickness at the very end of the overlaminate strengthening plies may induce peel stresses at the end of the repair that are above and beyond the expected design resulting in premature failure of the repair. Whether a delamination will propagate along the tapered interface in preference to an internal repair interface is uncertain but the fact that either could occur should raise some concern about the effect it will have on the

compressive and shear strength properties of the structure. Any reduction in either of these properties below the design limit could result in a catastrophic failure.

4.5.3 Effects analysis

The failure modes contained within the composite repair have now been identified. In this section, the effects of these failure modes upon the design criteria used for tapered structural repair will be considered. The design criteria were first introduced in Table 2.9 and are repeated below:

1. Stiffness and strength replacement
2. Stability
3. Durability
4. Restoration of functional requirements

Depending upon the severity of the processing or operational defects and its location within the repair scheme, it could significantly alter one or all of the design criteria.

4.5.4 Criticality Analysis

The criticality analysis is based upon the information determined in the 'Failure Mode' Analysis and the 'Effects' Analysis. The criticality assessment considers the influence of the type of defect and the defects location upon the design criteria, i.e. what type of defect will have the greatest influence upon the design performance of the tapered scarf repair.

The Criticality Analysis conducted for this research project is presented in Table 4.4. However, before proceeding to discuss the results, the assumptions used within the formulation of the table should be mentioned and discussed.

Firstly, during the development of Table 4.4 RNLI personnel where consulted about the design criteria and the influence certain types of defects have on the structure of the RNLI all-weather class of lifeboat. For example, to date, the RNLI have not observed any skin-core debonding or core shear cracks. In the former case, this is in part due to

the adhesive bondline used between the skin and the core, and in the latter case it is because (1) the sandwich structure is designed to take all the load through the outer skin, and (2) the 100mm thick foam core is bonded together (with a structural adhesive) in sections of 25mm. Also, the outer skin is manufactured from composite pre-impregnated material thereby eliminating the problem of laminate dry zones. It is due to these design details that the results in Table 4.4 are only applicable to rescue craft manufactured and operated by the RNLI, i.e. the Criticality Analysis in Table 4.4 would have to be undertaken again for any other type of sandwich structure.

Secondly, the nature of the impact damage has been assumed to be non-penetrating, i.e. if the damage had penetrated the outer skin all the design criteria would be compromised and therefore a full structural repair would be required. In this research programme, the question of manufacturing defects or impact damage to an existing tapered scarf repair is being considered.

Thirdly, the probability and severity rating has to consider the extreme operational and loading conditions experienced by RNLI rescue craft. In this context the Criticality Analysis detailed in Table 4.4 is overly conservative, i.e. a greater probability rating coupled with a higher severity rating has been used to reflect the extreme loading conditions experienced by the vessel when undertaking a rescue in bad seas. In reality, this loading may only last 1 to 10 hours (depending upon station location) over the course of a year, for the operational life of the vessel (typically 25 years). In terms of developing a damage tolerance approach for tapered scarf repairs to sandwich structures, the criticality analysis must reflect the situation when undetected damage will be subjected to these extreme loading patterns rather than the possibility that operational damage which actually occur during these periods.

It is based upon these assumptions that the assessment in Table 4.4 has been made.

Defect type		Defect location	Design Criteria											
			Stiffness and strength replacement			Stability (i.e. compressive performance)			Durability (fatigue; crack growth)			Restoration of functional requirements		
			Probability	*Severity*	*Risk*	*Probability*	*Severity*	*Risk*	*Probability*	*Severity*	*Risk*	*Probability*	*Severity*	*Risk*
Manufacturing flaws	Face/core interface debonds	Interface between the replacement foam core & repair	Improbable	III	D	Improbable	III	D	Improbable	III	D	Improbable	IV	D
	Core/ core adhesive debonds	Interface of the replacement and original foam core	Remote	IV	D	Remote	IV	D	Remote	IV	D	Remote	IV	D
	Face sheet laminate dry zones	Tapered interface between the repair plies and parent	Remote	III	C	Remote	III	C	Remote	III	C	Remote	III	C
		Horizontal interface between the repair plies and parent	Remote	II	C	Remote	II	C	Remote	II	C	Remote	II	C
		In the repair laminate	Remote	II	C	Remote	II	C	Remote	II	C	Remote	II	C
		In the parent laminate	Improbable	II	C	Improbable	II	C	Improbable	II	C	Improbable	II	C
In-service damage	Impact damage to face sheets	Interface of the replacement and original foam core	Improbable	IV	D	Improbable	IV	D	Improbable	IV	D	Improbable	IV	D
		Interface between the replacement core & repair	Remote	IV	D	Remote	IV	D	Remote	IV	D	Remote	IV	D
		Tapered interface between the repair plies and parent	Occasional	I – II	A - B	Occasional	I - II	A - B	Occasional	I - II	A - B	Occasional	I - II	A - B
		Horizontal interface between the repair plies and parent	Occasional	I – II	A - B	Occasional	I - II	A - B	Occasional	I - II	A - B	Occasional	I - II	A - B
		In the repair laminate	Occasional	I – II	A - B	Occasional	I - II	A - B	Occasional	I - II	A - B	Occasional	I - II	A - B
		In the parent laminate	Occasional	II - III	B - C	Occasional	II - III	B - C	Occasional	II - III	B - C	Occasional	II - III	B - C

	Core crushing	Interface of the replacement and the original foam core	Remote	IV	D	Remote	IV	D	Remote	IV	D	Remote	IV	D
		Interface between the replacement core & repair	Occasional	IV	C	Occasional	IV	C	Occasional	IV	C	Occasional	IV	C
	Impact induced skin/core debonding	Interface between the replacement core & repair	Improbable	II	C	Improbable	II	C	Improbable	II	C	Improbable	II	C
	Core shear cracks	Interface of the replacement and original foam core	Improbable	III	D	Improbable	II	C	Improbable	II	C	Improbable	III	D
	Fatigue and fracture at or near stress concentrations	End of overlaminate	Improbable	III	D	Improbable	III	D	Improbable	II	C	Improbable	II	C
		External edge of repair taper	Incredible	III	D	Incredible	III	D	Incredible	IV	D	Incredible	IV	D
		Internal edge of repair taper	Occasional	II	B	Occasional	II	B	Occasional	II	B	Occasional	IV	C

Table 4.4: Hazard severity and probability levels for manufacturing and operational defects on the design criteria of a tapered scarf repair to a marine composite sandwich structure

Table 4.4 details the hazard severity and probability levels for manufacturing defects and operational damage on the repair design criteria of a tapered scarf repair to composite marine sandwich structures used in the manufacture of rescue craft. To help visualise the critical hazards a colour-coding scheme originally employed in Table 4.3 has been used (green = low risk, blue = low to medium risk, orange = medium to high risk, red = high risk).

The critical hazards identified within the Criticality Analysis is as follows:

1. High risk
   - Impact damage to the tapered interface between the repair plies and parent
   - Impact damage to the horizontal interface between the repair plies and parent
   - Impact damage to the repair laminate
2. Medium to high risk
   - Impact damage to the parent laminate
   - Fatigue and fracture at or near the internal edge of a repair taper

The method for the characterisation of these hazards is discussed below.

Any form of impact damage to the tapered interface between the repair plies and parent is considered a high risk because it is likely to compromise the structural performance of the repair due to the reduction of available repair area to transmit the shear loads. In the work by Hart-Smith [Hart-Smith, 1973a] he observed that a certain minimum scarf taper is required to ensure the repair joint has superior mechanical properties to the parent laminate.

Impact damage to the horizontal interface between the repair plies and parent is perceived a high risk because it could open the leading edge of the repair and permit the operational loads and the environment to 'peel' the repair from the parent structure. In Table 4.4 this has been given an 'Occasional' probability rating with a severity rating of 'category 1 to II' (Catastrophic to Critical). The justification of the probability rating is based upon the observation that in marine craft impact damage during operational

service tends to occur in and around the waterline in specific locations around the vessel. Since the damage tends to be location specific there is a risk that a second impact event could occur on, or near to, the repair, i.e. it is likely to occur sometime in the life of the vessel. The justification for the severity rating of 'category I to II' concerns the risk that a damaged horizontal edge to the repair could be torn from the parent laminate thereby exposing the internal tapered scarf profile, or worst the skin-core interface. If either of this two failure modes were to occur as a result of the initial impact damage to the repair major property damage would occur which, at the very least, would result in major downtime (to undertake the repair) or a failure of the vessel, which may cause injury or death. In this context, there is considerable uncertainty and risk associated with the performance of an impact damaged structural repair. A key aim of this project is to define this risk.

Impact damage to the repair laminate is perceived as a high risk because the hand lay-up repair scheme may be less damage tolerant that the original parent prepreg laminate due to the inclusion of manufacturing defects and poor control of the adhesive bondline. It is therefore possible that the damaged repair scheme could failure prematurely.

Impact damage to the parent laminate is perceived as a medium-to-high risk because impact damage to the parent laminate surrounding the repair scheme could result in load transfer to the repair scheme resulting in premature failure via delamination growth through the parent laminate across the tapered repair interface and in to the repair laminate.

A second medium-to-high critical hazard concerns fatigue and fracture damage at or near the internal edge of repair taper. In tapered repair schemes a protective overlaminate is used to minimise the stress concentrations at the scarf tip. On the external edge of the scarf taper this is undertaken as standard but not on the internal edge, which rests against the foam core. Some concern exists about the performance of this internal scarf tip to operational loads, and whether it could initiate core shear cracks at this location.

The preceding discussion highlights the current uncertainty about the performance of a structural repair when it is damaged or containing internal stress concentrations. This knowledge will now be used in conjunction with load and environment definition and the results from the FMECA analysis to help design and define the experimental approach for the damage tolerance assessment of repaired sandwich structures. This methodology permits the determination and characterisation of the exact risk that these critical defects have. The precise implementation of these two approaches will be defined in the following sections.

4.6 Strength Based Assessment

4.6.1 Introduction

The methodology detailed in Figure 3.1 in Chapter 3 explained why a Strength Based Assessment is recommended for a damage tolerance assessment. The critical hazards identified in Table 4.4 (and discussed in Table 4.5) define the extent of the Strength Based assessment. The aim of this section is to draw together these ideals and define the methodology that will be implemented.

4.6.2 Implementation method for Strength Based Assessment

The key aims of the strength-based assessment are to capture damage tolerance performance of the high risk and medium-to-high risk defects identified in Table 4.4. To achieve this requirement a comparative assessment between pristine four-point bend beams and damaged four-point bend beams plus repaired four-point bend beams and damaged repair four-point bend beams must be undertaken. This has been illustrated in Figure 4.3.

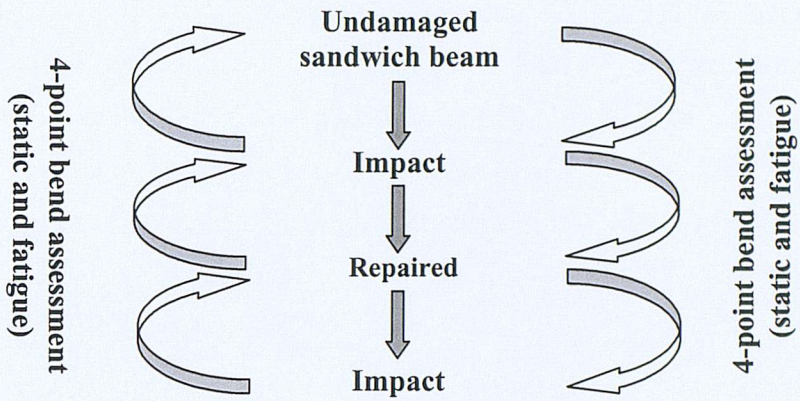

Figure 4.3: Strength based assessment

The precise mechanics of undertaking this assessment will be discussed in the following sections.

4.6.3 Flexural tests

The strength-based assessment could be undertaken in a variety of loading conditions, i.e. tension, compression, or flexure. In this research programme it was decided to employ a standard flexural test method, i.e. the four-point bend test. Two primary reasons exist for this selection. The first concerns the RNLI in-service observations of mid-panel deflection arising from wave slamming, and the second concerns the previous RNLI research conducted by [Clark, 1997] who also examined the static and fatigue of composite sandwich beams using 10-point flexural tests. By adopting a similar test method, a direct comparison between the original fatigue life obtained by [Clark, 1997] for undamaged beams could be compared with the fatigue life of repaired beams containing impact induced damage. This approach will also yield the fatigue performance for a sandwich beam representative of a structural panel experiencing mid-span deflection through wave slamming.

The static flexural bending tests were conducted to the ASTM C393-62 (1989) "Standard Test Method for Flexural Properties of Flat Sandwich Constructions" with the loading points located at two quarter-span points. The test method permits the

calculation of the sandwich beam flexural stiffness, the core shear strength and shear modulus, or the facings compressive and tensile strengths.

The specimen dimensions evolved from the recommendations within the test standard and were as follows; the total length of the specimens were 1800 mm, span length 1200 mm, width 200 mm, thickness of the foam core 100 mm and the thickness of the laminate before repair 5.4 mm.

4.6.4 Impact tests

For the damaged assessment of the beams and the repaired beams, impact damage was introduced by a purpose built impact-testing machine. A simple vertical drop weight frame with the option to vary the impact energy by changing the drop height, the weight of impactor, and the size of impactor was devised and used to conduct the low velocity impact tests. The design was very similar to the rig used by [Mines *et al*, 1994]. The frame was simple enough to design, allowing for the sandwich beam to fit underneath the impactor and be tall enough to be supported by an existing steel frame housed in the Civil Engineering Department of the University of Southampton. The design permitted the sandwich beams to be moved in a longitudinal direction so that several separate impacts could be dropped on the same beam but at different intervals along the length of the beam.

The sandwich beams were placed directly onto the concrete floor. A steel plate with a width of 50mm with chamfered 10mm edges and a length of 250mm (larger than the width of the specimens) was attached to a free falling steel body (see Figure 4.4).

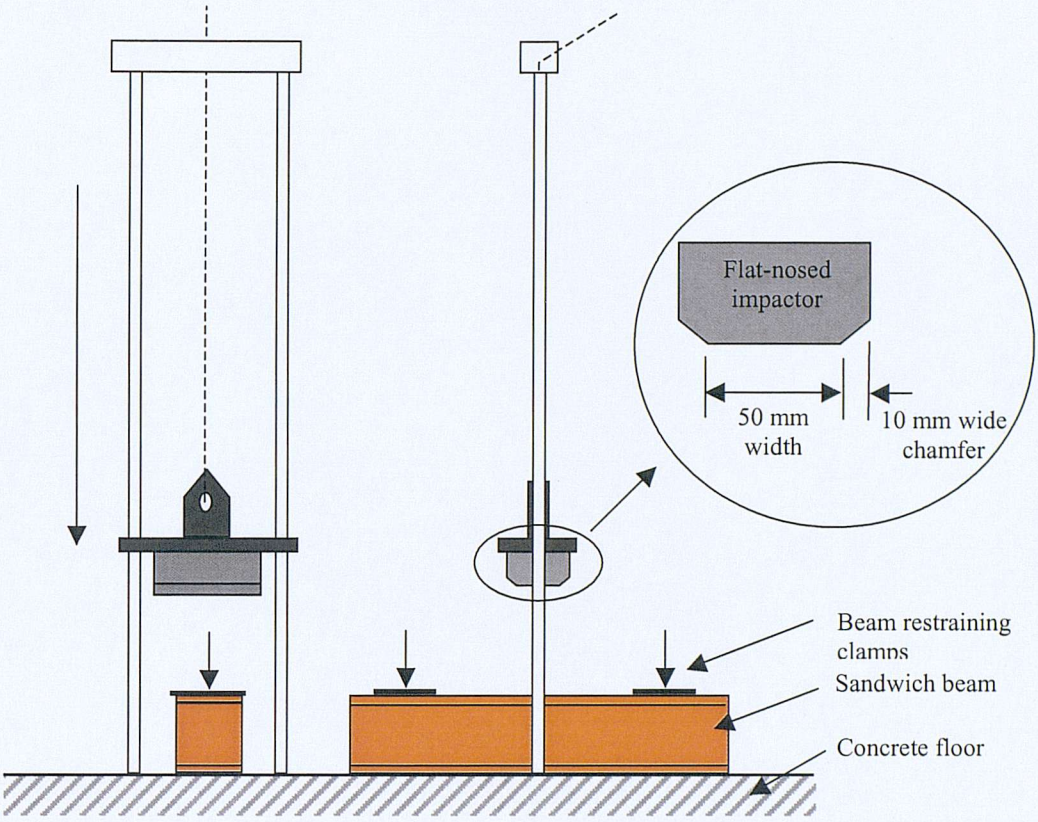

Figure 4.4: Schematic illustration of drop-weight impact testing rig

The impactor profile was selected to ensure that it did not penetrate the outer skin laminate but rather to produce internal damage within the repair scheme and the tapered interface, i.e. the impactor was selected to form barely visible impact damage. The total impact mass could be varied from 10kg to 60kg in steps of 5kg.

The impact energy was determined using the following equation from Gere and Timoshenko [Gere and Timoshenko, 1993] for the determination of Kinetic Energy (KE):

$$KE = \frac{1}{2} M v^2 \tag{4.1}$$

where

M is the mass, and

V is the velocity of the falling mass determined by:

$$v = \sqrt{2gh} \tag{4.2}$$

where

g is the acceleration of gravity (9.81 m/s^2)

h is the height dropped by the mass

Drop heights up to 2m could be used thus varying the impact energy from 98J to 1170J. The impact velocities were estimated assuming ideal free fall.

It was observed by [Mines *et al*, 1994] that drop weight impact tests could take two forms, namely sub-critical and integrity studies. The authors noted that in the former, the amount of energy due to impact is critical and so a single bounce test is required, i.e. the tup is captured after impact. In the case of integrity studies, [Mines *et al*, 1994] observed that a large range of impact energies tends to be studied and the post-critical behaviour of the structure is of importance. Hence in this context, a multiple bounce test could be accepted, if it is assumed that the majority of the damage occurs on the first bounce. To determine whether the majority of the impact damage was generated within the first impact event and not the subsequent rebound impacts a number of critical points have to be considered.

Firstly the rebound height and number of impacts were recorded for the maximum energy impact tests, i.e. 1270J (which equates to 64.7kg from 2m). In these experiments it was observed that an initial 300mm to 400mm rebound height occurred for a mass of 64.7kg. A further two rebounds occurred before the mass came to rest upon the beam. The damage site only indicated foam core crushing, laminate skin delamination and matrix cracking but no fibre fracture or surface penetration.

To gauge whether the first rebound has sufficient energy to introduce any additional damage (in the already damaged structure), two points should be considered, namely (1) the magnitude of the impact energy and whether this is greater than the threshold to initiate damage, and (2) whether this energy level would be sufficient to propagate a delamination in mode II.

The new rebound impact energy was calculated to be 507J, i.e. 64.7kg from 400mm assuming ideal free fall. This rebound energy maximum was compared to the threshold energy required for damage initiation. In the impact experimental work in Chapter 5 it was observed that an impact threshold energy of 635J existed for the pristine beams, whilst an impact threshold energy of 780J existed at impact location 1 on the tapered scarf repairs. Since both of these threshold energies are greater than the rebound energy level it is believed that no further damage has been introduced after the initial impact event.

The growth of delamination damage within a laminate skin of a sandwich structure is governed by the mode II fracture toughness [Olsson, 2002]. After the initial impact event a delamination has already propagate by mode II to a set distance related to the magnitude of the energy. For the existing delamination damage to propagate under a rebound event it must overcome the mode II fracture toughness initiation value. In Chapter 5 it was observed that a G_{IIC} initiation threshold of 3311±207 J/mm^2 for the parent laminate, 3956±487 J/mm^2 for the repair laminate, and 3224±307 J/mm^2 for the repair-parent interface was required to initiate delamination onset. This result indicates that the rebound event requires over 3200 J/mm^2 to initiate a crack at a new ply interface under the impact location or to extend the existing delamination, which coincidently is no longer directly below the impact site therefore requiring even more energy to propagate it.

The two preceding paragraphs have shown the impact threshold energy and the mode II fracture toughness required to initiate and propagate a crack is greater than the rebound energy available in the system. Therefore, it is the author's believe that the damage observed post impact is only attributed to the initial impact energy and not influenced by any rebound event.

The impact locations were selected to coincide with the centreline of the 'pristine' sandwich beams. On the 20:1 tapered repair scheme the impact locations were selected to coincide with the end of the overlaminate and the start of the scarf taper. The damage to the sandwich beams was recorded by measurement of the indentation depth and extent of damage width beyond the edge of the impactor.

A further investigation was undertaken using a stereoscopic photographic NDE technique that can determine the strain lines occurring in the core material after an impact event. This technique was first proposed by Sir Charles Wheatstone in 1938 [Wheatstone, 1999] where he described the theory of stereoscopic photography to the Royal Society. When viewed through the stereoscope the impression of depth would be recreated. The advantage of the arrangement was that one could cope with large pictures, which is why the principle is still in use today when viewing Xray stereoscopic pictures.

In the generation of contour maps, two photographs are taken of the same landscape with a known separation distance. These photographs are then viewed in 'stereo' using the equipment shown in Figure 4.5. Each photo is viewed by eye down each lens. Although each eye is viewing a different photo, the brain overlays both pictures so that a single picture is observed. This overlaid picture indicates the changes that have occurred since the first and second photography. In the context of developing a map, the brain identifies the changes by seeing raised or lowered contour regions of the picture. The gradient of the raised and lowered areas show the severity of the landscape.

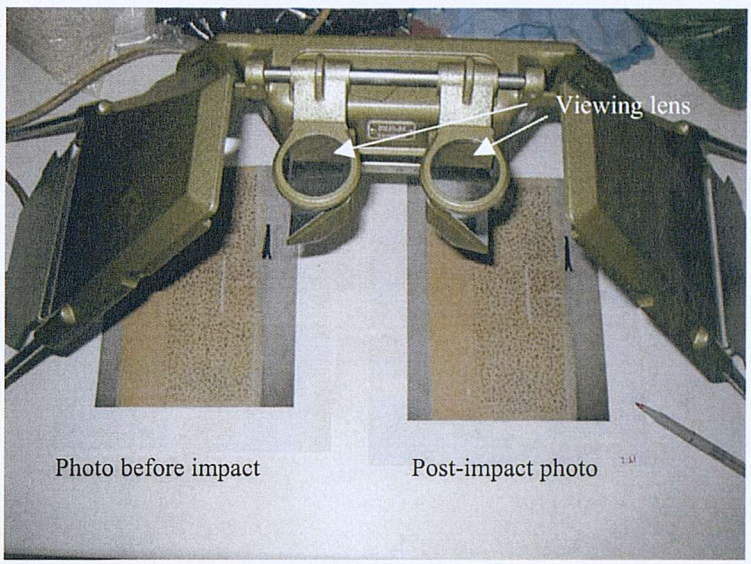

Figure 4.5: Stereoscopic photographic NDE - experimental set-up with before and after photographs of BVID in a tapered scarf repair scheme

In the context of these experiments, the stereoscopic photographic NDE technique was used to assess the behaviour of the foam core after an impact event. The relative movement of the reference grid or dots between the first and second photography indicate the deformation of the core material. In the 'overlaid' picture distinctive raised and lowered regions were observed. These regions show the areas that have relative movement between the two photographs, the gradient of the raised and lowered areas show the severity of the strain.

4.7 Fracture Mechanics Assessment

4.7.1 Introduction

The damage tolerance conclusions arising from the FMECA analysis identified four critical locations where a delamination could potentially initiate failure of the repair scheme. The locations identified where:

1. Parent laminate (medium to high risk)
2. Repair laminate (high risk)
3. Horizontal interface between the repair and the parent laminate (high risk)

4. Tapered face between the repair and the parent laminate (high risk)

The four different locations identified within the FMECA have been illustrated in Figure 4.6.

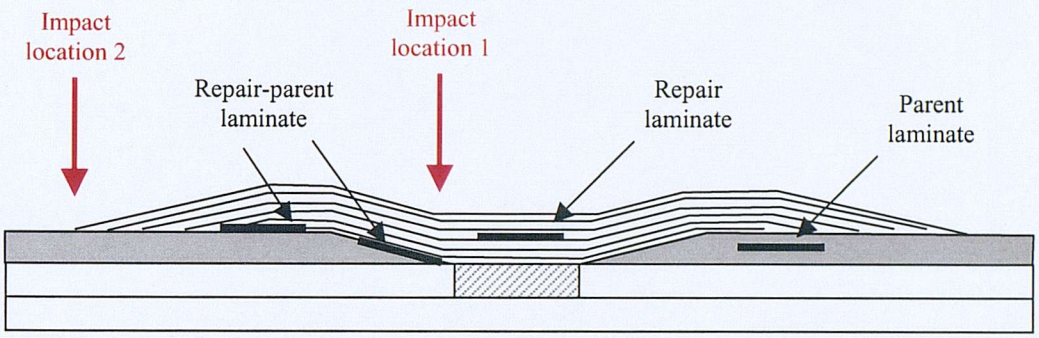

Figure 4.6: Schematic illustration of the four critical delaminate locations identified within the FMECA assessment

Figure 4.6 provides a schematic illustration of the possible damage locations. In a real marine sandwich structure when a repair is subjected to operational loading (bending, rotation, compression, or wave slamming) the crack tip could experience pure mode I crack propagation or pure mode II crack propagation, or any component between these two extremes. Due to the uncertain nature of the load path it was decided to follow a similar approach to [Olsson *et al*, 1996], who recommended that the application of fracture mechanics to delaminations in fibre composites requires the characterisation of the interlaminar toughness of angle ply interfaces in both pure and mixed mode conditions.

4.7.2 Implementation method for Fracture Mechanics Assessment

The fracture mechanics assessment and the test methods employed in this research have been defined in the test matrix illustrated in Table 4.5.

Fracture mechanics test	Test Method	Parent laminate	Repair laminate	Repair-parent interface
Pure mode I	DCB	√	√	√
75% Mode I / 25% Mode II	MMB	√	-	-
50% Mode I / 50% Mode II	MMB	√	√	√
25% Mode I / 75% Mode II	MMB	√	-	-
Pure mode II	ELS	√	√	√

Table 4.5: Fracture mechanics test matrix

At an earlier stage within the research project it was realised that trying to manufacture fracture mechanics specimens representative of the tapered repair-parent interface was not possible. A number of attempts were made to manufacture a 75mm thick panel that could be cut at 3° and 6° to produce the taper before a hand laid-up repair was applied to the machined side. Apart from the difficulty of curing such a large composite block, considerable problems were experienced in machining individual samples with the correct taper angle. During these trials it was also noted that when an E-glass/Kevlar – epoxy matrix ply is cut, significant Kevlar fibre brooming occurs at the cut face.

Whilst complicating the cutting process, the brooming aspect of the Kevlar fibres would also provide some form of mechanical locking across the interface between the parent laminate and the repair patch, in addition to the chemical bonding from the repair resin. This additional toughening mechanism, plus the change in geometry affecting the stress-field at the tapered interface, is likely to ensure that it's toughness is greater than the toughness of the horizontal interface between the repair and the parent laminate. Providing this assumption holds, and the fracture toughness of the horizontal repair-parent interface is superior to both the repair laminate and the parent laminate then damage is unlikely to propagate at the tapered interface. This point will have to be examined carefully within the fracture mechanics assessment.

4.7.3 Mode I fracture mechanics assessment

To undertake the pure mode I ratios, the double cantilever beam (DCB) test method was employed. The interlaminar fracture of composite materials for mode I loading (see Figure 4.7) can be determined by ASTM Standard D5528-94a.

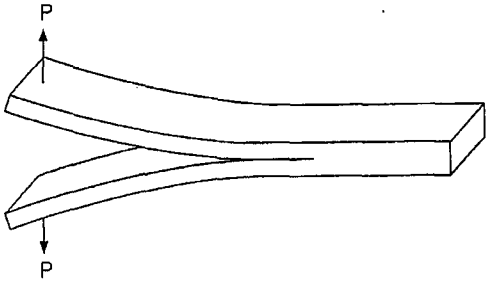

Figure 4.7: Mode I DCB test configuration

The typical DCB specimen as specified in ASTM standard D5528-94a is typically 150mm long, 25mm wide and 3mm thick. However, these dimensions were recommended for typical aerospace laminates, i.e. thin, unidirectional carbon fibre laminates manufactured by the autoclave-processing route. In reality, some deviation away from these dimensions will be required for laminates with different stacking fibre orientation and laminates manufactured by alternative processing routes.

The design of the fracture toughness specimens was complicated since three different test methods were being considered. During the initial phase of the programme it was decided to design the specimen so that it could meet the maximum width requirement of the MMB test and have sufficient length to be used in all three tests. The specimen dimensions are detailed in Figure 4.8.

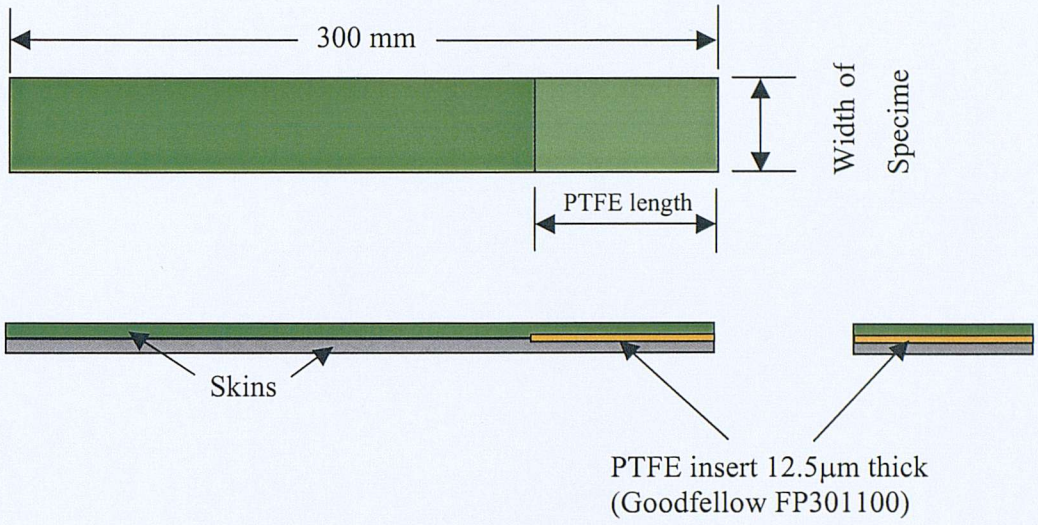

Note: Skin thickness 8mm (4mm each sub-laminate)

Figure 4.8: Fracture mechanics test specimen

Due to the quadriaxial fibre architecture, and the possibility that processing defects may occur within the specimen's cross-section, it was decided to use a specimen width of 35mm and a length of 250 mm.

The test laminates contained a symmetric stacking arrangement of eight plies. Between the fourth and the fifth ply there was a nonadhesive insert that served as an initiation site for the delamination. It was produced by placing a film at the panel mid-plane prior to processing. The DCB specimens were cut from multidirectional panels with a diamond impregnated saw blade.

The length of all the specimens was around 250 mm but the length of the inserted nonadhesive film varied between the different materials. The specimens of both fibre reinforced composite materials were about 35 mm in width. But their thickness differed. The glass/kevlar/epoxy laminates were about 8.5 mm in thickness and the glass/epoxy ones about 7.3 mm. The exact dimensions of the specimens are given in Appendix B. For mode I static testing a total of 20 specimens were tested.

The load was introduced through piano hinges. There is also the possibility of using end blocks with a pin but the piano hinges were chosen because they were more convenient for placing the specimen in the test machine (see Figure 4.9).

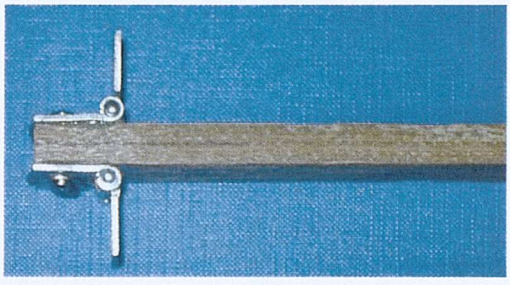

Figure 4.9: Location of piano hinges on DCB specimen

The piano hinges were bonded to the composite laminates with Araldite 2015 adhesive. Prior to bonding the surface of the specimens and the surface of the hinges were sanded and also cleaned with a volatile solvent. In addition, two screws were used on each side of the specimen to join the hinges to the specimen. These helped to distribute the applied load more uniformly by pre-stressing the specimen and the hinges. Mode I testing was carried out on an Instron testing machine.

After measuring the dimensions of the laminates, the polished edge of each specimen was coated with white correction fluid, which helped with the monitoring of the crack propagation when the load was applied. From the inner end of the inserted film marks were drawn at millimetre intervals for a distance of 10 mm and then at 5 mm intervals for the next 40 mm. Before loading, the plates of the hinges had to be fixed into the grips of the loading machine.

Load was then applied continuously at a displacement control rate of 2 mm per minute until the crack reached the 10 mm mark. After this point the crosshead speed was increased to 5 mm per minute. Figure 4.10 shows the testing set-up with the piano hinges applying the load to the specimen.

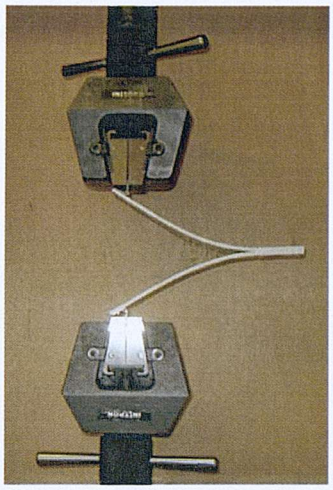

Figure 4.10: DCB loading arrangement

A chart recorder was used to draw the load versus displacement plot throughout the entire testing until the delamination length reached the 50 mm mark. With the help of an optical microscope the delamination length and, thus, the crack propagation were investigated by recording the load and the displacement at each mark. At the end of the test each specimen was loaded to complete failure. The mode I DCB tests were performed at room temperature.

4.7.4 Mode II fracture mechanics assessment

The inclusion of the Mode II fracture toughness tests in this research programme stems from the work of [Olsson, 2002]. In his work, the author stated that the development of internal delamination within the outer skin of a composite sandwich structure is controlled by the pure mode II performance of the laminate.

The pure mode II tests were undertaken by the end loaded split test (ELS), which promotes stable crack growth within the composite specimen. The loading arrangement is shown in Figure 4.11.

A total of 20 specimens have been investigated. The materials used were the same as in mode I testing. The multi-directional stacked laminates contained a mid-plane non-adhesive insert that served as an initiation site for the pre-cracking. The length of the specimens was 250 mm, the width was 35 mm. The thickness varied between 7.2 mm

for E-Glass and 8.5 mm for all Kevlar materials. An overview of the exact dimensions of the specimens is given in Appendix A.

Figure 4.10: Loading configuration of the ELS test method

In this research, stable crack growth was needed to evaluate the influence of the fibre architecture. To achieve this a specimen 35mm wide and 250mm long was used. The tests were conducted to test standard 'Mode II Determination Test: ELS – Specimen (99-06-03)'. The standard details the determination of the delamination resistance of a composite laminate. Stable delamination growth from a starter film or from a Mode I or Mode II precrack can be monitored. Data reduction yields the critical energy release rate G_{IIc} for initiation and propagation of a mode II delamination.

A mode I precrack 25 mm in length was introduced to the specimens to sharpen the initial crack created by the insert film and to provide an initial crack length to beam length ratio of at least 0.55 [Blackman, 2004], at which stable crack growth was expected. Furthermore, mode II testing without precracking would lead to incorrectly high values of G_{IIc} at the end of the insert due to the resin-rich region [Wang *et al*, 1995].

For mode II testing the same Instron machine was used as in mode I testing. In the ELS test a double cantilever beam is loaded by a transverse force at the split end, while the other end of the beam is clamped. This fixture has to be designed and manufactured to permit movement in the horizontal direction.

The load was applied through a roller 10 mm in diameter and a small roller 1.5 mm in diameter was placed between the two arms of the Double Cantilever Beam to reduce friction.

As for mode I testing one edge of the specimens was polished with sandpaper and coated with white correction fluid. Then, the width and the thickness of all specimens were measured at three positions along the length. The same points of measurement as in mode I testing were used.

The mode I pre-crack, 25 mm in length, was created by mode I loading applied with the help of hinges that were clamped to the grips of the apparatus (see Fig. 4.2). To ease the procedure the hinges were only fixed to the beams by screws and not with adhesive. While mode I loading was being carried out the exact end of the insert and finally, the end of the pre-crack were marked. From there onwards marks were drawn each mm for the first 5 mm and then each 2.5 mm for the next 25 mm giving a total mode II crack length of 30 mm. The specimens were clamped 20 mm beyond the last mode II mark (30 mm) as proposed by Corleto and Bradley [Corleto and Bradley, 1989].

The load was applied continuously under displacement control at a crosshead speed of 5 mm per minute until the delamination reached the 50 mm mark beyond the end of the insert foil. The chart recorder recorded a load versus displacement plot throughout the entire testing. With the help of a movable lamp delamination length and thus the crack propagation was detected and recorded with the corresponding load at each mark. After that all specimens were loaded in mode I to complete failure to be able to see the cracked surface. The mode II End Loaded Split tests were performed at room temperature.

4.7.5 Mixed-Mode fracture mechanics assessment

The decision to use a mixed mode bending test stems from two reasons; (1) the complex nature of the composite structure and the operational loads may impart a mixed-mode loading condition, and (2) the delamination damage within the composite repair will be influenced by the repair geometry which will impart mixed-mode crack growth as the delamination propagates along the tapered interface.

The mixed mode bending (MMB) test method was selected in preference to alternative methods because it is based upon the mode I DCB test (which permits continuity between the two test methods) and it can undertake a range of mixed-mode testing ratios with relatively simple adjustments to the test method (which permits standardisation across the test method).

The MMB test method is defined with ASTM D6671-01 test standard and it describes the determination of interlaminar fracture toughness, G_c, of composite materials at various mode I to mode II loading ratios. The Mixed-Mode Bending test (MMB) is a linear combination of two pure mode tests; the DCB (mode I) and the ENF (mode II). The MMB uses a lever arrangement to introduce the pure mode I and mode II components simultaneously into a conventional DCB test specimen. The test method is shown in Figure 4.12.

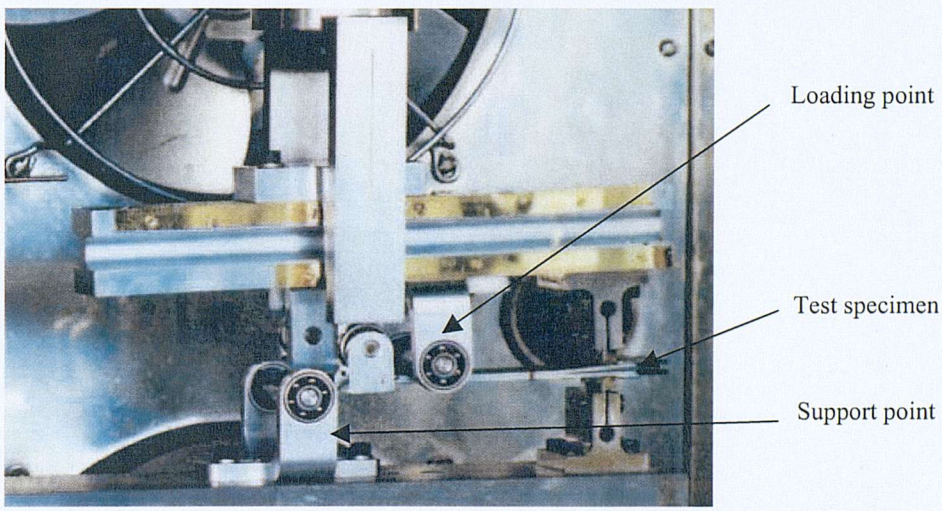

Figure 4.12: Test set-up for MMB

The lower surface of the specimen is attached by a hinge to the base of the rig and the other end of the specimen rests on a roller a distance 2L from this hinge. The loading lever is attached to the upper surface of the specimen via another hinge and rests on a roller (the fulcrum) a distance 'b' from the upper hinge. During the test, a downward load P is applied to the lever a distance 'c' from the fulcrum. This leads to the following expressions for G_I and G_{II} [Kinloch *et al*, 1993].

$$G_I = \frac{3P^2(a+\chi_I h)^2}{w^2 h^3 E_{11}}\left[\left(1-\frac{c+b}{2L}\right)-\frac{c}{b}\right]^2 \qquad 4.3$$

$$G_{II} = \frac{9P^2(a+\chi_{II} h)^2}{4w^2 h^3 E_{11}}\left[\left(1-\frac{c+b}{2L}\right)-\frac{c}{b}\right]^2 \qquad 4.4$$

where E_{II} is the axial stiffness, 'a' the crack length, 'w' and 'h' are the specimen width and half-thickness respectively. χ_I and χ_{II} are the mode I and mode II end-rotation corrections, given by the following expressions [Williams, 1989].

$$\chi_I = \sqrt{\frac{E_{II}}{11G_{12}}}\sqrt{\left[3-2\left(\frac{\Gamma}{1+\Gamma}\right)^2\right]} \qquad (4.5)$$

$$\chi_{II} = 0.42\chi_I \qquad (4.6)$$

where

$$\Gamma = 1.18\frac{\sqrt{E_{11}E_{22}}}{G_{12}} \qquad (4.7)$$

and E_{22} and G_{12} are the transverse and shear moduli respectively.

The mixed-mode ratio is given by:

$$\frac{G_I}{G_{II}} = \frac{4}{3}\left[\frac{\left(1-\frac{c+b}{2L}\right)-\frac{c}{b}}{\left(1-\frac{c+b}{2L}\right)+\frac{c}{b}}\right]^2\left[\frac{a+\chi_I h}{a+0.42\chi_I h}\right]^2 \qquad (4.8)$$

Thus, by changing the value of 'c' (and keeping 'L' and 'b' constant) a spectrum of mixed-mode loading ratios can be introduced by a single applied load, ranging from pure mode II ($G_I/G_{II} = 0$) to approaching pure mode I ($G_I/G_{II} \rightarrow \infty$). In this work, mixed-mode ratios of 75% mode I with 25% mode II, 50% mode I with 50% mode II, and 25% mode I with 75% mode II were evaluated.

Prior to the commencement of the experiments considerable preparation of the each sample was required. For example, after manufacture each specimen was labelled and the dimensions measured using a digital vernier at three locations along the width and thickness. The application of the hinges first required the cleaning of the surfaces to be bonded with acetone, abrading and then cleaning again. The hinges were bonded to the surface using an epoxy adhesive. After bonding, the hinges were inspected to ensure they were not deformed and also aligned with the specimen edges. The specimen edges were painted white and 1mm intervals marked from the tip of the insert.

The MMB specimens were tested on a screw driven Instron test machine with a 5kN load cell. The load and displacement were measured using a data logger and the crack length recorded at each 1mm along the edge of the specimen. All specimens were pre-cracked in Mode II to give a starter crack length of approximately 30mm. This was undertaken to avoid crack blunting at the tip of the insert.

The MMB tests were undertaken by Qinetiq staff at Qinetiq Farnborough, Cody Technology Park, Farnborough, Hampshire, UK.

In addition to understanding the fracture mechanics performance at the three different repair locations, the fracture mechanics test results are also required to undertake the impact damage threshold and impact damage propagation predictions identified in Table 2.6.

4.8 Repair Structural integrity assessment

The technical understanding and experimental findings arising from the Failure Mode and Effects Criticality Analysis, from the Strength Based Assessment and the Damage

Tolerance Assessment are all drawn together within the repair structural integrity assessment.

The assessment is used to determine whether the structural repair is damage tolerant and is based upon the following information:

1. Knowledge of the static and fatigue life performance of:
   - Pristine sandwich beam
   - 20:1 structural repair
   - Damaged composite sandwich beams

2. Knowledge of the residual strength performance of:
   - Damaged composite sandwich beams
   - Damaged 20:1 structural repairs

3. Knowledge of the damage initiation threshold of:
   - RNLI Ampreg 75/QEA1200 sandwich beams
   - Structural defect repair of (1)

4. Knowledge of the fracture toughness properties of:
   - Mode I, Mode II and mix-mode of parent laminate
   - Mode I, Mode II and mix-mode of the repair laminate
   - Mode I, Mode II and mix-mode of the repair-parent interface

5. Knowledge of the damage propagation within:
   - Parent laminate
   - Repair laminate
   - Repair-parent interface

The information detailed above will indicate whether the damage mode will influence the strength performance of the repair, and indicate whether the fracture toughness of the repair is sufficient to match or exceed the performance of the parent laminate thereby indicating that the repair is damage tolerant.

4.9 Concluding Remarks

The purpose of this chapter has been to provide the background information concerning each of the critical steps within Figure 3.1. Furthermore it has been shown how this methodology will be implemented within this research project to determine whether a

scarf tapered structural repair used within composite sandwich structures (representative of the RNLI all-weather class of lifeboat) is damage tolerant to non-penetrating impact damage.

5 FRACTURE MECHANICS ASSESSMENT OF SKIN LAMINATES

5.1 Introduction

In Chapter 3, the design methodology behind the damage tolerance assessment of repaired composite sandwich structures was defined previously, for clarification see Figure 3.1. In support of this methodology, Chapter 4 provides detailed information about the tools and test methods required to implement this approach. There are three critical elements within this methodology, namely the Fracture Mechanics Assessment, the Strength Based Assessment, and the Repair Structural Integrity Assessment. In this chapter, the Fracture Mechanics Assessment comprised of (1) Impact Damage Tolerance of Sandwich Beams and (2) Fracture and Crack Growth in the Outer Skin of Sandwich Beams, will be discussed.

5.2 Assessment of Tolerance to Impact Damage

5.2.1 Introduction

The aim here is to characterise the influence of impact damage on a 20:1 tapered scarf repair to a composite sandwich panel. In the FMECA (Chapter 4, section 4.5) two critical impact locations on a tapered scarf repair were identified, i.e. at the start of the scarf taper and at the end of the overlaminate plies, to understand how repair geometry could arrest or accelerate the damage failure modes.

5.2.2 Impact damage tolerance of 'Pristine' beams

To provide a baseline comparison for the 20:1 tapered scarf repairs a series of impact experiments were undertaken on pristine sandwich beams. This investigation used different damage measurements (indentation depth and crack length), coupled with viewing the damage site by the stereoscopic photographic NDE technique. Further microscopy investigations were used to understand the precise nature of the damage mechanisms within the sandwich beam. The experimental results for the impact damage on the sandwich beams for the 1m-drop height and 2m-drop height impacts are given in Tables 5.1 and 5.2 respectively.

The impact energy is calculated by equations (4.1) and (4.2) in Chapter 4 and assumes ideal free fall.

		Impact Weight [kg]	Impact Energy [J]	Side 1 [mm]		Side 2 [mm]		Av. Left [mm]	Av. Right [mm]	Total damage area [mm^2]	Stdev
				Left	Right	Left	Right				
1.1	Ampreg75	14.7	145	0	0	0	0	0	0	0	0
1.2	Ampreg75	19.7	194	0	0	0	0	0	0	0	0
1.3	Ampreg75	24.7	243	0	0	0	0	0	0	0	0
1.4	Ampreg75	29.7	292	0	0	0	0	0	0	0	0
1.5	Ampreg75	34.7	341	0	0	0	0	0	0	0	0
1.6	Ampreg75	39.7	390	0	0	0	0	0	0	0	0
1.7	Ampreg75	44.7	439	0	0	0	0	0	0	0	0
1.8	Ampreg75	49.7	488	0	0	0	0	0	0	0	0
1.9	Ampreg75	54.7	537	0	0	0	0	0	0	0	0
1.10	Ampreg75	59.7	586	0	0	0	0	0	0	0	0
1.11	Ampreg75	64.7	635	2.5	1.5	2	2.5	2.3	2.0	850	400
1.12	Ampreg75	64.7	635	4	4.5	6	4	5.0	4.3	1850	400

Table 5.1: 1-meter drop height impact tests and corresponding damage characteristics for E-glass/Kevlar composite and PVC foam core sandwich beams

		Impact Weight [kg]	Impact Energy [J]	Side 1 [mm]		Side 2 [mm]		Av. Left [mm]	Av. Right [mm]	Total damage area [mm^2]	Stdev
				Left	Right	Left	Right				
2.1	Ampreg75	14.7	289	0	0	0	0	0	0	0	0
2.2	Ampreg75	19.7	387	0	0	0	0	0	0	0	0
2.3	Ampreg75	24.7	485	0	0	0	0	0	0	0	0
2.4	Ampreg75	29.7	583	0	0	0	0	0	0	0	0
2.6	Ampreg75	34.7	635	12.5	0	7.5	0	10	0	2000	400
2.7	Ampreg75	39.7	780	0	23	0	23	0	23	4600	400
2.8	Ampreg75	44.7	878	8	5	19	23	14	14	5500	400
2.9	Ampreg75	49.7	976	19	22	18	27	18	24	8450	400
2.10	Ampreg75	54.7	1074	27	31	23	29	25	30	11000	400
2.11	Ampreg75	59.7	1172	35	30	27	15	31	23	10700	400
2.13	Ampreg75	64.7	1270	27	29	34	30	30.5	30	12000	400
2.14	Ampreg75	64.7	1270	27	26	25.5	30	26.25	28	10850	400
2.15	Ampreg75	64.7	1270	24	26	35	32.5	29.5	29	11750	400

Table 5.2: 2-meter drop height impact tests and corresponding damage characteristics for E-glass/Kevlar composite and PVC foam core sandwich beams

The two tables report the damage crack length in four locations, i.e. two sets of measurements taken on the left hand side and on the right hand side of the indented profile on the two external edges of the sandwich beam when viewed by the naked eye. Figure 5.1 illustrates the range of different damage mechanisms sustained by the outer laminate and foam core. Furthermore, Figure 5.1 indicates the definition for crack length left and crack length right on side 1. To maintain damage length continuity, the definition of left and right remain the same across the width of the sandwich beam even when the damage is viewed on side 2.

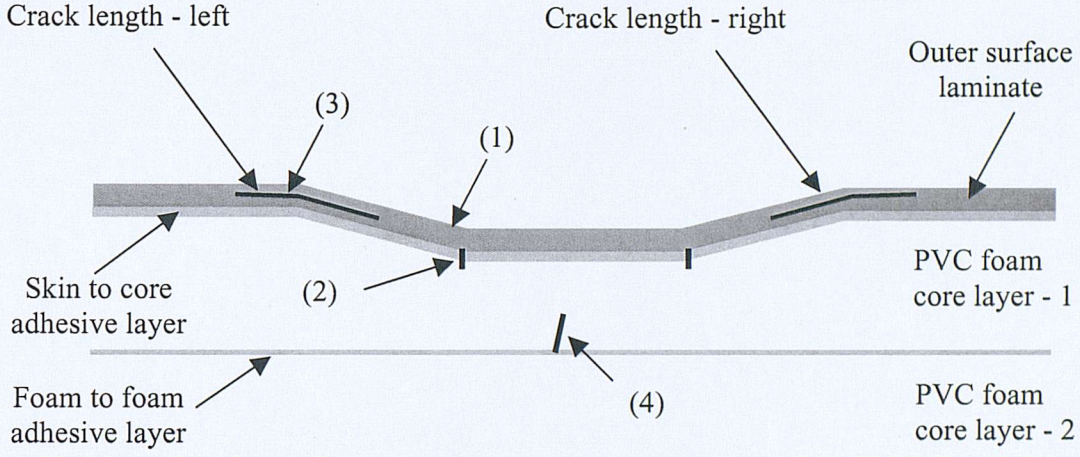

Figure 5.1: Impact damage contained within sandwich beam when viewed in cross-section on side 1.

The primary failure modes observed during this impact study, in order of occurrence was surface indentation (see point 1), followed by adhesive cracking (see point 2), followed by delamination formation (see point 3), and finally at the maximum impact energy vertical cracks occurred in the PVC foam core (see point 4). A full summary of the different energy levels to cause the different failure modes is given in Tables 5.3 and 5.4.

The impact velocity and energy was estimated from Equations (4.1) and (4.2).

Impact	Impact Mass (kg)	Impact Energy (J)	Impact Velocity (ms^{-1})	Max Indentation (mm)	Damage Description
1.1	14.73	145	4.43	0.00	No real damage, white lines from impactor edges
1.2	19.73	194	4.43	0.00	No real damage, white lines from impactor edges
1.3	24.73	243	4.43	0.64	No real damage, white lines from impactor edges
1.4	29.73	292	4.43	0.69	No real damage, white lines from impactor edges
1.5	34.73	341	4.43	0.73	No real damage, white lines from impactor edges
1.6	39.73	390	4.43	0.83	No real damage, white lines from impactor edges
1.7	44.73	439	4.43	0.94	No real damage, white lines from impactor edges
1.8	49.73	488	4.43	1.36	Starting to indent the surface of the beam
1.9	54.73	537	4.43	1.71	Larger indentation of the surface and slight core crushing below one of the impact edges
1.10	59.73	586	4.43	1.38	A greater indentation to 1.9 and the core moving as a section downwards below the impact area
1.11	64.73	635	4.43	1.65	An increase on the damage seen in 1.10
1.12	64.73	635	4.43	3.05	A slight indentation on the surface, no real damage apart from white lines from impactor edges

Table 5.3: Overview of failure modes for impact events conducted at 1-meter height

Impact	Impact Mass (kg)	Impact Energy (J)	Impact Velocity (ms^{-1})	Max Indentation (mm)	Damage Description
2.1	14.73	289	6.26	0.53	A slight indentation on the surface, no real damage apart from white lines from impactor edges
2.2	19.73	387	6.26	0.57	A slight indentation on the surface, no real damage apart from white lines from impactor edges
2.3	24.73	485	6.26	0.51	A slight indentation on the surface, no real damage apart from white lines from impactor edges
2.4	29.73	583	6.26	0.64	Greater indentation, slight adhesive cracking below impactor edges
2.5	34.73	681	6.26	2.16	Increase in indentation to previous beam, similar damage sustained
2.6	39.73	780	6.26	1.24	Increase in indentation to previous beam, similar damage sustained
2.7	44.73	878	6.26	2.39	Increase in indentation to previous beam, similar damage sustained
2.8	49.73	976	6.26	3.17	Larger indentation. Adhesive cracks below impactor edges, mid-plane delamination
2.9	54.73	1074	6.26	3.99	Increase in indentation to previous beam, similar damage sustained
2.10	59.73	1172	6.26	3.73	Increase in indentation to previous beam, similar damage sustained
2.11	64.73	1270	6.26	4.01	Increase in indentation to previous beam, similar damage sustained
2.13	64.73	1270	6.26	4.25	Adhesive cracks below each impactor edge. Core cracking below LHS impactor edge starting from first adhesive layer within the core. Mid-plane delamination
2.14	64.73	1270	6.26	4.23	Adhesive cracking below the impactor edges again. A core crack of greater magnitude than in 2.13, starting from the first adhesive layer within the core and situated in the middle of the impact
2.15	64.73	1270	6.26	4.69	The same damage as in 2.14 with a comparable crack in the first adhesive layer within the core
2.16	64.73	1270	6.26	4.51	The same damage as in 2.15 but without the adhesive crack within the core

Table 5.4: Overview of failure modes for impact events conducted at 2-meter height

In virtually all the impact tests discolouration of the matrix and a surface indentation was apparent. At the initial impact energies from the 1 metre drop height there was no visible damage other than the marks left by the impactor edges. However, once a mass of 10kg was added to the impact carriage, indentation became visible on the surface of the sandwich structure. The relationship between dent depth and impact energy is presented in Figure 5.2.

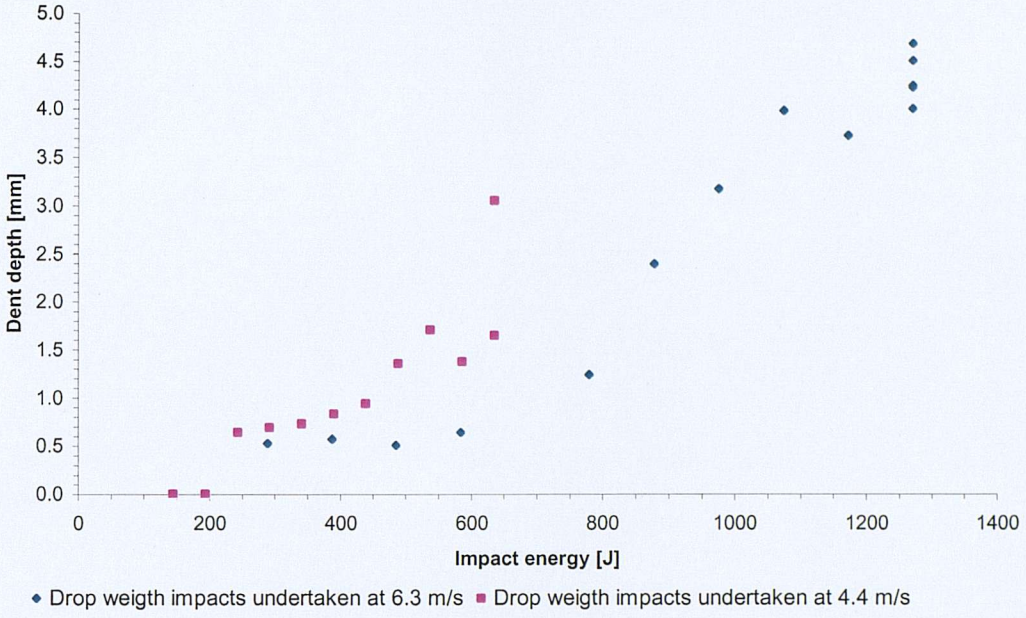

Figure 5.2: Relationship between residual indentation depth and impact energy for a range of impact energies

In Figure 5.2 the dent depth was measured at four locations across the width of the beam and averaged to give the final measurement. The figure clearly illustrates that dents in the outer skin are clear indications of damage (this point is confirmed later in Figure 5.3).

At the point where permanent indentation occurred in the laminate, a corresponding delamination within the laminate was observed when viewing the edge of the specimens. The relationship between the dent depth and the damage area has been presented in Figure 5.3.

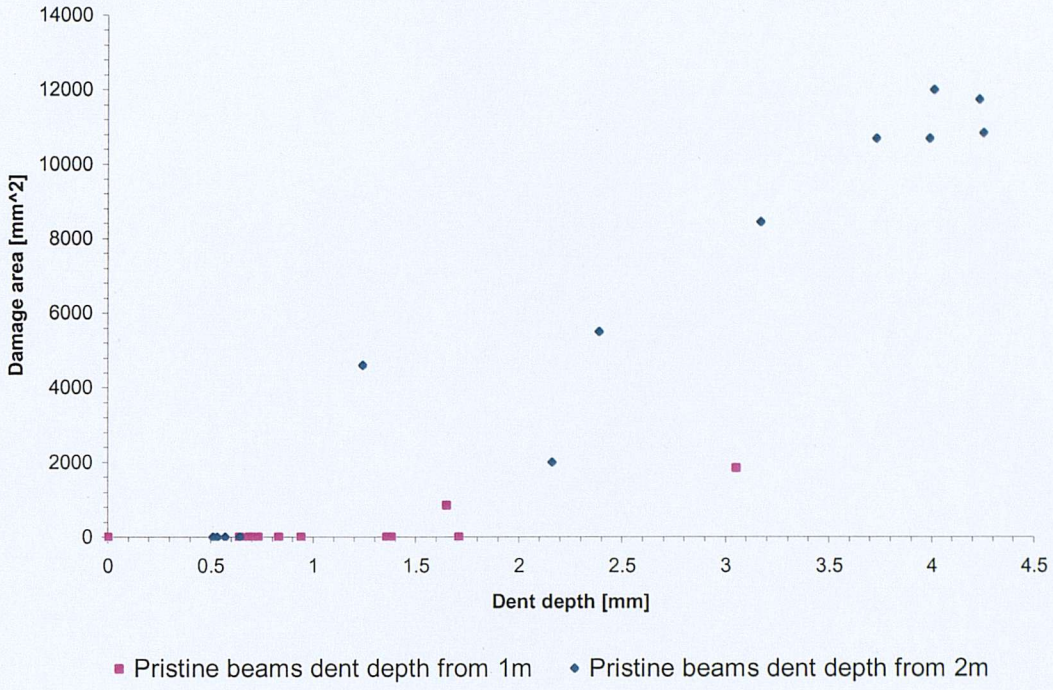

Figure 5.3: Relationship between damage area and dent depth for a range of impacts energies

Although larger dents generally correspond to a larger delamination size (as indicated in Figure 5.3) there is no direct correlation between dent depth and delamination size for different impact velocities for this impactor size and shape.

The extent of internal delamination area as a function of impact energy is presented in Figure 5.4.

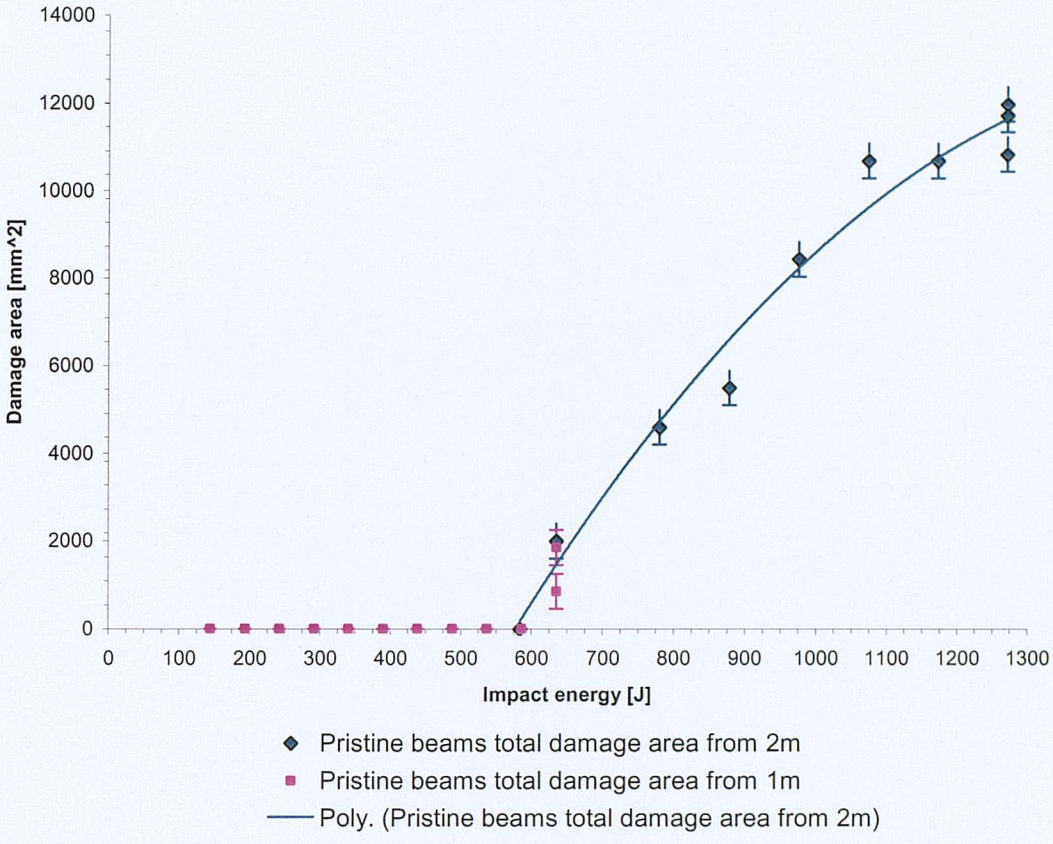

Figure 5.4: Relationship between delamination area and impact energy

The result in Figure 5.4 indicates that once a critical energy of 635J is reached, regardless of the impact velocity, there is rapid onset of delamination damage. There is also a suggestion that the delamination growth seems to be increasingly restrained, which is probably due to the energy being consumed by the formation of an increasing number of delaminations. This effect was observed at the higher energy levels where delaminations occurred at 3 or 4 discrete layers as opposed to one principal failure interface. Even at these energy levels no fibre fracture or skin penetration had occurred (which is probably due to the nature of the impactor chosen), but when they do start to occur they will effectively restrain any further delamination growth.

To confirm the precise location of the delamination within the lay-up, a section was removed from the beam and prepared for visual examination using a microscope. Figure 5.5 illustrates the delamination formation through the full thickness of the outer skin,

the figure shows a cross-section of the composite outer skin of a composite beam subjected to a 1270J impact.

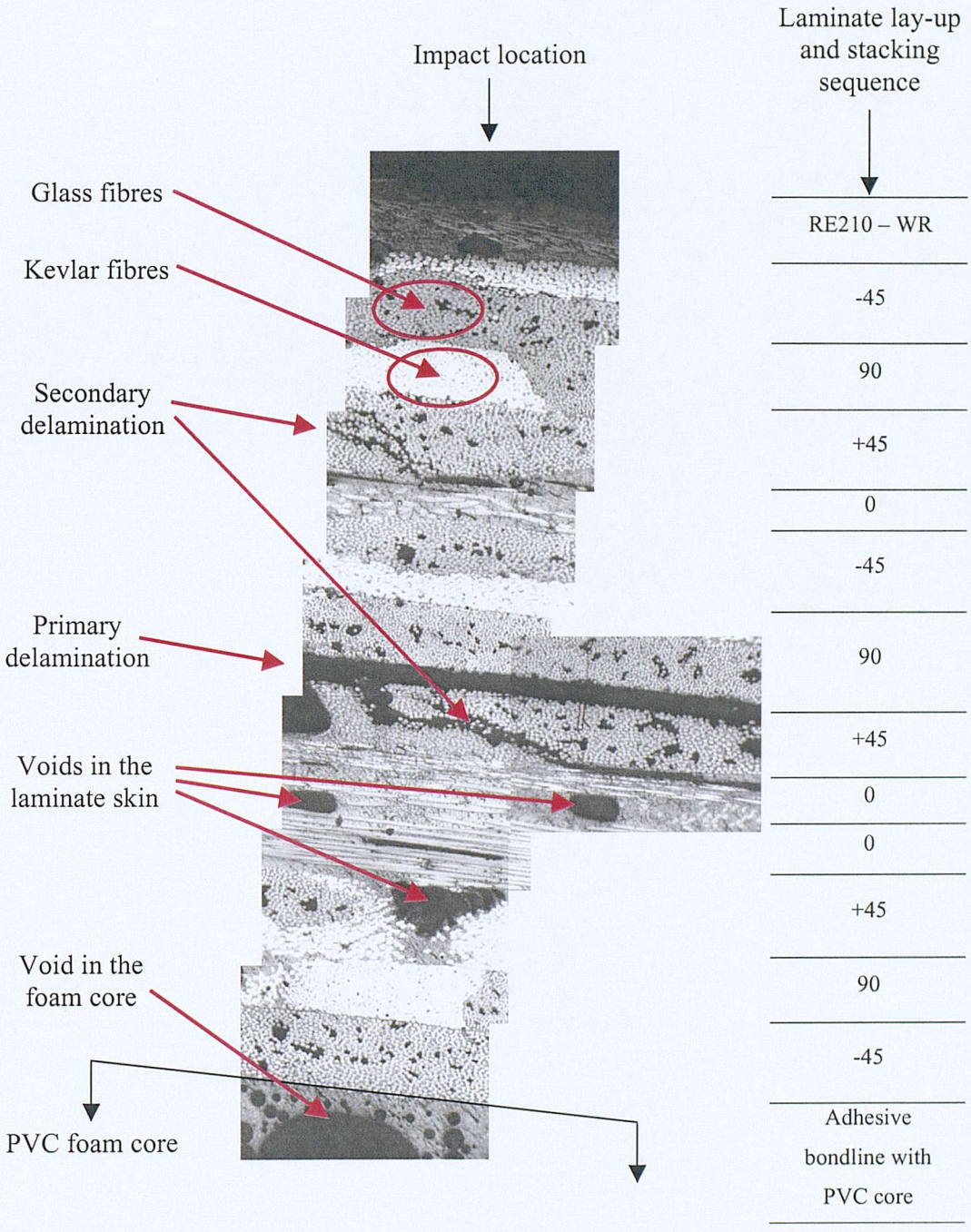

Figure 5.5: Damage formation in glass/Kevlar outer skin after a 1270J impact to a composite sandwich beam.

The impact occurred at the top of the figure, and the foam core which supports the outer skin is bonded below the bottom of the figure. The precise orientation of the individual

layers within the quadriaxial lay-up were determined from resin burn-off tests, which aided in determining the location of the principal damage mechanism. The fibre stacking sequence is indicated in the vertical column on the right-hand side of Figure 5.5. The dominant failure mode was observed to be delamination propagation midway through the stacking sequence at the 90°/+45° interface. Minor delaminations propagate from this major source damage and run parallel to the 0° interface. Secondary delamination failure mechanisms are also observed within the first +45° ply. Again these delaminations extend towards the 0° ply but do not pass through it. From these observations it appears that the 90°/+45° interface is the most susceptible to the formation of impact damage within this stacking sequence.

Whilst the damage formation within the composite outer skin can clearly be identified from microscopic examination, the damage failure mode within the PVC foam core is less clearly defined. Initially it was anticipated that a cavity in the core would be formed directly under the impact site, a phenomenon previously reported in the work by [Shipsha, 2001].

To characterise the damage within the foam core a series of optical examinations in conjunction with the stereoscopic photographic NDE technique were taken before and after the impact event. The stereoscopic photographic technique uses a reference grid system or random dots which when viewed using a stereomicroscope highlights the displacement difference between the first and second photo. Although this technique is unable to provide any physical data, it does provide some insight into how the core material is responding to an impact event.

The optical examination of the indented core material revealed some vertical cracking (typically 2mm in size) within the first adhesive bondline between the first and second 25mm thick foam core sections. It did not reveal a core cavity. In support of the optical observations, the sterography technique highlighted the influence of the adhesive bondline between the first and second layer of the PVC foam core. It showed that the deformation of the core material due to a 1270J impact was confined to the first 25mm. No strain line deformation was observed beyond this for the virgin beams. A typical

sterography representation of the deformation profile within a virgin beam subjected to 1270J impact is given in Figure 5.6.

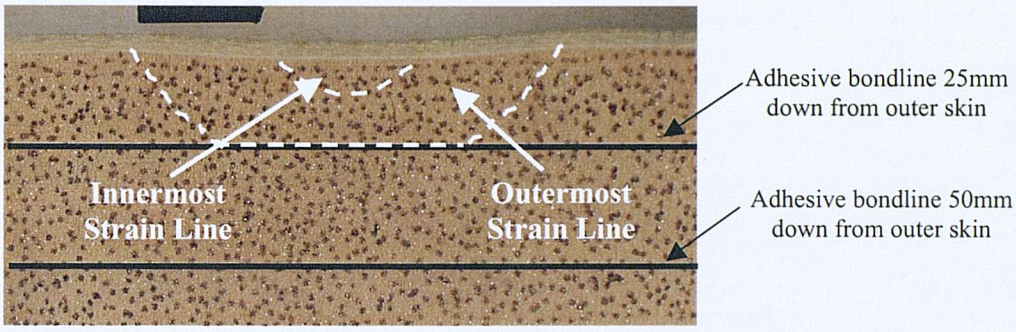

Figure 5.6: Strain line formation in PVC foam viewed by the stereoscopic photographic NDE technique

The two strain contours in Figure 5.6 provide some insight into the extent of the deformation experienced by the core material during the low velocity impact test. The methods of damage formation within the core will now be discussed.

At the moment the impactor strikes the surface a zone of crushed and compacted core occurs underneath the point of impact. Initial, the outermost individual cells start to crush. The plastic deformation of the core under compression is caused by cell-wall collapse due to cell wall buckling, cell wall breaking, and the formation of plastic hinges [Shipsha, 2001]. As the first cell starts to crush all plastic deformation is concentrated within this cell. Once the local compressive strain within this cell reaches the densification strain ($\varepsilon_{yy} \sim 70\%$) [Shipsha, 2001], the next connecting cell in the system starts to crush. This domino effect contains until the impact energy has been absorbed in the destruction of the foam core (the extent of the crushed and compacted core is indicated by the outermost strain line in Figure 5.6).

The elastic energy now stored within the indented skin laminate tries to return the skin to its original straightened position. However, the core material under the impacted region has now been permanently crushed and it is the crushed core that resists the skin laminate from popping back out, i.e. since the core and skin are still connect (bonded) to

one another, a tensile force exists across this interface will results in the skin exhibiting a dented profile post impact test. A final observation in Figure 5.6 concerns the influence of the adhesive bondline between the first and second foam core upon the crushed core zone. The stereoscopic photographic NDE investigation clearly indicated that no relative displacement of the core material occurred below the adhesive. It appears that the adhesive is providing an internal membrane that the first core block is being crushed against.

5.2.3 Impact damage tolerance of structural repairs

The experimental procedures used for the impact testing of the pristine beams were applied to the beams containing the structural repairs. Impact tests were undertaken at impact energy levels from 485J in steps of approximately 100J up to 1172J to evaluate the performance of the repair. As detailed in Chapter 4, 'Methodology Implementation', the range and the impact increments were determined by the testing approach and the mass size steps.

The impact investigation on the tapered scarf repair was based upon the findings of the FMECA given in Chapter 4. Table 4.5 details the critical hazards identified within the Criticality Analysis of the FMECA. The results from Table 4.5 are summarised below:

3. High risk
   - Impact damage to the tapered interface between the repair plies and parent
   - Impact damage to the horizontal interface between the repair plies and parent
   - Impact damage to the repair laminate
4. Medium to high risk
   - Impact damage to the parent laminate
   - Fatigue and fracture at or near the internal edge of repair taper

This result indicates that damage contained within the tapered interface or the horizontal interface of the repair, or the repair material itself has the greatest risk of causing failure to the repaired structure. Since any impact damage to the tapered interface or the horizontal interface is likely to induce damage to the repair laminate as well, it has been

decided to concentrate upon the two locations identified in Figure 4.5 to ascertain whether they are more or less damage tolerant than the pristine beams.

In these experiments only the delamination length was recorded and not the dent depth, unlike the impact investigation on the pristine beams. In the case of the pristine beams, the dent depth was easily obtained from a datum line bridging the impact site. However, in the case of the repair schemes, processing variability of bondline thickness, overlaminate step length and thickness and general increased thickness of repair material at the end of the tapered scarf (see Figures 4.5 and 5.8) presented considerable problems in obtaining a datum line that could be used for dent depth investigations. An additional problem concerns the vertical adhesive bondline and how it could influence the extent of the dent depth if the impactor was not correctly aligned over the exact same position on each beam. The extent of specimen variation and testing variation could significantly mask any similar trends observed in the pristine beams.

The delamination damage area versus impact energy for impact location 1 (on the tapered scarf profile) and impact location 2 (at the end of the over-laminate) is presented in Figure 5.7.

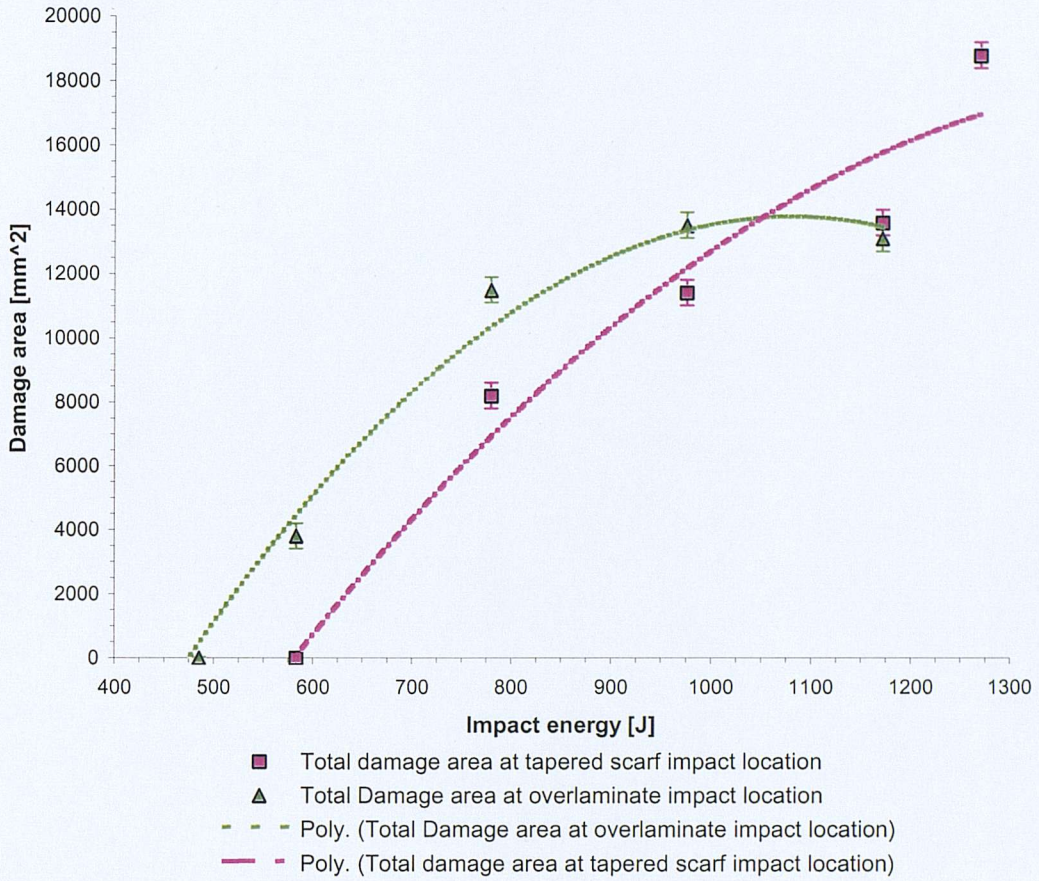

Figure 5.7: Delamination crack area at the commencement of the scarf repair taper and at the end of the scarf repair over-laminate for a range of impact energies

In Figure 5.7 the energy to initiate delamination damage in the repair when impacted on the taper scarf was found to be 780J. At this location the delamination damage was observed at the repair-parent interface and within the repair laminate above the foam core replacement. This corresponds to the same threshold energy to initiate delamination damage in the original sandwich beams at 6.3 m/s. Conversely, Figure 5.7 indicates that a lower energy is required to initiate damage at the end of the taper scarf over-laminate, typically 580J. At this location the damage initiated within the parent laminate directly underneath the increased thickness section of parent laminate and repair laminate, i.e. at the end of the scarf taper. The damage remains within the parent laminate until the energy level reaches 975J when damage is observed to occur at the end of the overlaminate plies between the parent and repair interface. Figure 5.8 has

been included to illustrate the sequence of damage formation at impact location (1) and impact location (2) when subjected to varying impact energies.

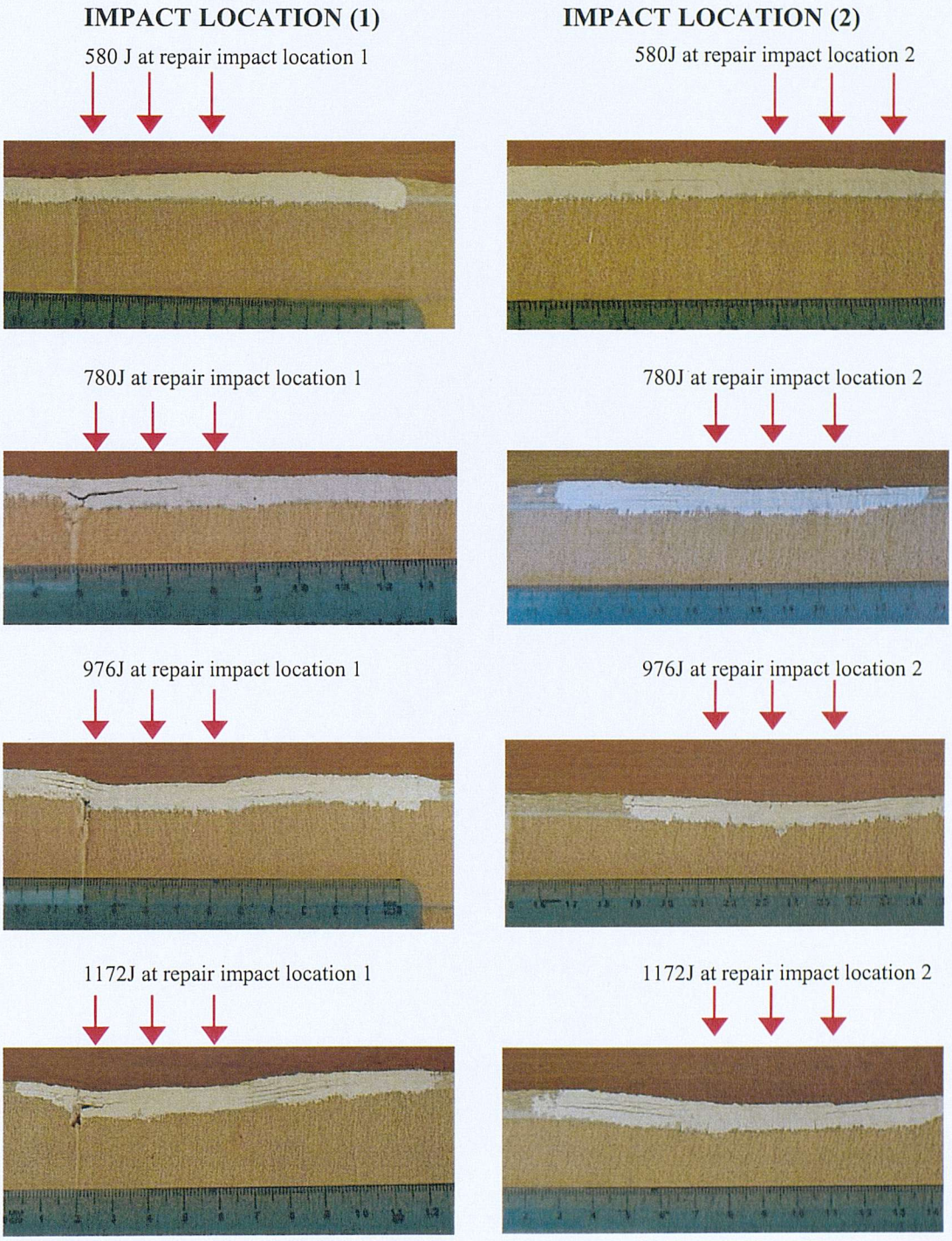

Figure 5.8: Damage formation at impact location (1) and impact location (2) in the 3° scarf taper repair for a range of impact energies

After the impact tests each sample was viewed under a microscope with 10x magnification. This approach permitted the characterisation of the various crack lengths occurring at each ply interface. In the tapered scarf repair on the outer skin, 6 individual plies are used to restore the structural efficiency of the original 4-ply outer skin laminate, i.e. in the tapered scarf repair 5 possible ply failure interfaces exist. The individual ply interfaces within the parent laminate (P1 to P3) and within the repair laminate (R1 to R5) have been illustrated in Figure 5.9.

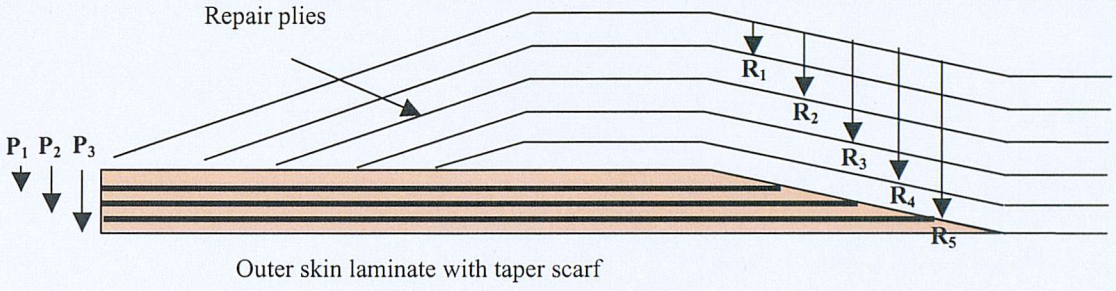

Figure 5.9: Schematic illustration of individual ply interfaces within a tapered scarf repair

The individual crack lengths at each of these interfaces have been detailed in Table 5.5 for impact location (1) and Table 5.6 for impact location (2).

Impact location (1): damage size measurements through the thickness of the laminate														
Impact energy (J)	Foam core side 1					Foam core side 2					Total delamination length [mm]	Max delam length foam core side 1 [mm]	Max delam length foam core side 2 [mm]	Average delam length between side 1 & 2 [mm]
	R_1	R_2	R_3	R_4	R_5	R_1	R_2	R_3	R_4	R_5				
580	0	0	0	0	0	0	0	0	0	0	0	0	0	0
780	0	7	14	16	43	0	0	0	12	39	131	43	39	41
976	0	15	23	0	0	10	5	19	0	0	72	23	19	21
1172	0	0	16	22	7	0	0	0	24	15	84	22	24	23
1270	0	0	10	23	10	0	0	10	15	25	93	23	25	24
Impact energy (J)	Taper end side 1					Taper end side 2					Total delam lengths Taper end [mm]	Max delam length Taper end side 1 [mm]	Max delam length Taper end side 2 [mm]	Average delam length between side 1 & 2 [mm]
	P_1	P_2	P_3	R_5	R_4	P_1	P_2	P_3	R_5	R_4				
580	0	0	0	0	0	0	0	0	0	0	0	0	0	0
780	0	0	0	0	0	0	0	0	0	0	0	0	0	0
976	4	10	37	0	0	11	14	35	16	0	127	37	35	36
1172	2	30	48	0	0	5	17	27	42	24	195	48	42	45
1270	0	10	60	0	0	20	20	80	0	0	190	60	80	70

Impact energy (J)	Total damage width (start + end)	Total damage area (mm^2)	Stdev (mm)
580	0	0	400
780	41	8200	400
976	57	11400	400
1172	68	13600	400
1270	94	18800	400

Table 5.5: Impact location (1): damage length measurements and total damage size for different impact energies

Impact location (2): damage size measurements through the thickness of the laminate														
Impact energy (J)	Start of overlaminate side 1					Start of overlaminate side 2					Total delamination length [mm]	Max delam length foam core side 1 [mm]	Max delam length foam core side 2 [mm]	Average delam length between side 1 & 2 [mm]
	P_1	P_2	P_3	R_5	R_4	P_1	P_2	P_3	R_1	R_2				
580	38	0	0	0	0	0	0	0	0	0	0	38	0	19
780	6	16	24	0	0	30	0	0	0	0	76	24	30	27
976	38	0	0	0	0	14	32	33	18	0	97	38	33	35.5
1172	34	39	39	0	0	20	22	32	18	0	204	39	32	35.5
Impact energy (J)	End of overlaminate side 1					End of overlaminate Side 2					Total delamination length [mm]	Max delam length Taper end side 1 [mm]	Max delam length Taper end side 2 [mm]	Average delam length between side 1 & 2 [mm]
	P_1	P_2	P_3	R_5	R_4	P_1	P_2	P_3	R_1	R_2				
580	0	0	0	0	0	0	0	0	0	0	0	0	0	0
780	12	27	16	0	0	0	34	0	0	0	0	27	34	30.5
976	6	29	22	0	0	9	35	0	0	0	101	29	35	32
1172	8	13	20	0	0	5	26	0	0	0	72	34	26	30

Impact energy (J)	Total damage width (start + end)	Total damage area (mm^2)	Stdev (mm)
580	19	3800	400
780	57.5	11500	400
976	67.5	13500	400
1172	65.5	13100	400

Table 5.6: Impact location (2): damage length measurements and total damage size for different impact energies

As the impact energy increases a number of trends become apparent for each location. Firstly, impact location 1 will be discussed, i.e. the impact to the scarf taper. Once above a threshold energy of 780J damage formation initiated at the vertical adhesive interface between the replacement core and the original foam core. At the same energy level, damage formation occurred at the tapered scarf repair interface. No damage was observed within the parent laminate. At the higher energy levels damage was observed to occur on either side of the flat-nosed impactor with the initiation of damage at the tapered interface and within the parent laminate. The damage did not appear to initiate within the repair laminate within this impact energy range.

To understand the fracture mode along the tapered interface a failure investigation using a scanning electron microscopy (SEM) was undertaken. A typical 3° scarf taper repair was subjected to two 1200J impacts along the length of the taper. The repeated impacts and their close proximity to each other ensured that a delamination extend along the full length of the beam. The failed repair patch was then extracted from the beam and the failed interface was examined using the SEM. The SEM investigation revealed that mode II fracture occurred directly under and in the immediate vicinity of the impact event. This was determined by an examination of the resin failure morphology. A typical mode I failure morphology would exhibit a clean smooth cleavage of the resin from the fibres. This was not observed on the sample. In comparison, the sample contained considerable surface debris, indications of fibre bridging (which was also observed optically) with resin shear cusps in between the individual fibres. Two SEM photographs have been included in Figure 5.10 for clarity. This first photograph shows considerable fibre pullout and surface damage to the composite repair. Closer examination between the damaged fibres shows smaller resin cusps standing up from the surface and being aligned towards the top left of the photograph. The second photograph is taken on the resin rich surface of the parent laminate. The rough surface with resin cusps is once again typical of a mode II fracture. This result would confirm the findings of [Olsson, 2002] that fracture initiation of delamination damage in the face sheet of a sandwich beam is based on pure mode II.

(a)

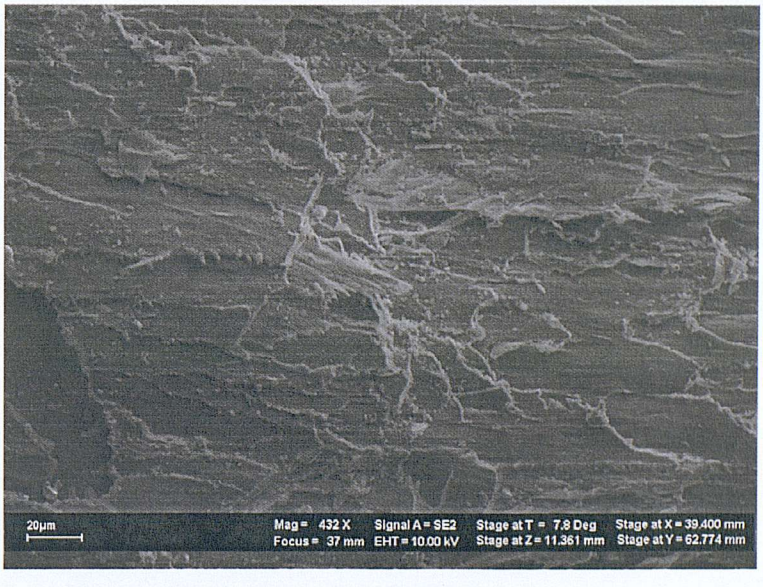

(b)

Figure 5.10: SEM photographs taken of the failed scarf repair (a) patch and (b) parent laminate surface

At impact location (2), the overlaminate impact location, the energy to initiate delamination damage within the parent laminate was observed to be 580J. At 780J the delamination damage was observed to occur within the parent laminate below the tapered section of the repair scheme and beyond the end of repair scheme. As the impact energy increased more damage was observed to occur at new ply interfaces within the parent laminate. Finally, at impact energies above 976J a crack was observed to occur between the final overlaminate ply and the parent laminate, i.e. the tensile stresses generated at the interface between the repair and the parent laminate were greater than the tensile strength of the Ampreg 26 laminating resin. If the impact induced debond did occur at a location where the environment could open the edge of the repair then it is possible that local failure of the patch could result in global failure of the panel/structure.

In an effort to understand the response of the replacement foam core to the 1270J impact a number of samples were examined with the stereoscopic photographic NDE technique. The strain line formation observed in the structural repair scheme subjected to a 1270J impact on the 20:1 scarf taper was similar to the 'pristine' beams (see Figure 5.11). The formation of these contour lines has been previously discussed but what effect this would have on the performance of the structure is uncertain.

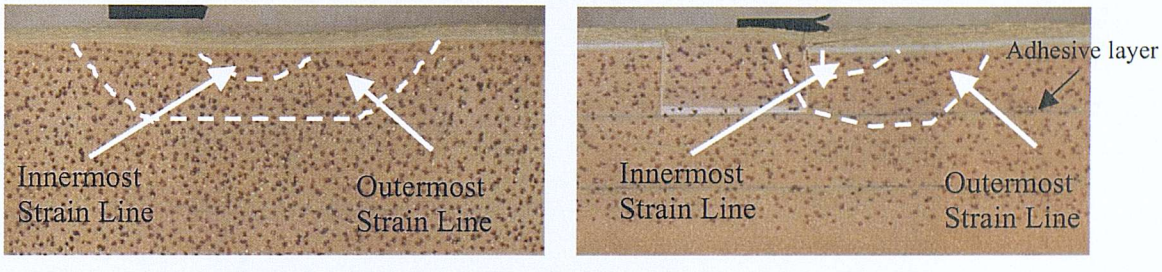

Figure 5.11: Strain line formation in PVC foam in pristine and repaired beams viewed by the stereoscopic photographic NDE technique

The stereoscopic photographic NDE technique suggested that there is an apparent high displacement plateau existing directly under impact location (1). As in the 'pristine' beams, a secondary displacement plateau existed but its profile was distorted due to the existence of the 25mm wide replacement PVC plug and the vertical adhesive bondline. It appears that the vertical adhesive bondline has significantly influenced the densification of the foam core.

The secondary displacement plateau also extended beyond the adhesive bondline between the first and second layer of PVC foam core although no damage was observed within the horizontal adhesive bondline. The movement of the core densification across the bondline was not observed within the pristine beams.

Finally, in the pristine beams a surface dent was readily apparent due to the tensile forces generated between the crushed core and the skin, i.e. the densification of the core resisted the 'spring-back' of the laminate skin. In the case of the tapered scarf repair no surface indentation value was recorded due to experimental difficulty (previous discussed). Whether the laminate skin would be indented to the same extent as the pristine skin is uncertain. Firstly the stereoscopic examination of the densification of the core material indicates that the core is compressed in a more localised region than for the corresponding impact energy on the pristine beams. This appears to be due to the vertical adhesive bondline. Secondly, the repair scheme has almost double the amount of laminate material compared to the pristine beams. This stiffer skin would protect the underlying core material from the impact event and it would have sufficient stiffness to overcome the tensile force of the compressed core and hence 'spring-back' to its starting position. This appears likely from the experimental evidence generated within this thesis however some uncertainties remain that could influence the magnitude of the spring-back, namely the destruction of the vertical adhesive bondline and the formation of delamination damage along the tapered interface.

5.2.4 Discussion of impact damage tolerance characteristics: pristine versus repair

Section 5.2 has evaluated the damage tolerance performance of 'pristine' and the tapered scarf repairs to BVID formed by a blunt-nosed impactor at different energy levels. Throughout this investigation a number of experimental observations were made about the damage threshold and the nature of the damage. These observations will now be discussed.

Whilst the same energy levels were used during these impact tests it became clear very early that understanding the precise failure mechanisms for each of the two repair locations was going to be very difficult. Besides the variables associated with the sandwich beams (laminate lay-up, laminate consolidation, adhesive bondline thickness

between skin and core), and the impactor (horizontal and vertical misalignment at the point of impact), there were also variables associated with the repair scheme (such as bondline thickness and replacement core width, taper angle and ply orientation). Finally, aligning the impactor to strike directly over a specific point required considerable precision and patience.

Although a vast number of possible variables could influence the experimental result, clear trends between repaired and pristine beams were observed. Figure 5.12 provides a comparison of the delamination width as a function of impact energy for the 'pristine' beams and the two impact locations on the structural repair.

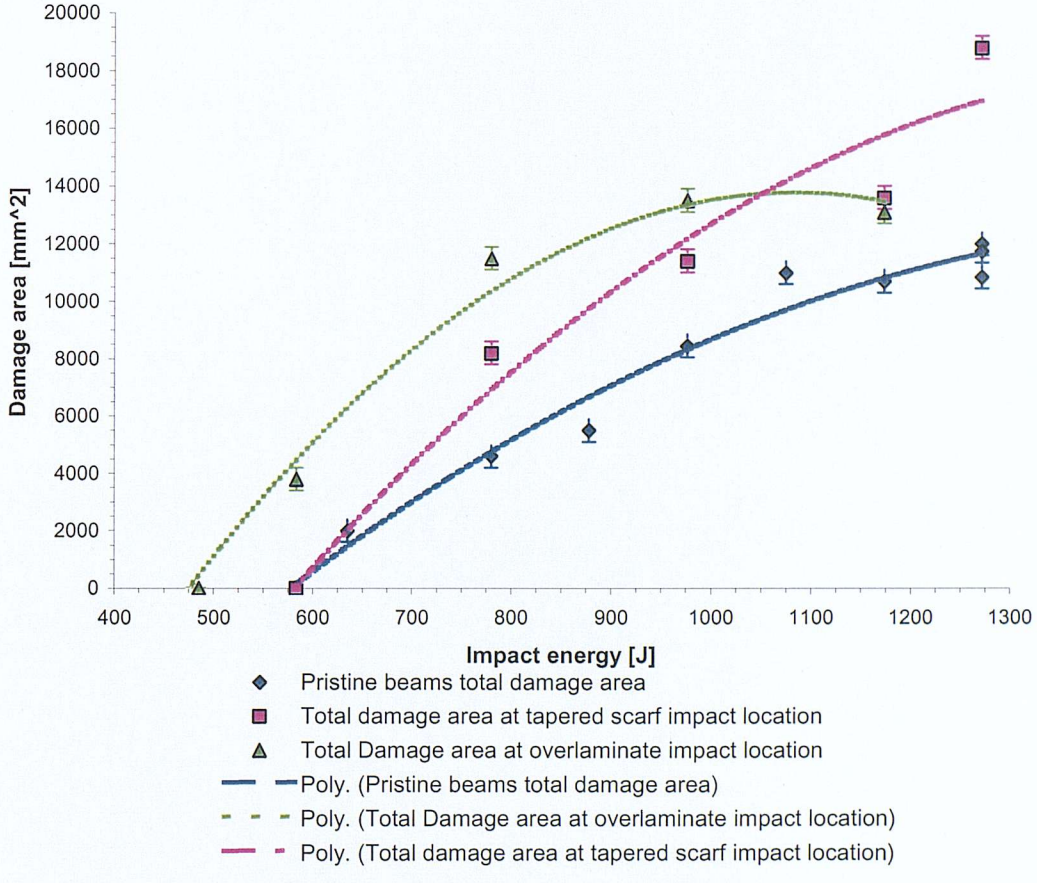

Figure 5.12: Relationship between average delamination area and impact energy for 3 ° tapered scarf repair and pristine beams.

In the context of these experiments (i.e. a flat nosed impactor 50mm wide) it was observed that the structural damage to the foam core was contained within the first 25mm, i.e. the adhesive bondline between the first and second foam core layer restrained any further crushing of the core. This was observed for both the 'pristine' and repaired beams. It was also observed that no interfacial separation between the outer skin and the foam core was observed in any of the tests. This experimental observation confirms the operational findings reported in Table 2.2 and the probability and severity ratings employed in Table 4.4.

In terms of a damage tolerance assessment it has been observed that a composite sandwich beam containing a 3° scarf taper repair is less damage tolerant to a 50mm wide flat-nosed impactor than the original laminate. The results illustrate that the threshold energy to initiate failure along the scarf taper is comparable with the 'pristine' beam in both cases. However, the damage area measurements revealed that the magnitude of the damage between the un-repaired and repaired beams is comparable at the end of the overlaminate impact location, whilst the damage area is almost doubled at the tapered scarf impact location (see Figure 5.12).

At the tapered scarf impact location, it appears that the bonded replacement core has considerable influence upon the way the damage manifests itself, i.e. the vertical column of adhesive disintegrates under the impact load thereby prompting a rapid increase of damage at the leading edge of the scarf taper repair (see Figure 5.13). Whether a concentration of damage at this location will drastically reduce the residual strength of the structure requires evaluation.

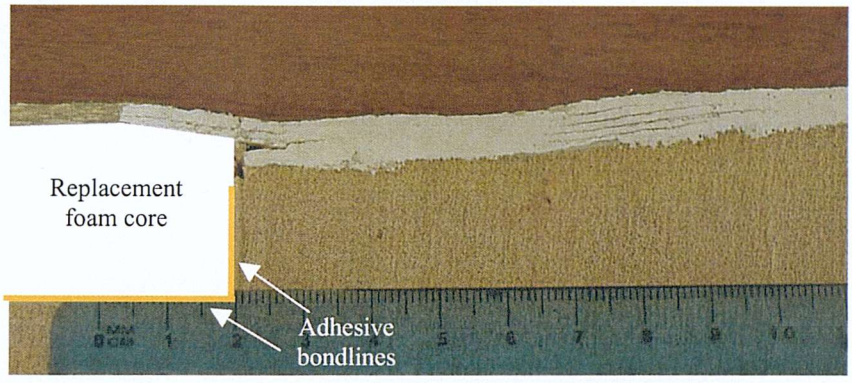

Figure 5.13: 1172J impact on the scarf taper interface of a tapered scarf structural repair

In the impact tests on the overlaminate, the outside edge of the impactor was aligned with the outside edge of the last overlaminate ply, i.e. the impact event was confined to the repair and not onto the parent laminate. It was therefore expected that the damage mechanisms would be biased towards to the repair overlaminate/parent laminate interface (where there are more ply interfaces and hence possible failure locations), with moderate damage occurring within the pristine laminate. This assumption did seem to be the valid for the majority of the impact damage observed at this impact location.

The threshold energy to introduce failure at the end of the overlaminate was lower than the threshold energy value for the 'pristine' beam and at impact location 1 on the repaired beams. The precise reason why the damage should initiate at a lower threshold is uncertain. The impact energy initially causes damage to start in the parent laminate underneath the repair scheme. As the impact energy increases the damage also starts to form at the leading edge of the repair resulting in the repair 'peeling' away from the original parent laminate. To highlight the location of the damage Figure 5.14 has been included for clarity.

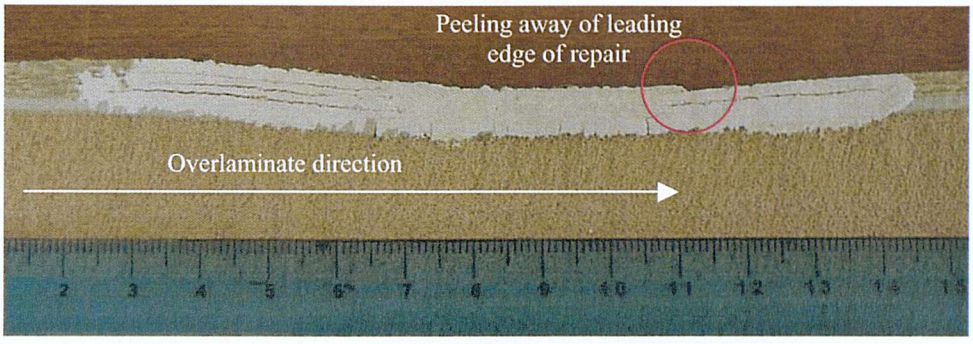

Figure 5.14: Representative 1172J impact on the overlaminate of tapered scarf repair structural repair.

This is quite a critical and important observation since the design rules for bonded joints proposed by Hart-Smith [Hart-Smith, 1973a] aim to reduce the tensile transverse stresses in the adhesive and the shear stress concentrations at the ends of the joint to maximise the durability of the repair scheme. However, if an impact energy threshold exists for the initiation of a 'peel' crack at the repair edge then the current repair design for the minimisation of peel stresses is inappropriate for repairs in regions of high impact probability. This research suggests that regardless of overlap length an impact event may be sufficient to overcome the tensile transverse stresses of the repair resin and cause failure of the patch/parent laminate interface. An alternatively approach must be considered.

5.3 Fracture and Crack Growth Assessment

5.3.1 Introduction

The purpose of this section is to present the results from the pure mode I (double cantilever beam), the pure mode II (end-loaded split) and the mixed-mode (mixed-mode bending) fracture mechanics tests. The results from these tests will be used to determine the energy required to propagate a crack within the three critical locations of a structural repair scheme (these are defined in Figure 4.6 and Table 4.6). The fracture mechanics results can then be directly compared with the experimental impact damage observations from section 5.2 to yield a better understanding of why the damage occurred within the different ply interfaces.

The fracture mechanics tests undertaken in Mode I, Mode II and at varying mixed-mode ratios on the parent laminate, the repair laminate and the repair-parent interface will now be presented. A full summary of the experimental data, the mode of failure, the load-displacement plots and the energy release rate versus crack length plots, for each of the testing configurations and different material combination, is given Appendix B.

5.3.2 Mode I fracture mechanics assessment

To obtain Mode I fracture toughness or critical strain energy release rate (G_{Ic}) of the different specimens a double cantilever beam specimen (DCB) was assessed using ASTM Standard D5528-94a. The modified beam theory has been used to calculate the mode I fracture toughness. The theory is given below:

$$G_{IC} = \frac{3 \cdot P \cdot \delta}{2 \cdot b \cdot (a + \Delta)} \tag{5.1}$$

This approach uses a correction factor Δ is added to the initial crack length 'a' thereby including stiffening effects, crack-tip rotation and large displacements [Hashemi *et al.* 1989] which simple beam theory neglects. The correction factor Δ can be found experimentally and it is constant during the entire crack propagation even though the factor Δ has no actual physical meaning.

Five samples from each material combination were evaluated on an Instron screw driven testing machine. The mean values and standard deviations of the energy release rates G_{IC} versus the crack length is presented in Figure 5.15.

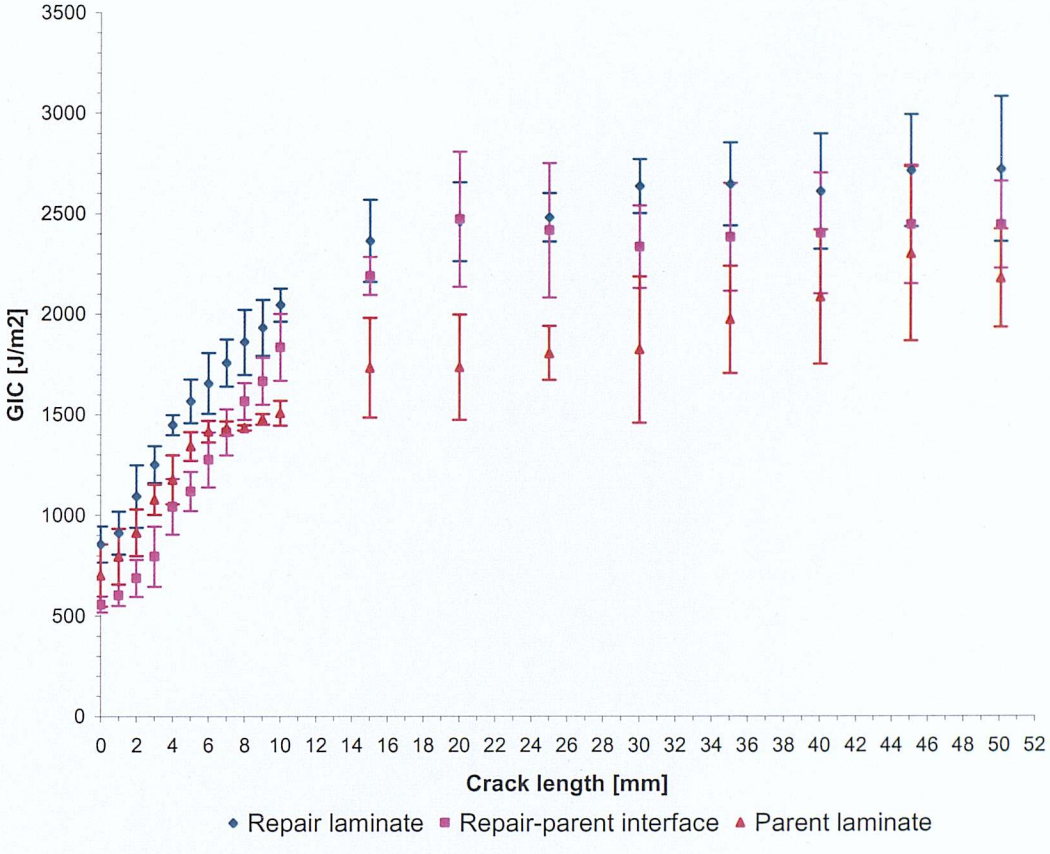

Figure 5.15: Mode I energy release rate versus crack length plot – mean values of all tested materials

Figure 5.15 clearly illustrates an increasing toughening effect as the crack propagates through the sample. This effect can be attributed to the extensive Kevlar fibre bridging observed during the tests (see Figure 5.16 for a typical example).

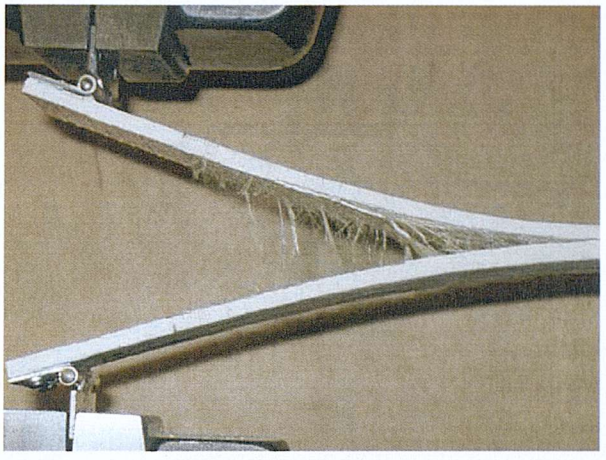

Figure 5.16: Fibre bridging in Parent laminate whilst loaded in mode I.

The mode I fracture toughness initiation threshold value and plateau values at 25mm are indicated in Table 5.7.

Material description	Number of specimens	G_{IC} initiation threshold	G_{IC} plateau (recorded at 25mm)
Parent laminate	5	699 ± 154	1818 ± 125
Repair laminate	5	855 ± 90	2481 ± 121
Repair-parent laminate	5	555 ± 40	2416 ± 336

Table 5.7: Mode I fracture toughness initiation threshold and plateau values

The first notable trend within the data is the similarity of the fracture toughness between the repair laminate (Kevlar/E-glass/Ampreg 26) and the repair-parent laminate (Kevlar/E-glass/Ampreg 26/75). This seems reasonable since the failure path in the repair-parent specimen was observed to occur in repair half of the repair-parent specimen. This is an interesting observation since the purpose of including the hybrid Ampreg 26/75 specimen was to characterise the interface of the composite repair and the parent laminate. However, if the crack growth instantly jumps away from the interface into the repair laminate it simplifies the design of composite repairs, i.e. the baseline performance of the repair laminate can be used as the design parameters for the

repair-parent interface and not rely on a new round of experimental testing to fully characterise the mechanical properties of the hybrid interface.

The second interesting trend is the performance difference between the Ampreg 75 and Ampreg 26 resin systems, i.e. the Ampreg 26 resin system is tougher than the Ampreg 75. The Ampreg 75 resin system is a standard pre-impregnated resin system produced by SP Systems that only requires consolidation with heat and vacuum to form a laminate. The Ampreg 26 resin system is supplied by SP Systems as a liquid two-part epoxy resin system that requires mixing before being drawn through the laminate by vacuum and cured by heat. The average thickness of the two laminates was 8.7mm for the Ampreg 75 laminate and 8.5mm for the Ampreg 26 laminate. The vacuum consolidation between the two laminates is almost identical, leading to a comparable volume fraction (V_f) and therefore comparable stiffness in each arm of the DCB specimens. If the variation in arm stiffness is comparable, the question about the difference in fracture toughness remains.

The only remaining aspect concerns processing variables and the affinity of the resin system to the fibres. In theory, the repair laminate system would have more processing variables than the pre-impregnated system because it is made outside of the optimum factory conditions (i.e. processing variation in vacuum control, temperature control and the introduction handling damage/defects are more likely with the repair laminate than the parent laminate). With all these possible-processing variations, it would be anticipated that the repair laminate would have lower fracture toughness. However this is not the case.

One possible reason for the repair resin having a higher fracture toughness is the resin's affinity to the different E-glass and Kevlar fibres. Both resin-fibre systems (eventually) have a global toughening due to fibre bridging, i.e. both materials reach a maximum energy release rate of ~2500 $J/m^2 \pm 200$ J/m^2 albeit at different crack lengths. However, the Ampreg 26 system attains this value considerable faster than the Ampreg 75 system. It seems reasonable to expect that the two resin systems have the same affinity to the E-glass but perhaps the Ampreg 26 resin system has greater affinity to the Kevlar fibres than the Ampreg 75 resin system. Following this assumption to its conclusion, it would

suggest that the Kevlar fibres impart some initial stiffening before sliding through the epoxy matrix and thus forming fibre bridging between the two failed surfaces.

5.3.3 Mode II fracture mechanics assessment

The mode II fracture toughness was characterised using the end loaded split test (ELS) configuration. In these tests two different pre-cracks were used to initiate the crack, namely a mode I and a mode II. Five specimens were evaluated in each configuration.

For the mode II End Loaded Split tests the corrected beam theory (CBT) data reduction method [Davies *et al*, 1999] have been used.

$$G_{IIC} = \frac{9P^2(a+\Delta_{II})^2}{4B^2Eh^3} \tag{5.2}$$

Where P is the load, a is the delamination length, Δ_{II} the correction for delamination tip rotation determined from Mode I tests using the DCB specimen, B is the width of the specimen, E is the Young's modulus parallel to the fibre direction, and h is the half-thickness of the specimen. Large displacement and load-block corrections have to be applied to equation (5.2) as follows:

$$G_{IIC(corrected)} = G_{IIC(CBT)}\left[1-\theta_1\left(\delta/L\right)^2-\theta_2\left(\delta I_1/L^2\right)\right] \tag{5.3}$$

with δ the displacement, I_1 the distance from the centre of the load-block to the midplane of the specimen beam to which the load-block is attached, and L the free length of the specimen. The correction factors θ_1 and θ_2 are calculated as follows:

$$\theta_1 = \frac{3}{20}\frac{\left[15+50\left(a/L\right)^2+63\left(a/L\right)^4\right]}{\left[1+3\left(a/L\right)^3\right]^2} \tag{5.4}$$

$$\theta_2 = -3\left(L/a\right)\frac{\left[1+3\left(a/L\right)^2\right]}{\left[1+3\left(a/L\right)^3\right]} \tag{5.5}$$

with a the delamination length and L the free length of the specimen.

The corrected beam theory (CBT) has been used to calculate the Mode II energy release rates. The full experimental data for the different Mode I and Mode II pre-cracks is contained in Appendix B.

A summary of the Mode II energy release rates with Mode I and Mode II pre-cracks for the parent laminate, the repair laminate and the repair-parent interface is presented in Figure 5.17 and Figure 5.18.

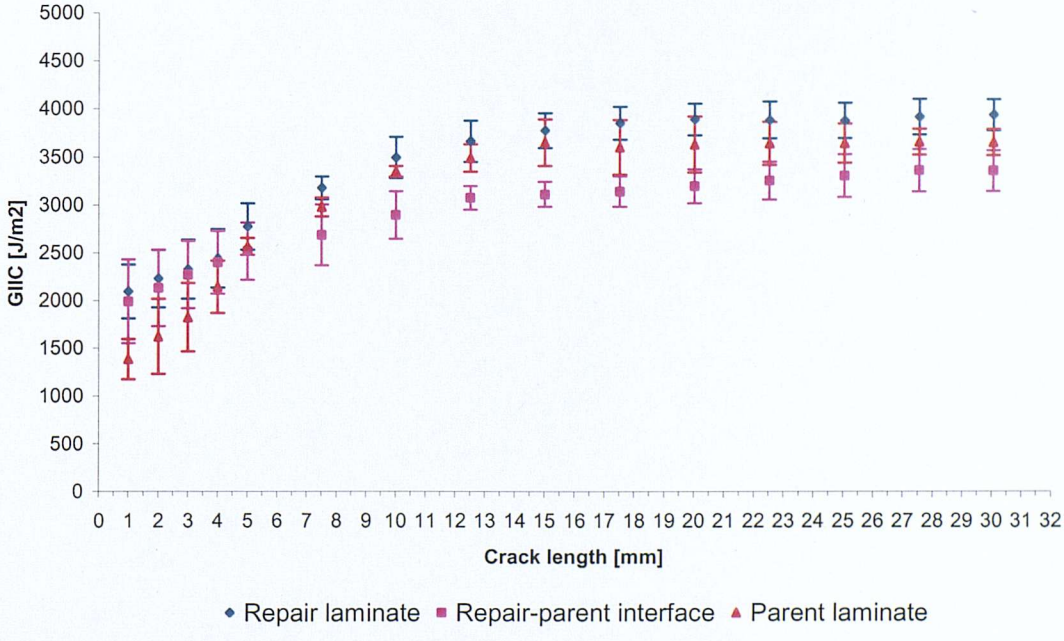

Figure 5.17: Summary of Mode II energy release rate versus crack length plot – mean values of all tested materials

The mode II fracture toughness results presented in Figure 5.17 for the three different material configurations illustrate similar characteristics to the G_{Ic} results in Figure 5.15.

In the G_{Ic} results the fracture energy appeared to plateau after the crack had propagated 25mm (typical energy levels of 2481 ± 121 J/m^2 for the repair laminate, 2416 ± 336 J/m^2 for the repair-parent interface laminate, and 1818 ± 125 J/m^2 for the parent laminate.

This observation can also be made of the G_{IIc} results with the repair laminate attaining a fracture plateau of 3883 ± 184 J/m^2, the repair-parent interface laminate attaining a fracture plateau of 3309 ± 223 J/m^2, and the parent laminate attaining a fracture plateau of 3647 ± 204 J/m^2. Whilst the formation of the fracture plateau occurs at the same time, the magnitude of the fracture energy is vastly different between the two different modes. At the start of the fracture plateau, the G_{IIc} results for the repair laminate are 1.7 times the G_{Ic} results. For the repair-parent interface the G_{IIc} results are 1.4 times the G_{Ic} results. The G_{IIc} fracture plateau is 2.1 times the G_{Ic} result.

A final observation concerns the extent of experimental scatter between the two different test methods. Composite materials tend to have extensive experimental scatter due to the variation in the basic constituents, variation in the manufacturing processes and experimental error. However, the experimental scatter is comparable for all the specimens tested in mode I and mode II with a mode I pre-crack.

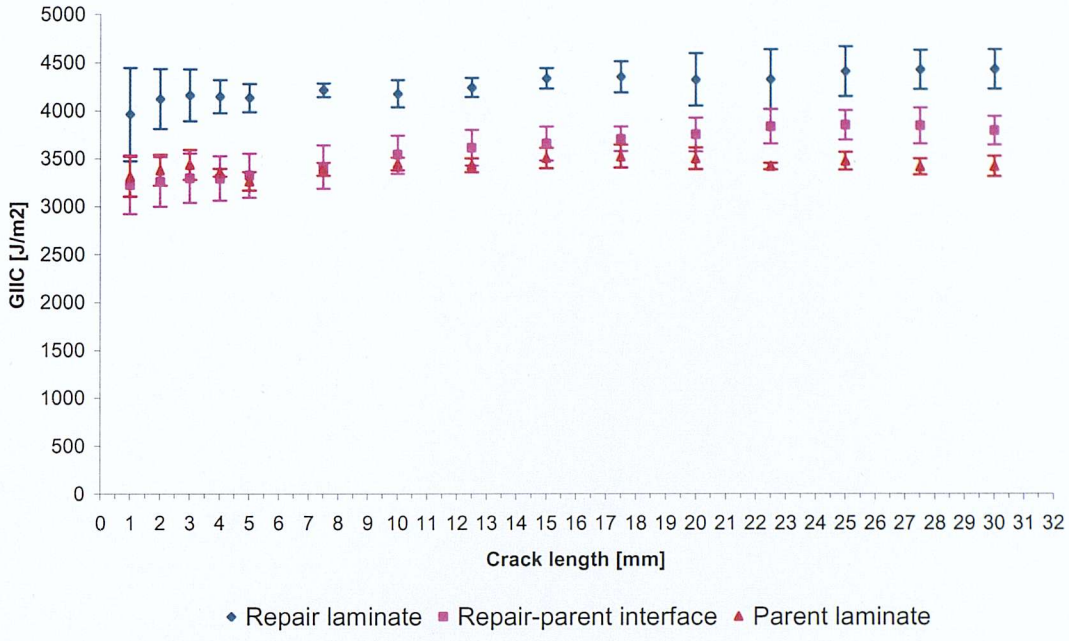

Figure 5.18: Summary of ELS fracture toughness result for all materials using a mode II pre-crack

Figure 5.18 confirms the results obtained by the ELS test method using a mode I pre-crack, i.e. the repair material has the highest fracture mode II toughness. The result for the parent laminate and the repair-parent interface is contrary to the result obtained through the application of a mode I pre-crack. The result for the parent laminate is comparable between the two different tests, i.e. 3476 ± 93 J/ m^2 with a mode II pre-crack and 3647 ± 204 J/m^2. However, the fracture toughness for the repair-parent interface is distinctively different, i.e. 3851 ± 154 J/m^2 for mode II pre-cracking compared with 3309 ± 223 J/m^2 for the mode I pre-cracking. Even considering the experimental scatter the results are still significantly different.

One possible explanation is due to the method of manufacture. The specimens represent the interface between a repair and the original parent laminate. To duplicate this interface the specimens are manufactured in two separate steps. Firstly the parent laminate is laid down and cured. Secondly, the repair laminate is applied via the hand lay-up process and then cured. Apart from the parent laminate having a second curing step that could alter the laminate behaviour, one obvious reason for the scatter concerns

the processing variability of the hand lay-up process. Since the specimens were extracted from different areas of the panel it can be speculated that the mode I pre-crack specimens contained more surface contamination. All that can be said with certainty is that the mode I pre-crack ELS specimens all came from the panel edge whist the mode II pre-crack ELS specimens came from the centre of the panel.

The influence of the pre-crack on the ELS fracture toughness has been summarised in Table 5.8. These results indicate that the mode I pre-crack influences the initial crack growth (~12mm) before the mode II fracture toughness attains a constant toughness plateau.

Material description	G_{IIC} initiation threshold	G_{IIC} plateau (recorded at 25mm)
Parent laminate – mode I pre-crack	1387 ± 214	3647 ± 204
Parent laminate – mode II pre-crack	3311 ± 207	3476 ± 93
Repair laminate – mode I pre-crack	2096 ± 281	3883 ± 184
Repair laminate – mode II pre-crack	3956 ± 487	4409 ± 259
Repair-parent laminate – mode I pre-crack	1996 ± 439	3309 ± 223
Repair-parent laminate – mode II pre-crack	3224 ± 307	3851 ± 154

Table 5.8: Influence of pre-crack upon mode II fracture toughness initiation threshold and plateau values

5.3.4 Mixed-mode fracture mechanics assessment

The Mixed-Mode Bending test (MMB) is a linear combination of two pure mode tests; the DCB (mode I) and the End notched flexure - ENF (mode II). The MMB uses a lever arrangement to introduce the pure mode I and mode II components simultaneously into a conventional DCB test specimen. By varying the length of the lever, a wide spectrum of mixed-mode loading ratios can be applied to the test piece. This section will detail the results obtained from the mixed mode tests conducted on the parent laminate, the repair laminate and the repair-parent interface. Due to resource constraints only the following ratios were considered:

- 75% G_I parent laminate

- 50% G_I parent laminate
- 25% G_I parent laminate
- 50% G_I repair laminate
- 50% G_I repair-parent interface

The experimental results for the mixed-mode fracture mechanics tests for the parent laminate, the repair laminate and the repair-parent interface is given in Table 5.9.

	Parent laminate		Repair laminate		Repair-parent interface	
	Initiation	Propagation	Initiation	Propagation	Initiation	Propagation
25% Mode II / 75% Mode I	539 ± 126	952 ± 30	-	-	-	-
50% Mode II / 50% Mode I	934 ± 111	1394 ± 216	1262 ± 169	2402 ± 245	1070 ± 17	1556 ± 150
75% Mode II / 25% Mode I	541 ± 190	1256 ± 252	-	-	-	-

Table 5.9: Crack initiation and propagation fracture toughness values obtained for various mixed-mode ratios for parent laminate, repair laminate and repair-parent interface

To illustrate the comparative performance of the different material configurations, a summary of the mixed-mode test results using the MMB test method, with the pure mode I (DCB) and pure mode II (ELS) test results has been detailed in Figure 5.19. Each specimen is represented with a crack initiation (dotted line) and crack propagation value (solid line).

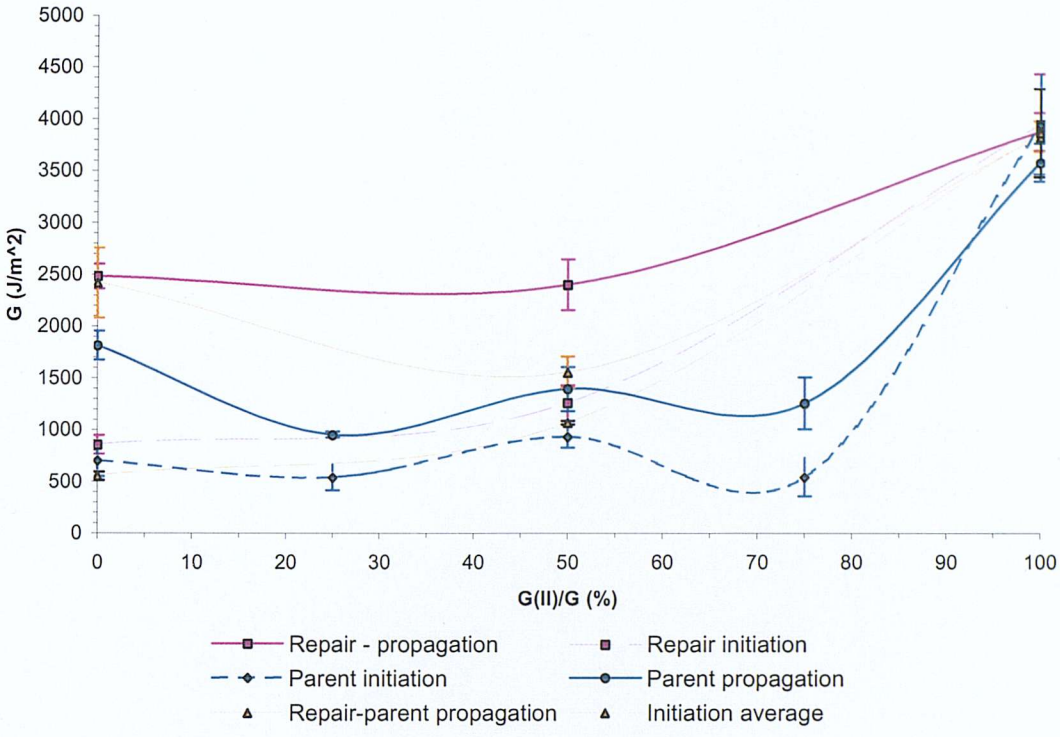

Figure 5.19: Summary of mixed-mode bending tests and pure mode I and pure mode II results

Figure 5.19 clearly indicates the fracture toughness hierarchy for the three different materials at varying mixed-mode ratios. These will now be discussed in turn.

The mixed mode evaluation for the parent laminate is presented in Figure 5.19 contains the MMB test results for 75% G_I, 50% G_I and 25% G_I with the pure mode I (DCB) and pure mode II (ELS) test data for crack initiation and crack propagation. The latter is defined as 25mm crack length in the DCB and ELS, and the maximum fracture toughness occurring after 10mm crack length in the MMB samples. The data is presented as initiation and propagation points. This approach was used to highlight the influence of crack branching and fibre bridging. In the case of pure mode I, the initiation and propagation values are over 1000 J/m^2 apart. Whilst at pure mode II, the initiation and propagation values are comparable, especially considering the experimental scatter. This result reflects the observations observed during the pure mode tests.

In general, as the mode II contribution of the MMB test increases the possibility of fibre bridging should reduce. However, the test data for the initiation and propagation crack growth for the parent laminate indicate the existence of fibre bridging at 75% G(II)/G.

Although the data in Figure 5.19 for the parent laminate contains considerable scatter, there is a suggestion of a 'hump' in the data at 50% mode I. Greenhalgh *et al* [Greenhalgh *et* al. 1999] reported humps in the mixed-mode failure loci but this occurred at higher mode I ratios where a small contribution of mode I interacts positively to improve the fracture toughness. The increase in fracture toughness was attributed to crack propagation on two different interfaces, namely the 0°/90° ply interface being tougher than the 0°/0° ply interface [Greenhalgh *et* al. 1999]. The MMB crack was initially propagated within the –45° ply before propagating along the -45°/90° ply interface and then at longer crack lengths in the 90°/45° ply interface. In addition to changing ply failure interfaces extensive fibre bridging was observed suggesting a complex crack path through the specimen that will increase the fracture toughness of the system.

In a similar approach to the mixed-mode tests undertaken on the parent laminate, the mixed-mode performance of the repair laminate was assessed. The mixed-mode failure envelope presented in Figure 5.19 follows a similar trend observed in the parent laminate with at least $1000J/m^2$ separating the initiation and propagation values at pure mode I and at 50% mode I. Conversely, at 100% mode II the initiation and propagation values are almost identical. The result again highlights the important role fibre bridging plays in arresting crack propagation. The principle observation arising from the G_I/G_{II} response of the repair laminate is its increased toughness, compared to the parent laminate, at the 50% mixed-mode ratio. Unfortunately, due to the lack of data at any other mixed-mode ratio, the fracture toughness 'hump' observed at 50% mode I in the parent laminate is not apparent within the repair laminate.

The G_I/G_{II} response for the repair-parent interface is considered in Figure 5.19. The fracture toughness tests presented in the figure only consider the pure mode I, pure mode II and the 50% mixed-mode ratio. Unfortunately, these results are insufficient to

determine whether the fracture toughness 'hump' phenomena would also occur within this material combination. The key observation that can be drawn from these experiments is that the 50% mixed-mode toughness value for the repair-parent interface lies between the corresponding mixed-mode ratios for the parent and repair laminates. The results once again illustrate the influence of crack toughening mechanism (i.e. Kevlar fibre bridging) at ratios containing a mode I component.

In summary, the repair laminate has the highest fracture toughness whilst the parent laminate has the lowest. The fracture toughness of the repair-parent interface is contained within the upper bounds of the repair laminate and the lower bounds of the parent laminate. At the pure mode I and pure mode II ends of the spectrum the fracture toughness of the repair-parent interface is biased towards the repair laminate but it migrates towards the parent laminate at 50% mixed-mode ratio. The changing influence of the mode ratio, and how this effects the crack front propagation, is of critical concern to the design engineer since the formation of dynamic damage to operational craft, and the subsequent crack propagation is likely to be outside the standard pure mode ratios. The role of the surrounding structure and the complex load paths within them are likely to have a significant influence over the damage formation and propagation within composite structures. In dynamic events that are governed by energy thresholds, the failure path will select the route of least resistance. In the case of an impact event to a structural repair, Figure 5.19 suggests that the parent laminate will experience the first crack formation. If the load path within the impact site only permits the delamination to grow in pure mode II a limited amount of damage will occur. Conversely, if the load path is such that a mixed mode component exists the delamination could initiate at an energy level a third lower, thereby producing a delamination area 3 times the size. This clearly is of concern to any structural engineer.

5.3.5 Discussion of experimental fracture mechanics results

The observations arising from the experimental fracture mechanics tests has indicated that the repair laminate has a higher fracture toughness than the corresponding parent laminate at all pure mode and mixed-mode ratios considered. Although both resin systems (the pre-impregnated version and the liquid resin) are supposed to be identical, one possible reason for the increased toughness of the repair material is the processing

route. In the hand lay-up process, the repair resin is manually introduced to the cloth and then vacuum consolidated. In comparison to the prepreg material the thickness of the individual repair plies is greater, suggesting a greater volume of resin to 'wet-out' the dry glass and Kevlar fibres. It is the repair resin's greater affinity to the Kevlar fibres that enhances the initial laminate toughness by resisting Kevlar fibre pullout before the fibre bridging has commenced. Fibre bridging of the Kevlar fibres across the crack interface was observed for all fracture mechanics tests containing a mode I component

At the pure mode I and pure mode II ends of the toughness spectrum the fracture toughness of the repair-parent interface is biased towards the repair laminate but it migrates towards the parent laminate at 50% mixed-mode ratio. Examination of the failure surfaces indicated the crack had migrated and then subsequently grown within the parent half of the repair-parent laminate. At the pure mode I and mode II loading the crack had grown within the repair halve of the repair-parent specimens.

Finally, in the FMECA assessment damage formation along the tapered interface was identified as a critical damage location. In Chapter 4 the problems of manufacturing a fracture mechanics specimen representative of the tapered interface were discussed and a recommendation was made not to include these specimens within this evaluation. Although no experimental data exists for this location, it is possible to hypothesise how this interface would perform in these tests. Firstly, it was observed that the repair material and the repair-parent (horizontal) interface all had higher fracture toughness than the parent laminate. Secondly, the influence of the fibre bridging by the Kevlar fibres significantly increased the toughness value when the crack experienced a Mode I contribution. Due to these experimental findings and the observation of the exposed fibre Kevlar fibre ends 'brooming' at the machined repair-parent tapered interface, it is the author's believe that the fracture toughness would be superior to the parent laminate at all mixed-mode ratios. Whether the toughness of repair-parent tapered interface would be greater than the repair-parent horizontal interface and closer to the pure repair laminate is also probable but not yet proven. Regardless of the fracture toughness hierarchy between the two repair interfaces (horizontal or tapered) it can be concluded that the repair-parent interface has a greater fracture toughness than the parent laminate,

and therefore a lower criticality risk for damage propagation. However, this can only be confirmed through residual strength testing.

5.3.3 Theoretical prediction of damage onset

In Table 2.5, analytical solutions were identified for the prediction of the impact damage within a composite laminate and composite sandwich structure. In Table 5.1 the experimental results for the different fracture mechanics tests are presented. In this section the experimental results will be used to assess the performance of the different formulas to predict the onset of impact delamination damage. This assessment is presented in Table 5.10 and compared with the experimental data determined in Section 5.2.

Author	**Formula**	**Predicted critical energy threshold for delamination onset (J)**					
		Parent		**Repair**		**Repair-parent overlaminate**	
Experimental data		*635*		*780*		*975*	
[Dorey, 1987]	$Energy = \frac{2\tau^2 wL^3}{9E_f t}$	544		443		423	
[Zhou, 1995]	$P = \frac{4\pi}{3}\tau tr$	654		770		657	
[Davies *et al*, 1996]	$P_c^2 = \frac{8\pi^2 E(2h)^3}{9(1-\upsilon^2)} G_{IIC}$	446 ±36	717 ±19	484 ±34	659 ±16	510 ±60	707 ±14
[Olsson, 2002]	$F_{dth} = \pi\sqrt{32 D_f G_{IIc}/3}$	623 ±46	1001± 51	756 ±102	961 ±52	926 ±205	1258 ±49

Table 5.10: Critical energy threshold predictions by ILSS and Mode II fracture toughness equations

The impact energy threshold predictions by [Dorey, 1987] and [Zhou, 1995] utilise the ILSS properties of the individual materials whilst the predictions by [Davies *et al*, 1996] and [Olsson, 2002] require detailed knowledge of the mode II fracture toughness. However, it should be noted that the prediction by [Zhou, 1995] is dependent upon the initial defect size (see equation 5.6):

$$a_0 = \frac{E_a G_c}{\pi \sigma_a^2} \tag{5.6}$$

where G_c is the critical mode II fracture toughness for each laminate system.

The mode II fracture toughness determined for the parent laminate, repair laminate and the repair-parent interface yield the initial defect sizes given in Table 5.11.

	Pure Mode II fracture toughness (J/m^2)	Corresponding defect size (mm)
Parent laminate	3583 ± 184	0.52 – 0.57
Repair laminate	3883 ± 184	0.61 – 0.66
Repair-parent interface	3309 ± 223	0.51 – 0.58

Table 5.11:Determination of critical defect size as a function of mode II fracture toughness

The result in Table 5.11 illustrates the importance of correctly determining the mode II fracture toughness of the laminate and how this property will influence the damage threshold prediction.

A comparison of the critical energy threshold predictions based on ILSS properties, with the experimental data for delamination onset within the parent laminate and the repair-parent interface, suggests that the closed form solution proposed by [Dorey, 1987] under-predicts the threshold whilst the approach by [Zhou, 1995] slightly over-predicts the parent laminate threshold. This result suggests that the initial defect size derived by Equation 5.5 and indicated in Table 5.11 is too small to be used as an initial defect size.

Table 5.10 also examines the variation in the impact threshold value when the mode I to mode II ratio is varied. Each result for the different ratios is split into two columns. The first column considers the threshold energy calculated with fracture toughness value

required for crack initiation whilst the second column considers the threshold energy calculated with the fracture toughness value for crack propagation. The reason both fracture toughness values were considered for this calculation was to consider the energy required by the initiation impact event to cause damage, and also the energy required to drive the 'formed' crack through the structure. As Table 5.10 suggests, the impact energy required to drive the 'formed' crack through the structure is greater than its initiation energy. Whilst the crack may not be driven any further along the laminate, the initial damage may still be sufficient to cause a significant drop in the mechanical performance of the structure.

5.3.4 Theoretical Prediction of Crack Growth

In addition to the prediction methods used for delamination onset, some authors have also tried to predict the size of delamination likely to occur for a known energy. Table 2.5 presents three methods for predicting the delamination size after an impact.

The theoretical predictions proposed by [Davies & Zhang, 1995] and [Olsson, 2002] for determining the delamination size for known impact energy have been plotted in Figure 5.20.

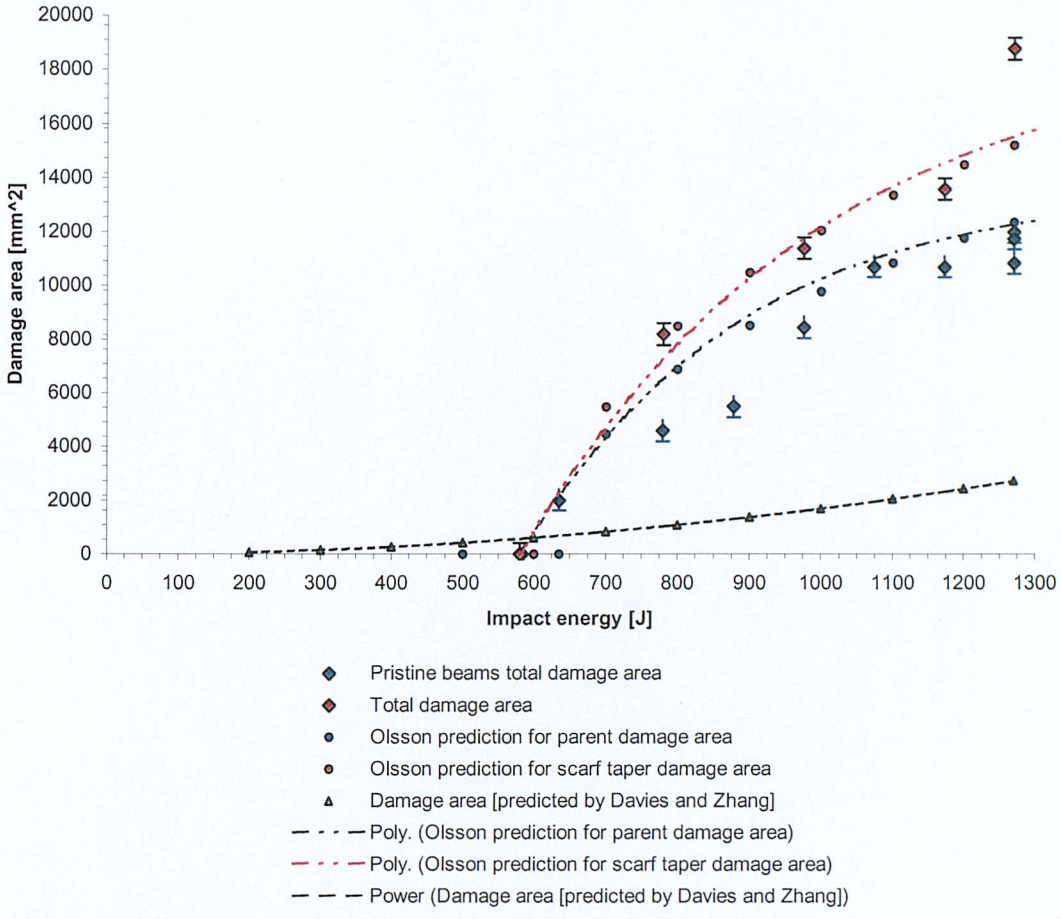

Figure 5.20: Delamination size predictions within the parent laminate and repair for known impact energies.

To determine which theoretical approach correctly predicts the damage size as a function of impact energy Figure 5.20 also includes the experimental results for damage length as a function of impact energy for the parent laminate and the repair laminate. The theory proposed by [Davies & Zhang, 1995], based upon the ILSS performance of the chosen material, suggests that damage progressively increases as the impact energy increases. This progressive damage build up was not observed during the experimental programme. The ILSS theory also significantly under predicts the magnitude of the damage occurring for known impact energy.

The theory developed by [Olsson, 2002] determines the magnitude of damage developed as a function of the dynamic crush stress of the core material, the number of

delaminations formed and the known energy for damage initiation. The dynamic crush stress (qd) of H130 PVC foam core was determined in the research by Hoo-Fat and Park [Hoo-Fat and Park, 2001] to be:

$$qd_{H130} = q_{H130static} \times 1.67 \qquad \text{Equation (5.7)}$$

where $q_{H130static}$ = 2.2MPa (obtained from DIAB Dinvinycell Technical Data Sheet)

The parent laminate delamination length prediction by Olsson in Figure 5.20 was determined using the H130 dynamic core stress of 3.67MPa assuming four dominant delaminations (n=4) and a parent laminate damage threshold of 635J. This result shows good agreement with the experimental results and captures the trend of damage formation within the parent laminate.

The second prediction by [Olsson, 2002] attempts to capture the damage formation within the tapered scarf repair scheme. In this particular case it is assumed that as many as five delaminations govern the failure process, i.e. four within the laminate (the same as the parent laminate) and one additional crack within the vertical adhesive (see Figure 5.2). The determination of the dynamic crush stress of the H130 PVC foam core at this location is complicated by the impact event being directly over a vertical adhesive joint. It is assumed that this additional bondline will improve the dynamic crush resistance of the foam. The magnitude of this additional hardening effect is uncertain but a 30% increase shows good agreement with the experimental results.

5.4 Concluding remarks

The purpose of this chapter is to generate the theoretical and practical understanding of 'Impact Damage Tolerance' and 'Fracture and Crack Growth' of a repaired composite sandwich structure in support of the fracture mechanics assessment identified in Figure 3.1, Chapter 3. In terms of the overall objectives of (1) evaluating the impact response of structural repairs contained within composite sandwich structures and (2) determining the damage tolerance performance of a structural repair, it has been observed that:

1. At damage locations coinciding with the start of the tapered scarf repair, the damage formation is influenced by the internal geometry of the taper angle and replacement foam core. At this location the damage size has almost doubled for the same impact energy indicating the tapered scarf repair is less damage tolerant than the parent laminate.
2. At a critical energy level, damage can form between the repair overlaminate and the parent laminate. This result suggests that an impact energy threshold exists for the initiation of a crack at the repair edge thus making the current repair designs for the minimisation of peel stresses inappropriate in regions of high impact probability.
3. The repair laminate has the highest fracture toughness at all pure mode and mix-mode ratios considered whilst the parent laminate had the lowest. Depending upon the mix-mode ratio, the fracture toughness of the repair-parent interface was either biased towards the repair laminate (Mode I and Mode II) or the parent laminate (50% Mode I).
4. The theoretical prediction by [Olsson, 2002] is able to capture the toughness value to initiate crack growth in all three laminates. In comparison, [Davies *et al*, 1996] is only able to capture the parent laminate.
5. The application of the damage propagation theories had mixed results. The theory based upon ILSS by [Davies *et al*, 1996] was unable to capture the damage trends. Conversely, the model proposed by [Olsson, 2002], which relies upon the dynamic crush performance of the core material and knowledge of the damage initiation threshold, is able to capture the magnitude and trend of the damage formation within the sandwich beams. The simplistic nature of this closed form solution is ideal as a tool to predict operational damage formation in real composite structures.
6. If the two theoretical predictions by [Olsson, 2002] are used in conjunction then the damage initiation and propagation characteristics of the tapered scarf repair to the sandwich beam can be successfully captured from the fracture mechanics data produce within this project.

The findings from this work will assist in the understanding of the strength based assessment in Chapter 6, in addition to help generate the damage tolerance guidelines within Chapter 7.

6 STRENGTH BASED ASSESSMENT

6.1 Introduction

In Chapter 3, the design methodology behind the damage tolerance assessment of repaired composite sandwich structures was defined. In this methodology there are three critical elements. The first, the Fracture Mechanics Assessment, was detailed in Chapter 5. The second element will be discussed in this Chapter, namely the Strength Based Assessment. The final part of the design methodology, the Repair Structural Integrity Assessment, encapsulating the damage tolerance assessment for structural repairs to composite sandwich structures will be addressed in Chapter 7.

In Figure 3.1 the format of the strength based assessment was defined, i.e. a static assessment and a fatigue assessment of the pristine, damaged-pristine, repaired and damaged-repaired beams. The purpose of this chapter is to illustrate the results for the strength-based assessment of the pristine, pristine-damaged, repaired and the damaged-repaired beams. To illustrate the scope of this test programme, Table 6.1 and 6.2 have been produced for the pristine and repaired beams respectively.

<table>
<tr><td rowspan="2">Sample ID</td><td colspan="4">Test evaluation method with corresponding test data location</td></tr>
<tr><td colspan="2">Impact testing (Impact energy/ data location)</td><td>Static strength assessment</td><td>Residual strength assessment</td><td colspan="2">Fatigue test (USL loading/ data location)</td></tr>
<tr><td>Pr. 1</td><td colspan="2" rowspan="4"></td><td rowspan="4">Table 6.3
Figure 6.1</td><td rowspan="4"></td><td colspan="2" rowspan="4"></td></tr>
<tr><td>Pr. 2</td></tr>
<tr><td>Pr. 3</td></tr>
<tr><td>Pr. 4</td></tr>
<tr><td>Pr. 5</td><td>200J</td><td rowspan="4">Figure 6.2</td><td rowspan="4"></td><td rowspan="4">Table 6.4
Figure 6.3</td><td colspan="2" rowspan="4"></td></tr>
<tr><td>Pr. 6</td><td>387J</td></tr>
<tr><td>Pr. 7</td><td>635J</td></tr>
<tr><td>Pr. 8</td><td>1200J</td></tr>
<tr><td>Pr. 9</td><td colspan="2" rowspan="8"></td><td rowspan="8"></td><td rowspan="8"></td><td>60%</td><td rowspan="8">Table 6.5
Table 6.6
Figure 6.9
Figure 6.10</td></tr>
<tr><td>Pr. 10</td><td>60%</td></tr>
<tr><td>Pr. 11</td><td>60%</td></tr>
<tr><td>Pr. 12</td><td>50%</td></tr>
<tr><td>Pr. 13</td><td>50%</td></tr>
<tr><td>Pr. 14</td><td>40%</td></tr>
<tr><td>Pr. 15</td><td>40%</td></tr>
<tr><td>Pr. 16</td><td>40%</td></tr>
</table>

Table 6.1: Overview of pristine beam testing programme

<table>
<tr><td rowspan="2">Sample ID</td><td colspan="5">Test evaluation method with corresponding test data location</td></tr>
<tr><td colspan="2">Impact testing (Impact energy/ data location)</td><td>Static strength assessment</td><td>Residual strength assessment</td><td colspan="2">Fatigue test (USL loading/ data location)</td></tr>
<tr><td>Rp. 1</td><td colspan="2" rowspan="4"></td><td rowspan="4">Table 6.5
Figure 6.5</td><td rowspan="4"></td><td colspan="2" rowspan="4"></td></tr>
<tr><td>Rp. 2</td></tr>
<tr><td>Rp. 3</td></tr>
<tr><td>Rp. 4</td></tr>
<tr><td>Rp. 5</td><td>583J</td><td rowspan="5">Figure 6.6</td><td rowspan="6"></td><td rowspan="6">Table 6.6
Figure 6.8</td><td colspan="2" rowspan="6"></td></tr>
<tr><td>Rp. 6</td><td>779J</td></tr>
<tr><td>Rp. 7</td><td>976J</td></tr>
<tr><td>Rp. 8</td><td>1171J</td></tr>
<tr><td>Rp. 9</td><td>1270J</td></tr>
<tr><td>Rp. 10</td><td>1270J</td><td>Table 6.6</td></tr>
<tr><td>Rp. 11</td><td colspan="2" rowspan="8"></td><td rowspan="9"></td><td rowspan="9"></td><td>80%</td><td rowspan="8">Table 6.9
Table 6.10
Figure 6.11
Figure 6.15</td></tr>
<tr><td>Rp. 12</td><td>60%</td></tr>
<tr><td>Rp. 13</td><td>60%</td></tr>
<tr><td>Rp. 14</td><td>60%</td></tr>
<tr><td>Rp. 15</td><td>40%</td></tr>
<tr><td>Rp. 16</td><td>40%</td></tr>
<tr><td>Rp. 17</td><td>40%</td></tr>
<tr><td>Rp. 18</td><td>30%</td></tr>
<tr><td>Rp. 19</td><td colspan="2">Table 6.9</td><td>20%</td><td>Figure 6.11</td></tr>
</table>

Table 6.2: Overview of tapered scarf repaired beam testing programme

6.2 Static strength assessment of undamaged and damaged 'pristine' beams

The static strength tests were completed following the American Society for Testing and Materials (ASTM) standard C393-00 for the four-point loading: "Standard Test Method for Flexural Properties of Sandwich Constructions". The specimen geometry and loading arrangement is outline in Chapter 4 with all tests being conducted on the Denison Mayes Group (DMG) 250 kN servo hydraulic testing machine located in the Civil Engineering Laboratory at the University of Southampton.

The tests on the virgin sandwich beams will provide the baseline comparison to assess all repaired and damaged beams against. The test results for the pristine beams loaded in four-point bend are provided in Table 6.3 and Figure 6.1.

The face bending stress and core shear stress were calculated according to ASTM C393-00, using the following formulas for two-point load at one-quarter span.

The face bending stress, σ, MPa, is given as:

$$\sigma = \frac{PL}{4t(d+c)b} \tag{6.1}$$

The tensile and compressive faces of the sandwich beam were defined in Chapter 4, Figure 4.3.

The core shear stress, τ, MPa, is given as:

$$\tau = \frac{P}{(d+c)b} \tag{6.2}$$

The face buckling stress, σ_{cr}, MPa, is given by Zenkert [Zenkert, 1995] as:

$$\sigma_{cr} = 0.85\sqrt[3]{E_f E_c G_c} \tag{6.3}$$

where:

P = load, N

L = span length, mm

t = facing thickness, mm

d = sandwich thickness, mm

c = core thickness, mm

b = sandwich width, mm

E_f = bending stiffness of the face

E_c = core out-of-plane stiffness

G_c = core out-of-plane shear stiffness

Loading	Samples	Failure Load (kN)	Failure Displacement (mm)	Core shear stress (MPa)	Tensile face bending stress (MPa)	Compressive face bending stress (MPa)	Failure Mode
Four point bending	Pr. 1	63.8	52.5	1.69	253.8	149.0	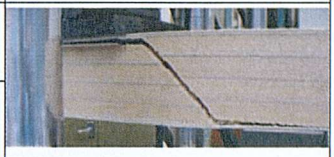
	Pr. 2	67.5	56.1	1.71	255.7	156.0	
	Pr. 3	64.0	54.8	1.69	252.5	153.5	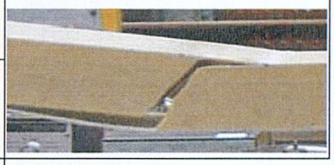
	Pr. 4	62.5	54.7	1.68	253.4	147.0	
Average		64.5	54.5	1.69	253.9	151.4	
Standard deviation		2.1	1.5	0.01	1.3	4.1	

Table 6.3: Failure load and failure mechanisms for pristine beams

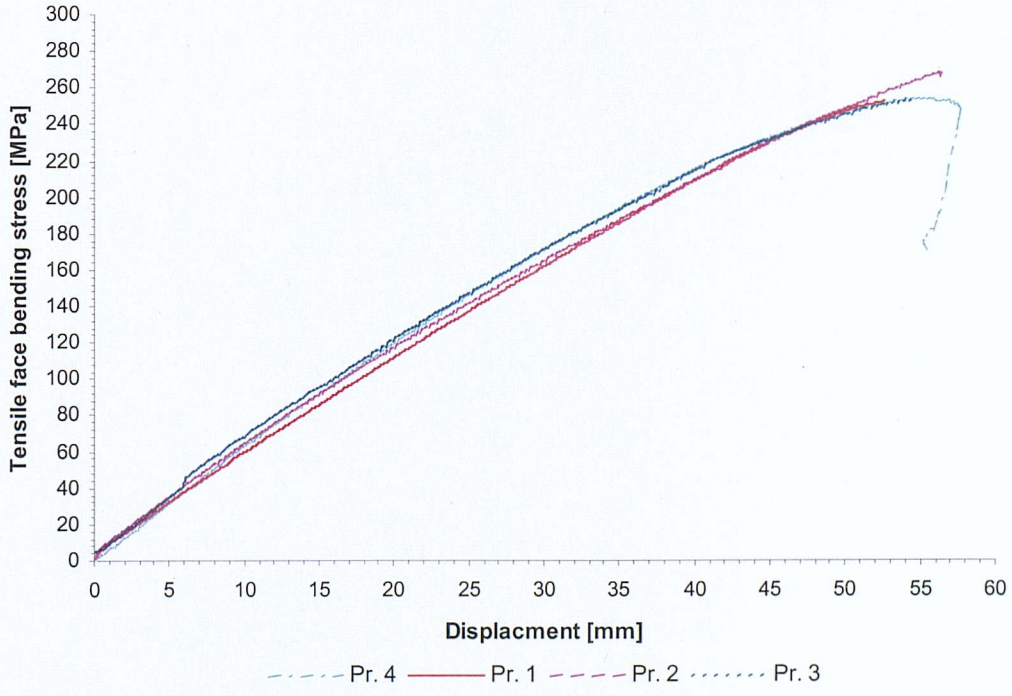

Figure 6.1: Inner skin tensile stress-displacement response for pristine beams

Figure 6.1 illustrates the compressive stress in the outer skin up to and including failure. The beams all failed by catastrophic core shear failure located between the outer support points and the inner loading points. No particular preference in failure side was observed, leading to the assumption that the test set-up was balanced. The inner and outer skin appeared to be free of any damaged.

To understand the influence of impact damage on the static performance of composite sandwich beams, a series of tests on pristine beams has been undertaken. The impact tests were conducted using the same test methodology developed in the previous chapter. The residual static outer skin stress as a function of varying impact energies is indicated in Figure 6.2.

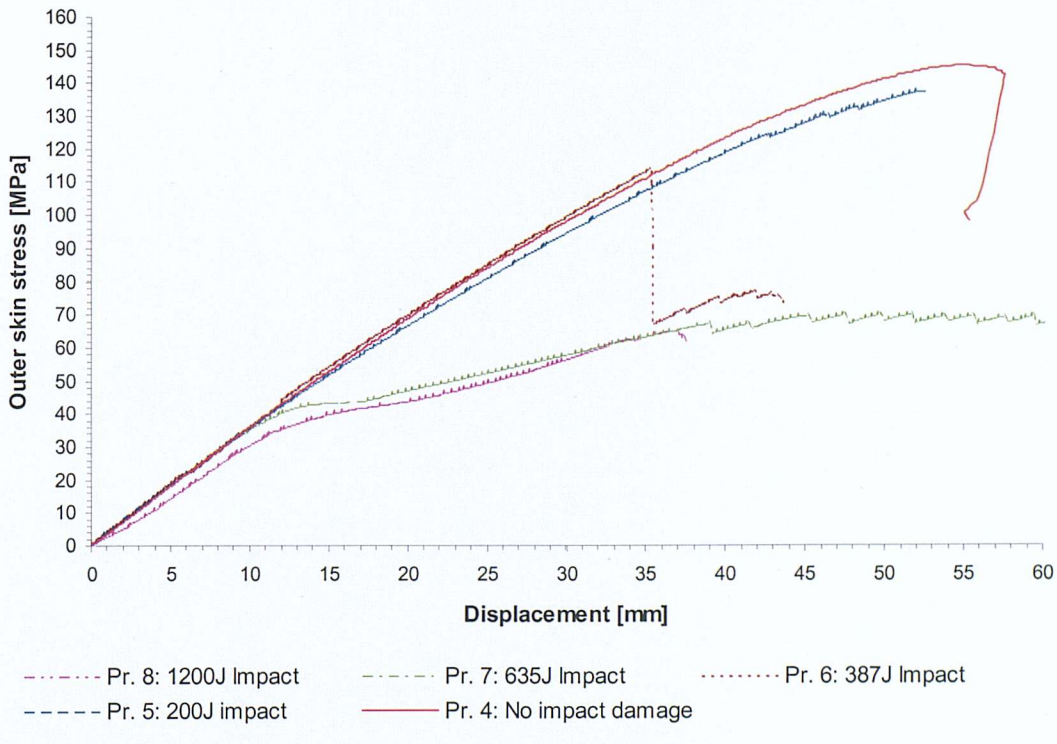

Figure 6.2: Outer skin stress versus varying impact energies.

Sample ID	Impact energy	Delamination area (mm^2)	Failure load (kN)	Compressive stress (MPa)	Failure mode
Pr. 4	0J	0	62.5	145.2	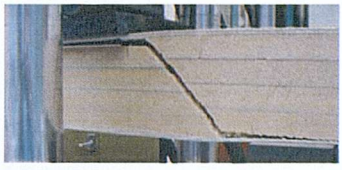
Pr. 5	200J	0	59.2	137.5	
Pr. 6	387J	360	46.1	107.1	
Pr. 7	635J	2565	15.2	35.3	
Pr. 8	1200J	20633	12.3	28.6	

Table 6.4: Static residual strength and failure mode results for pristine beams

The results in Figure 6.2 and Table 6.4 suggest that low impact energies (200J) have relatively little effect on the residual outer skin failure stress whilst high-energy impacts (>635J) have a significant effect on the residual failure stress. The slightly surprising result in Figure 6.2 is the reduction in stress for the 387J impact. In the previous impact work, a 387J impact was insufficient to cause any delamination damage in the outer skin but was sufficient to generate a residual dent of approximately 0.5mm. This research illustrates that the outer skin failure stress could be reduced by up to 18% for a skin indentation of only 0.5mm.

To illustrate the drastic reduction in the residual outer skin failure stress as a function of dent depth and delamination damage size Figure 6.3 has been generated. The residual strength is determined using the following formula:

$$\text{Compressive residual stress} = \frac{\text{compressive face bending stress for each impact energy level}}{\text{compressive face bending stress from static tests}} \tag{6.4}$$

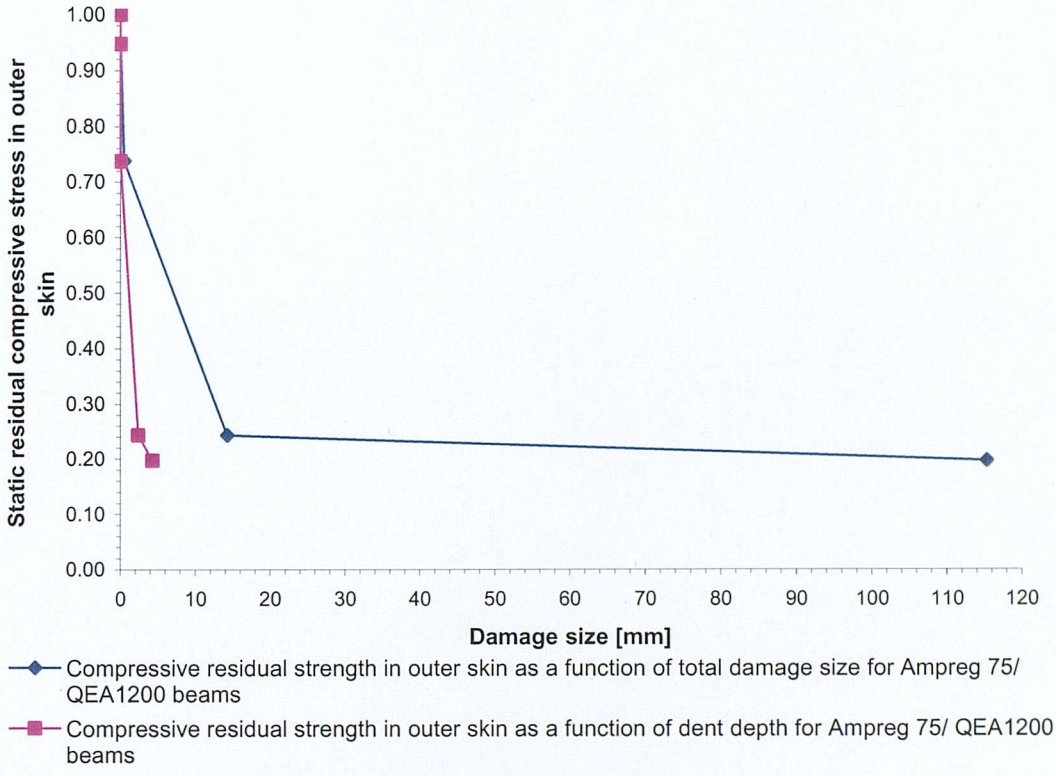

Figure 6.3: Residual compressive stress in the outer skin as a function of damage size for pristine beams

6.3 Static strength assessment of undamaged and damaged tapered scarf repair

The static flexural performance of the tapered scarf repair was assessed using the four-point bend test. The dimensions and terminology of the repair scheme within the sandwich beam was defined in Chapter 4, Figure 4.1. The experimental test set-up, with one roller and one fixed support above and below the specimen, was defined in Chapter 4, Figure 4.3 and is shown in Figure 6.4.

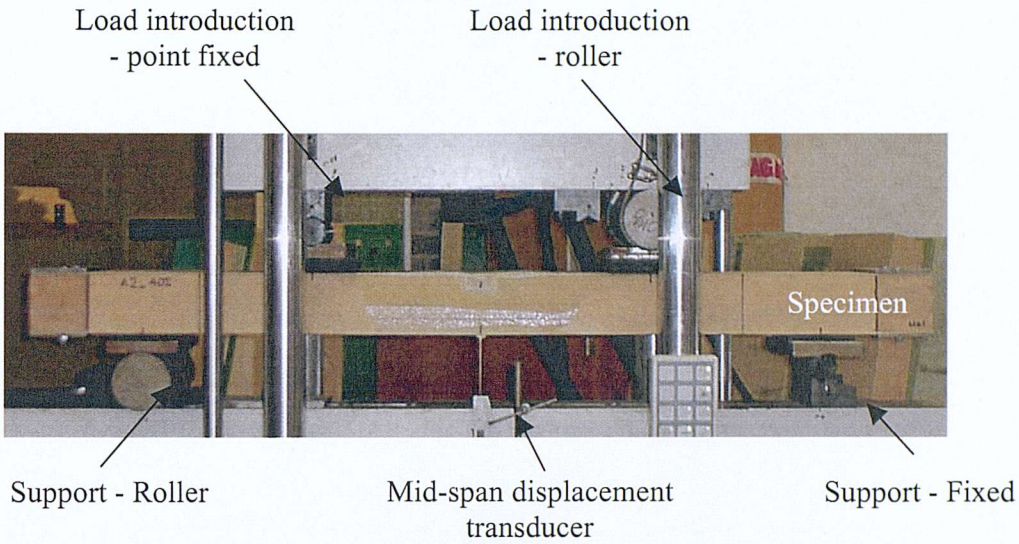

Figure 6.4: Four-point bend experimental set-up with two fixed and two roller load introduction/support points

Four different specimens were loaded to failure to ascertain the load-displacement response of the repaired sandwich beam. The results for these tests have been illustrated in Figure 6.5 and Table 6.5.

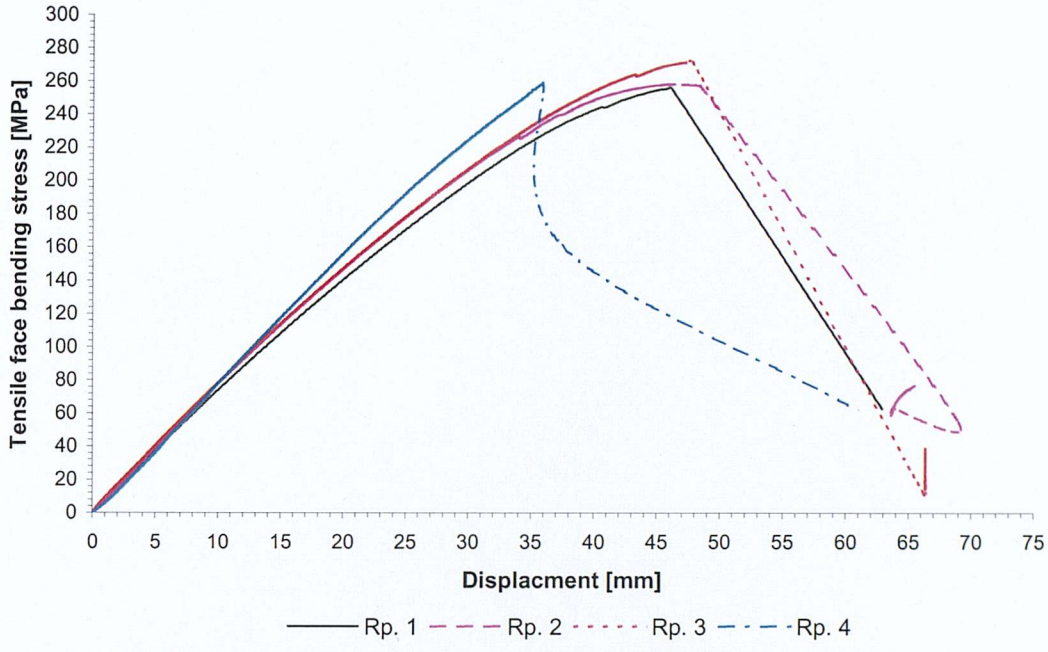

Figure 6.5: Tensile stress-displacement response for 20:1 tapered scarf repair

Loading	Samples	Failure Load (kN)	Failure Displacement (mm)	Core shear stress (MPa)	Tensile face bending stress (MPa)	Compressive bending stress (MPa)	Failure Mode
Four point bending	Rp. 1	69.7	46.1	1.70	256.6	155.0	
	Rp. 2	70.6	45.7	1.72	257.7	156.2	
	Rp. 3	75.8	47.7	1.81	271.1	155.1	
	Rp. 4	62.4	35.9	1.60	259.0	149.1	
Average		69.6	43.9	1.71	261.1	153.8	
Standard deviation		5.5	5.4	0.1	6.7	3.2	

Table 6.5: Failure load and failure mechanisms for 20:1 tapered scarf repair

The results presented in Table 6.5 show the relative experimental scatter for the 20:1 repair scheme. Typically, a failure load of 69.6 ± 5.5 kN resulting in a inner skin failure tensile stress of 261.1 ± 6.7 MPa. The mode of failure for each of the samples was governed by the performance of the core with core shear cracks between the inner and outer rollers causing catastrophic failure. The 20:1 repair scheme remained intact for the duration of the test.

To determine the static residual performance of the tapered scarf repairs, the beams used in Chapter 5 to determine the threshold energy for delamination initiation were tested in four-point bending using the test methodology outlined previously. The test results are given in Figure 6.6 and Table 6.6.

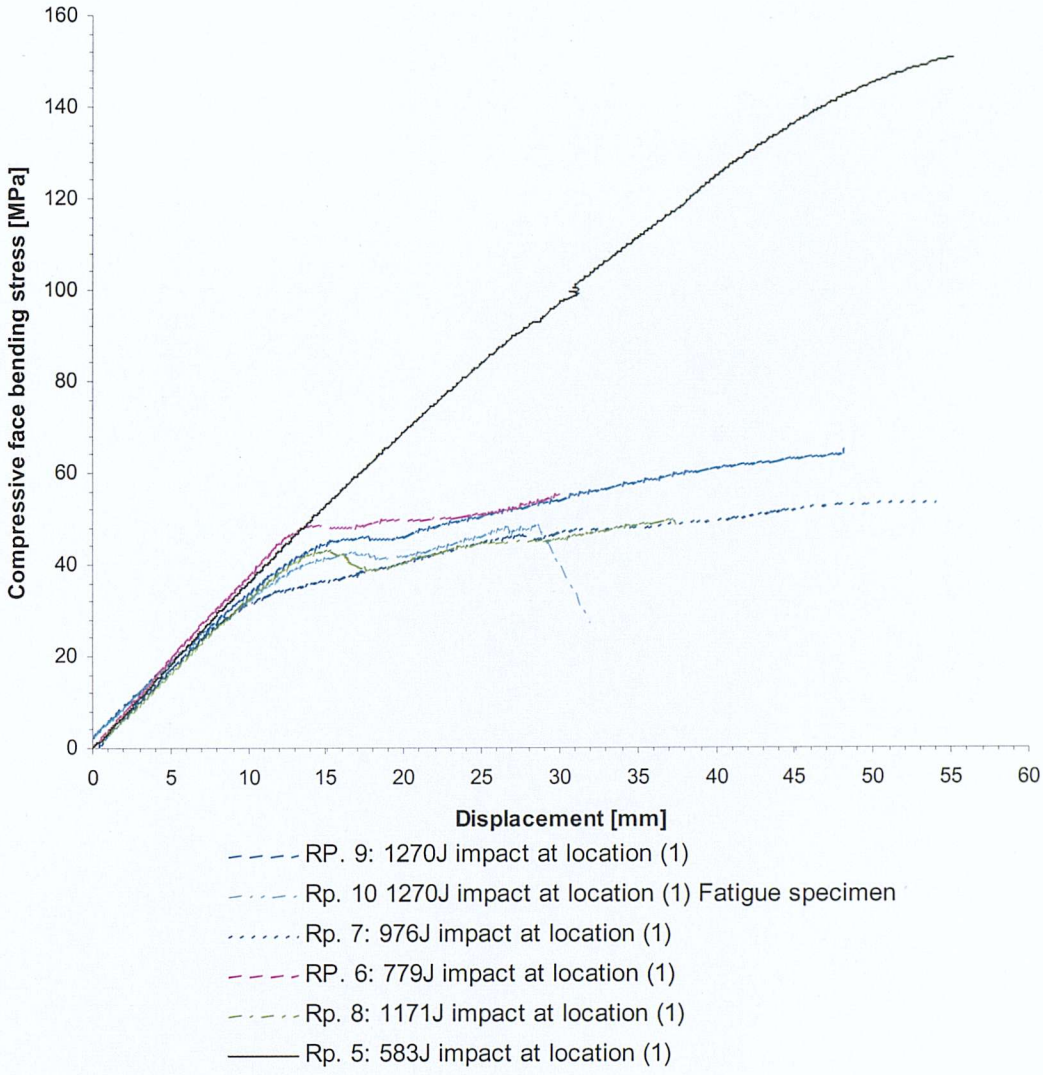

Figure 6.6: Outer skin compressive stress versus impact energy.

Loading	Impact energy	Delamination area (mm^2)	Failure displacement (mm)	Compressive stress (MPa)	Failure mode
Rp. 5	583 J	3800	55.1	151.0	
Rp. 6	779 J	8200	13.8	48.8	
Rp. 7	976 J	11400	10.0	32.5	
Rp. 8	1171 J	13600	15.0	42.9	
Rp. 9	1270J	18800	16.2	45.3	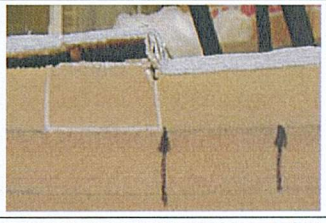
Rp. 10	1270J	16800	16.6	42.4	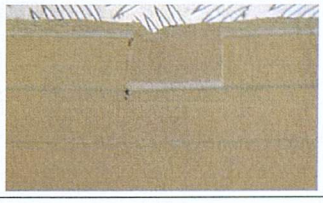

Table 6.6: Static residual strength and failure mode results for tapered scarf repairs

The failure mode of the 20:1 taper scarf repair was localised about the inner edge of the scarf taper and the vertical adhesive bondline of the replacement foam core. At low impact energies of 583J the damage formed has no effect on the residual outer skin failure stress. Conversely, at the high impact energy levels of 1270J the residual strength fell to a failure stress of 43.9 MPa ± 2.1 MPa.

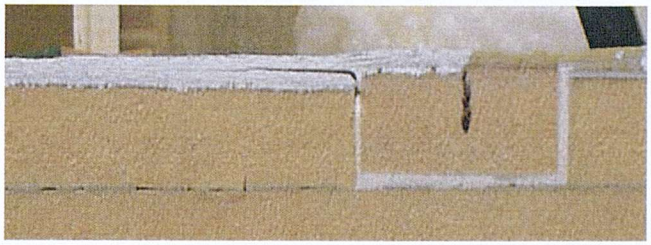

20:1 structural repair, impacted with 779J – initial unloaded condition

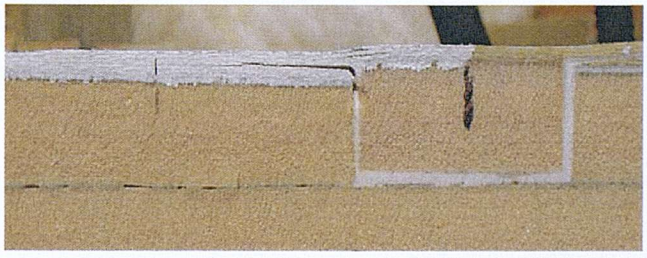

20:1 structural repair, impacted with 779J – 5kN load equivalent to 11.6MPa compressive stress in outer skin

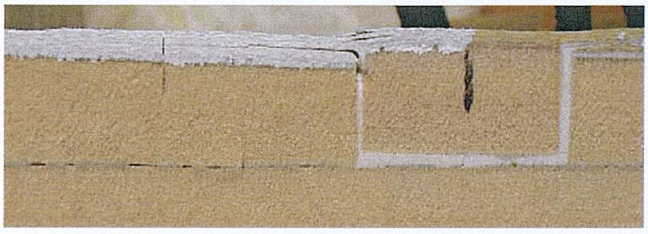

20:1 structural repair, impacted with 779J – 10kN load equivalent to 23.2MPa compressive stress in outer skin

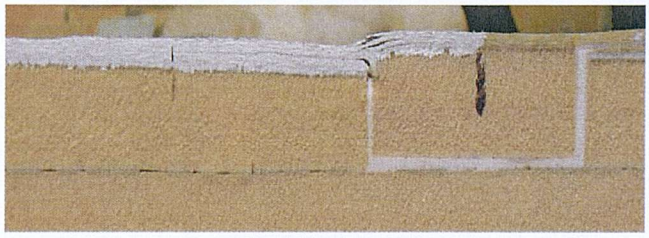

20:1 structural repair, impacted with 779J – 20kN load equivalent to 46.5MPa compressive stress in outer skin

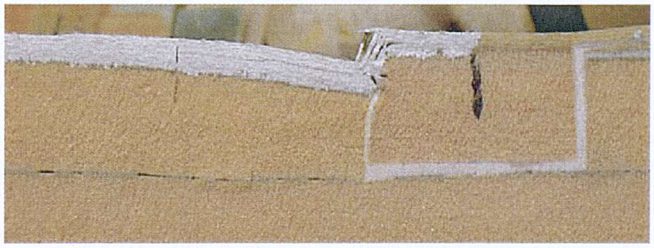

20:1 structural repair, impacted with 779J – 21kN load equivalent to 48.8MPa compressive stress in outer skin

Figure 6.7: Load-failure mode sequence for Sample Rp. 6 subjected to 779J blunt object impact.

Figure 6.7 shows the progressive failure of the 20:1 scarf repair loaded in four-point bending after it has been subjected to a 779J impact at repair location (1). Each

photograph is captured at a specific load/ stress level as indicated in the text description on the right hand side.

The extent of the damage already present in the sample is indicated in the first photograph, i.e. delamination damage along the tapered interface and two small delaminations in the repair material above the replacement foam core. During the test the delamination damage generated at the tapered interface remains static whilst the smaller delaminations start to grow and open. Eventually the outer skin kinks about the end of the taper, as indicated in the last photograph in Figure 6.7. At this point it is assumed that the composite beam has failed.

The static residual compressive stress in the outer skin of the 20:1 taper scarf repair as a function of damage size is indicated in Figure 6.8. The residual stress has been calculated using Equation (6.3).

The first striking difference between the static residual compressive stress for the virgin beams and the 20:1 taper scarf repair is the amount of delamination damage the structural repair can sustain before suffering a fall in the compressive stress. This is in direct contrast to the virgin beams that suffered a rapid fall in compressive stress for very small amounts of damage (i.e. 0.5mm indentation of the outer skin).

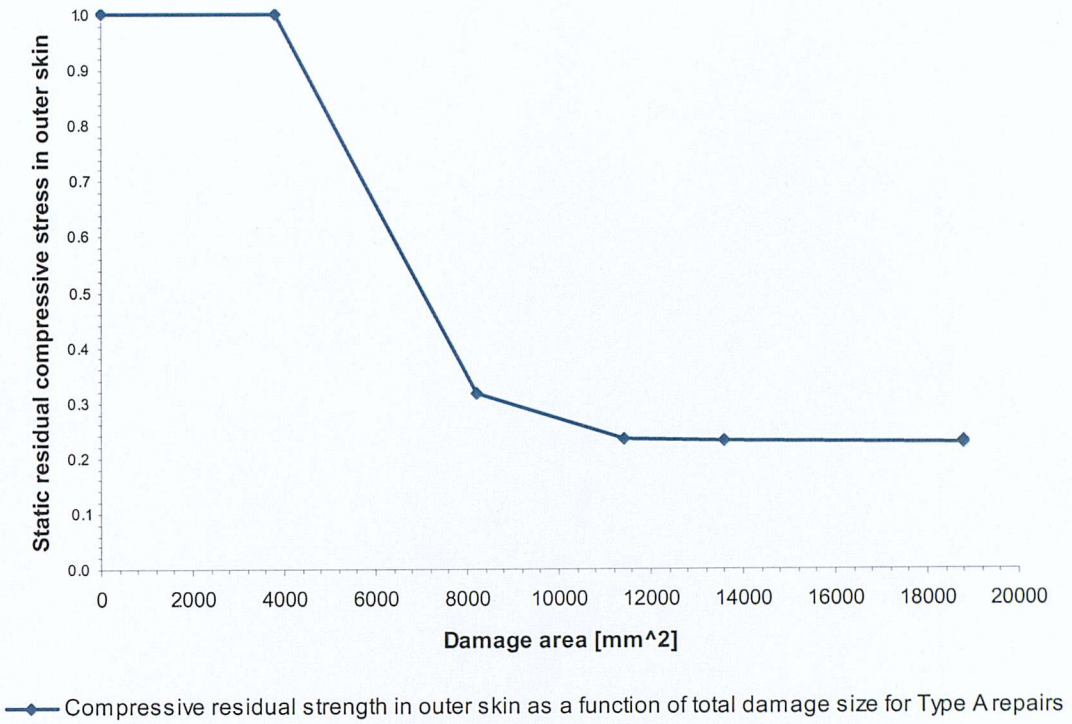

Figure 6.8: Normalised compressive stress in the outer skin as a function of damage size for 20:1 taper scarf repairs

6.4 Fatigue strength assessment of pristine beams

The fatigue loading range was determined from the average failure load obtained from the static tests (see Table 6.3). This provided the upper load limit for the fatigue tests, i.e. the ultimate static load (USL). The lower limit for the loading range was set to -1.0 kN. This nominal value was selected to ensure the load spectrum always remained negative, thus representing the slightly compressive load that a hydrostatic force would impart on the marine sandwich structure when it is afloat.

Using the average failure load and the lower testing limit, the fatigue test spectrum was established, i.e. the load amplitude was set to varying percentages of the ultimate static failure load. In these experiments a USL of 60%, 50% and 40% was used to determine the fatigue life. These results are presented in Table 6.7 and Figure 6.9.

Static Load Level	Specimen ID	Maximum Load (kN)	Max. tensile stress (MPa)	Number of cycles to failure
47%	Pr. 9	-37.9	119.8	3995
47%	Pr. 10	-37.9	119.8	4867
47%	Pr. 11	-37.9	119.8	3340
40%	Pr. 12	-31.6	103.2	24961
40%	Pr. 13	-31.6	103.2	23221
37%	Pr. 14	-25.3	93.3	79692
31%	Pr. 15	-25.3	79.9	126531
31%	Pr. 16	-25.3	79.9	231983

Table 6.7: Flexural fatigue results for Ampreg 75/ QEA1200 virgin beam tested at 1 Hz

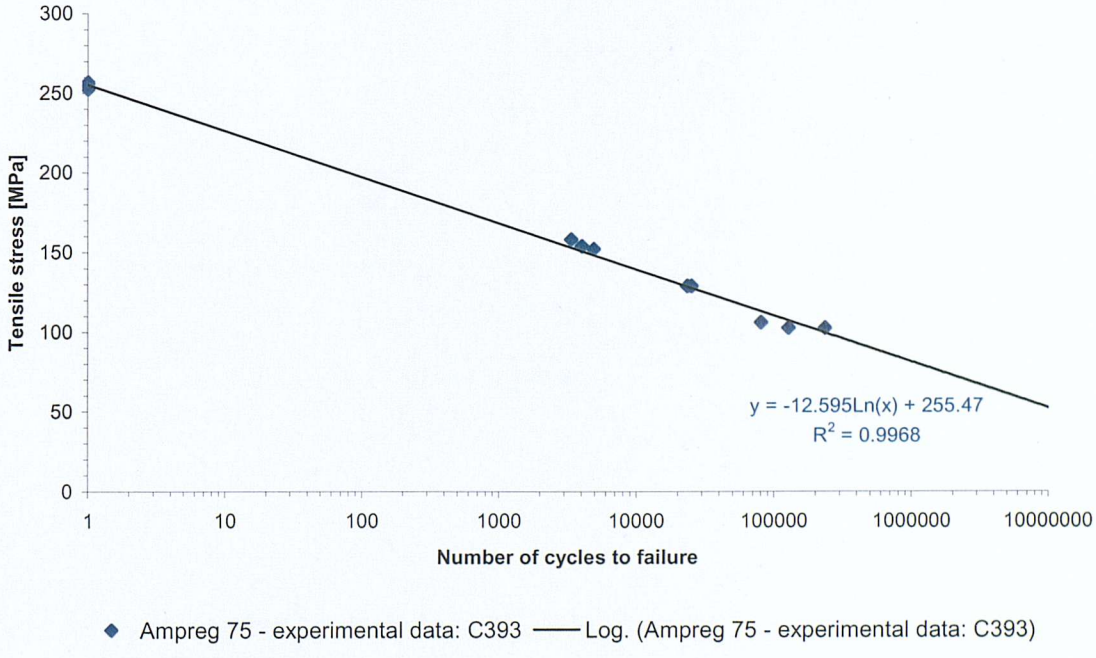

Figure 6.9: Tensile stress versus number of cycles to failure

The pristine beam's fatigue life result is presented in Figure 6.9 as a S-N curve, i.e. a tensile stress-number of cycles to failure. The fatigue result could have been presented

as the compressive stress to failure or the core shear stress to failure but since the fatigue specimens all failed by a tensile fatigue crack on the inner skin it was decided to present the fatigue result in this way.

To understand how the different loading levels affected the failure mode of the pristine beam, Table 6.8 has been generated.

Sample ID	Load Level	Failure mode description		Representative failure mode
	Static	Catastrophic core shear failure. No damage to inner or outer skin.	Side view	
Pr. 10	60%	No damage to outer skin. Diagonal crack in inner (tensile) skin with considerable fibre pull-out Foam core had a clean vertical crack	Side view	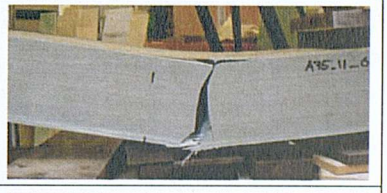
			Bottom view	
Pr. 14	40%	No damage to outer skin. Diagonal crack in inner (tensile) skin, clean fracture of fibres. Fatigue crack was observed to initiate at the edge of the 45° fibres and propagate across the tensile skin following this fibre orientation. Foam core had a clean vertical crack in the core.	Side view	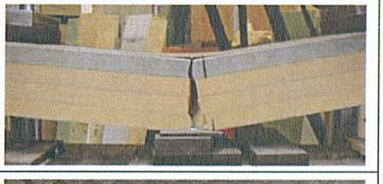
			Bottom view	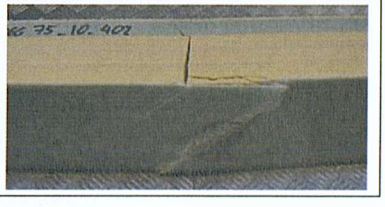

Table 6.8: Pristine beam failure mode for different fatigue load levels.

Two different failure modes existed between the static tests and the fatigue tests. In the static tests the failure load was dictated by the core shear strength of the core material. In the fatigue tests, the fatigue life of the sandwich beam is governed by the tensile

strength of the inner skin. The fatigue crack was observed to initiate from one outer edge and then propagate across the width following the line of the 45-degree fibres. At higher load levels considerable fibre pull-out was observed across the failure interface. Conversely, at the lower load levels a clean fatigue crack was observed.

In the work published by [Clark, 1997] on the 'Long term behaviour of FRP structural foam cored sandwich beams', he evaluated the fatigue and creep response of various marine sandwich beams. One of beam configurations, Type 3, was used as the structural design for the RNLI Severn and Trent composite sandwich hull structure, and hence evaluated as the baseline beam configuration in this investigation. The S-N fatigue curve for the Type 3 beams from Clark's work is reproduced in Figure 6.10. The figure also contains the experimental data derived in this test programme, i.e. Table 6.5.

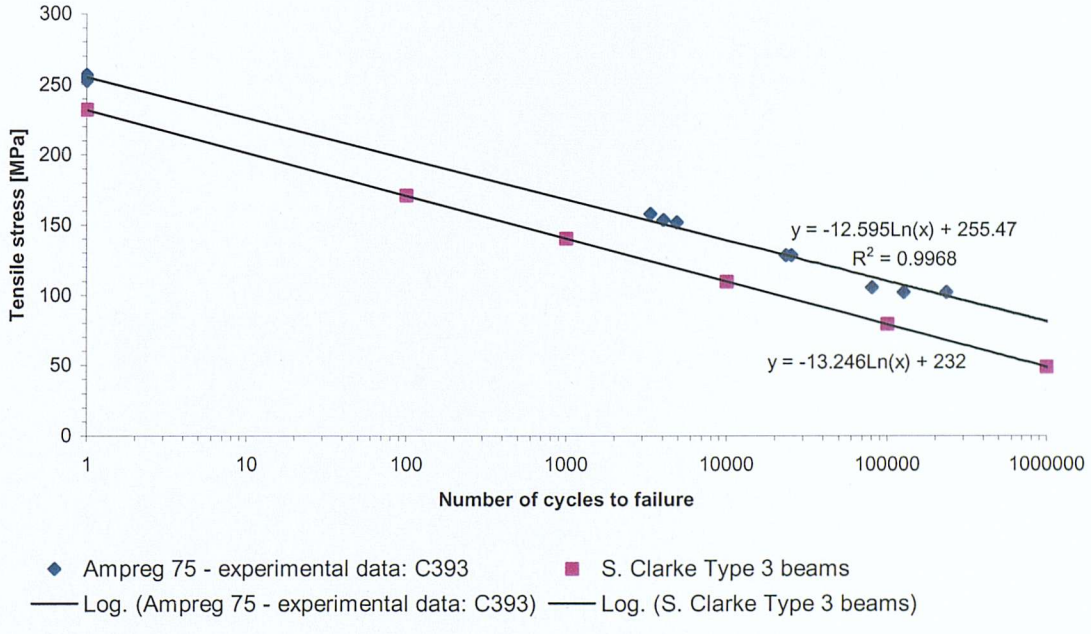

Figure 6.10: Comparison of S-N fatigue data between current test data and the Type 3 beams from Clark, 1997

The materials, fibre architecture, and processing methods are the same in Clark's work as the sandwich beams used in this investigation (i.e. QEA1200 outer skin, H130 PVC

core and QE1200 inner skin). In his tests, the author cited a skin tensile failure mode in the QE1200 as the cause of failure – the same failure mode as in these tests.

6.5 Fatigue strength assessment of undamaged and damaged tapered scarf repair

Table 6.1 contains the static test results for the 20:1 tapered scarf repair. The average failure load from these tests was used to determine the loading ranges for the fatigue tests (i.e. 80%, 60%, 40%, 30% and 20% of the ultimate static failure load). The fatigue results for the 80%, 60%, 40% and 20% of the USL are presented in Table 6.9 and Figure 6.11.

Load Level	Specimen ID	Maximum Load (kN)	Max. tensile stress (MPa)	Number of cycles to failure
80% of USL	Rp. 11	-57.4	210.0	7778
60%	Rp. 12	-43.0	157.5	10786
60%	Rp. 13	-43.0	158.3	9810
60%	Rp. 14	-43.0	160.7	9595
40%	Rp. 15	-28.8	105.0	203000
40%	Rp. 16	-28.8	107.6	167393
40%	Rp. 17	-28.8	106.0	181274
30%	Rp. 18	-21.2	79.2	> 1000000
20%	Rp. 19	-14.4	52.7	> 2000000

Table 6.9: Flexural fatigue results for 20:1 tapered scarf repair tested at 1 Hz

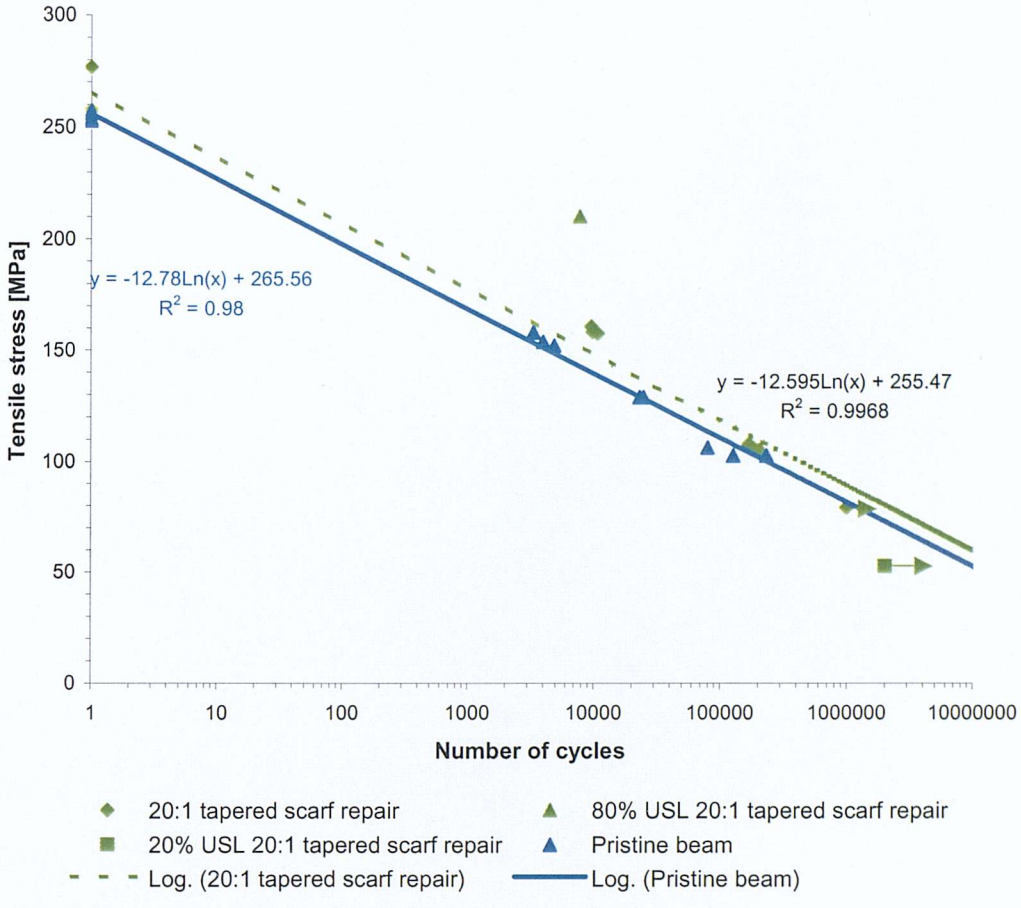

Figure 6.11: 20:1 tapered scarf repair: tensile stress versus number of cycles to failure

Figure 6.11 presents the fatigue life of the pristine beams and the repaired beams with a 20:1 tapered scarf. The fatigue life of the 20:1 tapered scarf repair has been determined without the inclusion of the 80% USL and 20% USL data points. The exclusion of the latter data point within the fatigue life determination is due to the fact that the specimen had not failed. In the case of the 80% USL level, the specimen failure was governed by core damage leading to catastrophic skin failure with substantial fibre pullout. These failure modes are more representative of a static test rather than a fatigue test (especially the fibre pullout) therefore due to this experimental evidence this data set was also excluded in the generation of the fatigue life. A full summary of the different failure modes for the 20:1 tapered scarf repair will now be discussed.

At the 100% USL the same failure mode pattern for the 20:1 tapered scarf repair specimens was observed for the pristine beams, i.e. in the static tests core shear failure between the inner and outer supports was observed. However, in the 20:1 tapered scarf repair beams two distinct failure modes exist depending upon the loading range (see Table 6.10 for the different failure mode for the structural repair as a function of fatigue loading level).

Sample ID	Load Level	Failure mode description		Representative failure mode
Rp.5	Static	Catastrophic core shear failure. No damage to inner or outer skin.	Side view	
Rp. 11	80%	No damage to outer skin. 45° diagonal crack in inner (tensile) skin with considerable fibre pull-out Extensive foam core damage	Side view	
			Bottom view	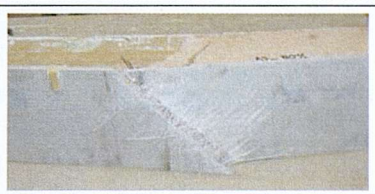
Rp. 12	60%	No damage to outer skin. 45° diagonal crack in inner (tensile) skin with considerable fibre pull-out Extensive foam core damage	Side view	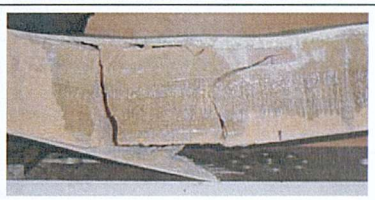
			Bottom view	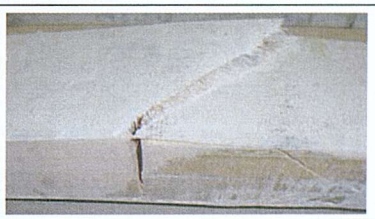
Rp. 17	40%	No damage to outer skin. Perpendicular crack in inner (tensile) skin, clean fracture of fibres. Fatigue crack was observed to initiate at the edge of the 45° fibres and propagate across the tensile skin. A serrated laminate failure edge was observed. Foam core had a clean vertical crack in the core.	Side view	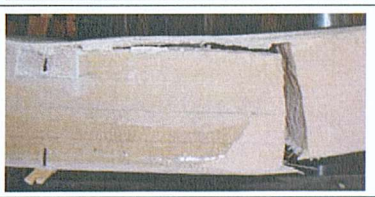
			Bottom view	
Rp. 18	30%	No failure		
Rp. 19	20%	No failure		

Table 6.10: 20:1 tapered scarf repair beam failure mode for different fatigue load levels.

At the higher loading percentage (i.e. 80% and 60% of the USL) the repaired structure was subjected to 37mm and 28mm deflection which has resulted in substantial damage to the foam core before leading to a complex fracture of the inner skin.

In comparison, the 40% loading percentage (mid-span deflection typically 19mm) has resulted in a progressive tensile failure of the outer skin. At this loading range, it was experimentally observed that the fatigue crack initiated at one edge before propagating across the full width of the beam. The crack propagation across the 200mm wide beam was observed to occur within 1000 cycles. Once the outer skin had completely failed the core was unable to support the load and failed in tension.

At 30% and 20% loading percentages (typically 14mm and 9mm deflection), no damage to the core or outer skin was observed for 1 million and 2 million cycles respectively. From this observation, it can be suggested that a fatigue limit of 30% of the static tensile strength of the inner skin can be set, i.e. the structure will not fail at a fatigue loading below this level.

The second observation concerns the lack of fatigue damage to the 20:1 tapered scarf repair, i.e. it is clear from these tests that the principal failure mode of the beam is governed by the fatigue life of the inner skin (QE1200/Ampreg 26) at low loads and the fatigue life of the core material at very high loads (loads approaching the static failure loads). In this test set-up the outer skin repair appears to be immune to any damage formation, i.e. it does not initiate any damage during the fatigue life of the structure and perhaps more importantly, it does not control the fatigue life of the beam.

In Chapter 5 the impact performance of the sandwich beams with and without the different repair techniques was considered. The objective of this research was to understand the damage tolerance performance of a tapered scarf repair scheme. A key element of this objective is to determine whether critical defects will propagate under fatigue loading.

To understand the fatigue performance of a damaged composite repair, a tapered scarf repair beam (sample ID Rp. 19) was subjected to a 1270J impact event, mirroring the testing approach outlined in Chapter 5. The damage contained within the repairs and the fatigue load spectrum is detailed in Table 6.11.

Specimen ID	Impact information	Damage size		Fatigue load level	Max compressive stress (MPa)
		Side 1	Side 2		
Rp. 19	1270J at impact location 1	62 mm	68mm	20% USL (14.4kN)	30.8

Table 6.11: Fatigue experimental summary of impact damaged Rp. 19 tapered scarf repair

To determine whether impact damage would grow when loaded with a fatigue load level below the load level sufficient to cause outer skin buckling, sample Rp. 19 was subjected to an impact at impact location 1 on the 20:1 scarf taper. The resulting damage is illustrated in Figure 6.12.

Figure 6.12: 1270J impact damage sustained by Specimen Rp.19

On side 1 of sample Rp. 19, the impact event generated a 42mm long crack propagating between the original laminate and the repair skin from the inside edge of the scarf taper towards the outer surface. Fibre bridging between the repair and the original laminate was also observed. On side 2, the impact event generated a 45mm long crack in the same location. Secondary cracks in the laminate and damage to the core material with vertical and horizontal cracks of various lengths was also observed.

The damaged beam was subjected to a fatigue loading of 20% USL (i.e. maximum load –14.4kN at 2Hz) to ascertain whether the inclusion of impact damage would alter the fatigue life of the structure. This fatigue load level was below that which caused outer skin buckling. After the first cycle is was apparent that the load level was unlikely to cause this failure mode.

Throughout the experiment, periodic examination of the damaged area (both side 1 and side 2) was undertaken to determine whether the damage had propagated further along the tapered repair or further into the core material. A summary of the observations at each cyclic interval is included in Table 6.12.

Number of cycles	Visual observation
0 cycle (i.e. impact damage)	Side 1: Dominant 42mm crack along tapered interface with secondary cracks of 15mm, slight vertical cracking (~5mm) in core material
	Side 2: 45mm crack along tapered interface with secondary cracks of 18mm, 5mm vertical crack, propagating diagonally into replacement core plug
40,000 cycles	As above, no indication of propagation
100,000 cycles	As above, no indication of propagation
454,000 cycles	Side 1: No crack extension along tapered interface. Extension of vertical cracking into foam core insert with new horizontal cracks contained within core plug.
	Side 2: No crack extension along tapered interface. Possible extension of original cracks within foam core.
1,080,000 cycles	Side 1: No crack extension along tapered interface. No further extension of foam core crack.
	Side 2: No crack extension along tapered interface. No further extension of foam core crack.
3,280,056 cycles	Tensile failure of inner skin. Side 1: No further crack extension from 1080000 cycles Side 2: No further crack extensions from 1080000 cycles

Table 6.12: Fatigue experimental summary of impact damaged to tapered scarf repair specimen Rp.19

A photograph of the extent of the damage at the maximum load after 400,000 cycles is indicated in Figure 6.13.

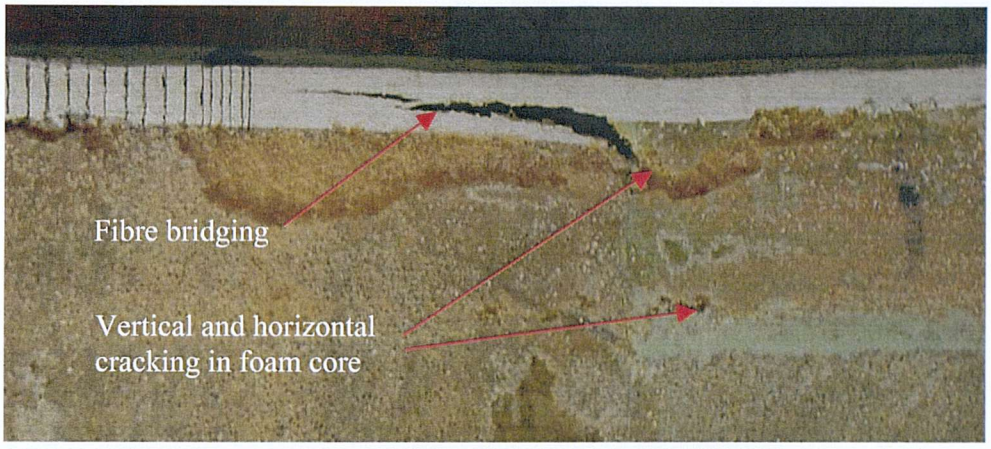

Figure 6.13: Damage mode in Rp. 19 tapered scarf repair subjected to 400,000 cycles at 20% USL

After 3,280,056 cycles, the impact damaged sample eventually failed by tensile failure of the inner skin (see Figure 6.14). The extent damage contained within the 20:1 tapered scarf repair had remained constant (at this load level) for over 2 million cycles.

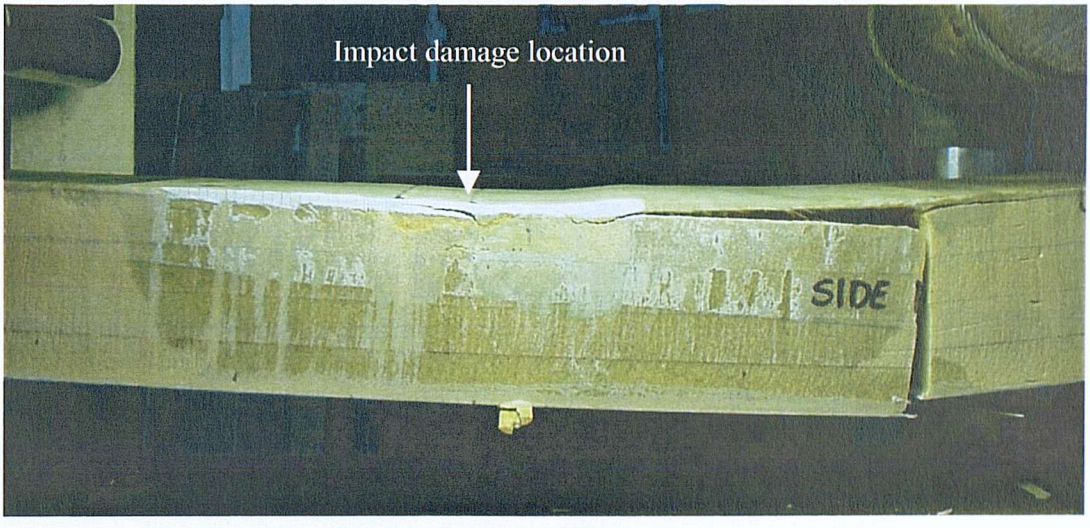

Figure 6.14: Fatigue failure mode of impacted damaged Rp. 19 tapered scarf repair

As Figure 6.14 illustrates the location of the inner skin tensile failure is on the opposite side to the location of the impact damage to the outer skin. It therefore appears that the impact damage had no influence on the failure mode of the specimen at this load level, i.e. 20% of the USL.

The S-N curve for the impact damaged 20:1 tapered scarf repair is presented in Figure 6.15. This figure contains the fatigue test data for the pristine beam and the undamaged 20:1 tapered scarf repair beams as well as the test result sample Rp. 19. The static residual strength for the 20:1 tapered scarf repair has also been included.

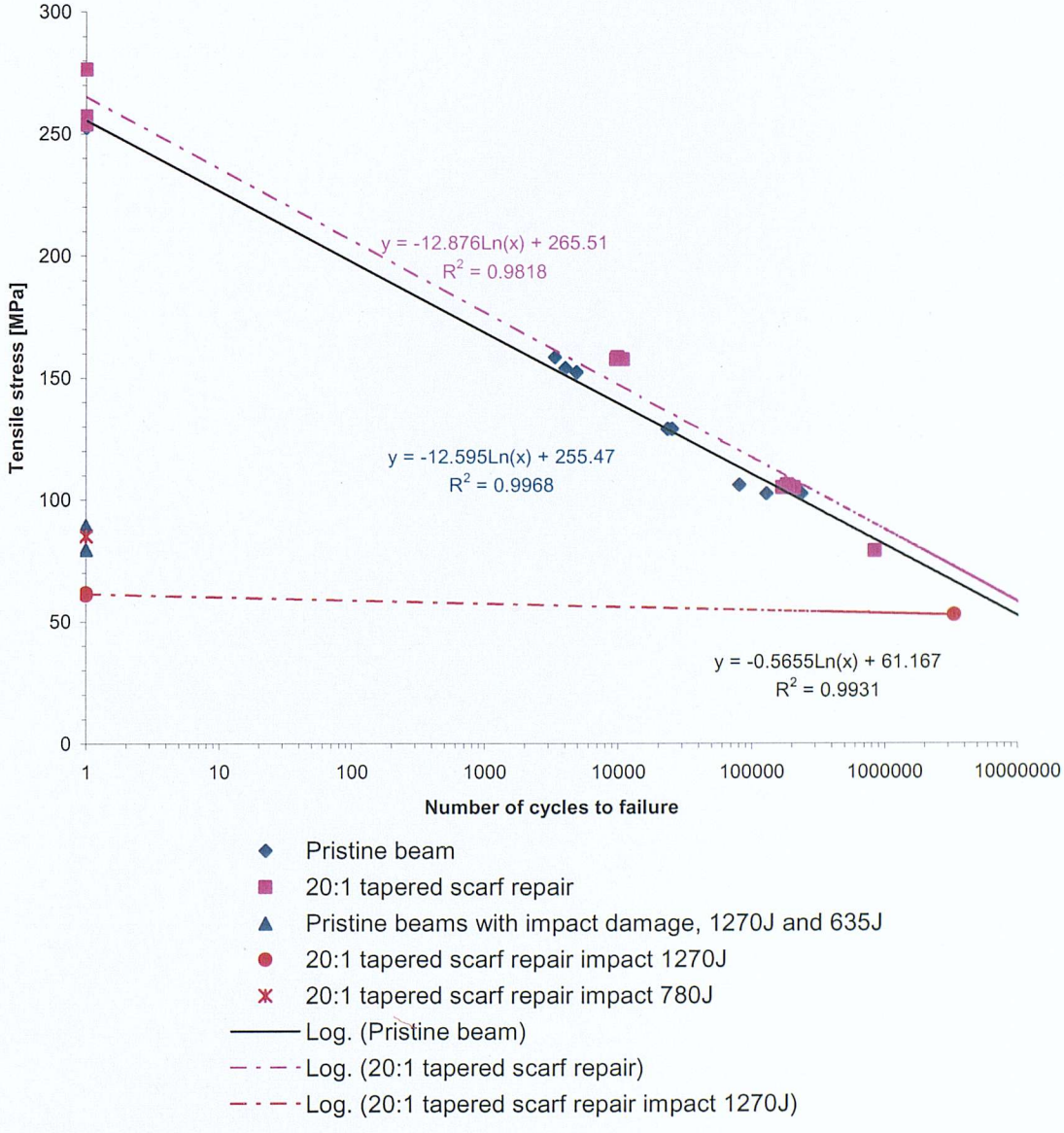

Figure 6.15: Comparison of impacted damaged 20:1 tapered scarf repair with undamaged pristine and undamaged 20:1 tapered scarf repair beams

The nature of the failure mode and the number of cycles to cause failure in the 20:1 tapered scarf repair would suggest that the delamination damage within the repair is benign for a tensile stress of 52.7MPa, which equates to a skin compressive stress of 31.2MPa. Any operational loading exceeding this stress level would result in buckling of the outer skin.

6.6 Discussion of strength based assessment

The strength-based assessment is based around two elements, namely a static strength and a fatigue strength assessment. The key findings from these two elements will now be discussed.

6.6.1 Static strength assessment of undamaged and damaged tapered scarf repair

A four-point bend static strength assessment of the pristine beams and the tapered scarf repair to the outer skin has been undertaken. Table 6.13 summarises the overall performance of these beams.

Specimen Identification		Failure load (kN)	Maximum displacement (mm)	Core shear stress at failure (MPa)	Inner skin tensile stress at failure (MPa)
Pristine Beams	Average	64.5	54.5	1.69	253.9
	St.dev	2.1	1.5	0.01	1.3
20:1 Repair	Average	69.6	43.9	1.71	261.1
	St.dev	5.5	5.4	0.10	6.7

Table 6.13: Summary table for pristine and repaired beams tested in four-point bend

Table 6.13 compares the average experimental results and the standard deviation for the failure load, deflection at failure, the core shear stress and the inner skin tensile stress at failure. An examination of the results highlights a number of interesting points. The first concerns the apparent appearance of the structural repair to be 'stiffer' than the pristine beam since it fails at a higher load with a lower deflection. The inner skin also experiences the highest tensile stress. One possible explanation for this increased beam stiffness can be directly related to the design of the 20:1 repair scheme, i.e. there is an increased amount of repair material between the inner loading points, typically the 20:1

repair extends over 95% of the beam between the inner loading supports. It is this increased material over a wide area that is believed to have caused the increase in bending stiffness.

A second observation arising from Table 6.13 concerns the core shear stress. In both cases the shear stress at failure is comparable (i.e. 1.71 ± 0.1 MPa) indicating that the performance of the pristine and repaired beams is governed by the performance of the core material rather than the composite skins. Any change in the performance of the foam core material will have considerable influence upon the static strength of the composite beams.

The investigation into the residual flexural strength of the pristine beams and the structurally repaired beams has illustrated the rapid reduction in residual outer skin compressive strength for a relatively low energy, low velocity impact. One interesting aspect of the research is the apparent improvement in damage tolerance between the structural repair and the pristine beam. Figure 6.16 illustrate the static residual stress (calculated using equation 6.3) versus damage size, whilst Figure 6.17 illustrates the static residual stress (calculated using equation 6.3) versus impact energy for both the virgin beam and the 20:1 taper scarf repair.

Figure 6.16: Comparison of the compressive residual stress as a function of total damage size for the virgin and 20:1 taper scarf repaired beams.

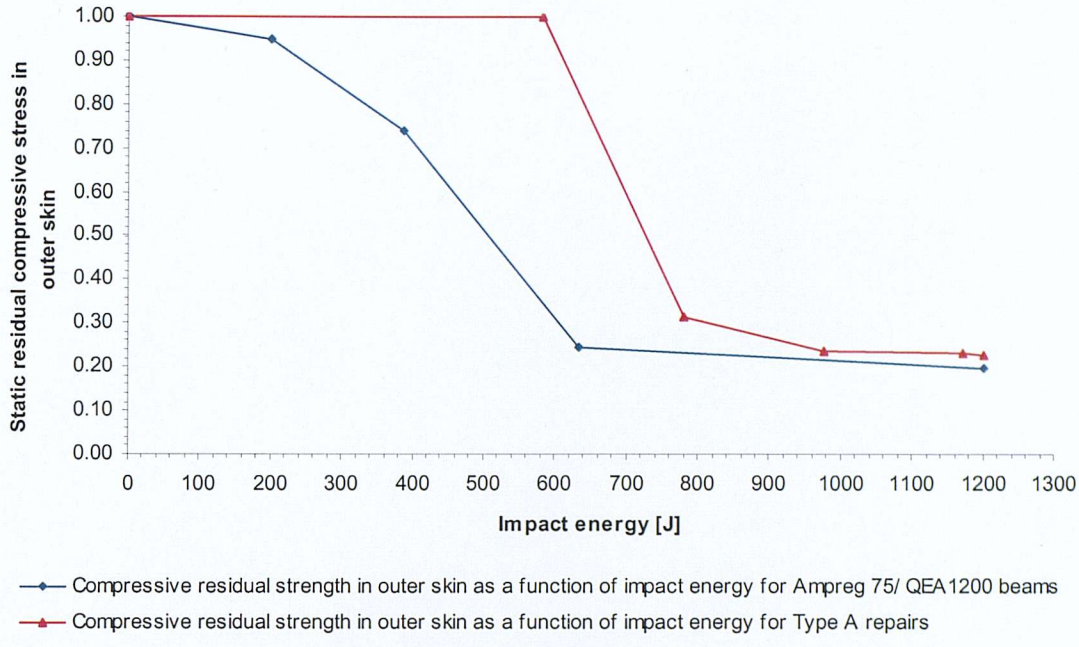

Figure 6.17: Comparison of the compressive residual strength as a function of impact energy for the virgin and 20:1 taper scarf repaired beams.

Figure 6.16 and Figure 6.17 indicate that for the same impact energy less damage will be formed in the 20:1 structural repair compared to the pristine beam, which leads to an improvement in the residual compressive stress. However, once a certain damage threshold is attained (approximately 640J for the virgin beams and between 779J and 976J for the structural repair) the residual compressive stress falls to the same level, i.e. between 20% and 25%.

6.6.2 Fatigue strength assessment of undamaged and damaged tapered scarf repair

The general observation arising from these tests for the pristine beam and the 20:1 tapered scarf repair is that at the lower load levels the fatigue life of the beams is dominated by the tensile skin fatigue life. At higher load levels the fatigue breakdown of the core caused by excessive displacement, which leads to tensile skin failure, is the dominant failure mode. The influence of the repair schemes upon the fatigue life of the beam is minimal. There is some suggestion that the tapered scarf configuration has slightly extended the fatigue life compared with the pristine beams. This is probable due to the increased amount of composite material on the outer skin that reduces the load

level experienced on the inner skin. However, it can be stated, for this particular loading arrangement, that the tapered scarf repair has not had an adverse effect upon the durability of the sandwich structure.

In addition to the undamaged beams, the fatigue life of two damaged composite beams has been assessed. A 1270J impact on the outer skin has been used to represent typical operational damage. In this assessment, it has been shown that the impact damage is benign at the low load levels (typically 20% USL) but if the damage is loaded in such a way that the stress in the outer skin exceeds the skin buckling stress then the specimen will fail (i.e. any damage within the outer skin will limit the maximum fatigue load to 32% of the USL). Although the structure cannot truly be considered damage tolerant, these results would suggest that it is damage tolerant for loads up to 32% USL. However, this may not always be the case. For example, in chapter 5, an impact energy above 975J was sufficient to cause a crack between the final overlaminate ply and the parent laminate, i.e. the tensile stresses generated at the interface between the repair and the parent laminate were greater than the tensile strength of the Ampreg 26 laminating resin. The environment can then attack this form of damage, i.e. in the case of a marine craft; the exposed edge would be attacked by the flow of water passing over it. In which case, it is possible that the patch could be torn from the repair and then the structure would fail at any load level below the fatigue threshold limit determined by this experimental programme. The fatigue life is then a function of the probability of an impact event of sufficient energy occurring directly on top a previously repaired area, and not a function of the tensile strength, and hence fatigue life, of the inner skin.

This observation from the static tests adds a cautionary warning to the fatigue test data generated within this programme. For example, the fatigue life of the undamaged pristine and 20:1 tapered scarf beams is valid using this the data obtained above. However, if impact damage has occurred to the structure, the maximum fatigue load supported by the two beams will be capped to the static residual strength of 24%. Providing the operational load remains below this threshold value the fatigue life of the structure will be unaffected. However, as the example above illustrated, if the impact damage is sufficient to generate a crack at the boundary of the repair then the fatigue life of the structure is no longer a function of the skin stress level. Rather, it is a

function of the bondline toughness and the speed of the water passing over the repair. It is these latter observations that must be included in a surveyor's design tool otherwise defective repairs will enter operational service or remain in operational service.

6.7 Conclusions

The purpose of this chapter has been to generate the theoretical and practical understanding of a repaired composite sandwich structure subjected to impact damage in support of the strength based assessment identified in Figure 3.1, Chapter 3. The key findings and observations arising from this investigation are:

1 The static strength performance of the pristine beams and the tapered scarf beams are governed by the core shear strength properties.

2 The residual strength performance of the pristine beams and the tapered scarf repair was governed by the compressive strength of the outer skin.

3 On the pristine beams, a residual dent in the outer skin resulting from a 387J impact was sufficient to cause an 18% reduction in the residual compressive stress. Once the damage size was greater than 3000 mm^2 the residual compressive stress fell to ~20%.

4 On the tapered scarf repair, once the impact damage (at impact location 1) had gained sufficient size (greater than 8200 mm^2) and the compressive stress in the outer skin has achieved ~49MPa the outer skin would fail in buckling about the start of the scarf taper.

5 In all fatigue loadings the dominant failure mode was catastrophic tensile failure of the inner skin. However, at high USL levels (80% and 60%) the tensile failure of the skin was initiated from the breakdown of the core material.

6 Crack growth from impact damage (at impact location 1) measuring 13000mm^2 did not occur when loaded below the buckling stress threshold of 24% USL. If the loading exceeded this value the outer skin would fail during the next fatigue cycle.

7 Tapered scarf repairs undertaken to hybrid E-glass/Kevlar fibre epoxy laminates bonded to PVC foam can be considered damage tolerant only if

- No damage has occurred within the vertical adhesive bondline of the tapered repair
- Outer skin delamination damage at impact location (1) remains below 8200 mm^2 in size, or delamination damage greater than this threshold is only loaded below the outer skin compressive buckling stress.
- Outer skin delamination damage at impact location (2) remains below 13500 mm^2 in size, or delamination damage greater than this threshold is only loaded below the outer skin compressive buckling stress.
- No 'peel' crack has occurred at the repair overlaminate edge

The findings from this work will be used to predict the damage tolerance performance of the repair within the 'Repair Structural Integrity Assessment'.

7 REPAIR STRUCTURAL INTEGRITY ASSESSMENT

7.1 Introduction

The purpose of this chapter is to draw together the improved technical understanding gained from the impact tests, the fracture mechanics tests, the static residual strength tests and the fatigue tests into a consolidated approach for the damage tolerance assessment of tapered scarf repairs. The approach for this was developed in Chapter 3, as defined in Figure 3.2, which is repeated here as Figure 7.1.

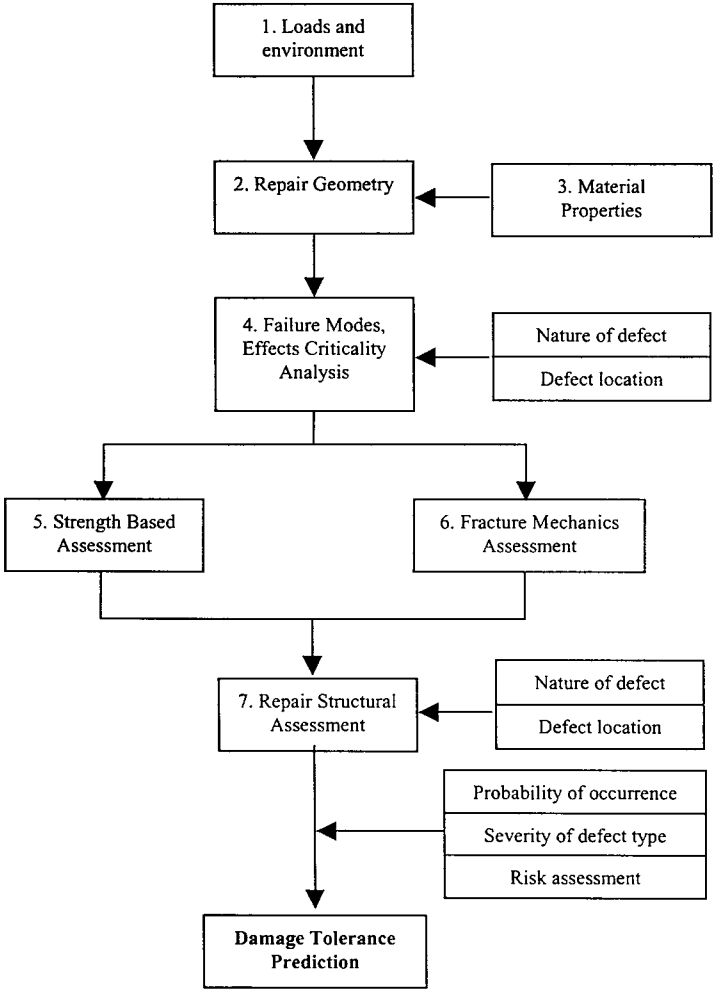

1. Loads and Environment.

The loads and environment were defined by the RNLI, for wave slamming fatigue life in UK coastal waters

2. Repair Geometry.

3° tapered scarf with 285mm overlaminate as indicated in Figure 4.1

3. Material Properties.

Standard skin laminate and foam core mechanical properties in Tables 4.1, A1, A2, and A3. Skin laminate and repair fracture toughness properties in Tables 5.7 and 5.8

4. FMECA Analysis.

Critical BVID hazards identified in Table 4.4:

1. High risk: (a) impact damage to the repair tapered interface, (b) impact damage to the repair horizontal interface, and (c) impact damage to the repair laminate
2. Medium to high risk: (a) impact damage to the parent laminate and (b) fatigue and fracture at or near the internal edge of a repair taper

5. Strength Based Assessment

Static strength of pristine and repair beams governed by core shear (see Fig. 6.1 & 6.5)
Residual strength of pristine and repair beams after formation of BVID governed by compressive strength of outer skin ~ 49MPa (see Fig. 6.16 & 6.17)
Fatigue life of pristine and repair beams governed by tensile failure of inner skin (see Fig. 6.15)
Fatigue crack growth did not occur for BVID (8200mm^2) at tapered scarf location (1) if the specimen is loaded below the buckling stress. Above this stress level and buckling failure occurs.

6. Fracture Mechanics Assessment.

Repair laminate has the highest fracture toughness (G_{Ic} = 2481J/m^2 G_{IIc} =4409J/m^2), followed by the repair-parent interface (G_{Ic} = 2416J/m^2 G_{IIc} =3851J/m^2), and then the parent laminate (G_{Ic} = 1818J/m^2 G_{IIc} =3476J/m^2). Composite repair is more damage tolerant than existing parent laminate

7. Damage tolerance prediction.

3° tapered scarf can be considered damage tolerant if: (a) no damage in vertical bondline, (b) Outer skin delamination damage at impact location (1) remains below 8200 mm^2 in size, or delamination damage greater than this threshold is only loaded below the outer skin compressive buckling stress, (c) outer skin delamination damage at impact location (2) remains below 13500 mm^2 in size, or delamination damage greater than this threshold is only loaded below the outer skin compressive buckling stress, and (d) no 'peel' crack has occurred at the repair overlaminate edge

Figure 7.1: Flow chart design methodology for the damage tolerance assessment of repaired composite sandwich structures

In addition to highlighting the technical flow in generating a damage tolerance methodology, Figure 7.1 also illustrates where the technical understanding generated within this thesis has been applied to derive a damage tolerance assessment of BVID in a 3° tapered scarf repair to composite sandwich structures. The over-riding conclusions are contained within the box detailing the 'damage tolerance prediction'.

Although the technical illustration in Figure 7.1 is specific to research undertaken in this thesis, the methodology behind the flowchart is applicable to structural repairs in any composite sandwich structure. There are three critical elements within this methodology, namely the Fracture Mechanics Assessment and the Strength Based Assessment, which feed into the Repair Structural Integrity Assessment. It is within this integrity assessment that the damage tolerance prediction for the tapered scarf repair is made.

7.2 Operational tool for repair verification

The repair of a composite structure is a complicated procedure made up of various skilled steps. To appreciate the full extent of this procedure, i.e. the 'repair cycle', Figure 7.2 has been compiled.

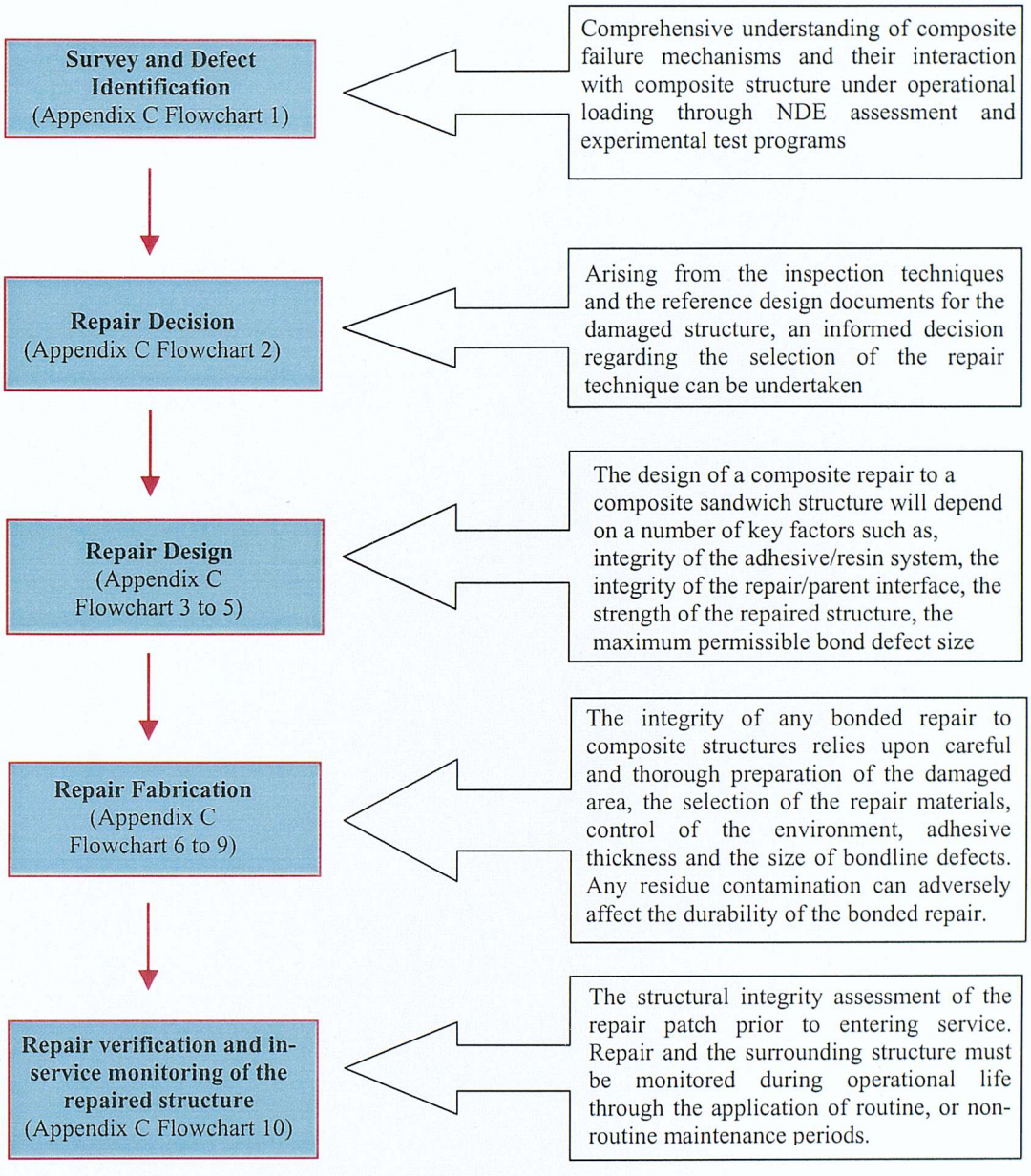

Figure 7.2: Repair cycle for marine composite sandwich structures

A full summary of the repair flowcharts derived in this study, to undertake a repair to composite sandwich structures, have been included in Appendix C. Flowchart C1.2 in Appendix C has been adapted from the RNLI/University of Southampton contribution (i.e. case study number 2) to the DTI/SSA link programme on Integrated Technology for Marine Construction [Shenoi *et al*, 2003]. The remaining flowcharts C1.3 to C1.11 have been derived in support of the repair cycle identified in Figure 7.2.

In Figure 7.2 there are two key stages where a damage tolerance assessment can be made, namely during the 'Repair Decision' and in the 'Repair Verification and In-service Monitoring of the Repaired Structure'. At these two stages within the repair cycle a critical decision can be made to leave the damage within the structure, or within the repair scheme, or to remove the damage and affect a new repair. It is therefore imperative that clear guidelines are produced to steer the repair engineer through a damage tolerance procedure.

7.2.1 Damage tolerant approach used within the 'Repair Decision' step

The first step in the design tool methodology considers the influence of the damage or defect upon the performance of the sandwich structure. This will then direct the surveyor to the correct course of action, i.e. repair immediately, repair within normal maintenance period or monitor throughout operational life. If the outer skin has been damaged by an impact event the surveyor needs to ascertain the size of the delamination and its influence upon the structure. In this situation the following design tool methodology should be employed.

The pristine sandwich damage tolerance evaluation is based around one key flowchart and two key assessment tables. The flowchart in Figure 7.3 presents the generic decision making process, whilst the Table 7.1 assesses the damage criticality and Table 7.2 are used to determine the probability of occurrence and level of risk each defect has on the structure.

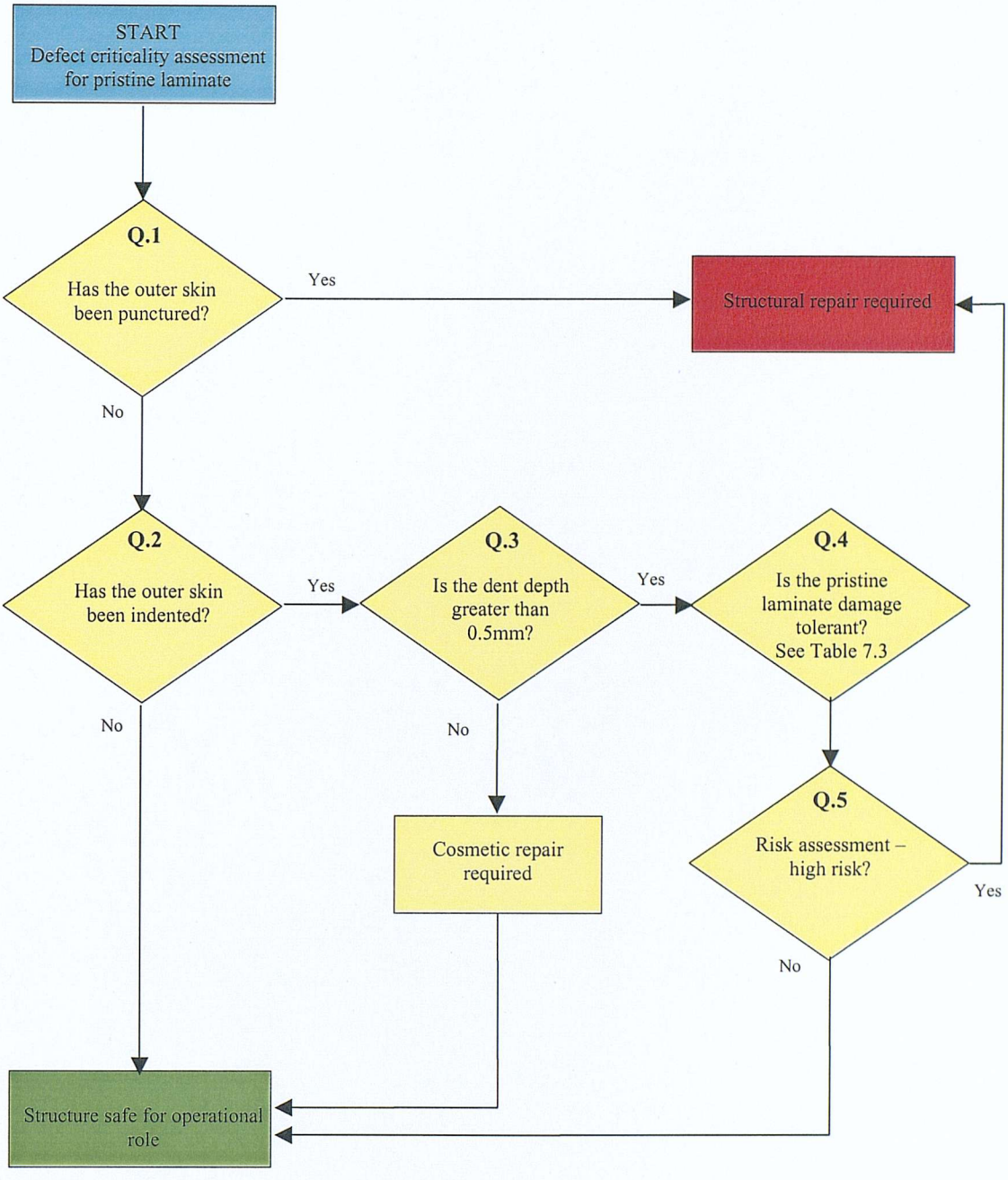

Figure 7.3: Damage tolerance methodology for BVID to outer skin of composite sandwich structures

The damage tolerance flowchart is shown in Figure 7.3. The flowchart leads the user from the 'defect criticality assessment' to the conclusion of whether a repair is, or is not, required for a particular defect. The process from initial assessment of operational damage to recommended action requires a detailed understanding of the defect type and

its influence on the structure. The logic employed in the formation of Figure 7.3 is detailed below.

Question 1.

A defect penetrating the outer skin of a composite sandwich structure cannot be considered damage tolerant. Baker *et al* [Baker *et al*, 1985] defined damage tolerance as '*the ability of the structure to contain representative weakening defects under representative loading and environment without suffering reduction in residual strength, for some stipulated period of service*'. In the case of full outer skin penetration a significant reduction in the residual strength would occur, thus requiring a structural repair to reinstate a minimal level of performance. This rationale has been used as the first decision within the flowchart, i.e. 'has the outer skin been penetrated?'

Question 2.

The residual strength evaluation in Chapter 6, Figure 6.3 and Table 6.4 indicated that a dent depth less than 0.5mm will not have an effect on the residual strength performance of the pristine beam. In Figure 7.3, this observation is used to make the distinction between undertaking a 'damage tolerance assessment' (presented in Table 7.1) and recommending that the 'structure is safe for operational use', providing the surface profile has been reinstated using a 'cosmetic repair' (this is typically a filler).

Question 3.

As stated above, in Chapter 6, a defect dent depth threshold existed which introduced a change in the mode of failure. Any dent depth greater than 0.5mm therefore requires a 'damage tolerance assessment' to determine whether the 'delamination is within acceptable limits?'. This has been undertaken in Table 7.1.

Question 4.

Damage tolerance assessment.

Dent depth	Delamination area [mm^2]	Compressive failure stress [MPa]	USL loading used in fatigue tests	Fatigue failure mode	Fatigue limit assessment
0 to 0.5mm	None	114.0	95%	Core shear	Operational structure will not be loaded to this USL therefore the structure can be considered damage tolerant
	360	88.8	73%	Core shear	
0.5mm and above	2565	29.3	24%	Buckling failure	Typically, an operational structure will be loaded to this USL. Since failure can occur within 1 cycle, the structure cannot be considered damage tolerant
	20633	23.7	20%	Buckling failure	

Table 7.1: Damage tolerance assessment for pristine laminates

Table 7.1 is based upon the experimental observations from the static residual strength assessment (Chapter 6, Sections 6.2) and the fatigue strength assessment in (Chapter 6, section 6.4). The table has been developed upon the following technical understanding, and supporting evidence:

a) The influence the dent depth (column 1) and delamination size (column 2) have upon the static compressive residual failure stress (column 3).

   Although no direct correlation exists between the dent depth and the delamination size in the outer skin was recorded, it was noted in Chapter 6 that a delamination size sufficient to alter the static residual strength occurred once the dent depth was greater than 0.5mm.

b) The influence of delamination size upon the compressive failure stress is shown between columns 2 and 3.

c) The static compressive failure stress values in column 3 can be mapped across to the fatigue life test results using the ultimate static load (USL) percentage using Equation 6.3.

The result in column 4 can be directly linked to Chapter 6, Figure 6.9 and Table 6.9 (these indicate the number of cycles to failure for each USL level)

d) The type of failure mode to cause failure during the fatigue life. This is indicated in column 5 and directly relates to the failure stress in column 3.

The fatigue lives of the pristine composite sandwich beams were governed at low USL levels by the tensile fatigue life of the inner skin and at high load levels by the fatigue live of the core properties (see Table 6.10). Both values that can be controlled through correct design. However, in the impact damaged pristine beams, the failure mode was observed to be compressive buckling of the outer skin (see Table 6.4), a failure mode not observed in the fatigue tests.

e) The 'fatigue limit' in column 6 is used to assess whether the structure is fatigue damage tolerant, or whether the damage has changed the mode of failure.

This assessment is made through the link between the USL level (column 4) and the type of damage mode to cause the structure to fail (column 5). At small dent depth/ delamination size, it was observed that the static residual compressive stress is still sufficient to ensure that core shear remains the dominant failure mode. Mapping this USL level to the fatigue tests also indicates that the fatigue life of the structure is governed by the performance of the sandwich core. Since the impact induced damage mode has not altered the performance of the core material, it can therefore be concluded that it will not alter the fatigue of the structure. The damage mode can considered damage tolerant.

At larger dent depth/ delamination size, it was observed that buckling of the outer skin occurs in preference to core shear failure, typically at USL levels of 24% and below. In the fatigue tests, at corresponding low USL levels the dominant failure mode was tensile failure of the inner skin, up to USL levels of 40% USL. At USL levels above 40% the core properties became dominant and therefore governed the fatigue life of the structure. It should be noted that at no point in the fatigue life did failure occur within the outer skin. Since the BVID has induced a new mode of failure at a USL level that would usually attain 1

million fatigue cycles (see Figure 6.9, Chapter 6) it can be concluded that this type of damage to the outer skin is not damage tolerant.

Question 5.

The final step in Figure 7.3 is to undertake a risk assessment. In Table 7.1 the level of damage that can be tolerated by the structure before it influences the fatigue failure mode was established. This is used as the basis for the risk assessment in Table 7.2.

Dent depth	Defect type and size [mm^2]	USL to cause failure	Probability of damage occurrence	Probability of damage growth	Category rating	Risk assessment	Recommended action
0 to 0.5 mm	No delamination	95%	Probable	Remote (Unlikely to occur but possible)	Minor	Low (D)	Reinstate to operational capability with routine service inspections
	360	73%	Probable	Remote (Unlikely to occur but possible)	Minor	Low (D)	Reinstate to operational capability with increased service inspections
0.5 mm and above	2565	24%	Probable	Probable (Likely to occur several times in the life of an item)	Critical	High (A)	Restrict operational stress levels below buckling stress, otherwise repair
	20633	20%	Probable	Probable (Likely to occur several times in the life of an item)	Critical	High (A)	Restrict operational stress levels below buckling stress, otherwise repair

Table 7.2: Probability of occurrence and growth of BVID in composite laminate sandwich skins

Table 7.2 assesses the consequences of the defect on the structure through 'Probability of occurrence' and 'Probability of growth'. This information is then used to form the recommended action. The table has been developed considering the following interactions:

a) The FMECA introduced in Chapter 3, Figure 3.1 and Chapter 4, Section 4.5.

b) The first 3 columns in Table 7.2 are the same for Table 7.1 and provide the continuity through the damage tolerance assessment.

c) The 'probability of damage occurrence' has been defined according to the definition in Table 4.2. The selection of 'probable' for damage occurrence is perceived by the author to best reflect the likelihood of impact damage occurring within the lifetime of the structure. This rating is specific to the hull form of the marine structures since impact damage tends to form in or around the waterline. In aerospace structures a probability rating of 'occasion' may be more appropriate.

d) The 'probability of damage growth' has been defined according the definition in Table 4.2. The selection of 'remote' for damage growth for dent depths of 0.5mm or below is perceived by the author to reflect the likelihood of the damage propagating under operational loading, i.e. USL levels of 73% or higher will have to occur within the lifetime of the structure. It is felt that this is unlikely.

   Conversely, the selection of 'probable' for damage growth for dent depths greater than 0.5mm is felt more realistic for this type of damage. In this particular case, the mode of damage growth will be outer skin buckling which could occur at USL levels of 24% or below. It is felt that this USL level is likely to occur during operational loading and therefore there is a risk to the sandwich structure.

e) The 'category rating' is a measure used to rate each defect type. This is established from the definition in Chapter 4 and the technical understanding gained within this project. For example, dent depths below 0.5mm were not observed to alter the residual strength performance of the structure, whereas dent depths greater than this value altered the failure mode in the static and fatigue tests. Hence the later are given a more sever rating.

f) The risk assessment in column 7 is the derived from the combination of the 'probability of damage growth' and the 'category rating'. This interaction was first defined in Table 4.3, where 'A' is the highest risk and 'D' is the lowest.

Dent depths below 0.5mm are given a rating of 'D', i.e. the defect growth is remote (see point 'd' above) and the defect category rating is minor (see point 'e' above). Conversely, dent depths greater than 0.5mm have BVID in the outer skin that was observed to initiate failure. Therefore this type of defect has been assigned a risk assessment of 'A' due to the high risk that the defect may propagate (i.e. induce buckling failure) during operational service, even though the probability of the defect occurring remains the same.

g) The 'recommended action' in column 8 details the repair strategy for the category determined in the risk assessment in column 7. This information is also provides the final instructions in the flowchart in Figure 7.3

The preceding bullet points (1, 2, 3{a to e} and 4{a to g)} provide the technical information and justification to the questions in the flowchart in Figure 7.3. Although the specific damage threshold values are only applicable to the type of materials and form of BVID used in this project, the generic damage tolerance methodology of (1) assessing the residual strength failure mode, (2) determining whether the type of damage changes the fatigue failure mode and (3) determining whether the BVID will occur, propagate or cause the structure to fail through the application of a FMECA methodology, can be applied to any composite structure. This approach will again be applied in the next section.

In conclusion, the application of this methodology to the BVID to the pristine beams indicates that any dent depth less than 0.5mm can be considered damage tolerant. Any damage greater than 0.5mm dent depth can be considered damage tolerant if the operating stress of the sandwich beams remains below the buckling stress. If there is a risk that the operating stress will exceed this failure stress then the structure should not be considered damage tolerant and therefore should be repaired.

7.2.2 Damage tolerant approach used within 'Repair Verification' step

The objective of a tapered scarf repair is to return the structure to its undamaged condition, such that it can support all design loads for the intended service life. If the repair is found to contain any type of defects a damage tolerance assessment must be undertaken to determine the severity the defective repair will have on the operational performance of the vessel and the safety of the crew, i.e. is the defect within acceptable limits?

In a tapered scarf repair, two critical defect locations have been considered (1) tapered interface and (2) overlaminate. These locations are considered in Figure 7.4 and discussed within this section.

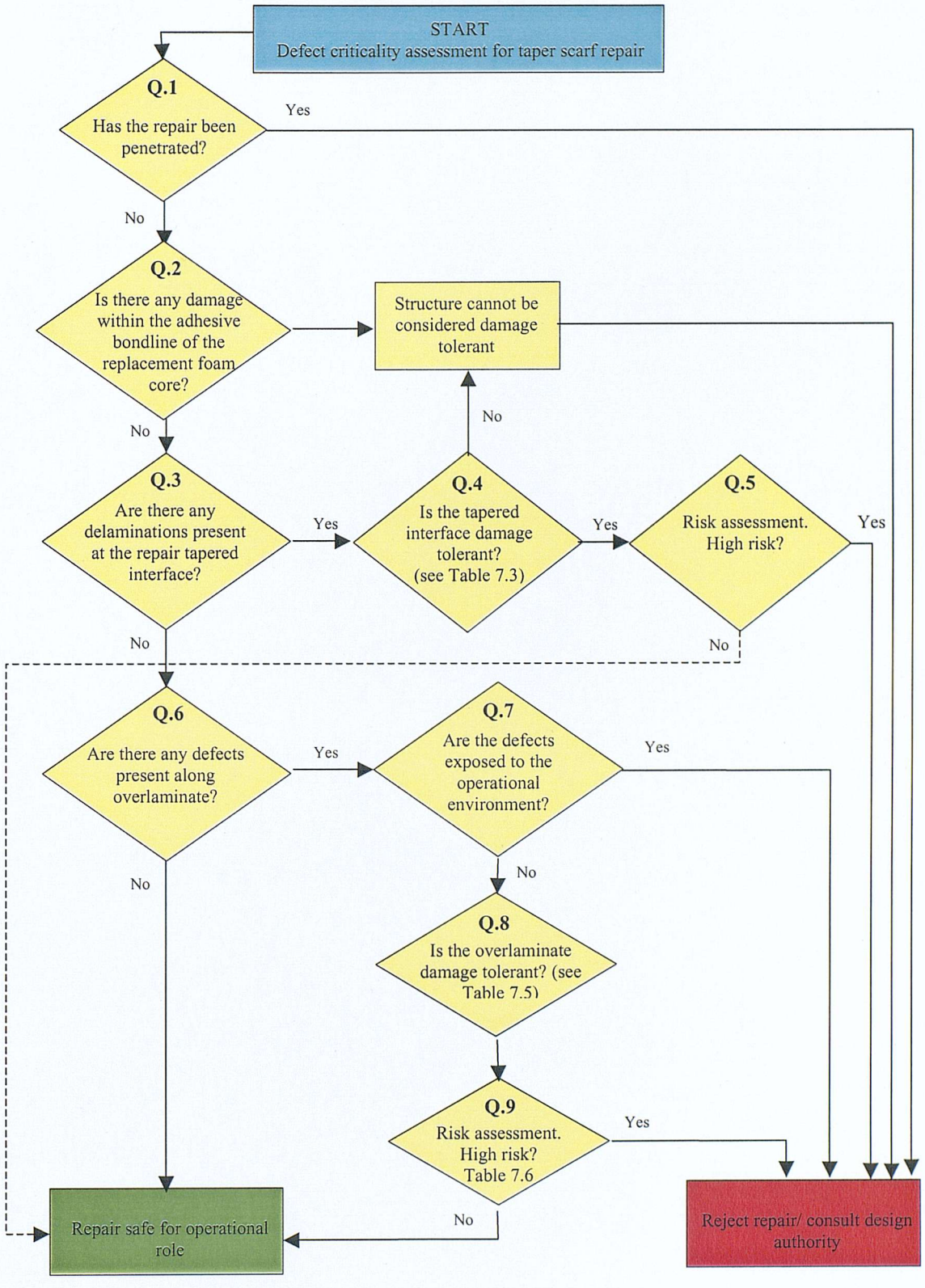

Figure 7.4: Design methodology flowchart for the defect criticality assessment of the taper scarf structural repair

The technical logic employed in the formation of Figure 7.4 follows the same approach foe Figure 7.3. In the previous sub-section a detailed explanation was given for each step within the Figure 7.3. Since most of these points are also applicable to Figure 7.4, the following text will discuss the critical and pertinent points of BVID to a tapered scarf repair, and refer back to the previous supporting text when required.

The formation of Figure 7.4 is based upon the following questions

Question 1.

The damage penetrating the tapered scarf repair cannot be considered damage tolerant (see previous sub-section for full explanation).

Question 2.

BVID forming in the vertical adhesive bondline within the tapered scarf repair was observed to initiate buckling failure of the repair (see Figure 5.8 for damage location and Figure 6.8 for damage induced failure mode).

The fatigue life of the sandwich structure is governed by the tensile skin properties but since this damage is contained within the foam core there is considerable risk that this type of damage could change the mode of failure and propagate at low fatigue loadings.

In conclusion, BVID in the vertical adhesive bondline cannot be considered damage tolerant and therefore must be repaired (as indicated in the flowchart).

Question 3.

This requires direct input from an NDE technique.

Question 4.

BVID forming on the tapered adhesive interface within the tapered scarf repair could be damage tolerant. This assessment is made in Table 7.3.

Impact energy	Delamination area [mm^2]	Compressive failure stress [MPa]	USL loading used in fatigue tests	Failure mode	Fatigue limit
583J	3800	151.0	98%	Core shear	Operational structure will not be loaded to this USL therefore the structure can be considered damage tolerant
779J	8200	48.8	31%	Buckling failure	The USL to cause failure is typical of the operational loads likely to be experienced by the structure. Since failure could occur within 1 cycle, the structure cannot be considered damage tolerant
976J	11400	38.5	25%		
1171J	13600	42.9	28%		
1270J	Ranging between 16800 - 18800	42.4 – 45.3	28 - 29%		

Table 7.3: Damage tolerance assessment for repair tapered interface

Table 7.3 is based upon the experimental observations from the static residual strength assessment (Chapter 6, Sections 6.3) and the fatigue strength assessment in (Chapter 6, section 6.5). The table has been developed upon:

a) The impact energy (column 1) to initiate delamination size (column 2) have upon the static compressive residual failure stress (column 3).

b) The influence of delamination size upon the compressive failure stress is shown between columns 2 and 3.

c) The static compressive failure stress values in column 3 can be mapped across to the fatigue life test results using the ultimate static load (USL) percentage using Equation 6.3.

d) The type of failure mode to cause failure during the fatigue life. This is indicated in column 5 and directly relates to the failure stress in column 3. The fatigue lives of the tapered scarf repaired sandwich beams was governed at low USL levels by the tensile fatigue life of the inner skin and at high load levels by the fatigue live of the core properties (see Table 6.12). However, in the impact

damaged repaired beams, the failure mode was observed to be compressive buckling of the outer skin above 20% USL (see Table 6.6). Below 20% USL the fatigue failure mode of the damage tapered scarf repaired beams was tensile failure of the inner skin.

e) The 'fatigue limit' in column 6 is used to assess whether the structure is fatigue damage tolerant, or whether the damage has changed the mode of failure. The results from this research indicate that a 20:1 tapered scarf repair is damage tolerant to a delamination area of 3800mm^2. Conversely, it was noted that a defect within the tapered scarf repair measuring 8200mm^2 or greater will reduce the ultimate stress of the repair scheme down to 28% USL (which equates to approximately 42MPa).

Question 5.

The final step in the damage tolerance assessment of BVID on the tapered interface in Figure 7.4 is to undertake a risk assessment. The probability of a BVID defect occurring within the repair interface and its severity rating is considered in Table 7.4.

Defect type and size [mm^2]	USL to cause failure	Probability of damage occurrence	Probability of damage growth	Category rating	Risk assessment	Recommended action
< 3800 mm^2	98%	Probable	Probable (likely to occur several times in the life of an item) to Occasional (likely to occur sometime in the life of an item)	Minor	Medium to low (C)	Reinstate to operational capability with routine service inspections
4000 mm^2 to 8200 mm^2	~98%	Probable	Probable (likely to occur several times in the life of an item) to Occasional (likely to occur sometime in the life of an item)	Minor	Medium to low (C)	Reinstate to operational capability with routine service inspections
> 8200 mm^2	31%	Probable	Frequent (Likely to occur frequently) to Probable (Likely to occur several times in the life of an item)	Critical	High (A)	Reject repair and replace

Table 7.4: Damage tolerance and probability of delamination growth guidelines for tapered interface

Table 7.4 assesses the consequences of the defect on the tapered interface of the structural repair through 'Probability of occurrence' and 'Probability of growth'. This information is then used to form the recommended action. The table has been developed by the author and considers the following interactions:

a) The FMECA introduced in Chapter 3, Figure 3.1 and Chapter 4, Section 4.5.
b) The 'probability of damage occurrence' has been defined according to the definition in Table 4.2. The selection of 'probable' for damage occurrence is

perceived by the author to best reflect the likelihood of impact damage occurring within the lifetime of the structure.

c) The 'probability of damage growth' has been defined according the definition in Table 4.2.

The selection of 'probable' to 'occasional' for delamination damage < 8200mm^2 growing along the tapered interface is perceived by the author to reflect the likelihood of the damage propagating under operational loading, i.e. to cause static failure of the beams USL levels of 93% or higher will have to occur within the lifetime of the structure. It is felt that this is unlikely. Furthermore, in the fatigue tests the damage remained unaffected and benign until the static buckling stress of the outer skin was exceeded.

The selection of 'frequent' to 'probable' for the growth of damage sizes greater than 8200mm^2 is based upon the experimental evidence that the damage was observed to initiate outer skin buckling at USL levels of 31% or below. It is felt that this USL level is likely to occur during operational loading and therefore there is a risk of repair failure.

d) The 'category rating' in column 5 is a measure used to rate each defect type. This is established from the definition in Chapter 4 and from the technical understanding gained within this project.

The defect rating of 'minor' has been given to delamination damage below 8200mm^2 because the damage does not influence the static mode of failure, i.e. the sandwich structure can be considered damage tolerant to BVID upto 8200mm^2.

The defect rating of 'critical' has been given to delamination damage above 8200mm^2 because this defect size is likely to initiate outer skin buckling at typical operational loading levels. This could cause major damage to the repair and risk failure of the structure.

e) The risk assessment in column 6 is the derived from the combination of the 'probability of damage growth' and the 'category rating'. This interaction is defined in Table 4.3, where 'A' is the highest risk and 'D' is the lowest.

In this case, any damage greater than 8200mm^2 is a high risk to the structure.

f) The 'recommended action' in column 7 details the repair strategy for the category determined in the risk assessment in column 6. This information is also provides the instructions in the flowchart in Figure 7.4.

Question 6.

Figure 7.4 also considers the possibility of BVID occurring to the repair overlaminate. The size of the defect is determined from NDE.

Question 7.

If the defects are exposed to the environment this could influence the rate at which the defect grows, i.e. through material degradation or external peeling forces associated with the movement of water across the fractured edge.

Question 8.

The methodology behind this element of the flowchart considers whether the environment could influence the failure mode of the defect.

a) This research has indicated that an impact threshold (976J) exists for the separation of the overlaminate 'tip' from the original parent laminate. Any damage observed at this location must be repaired because failure could be accelerated by environmental attack.
b) The overlaminate design used in this project was able to support internal damage up to 13500mm^2 before the impact threshold for overlaminate peeling occurred (point (a) above).

The damage tolerance philosophy for the overlaminate is given in Table 7.5.

Impact energy	Delamination area [mm^2]	Compressive failure stress [MPa]	USL loading used in fatigue tests	Failure mode	Fatigue limit
<976	13500	151.0	98%	Core shear	Operational structure will not be loaded to this USL therefore the structure can be considered damage tolerant
>976	Impact energy initiates failure between the overlaminate and the parent	Failure stress influenced by environmental attack	Not undertaken	Overlaminate peeling	The structure cannot be considered damage tolerant because the fatigue life is dependent upon the environmental degradation of the overlaminate interface

Table 7.5 Damage tolerance assessment for repair overlaminate

Question 9.

The final step in the damage tolerance assessment of BVID within the overlaminate in Figure 7.4 is to undertake a risk assessment. The probability of a BVID defect occurring within the overlaminate interface and its severity rating is considered in Table 7.6

Defect type and size [mm^2]	USL to cause failure	Probability of damage occurrence	Probability of damage growth	Category rating	Risk assessment	Recommended action
<13500 mm^2	98%	Probable	Remote	Minor	Medium to Low (C)	Reinstate to operational capability with routine service inspections
>13500 mm^2 leads to exposed edge of the overlaminate	Governed by attack from environment	Probable	Frequent (if on or under waterline)	Critical	High (A)	Reject repair and replace

Table 7.6: Damage tolerance and probability of growth guidelines for overlaminate

The damage tolerance summary in Table 7.6 illustrates the complex interaction between the overlaminate, the types of damage that could occur and the influence they have upon the overall performance of the repair scheme. Since the overlaminate is employed to protect the taper scarf from stress concentrations the extent of the damage that can be accommodated within it has to be balanced against the effect this will have upon the tapered scarf repair. The assumptions used in Table 7.6 are detailed below:

a) The 'probability of damage occurrence' has been defined following the same approach for the tapered interface (Note 4b).
b) The 'probability of damage growth' for delamination damage less than 13500 mm^2 has been determined as 'Remote' since this type of damage was observed to propagate during the static tests. Conversely, delamination damage greater than 13500 mm^2 has been set as 'Frequent' because the exposed edge of the overlaminate would be under attack from the environment, which may accelerate failure.
c) The 'criticality rating' was set at 'Minor' for the delamination less than 13500 mm^2 because it is unlikely the damage will propagate before core shear failure

occurs. For delaminations greater than 13500 mm^2 it was set at 'Critical' because the exposed edge of the overlaminate could initiate failure of the composite repair.

d) The outcome of the 'Probability of damage growth' and the 'Criticality rating' is reflected in 'Risk Assessment' ratings which indicates the high risk of having an exposed overlaminate edge.

e) The 'recommended action' in column 7 details the repair strategy for the category determined in the risk assessment in column 6. This information is also provides the final instructions in the flowchart in Figure 7.4.

7.2.3 Damage tolerance observations

The damage tolerance approach for the 'Repair Decision' step and the 'Repair Verification' step within the repair cycle identified in Figure 7.1 has been defined. The flowcharts in Figure 7.3 and Figure 7.4 map out the damage tolerance methodology whilst Tables 7.1 and 7.2 details the damage tolerance assessment for the 'Repair Decision' step, and Tables 7.3, 7.4, 7.5 and 7.6 provide the damage tolerance assessment for the tapered interface and the overlaminate interface.

The technical information, justification and specific damage threshold information supporting the flowcharts in Figure 7.3 and 7.4 are applicable to the type of materials used in the sandwich structure, the design of the repair scheme and form of BVID used in this project. However, the damage tolerance methodology contained within this section is generic in nature and therefore can be applied in other situations.

7.3 SURVEYOR'S CHECKLIST

7.3.1 Introduction

In Chapter 2 it was identified that the development of clear guidelines for the assessment of damaged structural repairs is required. It was postulated that a design tool could form the basis of an 'intelligent' interrogation system that skilled and unskilled workers can use to make an informed decision about a defects criticality. The purpose of this section is to propose a generic approach that could form the basis of a damage tolerance design tool.

7.3.2 Damage tolerance design tool

In the assessment of a damaged or defective structural repair the surveyor will have to consider the information contained within the repair cycle flow-chart, the defect criticality flowcharts and the damage tolerance tables introduced in Section 7.5.

The aim of the damage tolerance design tool is to present the pertinent damage tolerance information to the end-user without over-complicating the information. Ideally, a full summary of the damage tolerance results for the tapered scarf repair should be presented in a simple tabular format. Table 7.7 has been included (with the findings from this project) as an example of the required format.

Defect type	USL to cause failure	Probability of damage occurrence	Probability of damage growth	Category rating	Risk assessment	Recommended action
Adhesive bondline in replacement foam core	25%	Probable	Probable to Occasional	Marginal	High to Medium (B)	Reject the repair and replace
Repair tapered interface <8200mm^2	98%	Probable	Probable to Occasional	Minor	Medium to low (C)	Reinstate to operational capability with routine service inspections
Repair tapered interface >8200mm^2	31%	Probable	Frequent to Probable	Critical	High (A)	Reject the repair and replace
Overlaminate interface <13500 mm^2	98%	Probable	Remote	Minor	Medium to Low (C)	Reinstate to operational capability with routine service inspections
Overlaminate interface >13500 mm^2	Governed by attack from environment	Probable	Frequent (if on or under waterline)	Critical	High (A)	Reject the repair and replace

Table 7.7: Summary of damage tolerance findings

The results in Table 7.7 are taken directly from Tables 7.4 and 7.6. The damage tolerance recommendations in Table 7.7 are used to supplement a standard repair methodology for composite structures. An example of such a methodology for the repair of composite structures was proposed in Figure 7.2 and it recommended from this study that the damage tolerance flowcharts (Figures 7.3 and Figure 7.4) be directly incorporated within this existing methodology and employed as a damage tolerance design tool.

In addition to the existing flowcharts it is recommended that the technical information be consolidated in to a clear visual representation for a surveyor to understand the complex damage tolerance methodology that exists within a tapered scarf repair in a composite sandwich structure. To generate a failure map for increasing damage size within the tapered scarf interface, the theoretical equations for the design of a tapered scarf repair first introduced in Chapter 2, Table 2.9 and Chapter 6, Section 6.2 have to be considered. A summary of these critical equations has been detailed in Table 7.8.

Description	Author	Equation	Equation number
Theoretical compressive stress limit of the pristine laminate	[Hart-Smith, 1973a]	$P = E\varepsilon_u t$	(7.1)
Ultimate stress variation in the tapered scarf repair	[Soutis & Hu, 1997]	$\theta_{opt} \cong \tan^{-1}(0.816\tau_s/\sigma_{un})$	(7.2)
Theoretical buckling stress limit	[Zenkert, 1995]	$\sigma_{cr} = 0.85\sqrt[3]{E_f E_c G_c}$	(7.3)

Table 7.8: Theoretical equations for buckling stress limit and the design of composite repairs

The theoretical maximum load that a composite repair could attain is based upon the ultimate design strain (ε_u) in equation 7.1. This value provides a ceiling for the failure map. The ultimate stress within a tapered scarf repair subjected to compressive loads is based upon the work by Soutis and Hu [Soutis and Hu, 1997] and given as equation 7.2. The ultimate stress within this equation is governed by the ultimate design strain (ε_u) in equation 7.1. Therefore it is the shear stress of the repair resin in equation 7.2 that determines the tapered scarf stress transfer efficiency. Any variation to this material property, via poor bonding of the resin or the inclusion of defects, will significantly influence the mechanical performance of the repair.

In an effort to understand the influence of damage length upon the ultimate stress within the tapered scarf joint, the Soutis equation [Soutis & Hu, 1997] (which determines the

ultimate stress in the tapered scarf repair) has to be modified to take account of the reduction of the available taper area, as the defect increases along the length of the tapered interface. This revised equation is given below.

$$\theta_{Defect} = 200 \times ATAN\left(\frac{Skin_{Thk}}{Area_{Taper} - Area_{Defect}}\right) \tag{7.4}$$

$$\sigma_{Defect} = \frac{0.816 \times \tau_{\text{Re } pair}}{Tan\left(\theta_{Defect}\right)} \tag{7.5}$$

The resulting intersection of the theoretical equations in Table 7.8 and experimental data illustrates the dominant failure mode within the repaired tapered interface as the damage area increases has been indicated in Figure 7.5.

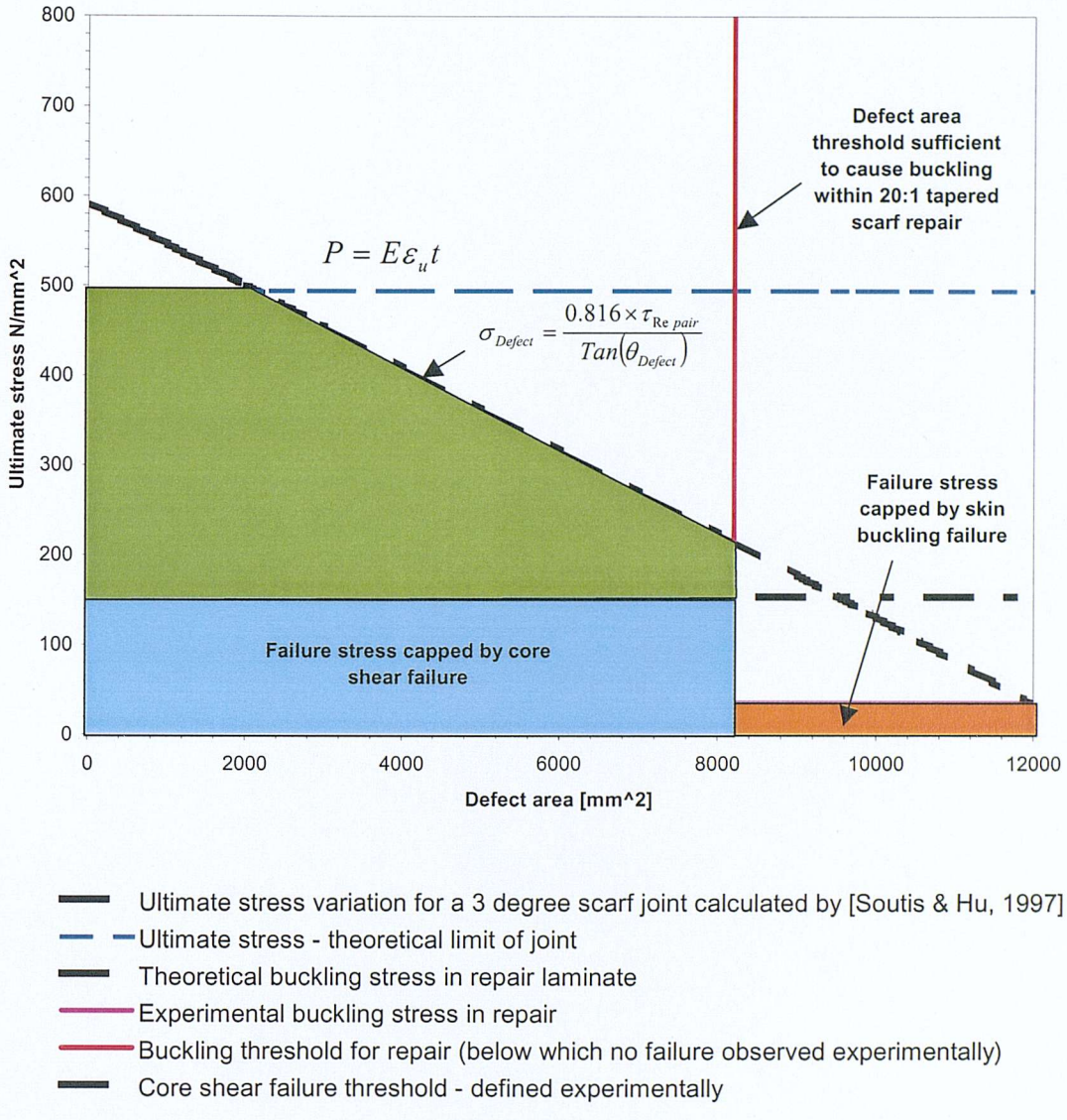

Figure 7.5: Damage tolerance zone as a function of defect size in tapered scarf repair

Figure 7.5 indicates that at the lower damage sizes the failure stress within the beam is capped by the stress to initiate core shear failure (the blue zone). The green zone shows the influence of the damage size upon the failure stress within the tapered interface. However, since the repair failure stress is above the stress to initiate core shear failure, the core will fail in preference to the tapered interface.

As the defect size increase, the stress at the tapered interface approaches the core shear failure stress. However, when the defect attains a damage area of 8200mm^2 it is

sufficient to initiate buckling failure within the outer skin. The dominant failure mode then switches from core shear to outer skin buckling. Once again, the stress to initiate failure in the repair is above the buckling stress of the outer skin and hence it is unlikely to be dominant. This situation is unlikely to change unless the buckling stress in the outer skin is increased by the application of a different laminate configuration or by using a damage tolerant adhesive in the vertical bondline for the replacement foam core.

7.4 DAMAGE TOLERANCE QUESTIONS

To further assist, and prompt, the surveyor to address the critical points of undertaking a damage tolerance assessment a series of questions have been composed for some assistance.

1. Is the damage zone above or below the waterline?
2. Has a dynamic impact event greater than the impact energy threshold occurred?
3. Has the outer skin been dented or penetrated?
4. Can the defect size be resolved with the current NDE equipment?
5. What repair manufacturing technique was used?
6. Were standard/recommended repair materials used?
7. Was the repair manufacture kept within processing controls?
8. Was the repair environment controlled?
9. Is the quality of workmanship very good, good or bad?
10. What is the precise location of the defect within the repair?
11. Has the residual strength performance been compromised?
12. What are the typical operational loads for the vessel?
13. How often will the vessel operate at its extreme limit?
14. Is the defect within its damage tolerance zone?
15. Are the load levels sufficient to propagate the known defect?
16. What is the probability of defect growth?
17. What are the consequences of defect growth?

7.5 CONCLUDING REMARKS

The purpose of this section has been to introduce the starting blocks for the formation of a damage tolerance design tool for structural repairs to marine sandwich structures. Through the application of the flow charts and the damage tolerance tables developed in Section 7.2, with the damage tolerance zone chart (Figure 7.5 in Section 7.3) and supporting questions presented in Section 7.4, the surveyor will be able to undertake an instantaneous evaluation of a damaged or defective repair in a composite sandwich structure and determine what corrective action is required, i.e. the repair is damage tolerant or it requires replacement.

8 CONCLUSIONS AND SUGGESTIONS FOR FUTURE WORK

8.1 Conclusions

1 The research undertaken in this project is the first to extensively review the repair of composite sandwich structures by examining the nature of operational defects, the basis for the design of structural repairs and the examination of typical repair techniques employed by military and commercial organisations in the marine and aerospace communities.

2 The research presented here uniquely characterises the damage tolerance performance of a structural repair, in a composite sandwich structure, in relation to barely visible impact damage (BVID). This has been achieved through:

- Characterisation of the damage formation and impact damage tolerance threshold for critical defects in tapered scarf repairs in composite sandwich structures;
- Determining the damage tolerance performance of a tapered scarf repair through the characterisation of the residual strength and fatigue performance.

This specific conclusions arising from this part of the research are:

2.1 A relationship between delamination size in sandwich panels and impact energy shows good agreement for the two different impact velocities used within this research. This relationship indicated that once a critical energy of 635J was reached, regardless of the impact velocity, there is a rapid increase in the delamination size.

2.2 The threshold energy to initiate impact damage failure along the scarf taper is comparable with the 'pristine' beam, but the magnitude of the damage within the repair is almost double the pristine beam at an impact energy of 1270J.

2.3 The static strength performance of the pristine beams and the tapered scarf beams are governed by the core shear strength properties (~1.70 MPa).

2.4 The residual strength performance of the pristine beams and the tapered scarf repair was governed by the compressive strength of the outer skin. The residual strength performance of the tapered scarf repair is superior to the pristine beam. This can be attributed to the greater amount of material within the repair scheme.

2.5 On the pristine beams, a residual dent in the outer skin resulting from a 387J impact was sufficient to cause an 18% reduction in the residual compressive stress. Once the damage size was greater than 3000 mm^2 the residual compressive stress fell to ~20%.

2.6 On the tapered scarf repair, once the impact damage (at impact location 1) had gained sufficient size (greater than 8200 mm^2) and the compressive stress in the outer skin has achieved ~49MPa the outer skin would fail in buckling about the start of the scarf taper.

2.7 In all fatigue loadings the dominant failure mode was catastrophic tensile failure of the inner skin. However, at high USL levels (80% and 60%) the tensile failure of the skin was initiated from the breakdown of the core material. Fatigue lives in excess of 1 million cycles was attainable for both the pristine and repaired beams when loaded to 30% USL.

2.8 Crack growth from impact damage (at impact location 1) measuring 13000mm^2 did not occur when loaded below the buckling stress threshold of 25% USL. If the loading exceeded this value the outer skin would fail during the next fatigue cycle.

2.9 Tapered scarf repairs can be considered damage tolerant only if the operational loading remains below the outer skin compressive buckling stress, i.e. 49MPa.

2.10 The G_{Ic} tests undertaken for the three different material combinations established that the repair laminate had the highest toughness, followed by the laminate representing the repair-parent interface, which was superior to the fracture toughness of the parent laminate. The same performance hierarchy was also observed for the G_{IIc} tests.

2.11 The fracture toughness of all the laminates was influenced by the formation of fibre bridging by the Kevlar fibres. The selection of the initial pre-crack in the mode II fracture toughness tests was observed to influence the fracture initiation threshold, and have some influence upon the energy required for crack propagation.

2.12 The two theoretical predictions by [Olsson, 2002] are able to capture the damage initiation and propagation characteristics of the tapered scarf repair from the fracture mechanics data determined within this project.

3 It has been previously suggested that the inclusion of the overlaminate plies protects the tapered scarf tip from damage and minimises stress concentrations at the scarf tip end [Deaton, 1990; Smith 1995]. However, in this thesis it has been shown for the first time than an impact energy threshold exists for the initiation of a 'peel' crack at the repair overlaminate edge. This result importantly indicates the need to update the design guidelines originally developed in the 1970s.

3.1 An impact energy threshold of 976J exists for the initiation of a 'peel' crack at the repair overlaminate edge of a 20:1 tapered scarf repair manufactured from E-glass/ Aramid fabric with a epoxy matrix.

3.2 This research suggests that regardless of overlap length an impact event may be sufficient to overcome the tensile transverse stresses of the repair resin and cause failure of the patch/parent laminate interface.

4 This project is the first to generate comprehensive damage tolerance guidelines (using flowcharts and damage tolerance tables) for tapered scarf repairs in composite sandwich structures. This unique approach forms the basis of an 'intelligent' interrogation system that skilled and unskilled workers can use to make an informed decision about the criticality of defects in operational composite sandwich structures. Validation of the generic damage tolerance methodology has been undertaken through the examination of a specific marine composite sandwich structure used in the manufacture of the RNLI all-weather class of lifeboat, and subsequently guidelines have been developed that can now be applied to the RNLI fleet.

5 In addition to this specific application, the methodology applied in this research project is transferable to sandwich structures used in other industrial environments, and therefore has a great value as a practical tool.

8.2 Suggestions for future work

The work undertaken in this project has illustrated the need to revise the existing approach to designing composite structural repairs. The current approach used by composite engineers is based upon the pioneering work undertaken by Hart-Smith in the 1970s. Since its development the understanding of composite materials has significant evolved and this work is conservative in nature. It is recommended that future work in this area consider the following:

1. The stress and strength interaction between the tapered scarf profile and the overlaminate plies should be determined. This will lead to better and more efficient repair designs.

2. Clear guidelines about the overlaminate recommended lengths should be devised.

3. The stress concentration on the internal edge of a tapered scarf repair undertaken to a composite sandwich structure should be evaluated and design solutions developed to minimise this problem.

4. Design guidelines should be developed specifically for repairs located within regions having high impact probability. The role of compliant adhesives on the short-term and long-term performance of the outer ply should be considered.

The strength-based and fracture based assessment of the damaged repairs has also indicated areas for future work, namely:

1. Scaling of impact damage from beams to panels should be undertaken. The current research has indicated a detailed knowledge of the failure mechanisms within composite sandwich beams. Scaling of the failure mechanisms is critical in the development of a damage tolerance methodology.

2. Scaling of residual strength results should also be undertaken. The work within this research has been undertaken on semi-structural components but work is now needed to understand the interaction of internal structural (i.e. stiffeners, bulkheads) upon the external panels. It is likely that theses internal supporting structures will redistribute the stress concentrations and are therefore more likely to increase the damage tolerance performance of the sandwich structure.

3. The influence of environmental attack upon the damage tolerance performance of the impact-exposed edge of the E-glass/Kevlar overlaminate is required.

4. A fracture mechanics assessment of a crack propagating along the tapered interface of a composite repair is required. In this research damage was observed to occur at this interface hence, if the design of the repairs are optimised in the future, there is a possibility that damage propagation at this interface will occur and become critical.

9 REFERENCES

Abrate, S. 'Localised impact on sandwich structures with laminated facings', *Applied Mechanics Reviews*, 50(2), pp 47-55, 1994

Adkins D.W. and Pipes R.B. 'Tensile Behaviour of Bonded Scarf Joints Between Composite Adherends', presented at Proceedings of the 4th Japan-US Conference on Composite Materials. Washington, D.C., pp. 845-854, 1988.

Allen H.G. 'Analysis and Design of Structural Sandwich Panels', Pergamon Press, Oxford, 1969.

Armstrong K.B. and Barrett R.T. 'Care and repair of advanced composites', Society of Automotive Engineers, Inc., Warrendale, PA, USA, 1998.

Attia O., Kinloch A.J. and Matthews F.L. 'Modelling the fatigue life of polymer-matrix fibre-composite components', *Composite Science and Technology*, **61**, pp 2273-2283, 2001.

Austen S 'Repair Specification for ON1202 (Harwich Lifeboat)', Royal National Lifeboat Institution, Poole, Dorset, UK, June 2001.

Austen S 'Repair Specification for ON1210 (Exmouth Lifeboat)', Royal National Lifeboat Institution, Poole, Dorset, UK, February 2000.

Austen S 'Repair Specification for ON1217 (Aran Lifeboat)', Royal National Lifeboat Institution, Poole, Dorset, UK, May 1999.

Austen S 'Repair Specification for ON1217 (Aran Lifeboat)', Royal National Lifeboat Institution, Poole, Dorset, UK, May 2000.

Austen S 'Repair Specification for ON1243 (Newhaven Lifeboat)', Royal National Lifeboat Institution, Poole, Dorset, UK, March 2001.

Baker, A.A. and Jones, R., 'Bonded Repair of Aircraft Structures', Martinus Nijhoff Publishers, Dordrecht, The Netherlands, 1988.

Baker, A.A., Jones, R. and Callinan, R.J. 'Damage tolerance of graphite/epoxy composites', *Composite Structures*, **4**, pp15-44, 1985.

Beheshty M.H., Harris B. and Adam T. 'An empirical fatigue-life model for high-performance fibre composites with and without impact damage', *Composites Part A*, **30**, pp 971-987, 1999.

Blackman, B.R.K. Telephone correspondence with Dr B. R. K. Blackman, Department of Mechanical Engineering Imperial College London, UK, 2004

Bristow J.W. and Goudie A.D. 'The Three 'R's – Repair, Replacement and Regulation' In-service Structural Integrity, NDE and Repair, IMechE, Bristol, May 2002.

Burman M. and Zenkert D. 'Fatigue of foam core sandwich beams – 2: effect of initial damage', *Int. J. Fatigue*, **19**(7), pp 563-578, 1997.

Caprino, G and Teti, R '*Sandwich Structures Handbook*', Il Prato, Italy, 1989

Chaplin N and Austen S 'Repair Specification for ON1227 (Oban Lifeboat)', Royal National Lifeboat Institution, Poole, Dorset, UK, May 2002.

Choi H.Y., Downs R.J. and Chang F. –K. 'A new approach to understanding damage mechanisms and mechanics of laminated composites due to low-velocity impact: Part I – Experiments' *J. Compos. Mater.* **25** pp 992-1011, 1991.

Christoforou A. P. 'Impact dynamics and damage in composites structures', *Composite Structures* **52**, pp 181-188, 2001.

Clark, S.D., 'Long Term Behaviour of FRP Structural Foam Cored Sandwich Beams' Doctorial Thesis 1997, University of Southampton, Southampton, UK.

Cochran R.C., Donnellan T.M., Rosenzweig E.L. and Trabocco R.E. 'Composite repair material and design development efforts' in AGARD-CP-402 'The repair of aircraft structures involving composite materials', Oslo, Norway: NATO, pp 16.1/16.13, 1986.

Cole, W.F. 'Technical justification of repairs to composite laminates', *Int. J Adhesion and Adhesives*, 1999, **19**,107-120.

COMPOSITES I, Seahorse, 159, p. 49, May 1993

Corleto, C. R., Bradley, W. L., Mode II delamination fracture toughness of unidirectional graphite/epoxy composites, *Composite Materials: Fatigue and Fracture, 2nd Vol.*, ASTM STP 1012, Philadelphia, pp. 201 - 221, 1989.

Curley A.J., Hadavinia H., Kinloch A.J. and Taylor A.C. 'Predicting the service-life of adhesively-bonded joints', *Int. J Fracture*, **103**, pp 41-69, 2000.

Davies G.A.O., Hitchings D. and Zhou G. 'Impact damage and residual strengths of woven fabric glass/polyester laminates', *Composites Part A* **27A**, 1147-1156, 1996.

Davies P., Sims G.D., Blackman B.R.K., Brunner A.J., Kageyama K., Hojo M., Tanaka K., Murri G., Rousseau C., Gieseke B., Martin R.H.. '*Comparison of test configurations for determination of mode II interlaminar fracture toughness results from international collaborative test programme.* Plastics, Rubber and Composites, Vol **28**, Number 9, p.432-437, 1999.

Davis M.J. 'The development of an engineering standard for composite repair' in *Composite Repair of Military Aircraft Structures*, AGARD-CP-550. Seville, Spain: NATO, pp 24.1/24.11, 1995.

Davis M. and Bond D. 'Principles and practices of adhesive bonded structural joints and repairs', *Int. J. Adhesion & Adhesives,* **19**, pp91-105, 1999.

Deaton, J.W. 'Repair of Advanced Composite Commercial Aircraft Structures' in *Engineering Materials Handbook, Vol. 3: Adhesives and Sealants:* ASM, pp 830-839, 1990.

Decobert, F. 'WP3 Damage Repair Methodology State of the Art Survey Synthesis Report', EUCLID CEPA3 – RTP 3.8, TD-03116-9401 Rev 1, March 1994.

Dorey, G. 'Impact damage in composites – development, consequences and prevention', in *Proc 6th Int Conf Comp Mat comb 2nd European Conf Comp Mat*, London, 3.1-3.26, 1987.

Finn S. R., He Y. –F. and Springer G.S. 'Delaminations in composite plates under transverse impact loads – experimental results' *Compos. Struct.* **23**, 191-204, 1993.

Fraisse P. and Schmit F. 'Analyse par la mecanique de la rupture de la tenue des junctions collees', Materiaux et Techniques, n 4-5, 1992.

Frame C.S. 'Composite Repair of Composite Structures' in *Composite Repair of Military Aircraft Structures*, AGARD-CP-550. Seville, Spain: NATO, pp 17.1/17.11, 1995.

Gere, J.M. and Timoshenko, S.P. 'Mechanics of Materials' Third SI Edition, Chapman and Hall, London, UK, 1993.

Greenhalgh, E., Asp, L. and Singh, S. 'Delamination resistance, failure criteria and fracture morphology of 0°/0°, 0°/5° and 0°/90° ply interfaces in CFRP', 5th International Conference on Deformation and Fracture of Composites, ImechE, London, UK, 18-19 March 1999.

Grosko J. 'Structural modification and repair of C-130 wing structure using bonded composites' in *Composite Repair of Military Aircraft Structures*, AGARD-CP-550. Seville, Spain: NATO, pp 8.1/8.9, 1995.

Hahn M 'Design for repairability of helicopter composite blades', in *The Repair of Aircraft Structures Involving Composite Materials*, AGARD-CP-402. Oslo, Norway: NATO, pp 3.1/3.15, 1986.

Hashemi, S., Kinloch, A. J., Williams, J. G., Corrections needed in double cantilever beam tests for assessing the interlaminar failure of fiber-composites, *J Materials Science Letters, Vol. 8,* pp. 125 – 129, 1989.

Hart-Smith, L.J. 'Adhesive bonded scarf and stepped-lap joints', *NASA CR-112237*, January 1973.

Hart-Smith, L.J. 'Adhesive bonded single lap joints', *NASA CR-112236*, January 1973.

Hoo-Fatt, M.S., Park, K.S., 'Modelling low-velocity impact damage of composite sandwich panels', *J Sandwich Structures and Materials*, **3**, pp. 130-168, 2001.

Ireman T. and Purin P. 'Evaluation of factors affecting the design of bolted composite laminates' in the 'International conference on Joining and repair of plastics and composites, IMechE Conference Transactions, 16-17 March 1999, The Institution of Mechanical Engineers, London, UK.

Irving P.E., 'Achievement of damage tolerant designs in metal and composite aircraft structures', IMechE conference on 'In-service structural integrity, NDE and repair', 30th May 2002, BAWA, Bristol, UK.

Kinloch, A., Wang, Y., Williams, J.G. and Yayla, P., 'The Mixed-Mode Delamination of Fibre-Composite Materials', *Comp Sci and Tech*, **47**, pp225-237, 1993.

Kinloch A.J. and Osiyemi S.O. 'Predicting the fatigue life of adhesively-bonded joints', *J. Adhesion*, **43**, pp 79-90, 1993.

Krueger R., Paris I. L. and O'Brien T. K. 'Fatigue life methodology for bonded composite skin/stringer configurations', in Proceedings of the America Society for Composites, Fifteenth Technical Conference, Technomic Publishing, pp 729-736, 2000.

L.J. Hart-Smith, 'Designing to minimise peel stresses in adhesively-bonded joints', Delamination and Debonding of Materials, ASTM STP 876, W.S Johnson, Ed., American Society for Testing and Materials, Philadelphia, 1985, pp. 238-266.

Li X. and Carlsson L. A. 'A test specimen for determining the fracture resistance of a facing/core interface', 4th International Conference on Sandwich Construction, Vol. 2, Stockholm, Sweden, June 9-11, pp 616-627, 1998.

Lubkin J.L. 'A theory of adhesive scarf joints', *J. Appl. Mech.*, pp 255-260, June 1957.

Madenci E, Shkarayev S, Shipilov Y and Scotti S 'Analysis of double-lap composite joints with multiple-row bolts under combined mechanical and thermal loading', in the 'International conference on Joining and repair of plastics and composites, IMechE Conference Transactions, 16-17 March 1999, The Institution of Mechanical Engineers, London, UK.

Mahler M. 'Bonded Composite Repair of Composite Structures', PhD Thesis, University of California, Los Angeles, 1999.

Maier A.E. and Günther G. 'Composite Repair of a CF18 – Vertical Stabiliser Leading Edge', in *Composite Repair of Military Aircraft Structures*, AGARD-CP-550. Seville, Spain: NATO, pp 13.1/13.16, 1995.

'Marine Composites' Second Edition, Eric Green Associates, Annapolis, Maryland, USA.

Matthews F.L. 'Joining FRP with mechanical fasteners' in the 'International conference on Joining and repair of plastics and composites, IMechE Conference Transactions, 16-17 March 1999, The Institution of Mechanical Engineers, London, UK.

MIL-STD-1629A 'Procedures for performing a Failure Mode, Effects, and Criticality Analysis' DEPARTMENT OF DEFENSE, Washington, DC 20301, 1980.

Mines R.A.W., Worrall C.M. and Gibson A.G. 'The static and impact behaviour of polymer composite sandwich beams', *Composite*, **25** (2), pp 95-110, 1994.

Mouritz A. P. and Thomson R. S. 'Compression, flexure and shear properties of a sandwich composite containing defects', *Composite Structures*, **44**, pp 263-278, 1999.

Noury P. M. C., Shenoi R. A. and Sinclair I. 'Fatigue crack growth in rigid PVC foam under combined mode-I and mode-II loading', 4th International Conference on Sandwich Construction, Vol. 2, Stockholm, Sweden, June 9-11, pp 493-504, 1998.

Olsson, R., Thesken, J.C., Brandt, F., Jönsson, N. and Nilsson S. 'Investigations of delamination criticality and the transferability of growth criteria', *Composite Structures* **36** (1996) 221-247

Olsson, R. 'Engineering method for prediction of impact response and damage in sandwich panels', *Jn.* Sandwich Structures and Materials, pp 3-29, Vol. 4, 2002.

Pavier M. and Clarke M., 'Experimental Techniques for the investigation of the effects of impact damage on carbon-fibre composites', *Composites Science and Technology*, **55**, pp157-169, 1995.

PERA 'DTI Composite performance and design programme: CPD 4A Repair Technology Project'. November 2000.

Potter D.L. 'Primary Adhesively Bonded Structure Technology (PABST). Design Handbook for Adhesive Bonding', Douglas Aircraft Co, Long Beach, California, US. AFFDL-TR-79-3129, November 1979.

Raizenne M. D., Benak T. J., Heath J. B. R., Simpson D. L. and Baker A. A. 'Bonded composite repair of thin metallic materials: variable load amplitude and temperature cure effects', in *Composite Repair of Military Aircraft Structures*, AGARD-CP-550, Seville, Spain, pp 5.1-5.12, 1994.

Ratcliffe J. and Cantwell W. J. 'Centre notch flexure sandwich geometry for characterising skin-core adhesion in thin-skinned sandwich structures' *J. Reinforced Plastics and Composites*, **20** (11), pp 945-970, 2001.

Reeder, J.R. and Crews, J.H. 'Mixed-mode bending method for delamination testing' *AIAA Journal*, **28** (7): 1270-1276, 1990

Richardson M. O. W. and Wisheart M. J. 'Review of low-velocity impact properties of composite materials', *Composite Part A* **27A**, pp1123-1131, 1996.

Romanko J., Liechti K. M. and Knauss W. G. 'Life prediction methodology for adhesively bonded joints', in Proceedings of the International Symposium on Adhesive Joints, Formation, Characteristics, and Testing, Plenum Press, New York, pp 567-586, 1984.

Schwan F.J. 'Design of Structure with Composites' in Handbook of Composites 2nd Ed, ed. Peters S.T., Chapman & Hall, 1998.

Shah-Khan, M.Z. and Grabovac I. 'Repair to damage to marine sandwich structures: Part II – Fatigue testing', DSTO-TN-0275, DSTO Aeronautical and Maritime Research Laboratory, Defence Science and Technology Organisation, Melbourne Victoria, Australia, 2000.

Shenoi, R.A., Dulieu-Barton, J.M., Jeong, H.K., Cripps, R.M. and Phillips, H.J., ''Case Study 2 – Application of FRP Repair Technology to Small FRP Vessels, Doc No. R.1.20.1342 – B2a', DTI/SSA Link Programme on Integrated Technology for Marine Construction (ITMC) #42: Design Production Guidance for the Use of FRP Composite Materials for Shipbuilding Applications, School of Engineering Sciences, University of Southampton, January 2003.

Shipsha, A., Burman, M. and Zenkert, D. 'On mode I fatigue crack growth in foam core materials for sandwich structures', *Journal of Sandwich Structures and Materials*, Vol. 2, April 2000, p103-116

Shipsha A. 'Failure of sandwich structures with sub-interface damage', Doctorial Thesis report 2001-13, Royal Institute of Technology, Stockholm, Sweden.

Shipsha, A. 'Edgewise compression of sandwich panels with impact damage', in 6th International Conference on Sandwich Structures, 31st March to 2nd April, 2003, Ft. Lauderdale, Florida, CRC Press, Washington, 2003, pp154 – 162

Sjögren J., Celsing C. G., Olsson, K. A., Levander C. G. and Hellbratt S.E. 'Swedish Development of MCMV – Hull Design and Production', International Symposium on Mine Warfare Vessels and Systems, The Royal Institution of Naval Architects, London, June 1984.

Smith, J. 'Design and structural validation of CF116 upper wing skin boron doubler' in *Composite Repair of Military Aircraft Structures*, AGARD-CP-550. Seville, Spain: NATO, pp 6.1/6.11, 1995.

Soutis C. and Hu F. Z. 'Repair designs of composites and efficiency of scarf patch repairs' Vol. 5, Proceedings of ICCM-11, Gold Coast, Australia, 14^{th}-18^{th} July 1997

Sutherland L. S. and Guedes Soares C. 'The effects of test parameters on the impact response of glass reinforced plastic using experimental design approach' *Composites Science and Technology* **63**, pp 1-18, 2003

Thiele T.H. 'Repair procedures for composite parts on the alpha jet' in *The Repair of Aircraft Structures Involving Composite Materials*, AGARD-CP-402. Høvik (Oslo), Norway: NATO, pp 2.1/2.7, 1986.

Thomas R., Luescher R. and Grabovac I. 'Repair to damage to marine sandwich structures: Part I – Static testing', DSTO-TR-0736, DSTO Aeronautical and Maritime Research Laboratory, Defence Science and Technology Organisation, Melbourne Victoria, Australia.

Thomson R. S., Shah Khan M. Z. and Mouritz A. P. 'Shear properties of a sandwich composite containing defects', *Composite Structures*, **42**, pp 107-118, 1998.

Tomblin J., Lacy T., Smith B., Hooper S., Vizzini A. and Lee S., 'Review of damage tolerance for composite sandwich airframe structures', DOT/FAA/AR-99/49, 1999.

Torres M and Plissonneau B 'Repair of helicopter composite structure: techniques and substantiations', in *The Repair of Aircraft Structures Involving Composite Materials*, AGARD-CP-402. Oslo, Norway: NATO, pp 6.1/6.21, 1986.

Trabocco R.E., Donnellan T.M. & Williams J.G. in Bonded repair of Aircraft Structures, Ed. Baker A.A. & Jones R., Dordrecht: Martinus Nijhoff, 1988.

Tran-Cong, T. and Heller, M. 'Reduction in adhesive shear strains at the ends of bonded reinforcements', DSTO-RR-0115, DSTO Aeronautical and Maritime Research Laboratory, Defence Science and Technology Organisation, Melbourne Victoria, Australia.

Vinson, J.R., 'The behaviour of sandwich structures of isotropic and composite materials', Technomic Publishing Company, Inc., Lancaster, Pennsylvania, USA, 1999.

Wang, H., Vu-Khanh, T., Le, V. N., Effects of large deflection on mode II fracture test of composite materials, *Journal of Composite Materials, Vol. 29*, **6**, pp. 833 - 849, 1995.

Webber J. P. H. 'Scarf Repair Joints in Carbon Fibre Reinforced Plastic Strips' *J. Adhesion,* **12**, pp 257-281, 1981

Wheatstone, C., http://www.rleggat.com/photohistory/history/wheatsto.htm, 1999.

Williams, J. G., Large displacement and end block effects in the DCB interlaminar test in Mode-I and Mode II, *Jn. Composite Materials*, **21** (4) pp 330-347, 1987

Williams J.G. 'End corrections for Orthotropic DCB Specimens', *Comp Sci and Tech,* **35**, pp 367-376, 1989.

Whitehead S., McDonald M. and Bartholomeusz R.A. 'Loading, degradation and repair of F-111 bonded honeycomb sandwich panels – preliminary study', Report No. DSTO-TR-1041, DSTO Aeronautical and Maritime Research Laboratory, Australia, 2000.

Wu C.L. and Sun C.T. 'Low velocity impact damage in composite sandwich beams', *Composite Strucutres,* **34**, pp 21-27, 1996.

Zenkert, D., 'An Introduction to Sandwich Construction', Chameleon Press Ltd., London, 1995

Zhou G. 'Prediction of impact damage thresholds of glass fibre reinforced laminates', *Composite Structures*, **31**, pp 185-193, 1995.

Zhou G. 'The use of experimentally-determined impact force as a damage measure in impact damage resistance and tolerance of composite structures', *Composite Structures*, **42**, pp375-382, 1998.

APPENDIX A

A.1 Introduction

The purpose of this appendix is to provide background information and sources of further information about the RNLI and composite rescue craft that they operate.

A.2 RNLI

The Royal National Lifeboat Institution (RNLI) is a charity organisation which provides life saving cover for the United Kingdom's and the Republic of Ireland's waters. The RNLI provides all weather lifeboat cover up to a range of 50 miles offshore within two and a half hours. The cover is 24 hours a day 365 days a year and the fleet of lifeboats can operate in the wide range of water conditions experienced around the UK and Ireland. This service is provided by a wide variety of craft ranging from very fast inshore rigid inflatable boats (RIBs) to far larger fibre-reinforced composite hulled offshore all-weather crafts. To guarantee these requirements, the RNLI has at its disposal an active fleet of 320 lifeboats, and a relief fleet of 131 lifeboats distributed in 230 stations strategically placed. In 2001, according to its rates, this institution saved 770 lives which is an average of 2 a day, landed 2,059 people and brought 4,093 people ashore. Since it was founded in 1824, the RNLI has saved over 135,500 lives.

A.3 Lifeboat History

The introduction in the UK of the Waveney class, a development of the United States coastguard 44 feet vessel, in the 1960's heralded the beginning of the modern fast afloat lifeboat. During the mid 1980's, increasing weight problems, resulting from the need for increased speed and additional operational equipment to meet increasing additional operational requirements, led to a progressive re-evaluation of materials to be used in the construction of lifeboats [RNLI, 1987]. To establish the relative performance of materials available, 1.5 m^2 panels made from steel, wood, aluminium and Fibre Reinforced Plastic (FRP) laminate and sandwich, representative of an RNLI boat structure, were tested under pressure and for impact performance [Hudson et al., 1993]. Following the satisfactory completion of the tests, there was evidence [Lloyds, 1989a; Lloyds, 1989b] to support the theory that an FRP boat could be satisfactorily built to withstand similar design pressures but at a lower weight than steel or aluminium.

Further abrasion and shock tests were undertaken [PERA, 1987] on a FRP sandwich prototype Mersey class lifeboat completed in 1988 [PERA, 1988].

The service profile of these vessels make them ideally suited for FRP construction in that they are required to be ready for service after years of sitting idle in a marine environment. Additionally, the craft must be able to withstand the impact of being launched and colliding into the host vessel. The ability to economically produce lightweight hull and canopy structures with highly visible gel coat finishes is also an attribute of FRP construction

A.4 Design Requirements For RNLI All-Weather Class Of Lifeboat

The Severn and Trent class lifeboats are the latest designs utilising fibre-reinforced composite and are shortly to be joined by a new class of slipway launched lifeboat, the Tamar class. These vessels are designed to have an operational capability of not less than 25 knots in Beaufort 2, a mean speed of 15-17 knots in Beaufort 7 and safe operation in wave heights of 11-15 meters and 60 knot winds. Furthermore, they have to be inherently self-righting after capsize and hence constructed from a material in such a manner as to withstand these operational requirements. Figure A1 illustrates a Severn class all-weather lifeboat.

Figure A1: Severn class all-weather lifeboat on operational duties in UK coastal waters

A.5 Lifeboat Design and Operational Loading Requirements

The major structural load for small fast craft is slamming loads on the base of the hull. The RNLI have developed a design procedure for the determination of the maximum design pressure for the bottom structure of their lifeboats based on service experience. This design approach culminates in a structure design for robustness, i.e. a design that accounts for slam pressures, beaching loads and the operational nature of a lifeboat. Typically, a uniform pressure of 620kPa is applied to the bottom shell whilst 310kPa is typically observed on the side shell of the boat, which is distributed over the middle two thirds of the hull structure [Cripps *et al*, 2004]. At present the RNLI is developing a modelling environment capable of simulating three-dimensional wave slam pressure distributions on a given hull form in a range of sea-states [Cripps *et al*, 2004]. Although still in the design validation stage, the CFD modelling has reported outer skin stress up 65MPa in extreme sea-states [Phillips, 2004]. The fatigue life of the composite structure has been validated against sandwich beam flexural fatigue tests undertaken in controlled laboratory conditions [Allen, 1992; Clark *et al*, 1998].

A.6 Materials And Construction

The Trent class lifeboat is made entirely from sandwich construction whilst the Severn class is similar except for the hull below the chine, which is single skinned and has top hat stiffening inside. For a comprehensive review of the design and development of the RNLI lifeboats see reference [Hudson, 1990; Hudson, 1992; Hudson et al., 1993].

The two vessels employ similar materials in the composite skins and cross-linked PVC core materials (typically 100-200kg/m^3).

The outer skin is constructed of 3 layers of a quadriaxial E-glass/ Aramid fabric with a single light biaxial E-glass/ Aramid surface cloth. The matrix material is an epoxy resin, specified Ampreg 75. This composite material is supplied as a pre-impregnated lamina, which are stacked in sequence prior to consolidating with a vacuum pressure and temperature.

The inner skin is constructed of 2 layers of an E-glass quadriaxial fabric. The matrix material is an epoxy resin, specified Ampreg 26. The composite laminate is

manufactured by the hand lay-up process and then vacuum consolidated against the foam core.

Typical material properties for the outer skin, inner skin and the repair material, as specified by the manufacturing company SP Systems [SP Systems], is provided in Table A.1 and A.2

Skin type	Lay-up	Ply thickness (mm)	Fibre volume fraction	Young's modulus (kN/mm^2)	Tensile strength (N/mm^2)
Outer skin	3 * QEA 1200 and RE 210	1.07	0.52	21.3	319
Inner skin	2 * QE 1200	0.99	0.48	18.4	276
Repair material	4 * QEA 1200	1.15	0.48	19.7	295

Layup code : E E-glass
A aramid
R reinforced balanced 0/90 woven roving
Q balanced quadriaxial 0°/90°/+45°/-45° woven roving
No. weight of cloth per unit area (g/m^2)

Table A.1: Material properties for the outer skin, inner skin and the repair material

Resin type	Hardener type	Curing temperature (°C)	Tensile strength (N/mm^2)	Young's Modulus (N/mm^2)
Ampreg 26	slow hardener	45-50	80	3200
Ampreg 75	fast hardener	80	76	3100

Table A.2: Typical material properties for resin systems Ampreg 26 and Ampreg 75

The core material used in the lifeboats is a closed-cell PVC core material, i.e. Divinycell H130 with a density of $130kg/mm^2$. Each layer is 25mm wide and four individual core sheets are bonded together to produce a core material with a total thickness of 100 mm.

Typical material properties for H130 as specified by Divinycell [] is indicated in Table A.3.

Core material	Density (kg/m^3)	Tensile modulus (MPa)	Tensile strength (MPa)	Shear modulus (MPa)	Shear strength (MPa)
Divinycell H130	130	140	4.2	52	2.0

Table A.3: Material properties for H130 PVC foam core [].

The two sandwich construction halves of the vessel are manufactured in female moulds. When the two halves of each hull are completed, they are joined and bonded along the centreline to provide a single hull moulding. This has been illustrated in Figure A.2

Figure A.2: Bondline joint between the two halves of the hull

Once bonded together, top-hat stiffeners are used to reinforce the hull form. A typical cross-section of a out-plane stiffener is illustrated in Figure A.3.

Figure A3: Out-of-Plane Stiffener

These stiffeners are constructed from PVC foam with the composite being applied via hand lay-up process. Once adhesively bonded in position to the hull additional composite plies are added on top to provide addition toughness and strength.

In addition to the top hat stiffeners, composite bulkheads are manufactured and bonded to the outer hull. Figure A4 shows an example of fitted bulkhead in the bow of a Trent class lifeboat, whilst Figure A5 shows the stiffening arrangement within a Severn class lifeboat. The vertical bulkheads are typically spaced 1.2m apart along the length of the vessel.

Figure A4: Bulkhead joints in bow section of Trent Lifeboat

Figure A5: Stiffening arrangement within the hull of a Severn class lifeboat

A.7 References

Allen, H.G. and Shenoi, R.A. 'Flexural fatigue tests on sandwich structure', Second Internal Conference on Sandwich Construction, Florida, March, 1992.

Clark, S.D., Shenoi, R.A., Hicks, I.A. and Cripps R.M. 'Fatigue considerations for FRP sandwich structures of RNLI lifeboats', *The Royal Institution of Naval Architects*, Spring Meeting 1998, Paper No 3.

Cripps, R.M., Phillips, H.J., Cain, C., 'Development of Integrated Design Procedures for Lifeboats.', *SURV 6: Surveillance, Pilot & Rescue Craft, RINA,* 17-18 March 2004, pp 9-15.

Hudson, F.D., Hicks, I.A. and Cripps, R.M. 'The design and development of modern lifeboats', *Proc Instn Mech Engrs Part A: Journal of Power and Energy,* 1993, pp 207.

Hudson, F.D. 'Design and development of fast carriage lifeboat', Institution of Martine Engineers, April, 1990.

Hudson, F.D. 'The development of composites for fast rescue craft', SNAME, 1992.

Lloyd's Register of Shipping, 'Royal National Lifeboat Institution Fast Afloat Lifeboat Mk III Structural Analysis, Report No YSCS/620025, April 1989

Lloyd's Register of Shipping, 'Royal National Lifeboat Institution Fast Afloat Lifeboat Mk III Structural Analysis, Report No YSCS/620030, June 1989

PERA report No 87-72286, 'Testing of Lifeboat Hull FRP Laminate', 1987.

PERA report No 88-71581, 'High Impact Damage – Abrasion resistant future composites', 1988.

Phillips, H.J. Private communication 03 November 2004.

RNLI, 'Pressure and Impact Tests of Lifeboat Construction Materials' Internal Report 1987.

SP Systems, http://www.spsystems.com/main.htm

APPENDIX B

B.1 Dimensions of DCB Specimens

B.1.1 E-Glass-Kevlar Ampreg 75 parent laminate

Kevlar-Glass-Epoxy Specimens: K01-XX ... KN-XX where N is the total number of specimens

Points where dimensions are taken: 1 and 3 50 mm from the end

2 at the mid-point

	Width					Thickness				
	B - 1	B - 2	B - 3	B mean	max d	2h - 1	2h - 2	2h - 3	2h mean	max d
Nr.	[mm]	[mm]	[mm]	[mm]	[mm]	[mm]	[mm]	[mm]	[mm]	[mm]
K01-75	34.00	34.40	34.80	**34.40**	0.80	8.85	8.85	8.85	**8.85**	0.00
K02-75	33.90	34.50	34.80	**34.40**	0.90	8.55	8.65	8.55	**8.58**	0.10
K03-75	34.30	34.40	34.50	**34.40**	0.20	8.85	8.60	8.70	**8.72**	0.25
K04-75	34.25	34.50	34.70	**34.48**	0.45	8.90	8.85	8.80	**8.85**	0.10
K05-75	34.45	34.50	34.25	**34.40**	0.25	8.85	8.80	8.75	**8.80**	0.10
K06-75	34.30	34.40	34.60	**34.43**	0.30	8.85	8.75	8.85	**8.82**	0.10
K07-75	34.25	34.35	34.50	**34.37**	0.25	8.80	8.85	8.75	**8.80**	0.10
K08-75	34.00	34.30	34.70	**34.33**	0.70	8.85	8.75	8.80	**8.80**	0.10
K09-75	34.20	34.30	34.65	**34.38**	0.45	8.50	8.80	8.70	**8.67**	0.30
K10-75	33.90	34.30	34.65	**34.28**	0.75	8.75	8.70	8.60	**8.68**	0.15
K11-75	36.25	36.65	36.00	**36.30**	0.65	8.90	8.85	8.80	**8.85**	0.10
K12-75	35.75	35.90	35.90	**35.85**	0.15	8.85	8.80	8.75	**8.80**	0.10
K13-75	36.25	36.80	36.30	**36.45**	0.55	8.85	8.75	8.85	**8.82**	0.10
K14-75	35.85	35.30	36.00	**35.72**	0.70	8.80	8.85	8.75	**8.80**	0.10
K15-75	36.00	35.85	35.70	**35.85**	0.30	8.85	8.75	8.80	**8.80**	0.10
K16-75	35.95	35.45	35.60	**35.67**	0.50	8.95	8.65	8.85	**8.82**	0.30
K17-75	35.50	35.70	35.75	**35.65**	0.25	8.80	8.75	8.70	**8.75**	0.10
K18-75	35.80	35.75	35.80	**35.78**	0.05	8.80	8.65	8.75	**8.73**	0.15
K19-75	36.70	35.95	35.85	**36.17**	0.85	8.85	9.00	8.80	**8.88**	0.20
K20-75	36.05	36.10	36.15	**36.10**	0.10	8.85	8.90	8.80	**8.85**	0.10

B.1.2 E-Glass-Kevlar Ampreg 26 repair laminate

	Width					Thickness				
	B - 1	B - 2	B - 3	B mean	max d	2h - 1	2h - 2	2h - 3	2h mean	max d
Nr.	[mm]	[mm]	[mm]	[mm]	[mm]	[mm]	[mm]	[mm]	[mm]	[mm]
K01-26	35.30	35.10	34.90	**35.10**	0.40	8.65	8.55	8.50	**8.57**	0.15
K02-26	35.00	34.90	34.70	**34.87**	0.30	8.50	8.50	8.50	**8.50**	0.00
K03-26	34.75	34.85	35.00	**34.87**	0.25	8.50	8.40	8.30	**8.40**	0.20
K04-26	34.75	34.70	34.60	**34.68**	0.15	8.55	8.50	8.50	**8.52**	0.05
K05-26	34.80	34.90	34.60	**34.77**	0.30	8.60	8.60	8.50	**8.57**	0.10
K06-26	35.05	34.90	34.90	**34.95**	0.15	8.40	8.45	8.45	**8.43**	0.05
K07-26	35.70	35.65	35.10	**35.48**	0.60	8.50	8.40	8.45	**8.45**	0.10
K08-26	34.85	34.90	34.80	**34.85**	0.10	8.45	8.24	8.44	**8.38**	0.21
K09-26	35.30	35.05	35.00	**35.12**	0.30	8.45	8.30	8.45	**8.40**	0.15
K10-26	34.80	34.65	34.60	**34.68**	0.20	8.60	8.45	8.50	**8.52**	0.15
K11-26	35.30	35.10	34.90	**35.10**	0.40	8.50	8.45	8.35	**8.43**	0.15

B.1.3 E-Glass-Kevlar Ampreg 26 and Ampreg 75 repair-parent laminate

	Width					Thickness				
	B - 1	B - 2	B - 3	B mean	max d	2h - 1	2h - 2	2h - 3	2h mean	max d
Nr.	[mm]	[mm]	[mm]	[mm]	[mm]	[mm]	[mm]	[mm]	[mm]	[mm]
K01-26/75	34.90	35.00	34.80	**34.90**	0.20	8.45	8.45	8.45	**8.45**	0.00
K02-26/75	35.00	34.80	34.65	**34.82**	0.35	8.60	8.45	8.45	**8.50**	0.15
K03-26/75	34.80	34.95	34.95	**34.90**	0.15	8.50	8.40	8.40	**8.43**	0.10
K04-26/75	34.85	34.85	34.80	**34.83**	0.05	8.50	8.35	8.40	**8.42**	0.15
K05-26/75	35.30	35.25	34.85	**35.13**	0.45	8.55	8.45	8.55	**8.52**	0.10
K06-26/75	34.70	34.80	34.70	**34.73**	0.10	8.40	8.45	8.45	**8.43**	0.05
K07-26/75	34.95	34.70	34.65	**34.77**	0.30	8.50	8.55	8.55	**8.53**	0.05
K08-26/75	34.85	34.55	34.60	**34.67**	0.30	8.60	8.45	8.50	**8.52**	0.15
K09-26/75	34.35	34.55	34.55	**34.48**	0.20	8.60	8.50	8.60	**8.57**	0.10
K10-26/75	34.85	34.95	35.00	**34.93**	0.15	8.35	8.40	8.40	**8.38**	0.05
K11-26/75	35.40	35.10	34.90	**35.13**	0.50	8.55	8.50	8.50	**8.52**	0.05

B.2 Mode I fracture mechanics test data

B.2.1 E-Glass-Kevlar Ampreg 75 parent laminate

Figure B.1: Fibre bridging at a Kevlar/E-Glass/Ampreg 75 specimen whilst loaded in opening mode

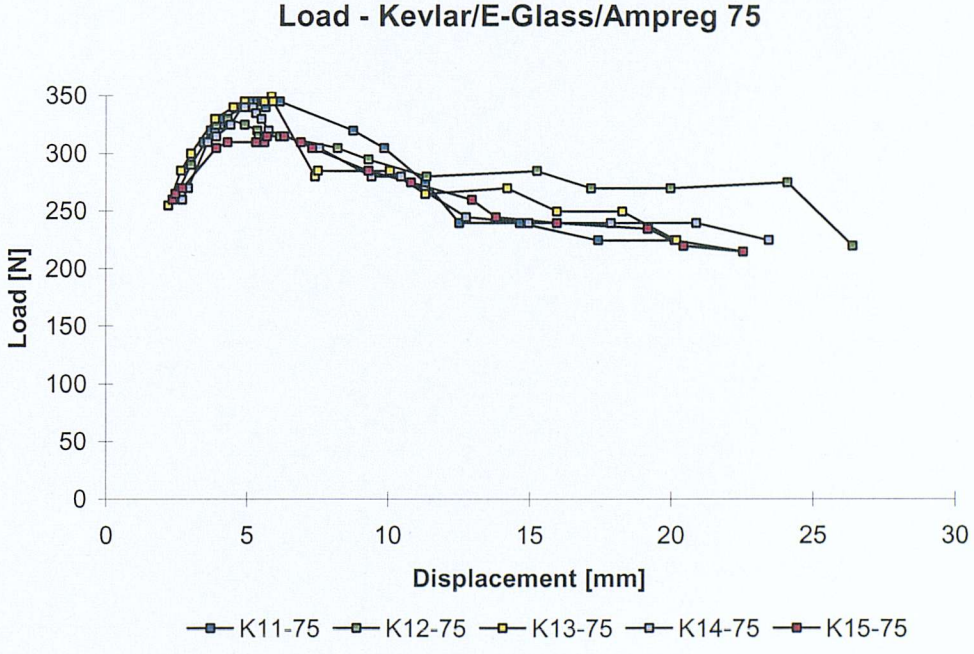

Figure B.2: Mode I load-displacement plot of Kevlar/E-Glass/Ampreg 75 specimens

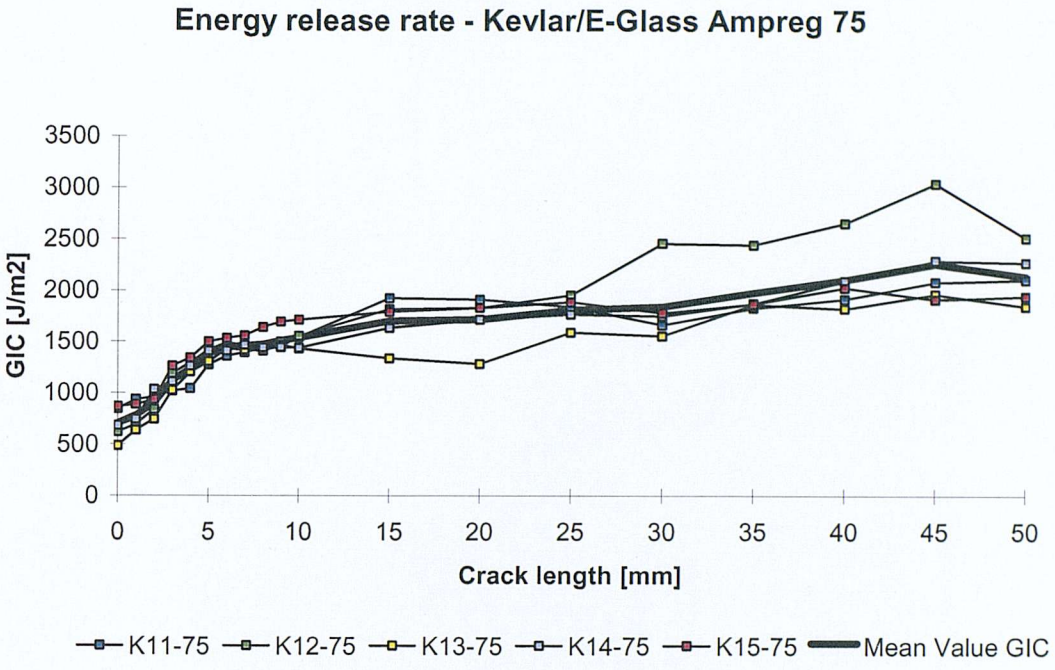

Figure B.3: Mode I energy release rate versus crack length plot of Kevlar/E-Glass/Ampreg 75 specimens

Figure B.4: Interfaces of two typical Group A Kevlar 75 specimens after complete failure

B.2.2 E-Glass-Kevlar Ampreg 26 repair laminate

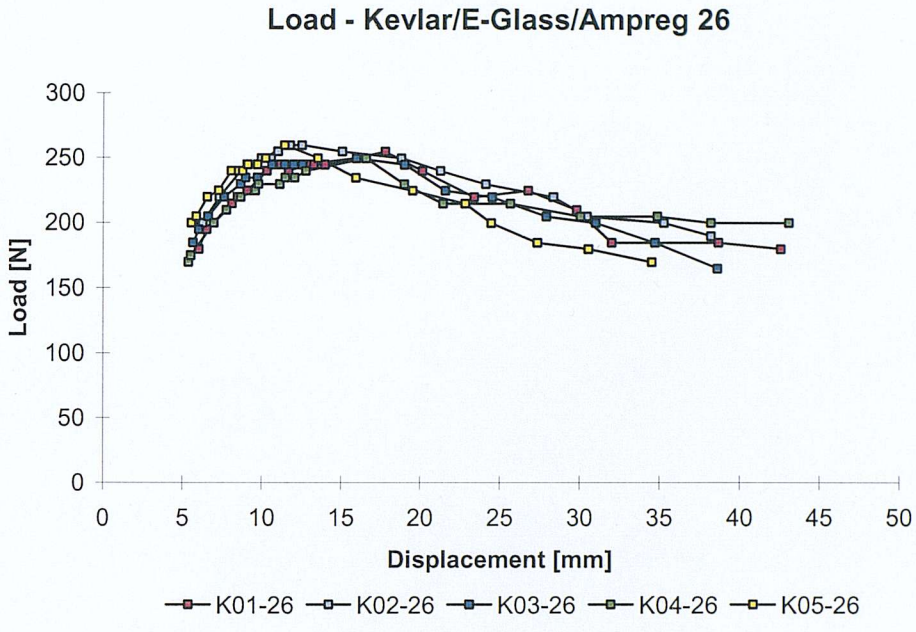

Figure B.5: Mode I load-displacement plot of Kevlar/E-Glass/Ampreg 26 specimens

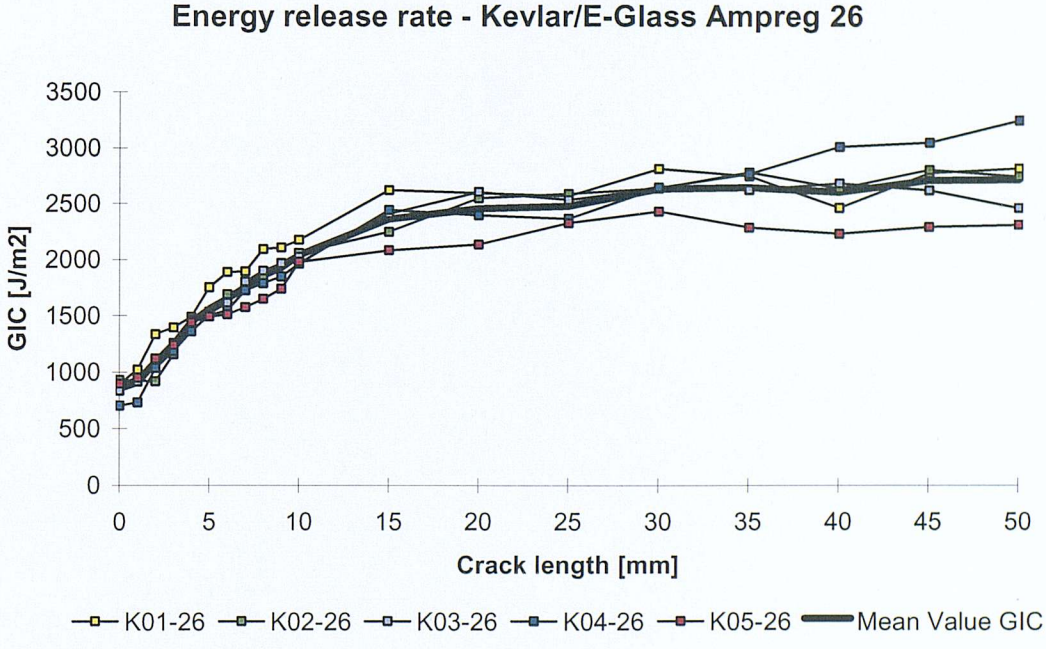

Figure B.6: Mode I energy release rate versus crack length plot of Kevlar/E-Glass/Ampreg 26 specimens

-a- : -45°/45° interface

-b- : within -45° layer

-c- : 0°/-45° interface

Figure B.7: Interfaces of two typical Kevlar/E-Glass/Ampreg 26 specimens

B.2.3 Kevlar/ E-Glass Ampreg 26 and Ampreg 75 repair- parent laminate

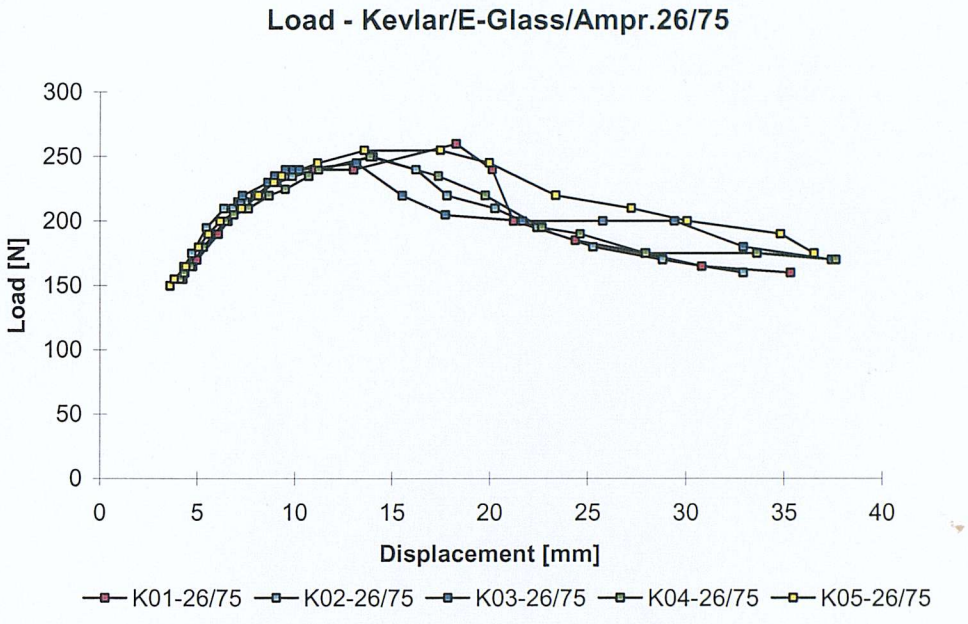

Figure B.8: Mode I load-displacement plot of Kevlar/E-Glass/Ampreg 26/75 specimens

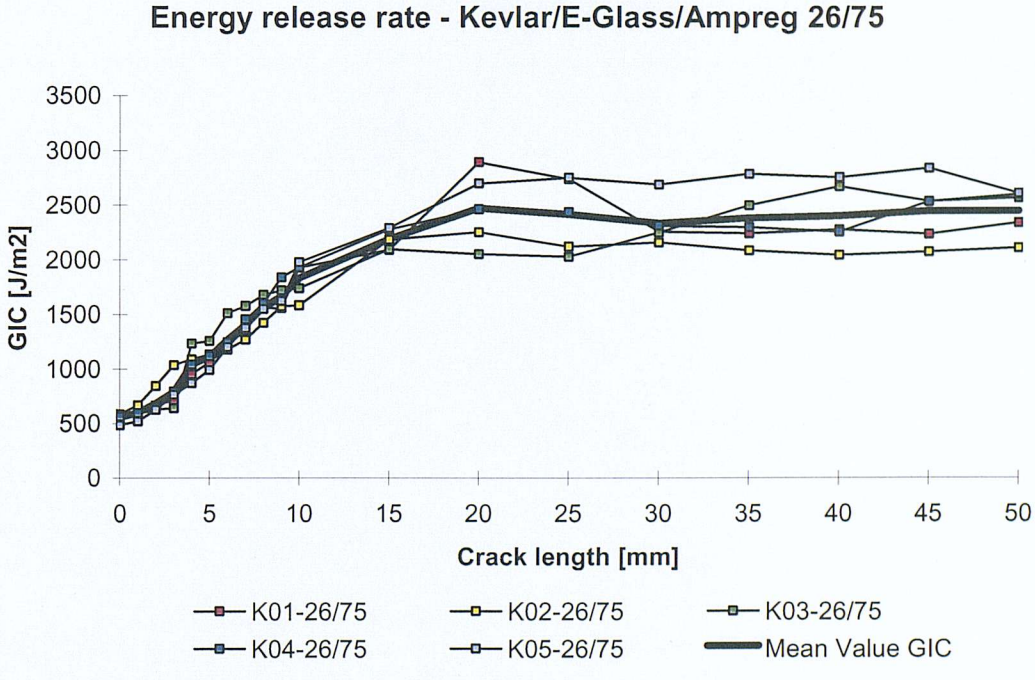

Figure B.9: Mode I energy release rate versus crack length plot of Kevlar/E-Glass/Ampreg 26/75 specimens

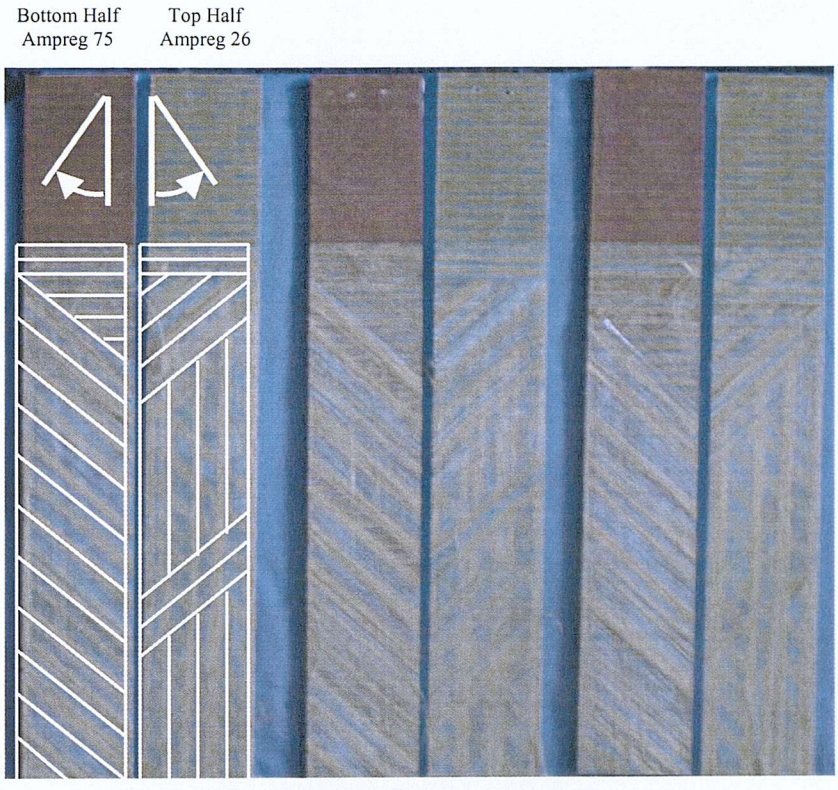

Figure B.10: Interfaces of three Kevlar/E-Glass/Ampreg 26/75 specimens

B.3 Mode II fracture mechanics test data with mode I pre-crack

B.3.1 E-Glass-Kevlar Ampreg 75 parent laminate

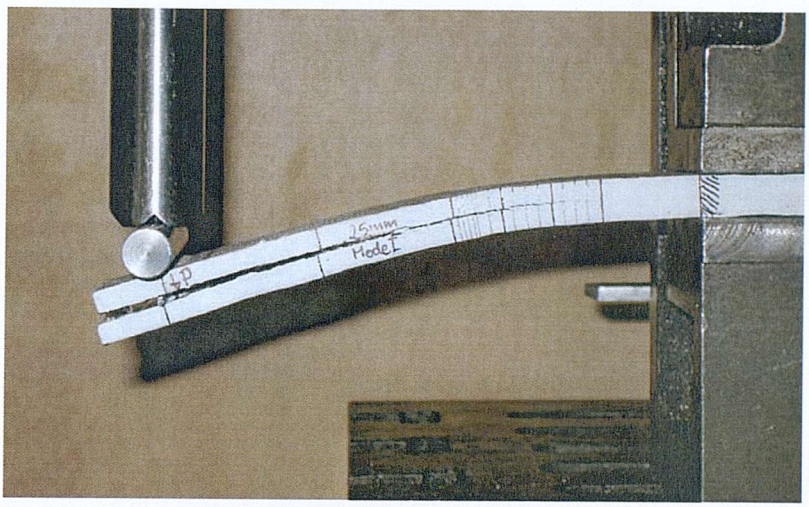

Figure B.11: Mode II test configuration and crack propagation

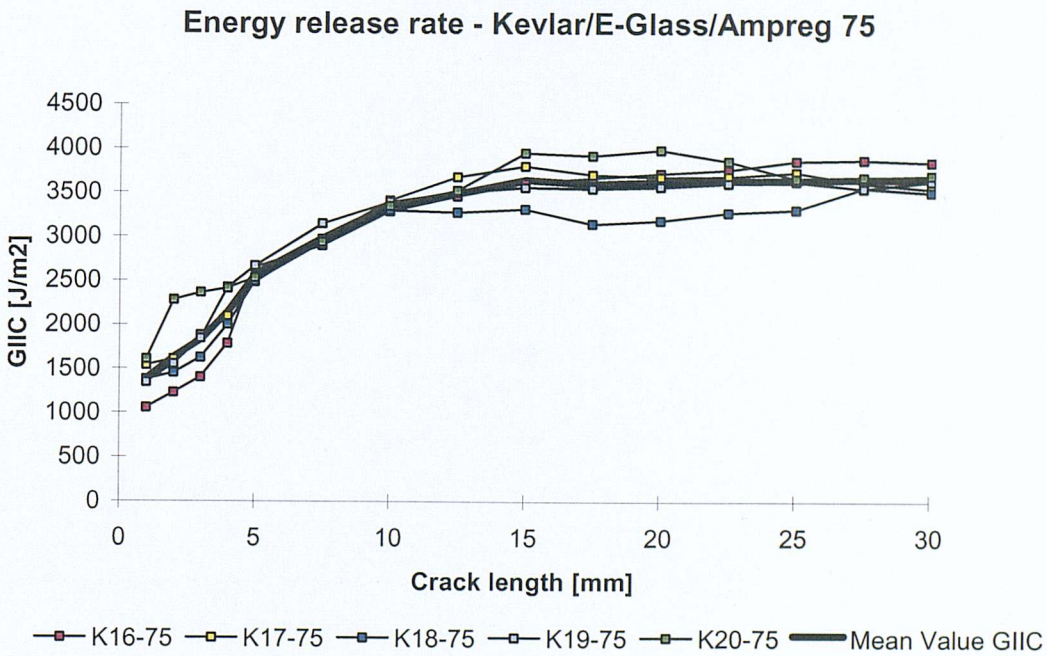

Figure B.12: Mode II energy release rate versus crack length plot of Kevlar/E-Glass/Ampreg 75 specimens

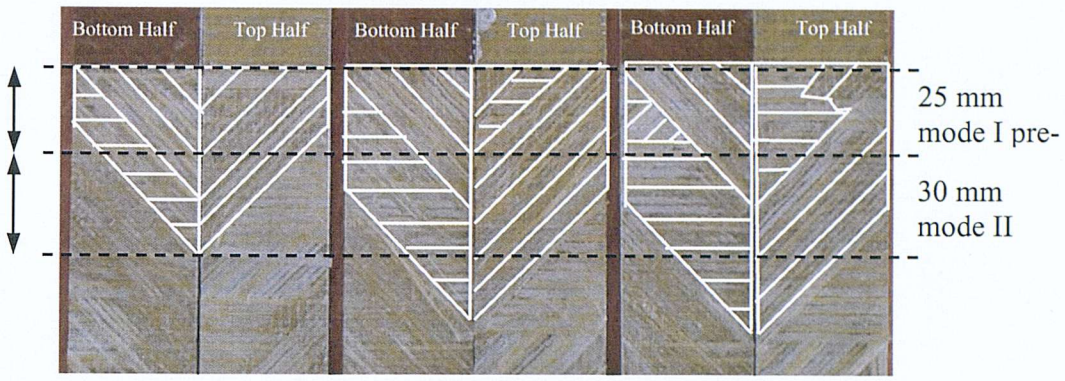

Figure B.13: Failure interfaces of three different Kevlar/E-Glass/Ampreg 75 specimens

B.3.2 E-Glass-Kevlar Ampreg 26 repair laminate

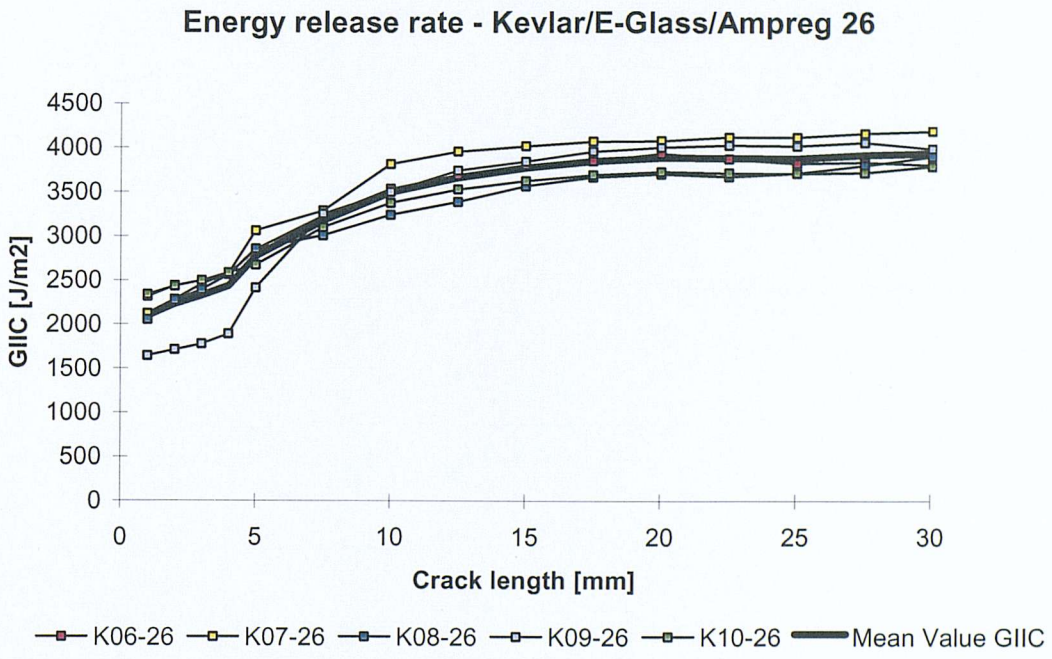

Figure B.14: Mode II energy release rate versus crack length plot of Kevlar/E-Glass /Ampreg 26 specimens

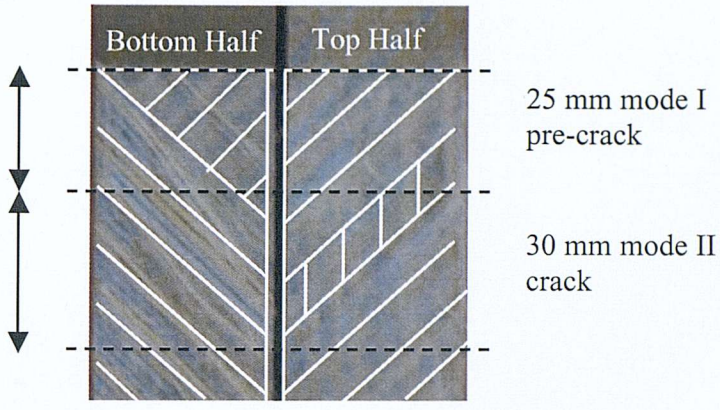

Figure B.15: Typical failure interface of the Kevlar/E-Glass /Ampreg 26 specimen

B.3.2 E-Glass-Kevlar Ampreg 26 and Ampreg 75 repair- parent laminate

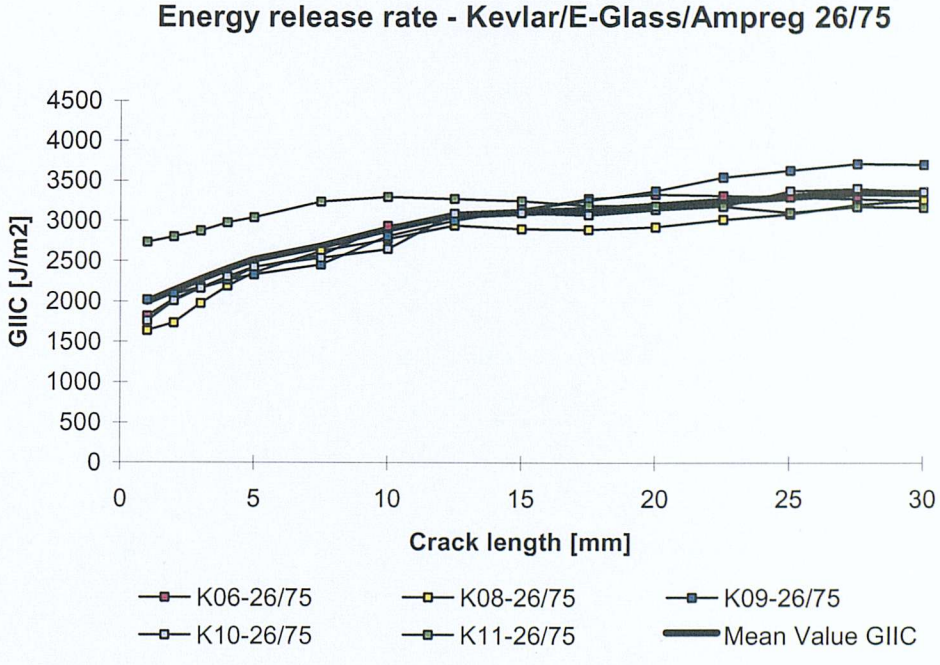

Figure B.16: Mode II energy release rate versus crack length plot of QEA1200/Ampreg 26/75 specimens

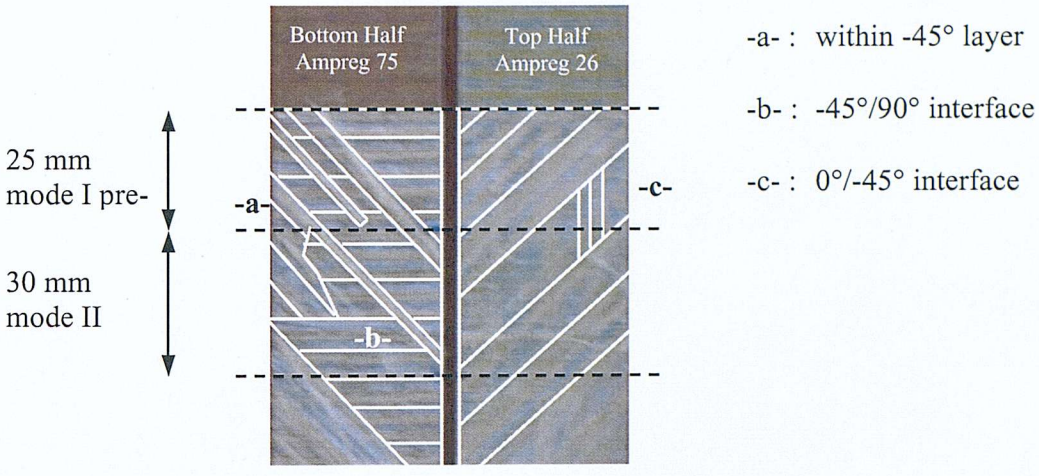

Figure B.17: Typical failure surface of QEA1200/Ampreg 26/75 specimen

B.4 Mode II fracture mechanics test data with mode II pre-crack

B.4.1 E-Glass-Kevlar Ampreg 75 parent laminate

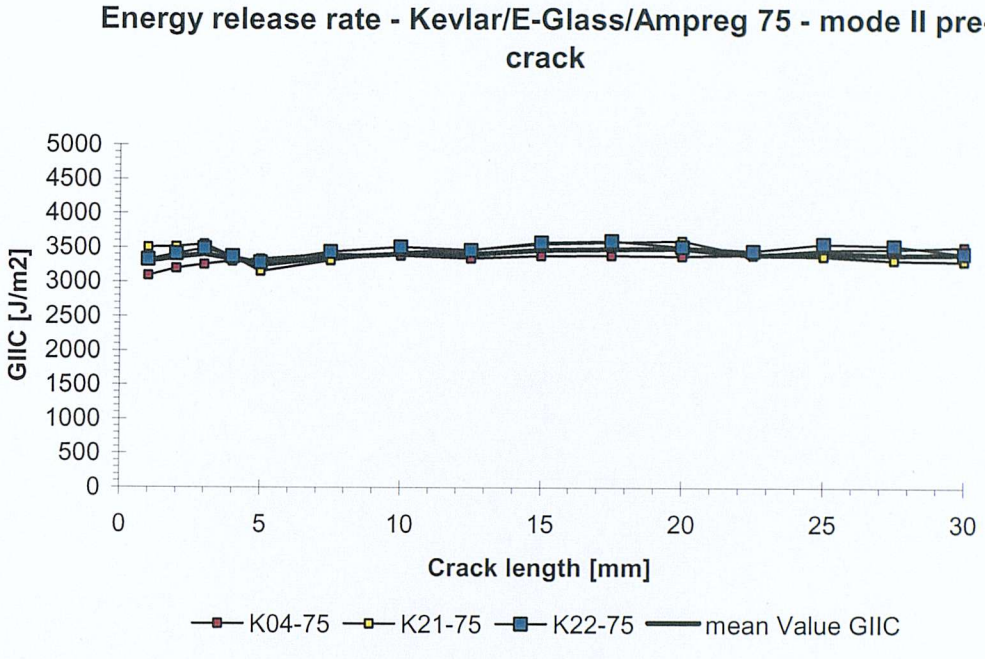

Figure B.18: Mode II energy release rate versus crack length plot of parent interface with a mode II pre-crack

B.4.2 E-Glass-Kevlar Ampreg 26 repair laminate

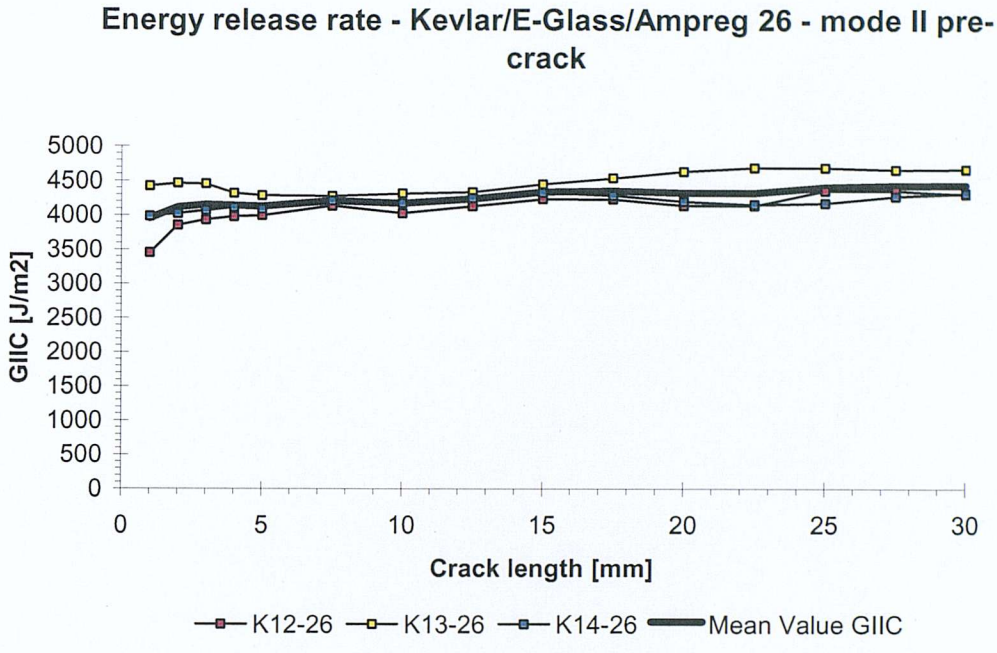

Figure B.19: Mode II energy release rate versus crack length plot of repair laminate with mode II pre-crack

B.4.3 E-Glass-Kevlar Ampreg 26 and Ampreg 75 repair- parent laminate

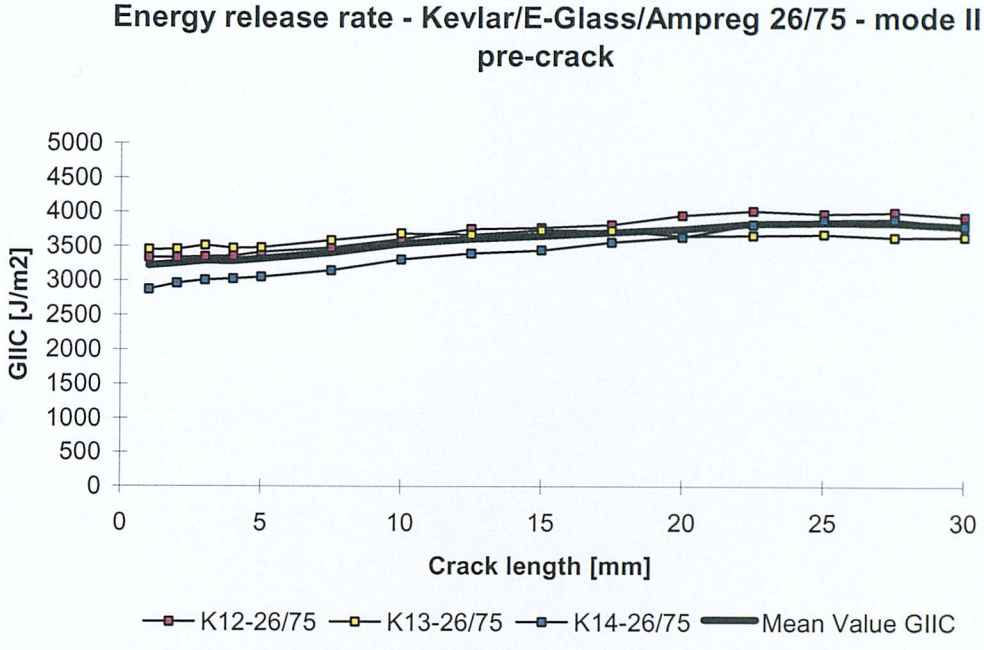

Figure B.20: Mode II energy release rate versus crack length plot of repair-parent interface with a mode II pre-crack

B5 Mixed Mode fracture mechanics test data

B5.1 E-Glass-Kevlar Ampreg 75 parent laminate

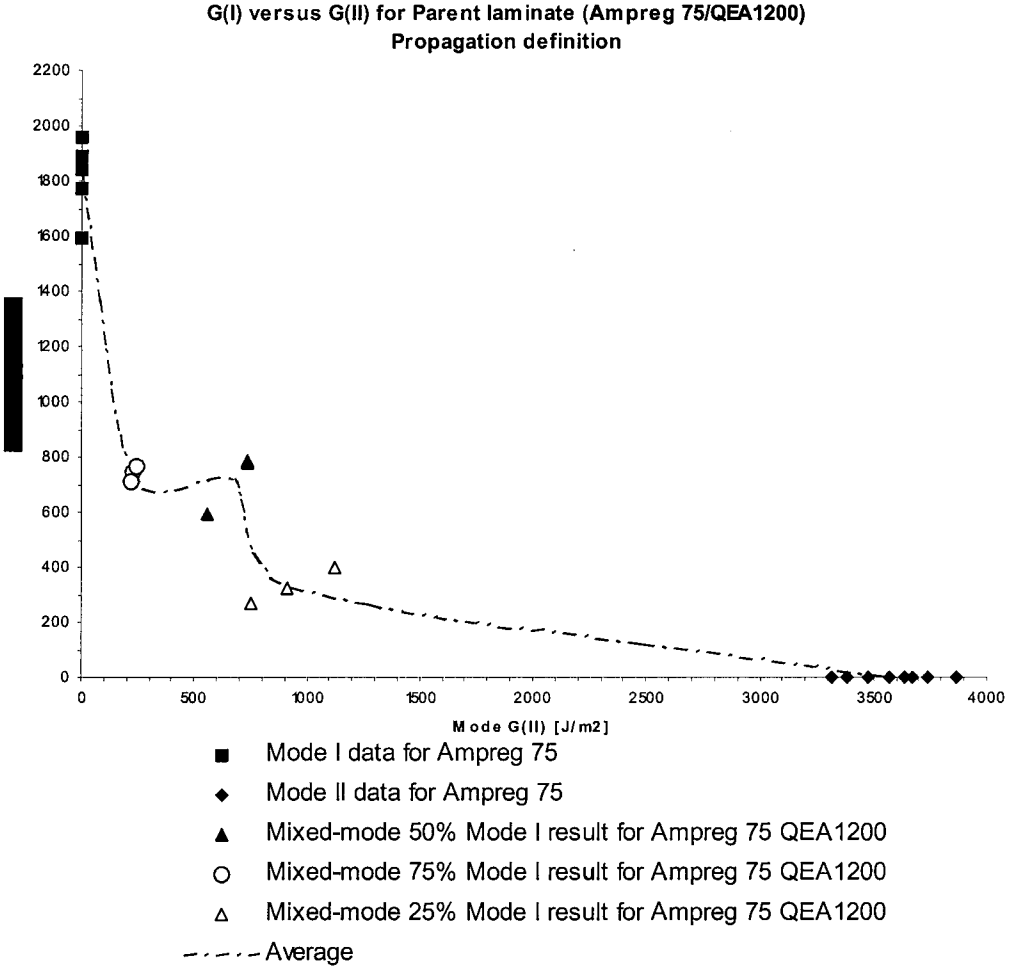

Figure B.21: G_I versus G_{II} for the Kevlar/ E-Glass Ampreg 75 parent laminate

B5.2 E-Glass-Kevlar Ampreg 26 repair laminate

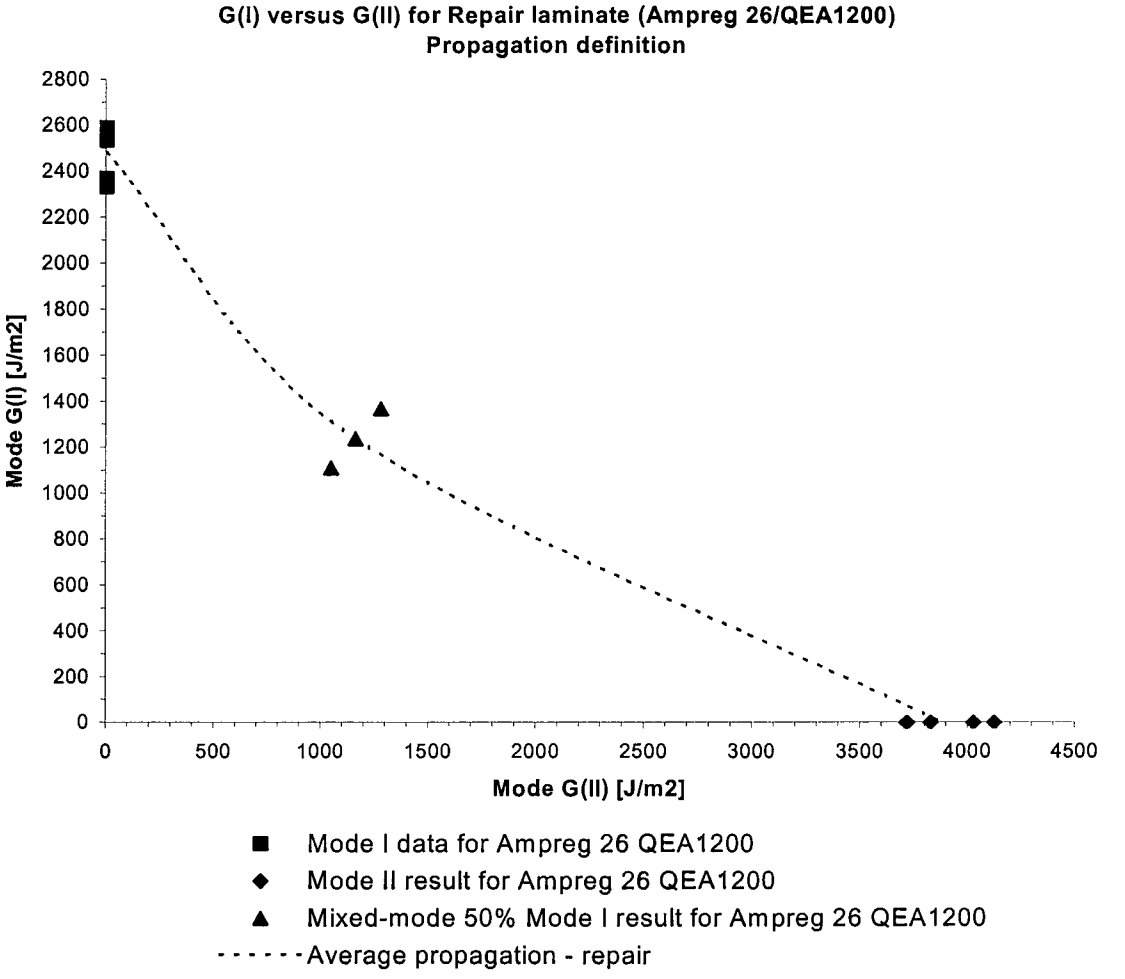

Figure B.22: G_I versus G_{II} for the Kevlar/ E-Glass Ampreg 75 parent laminate

B5.3 E-Glass-Kevlar Ampreg 26 and Ampreg 75 repair- parent laminate

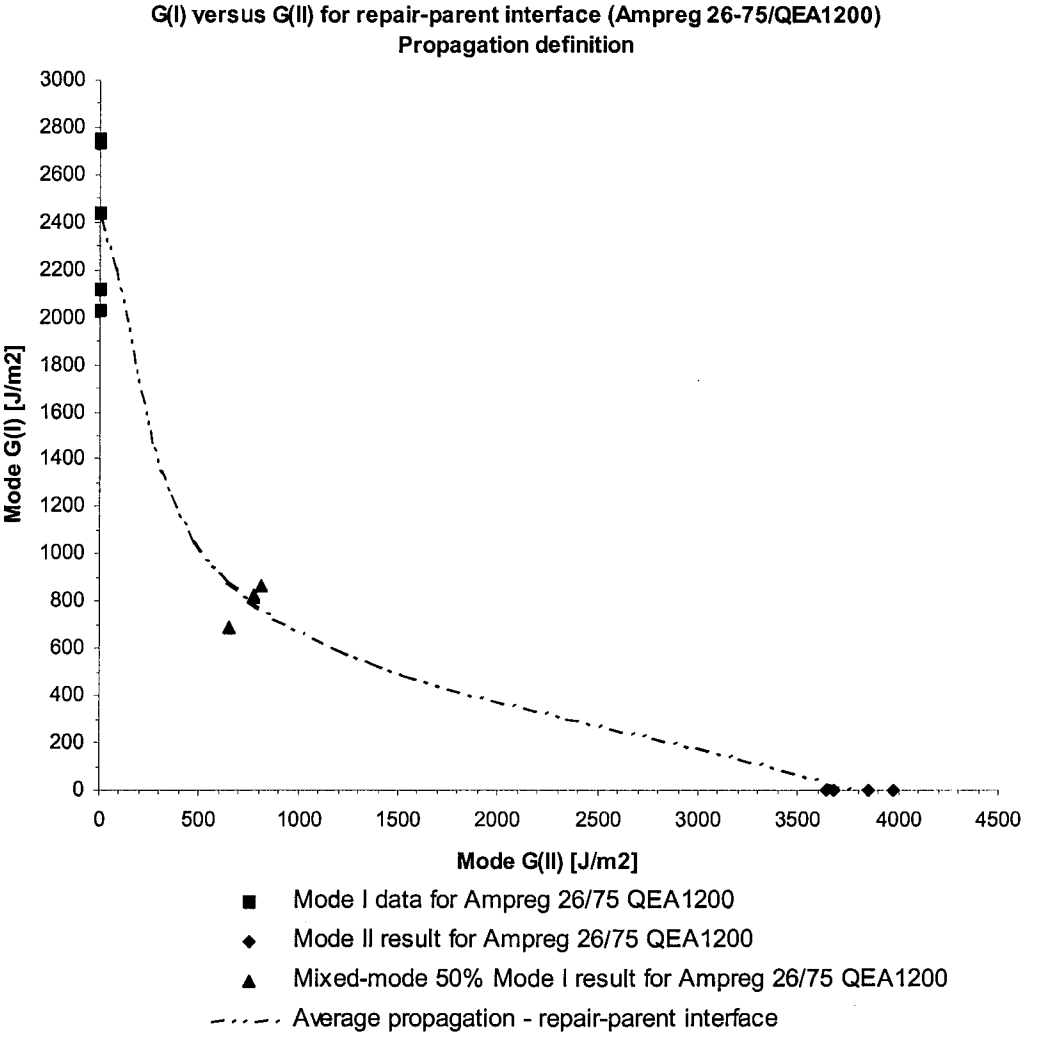

Figure B.23: G_I versus G_{II} for the repair-parent interface

APPENDIX C

C.1 Repair Cycle

This appendix contains the repair flowcharts for all of the key stages within the repair cycle identified in Figure C.1.

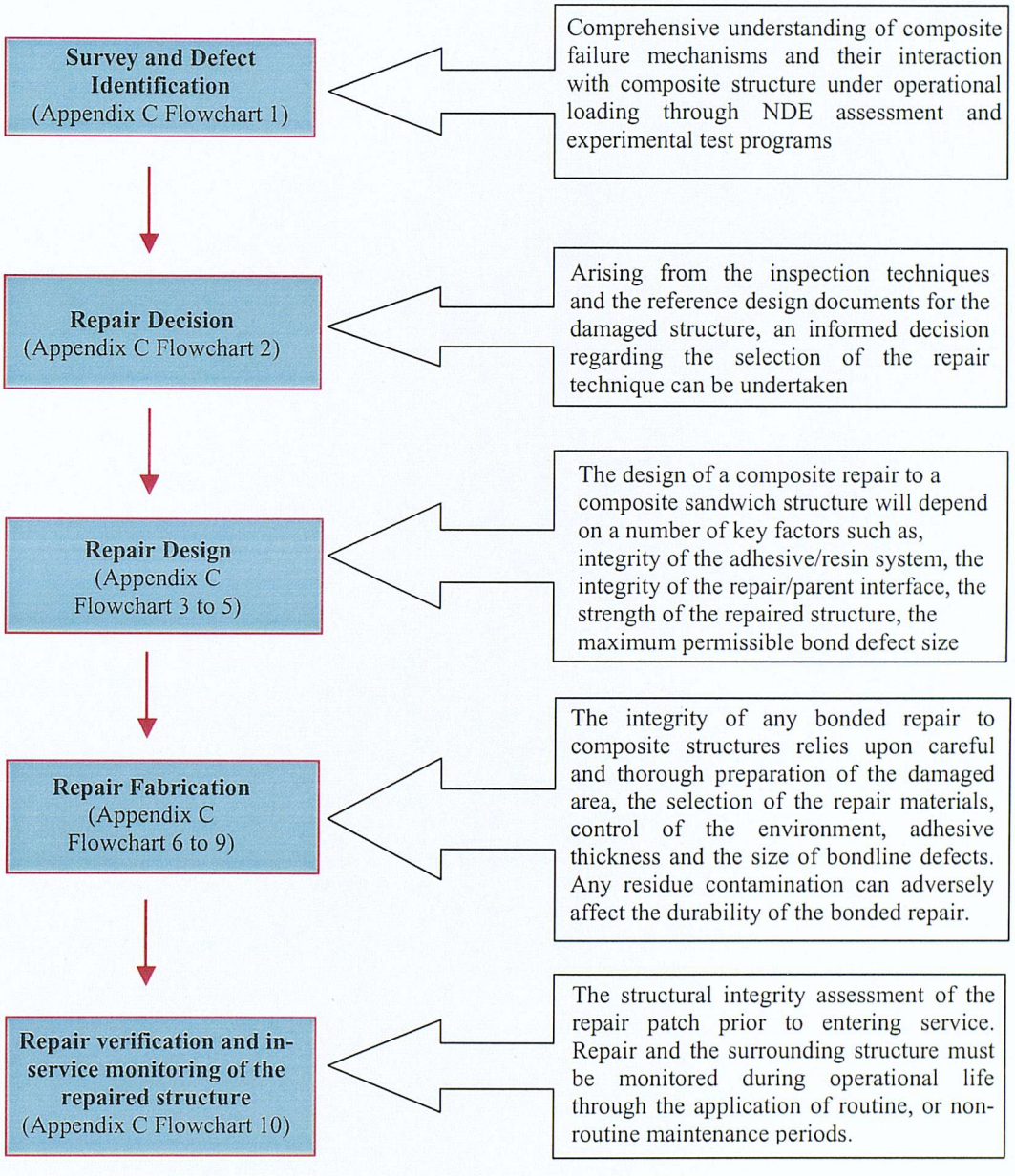

Figure C.1: Repair cycle for composite structures

C.2 Repair Flowcharts

Flowchart C1.2 has been adapted from 'Case Study 2 – Application of FRP Repair Technology to Small FRP Vessels, Doc No. R.1.20.1342 – B2a' from the DTI/SSA Link Programme on Integrated Technology for Marine Construction (ITMC) #42: Design Production Guidance for the Use of FRP Composite Materials for Shipbuilding Applications, School of Engineering Sciences, University of Southampton, January 2003.

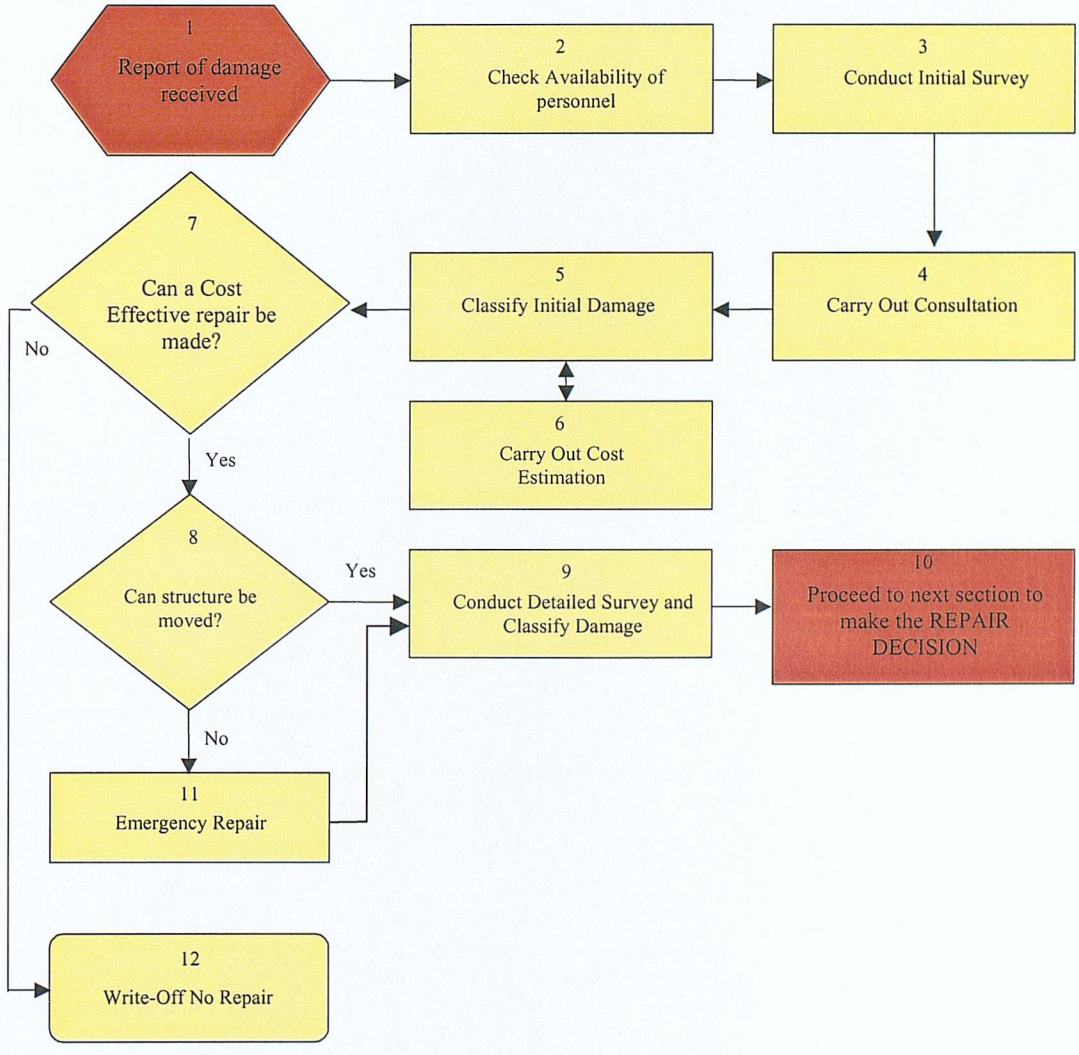

Figure C1.2: Flowchart 1- Survey and Defect Identification

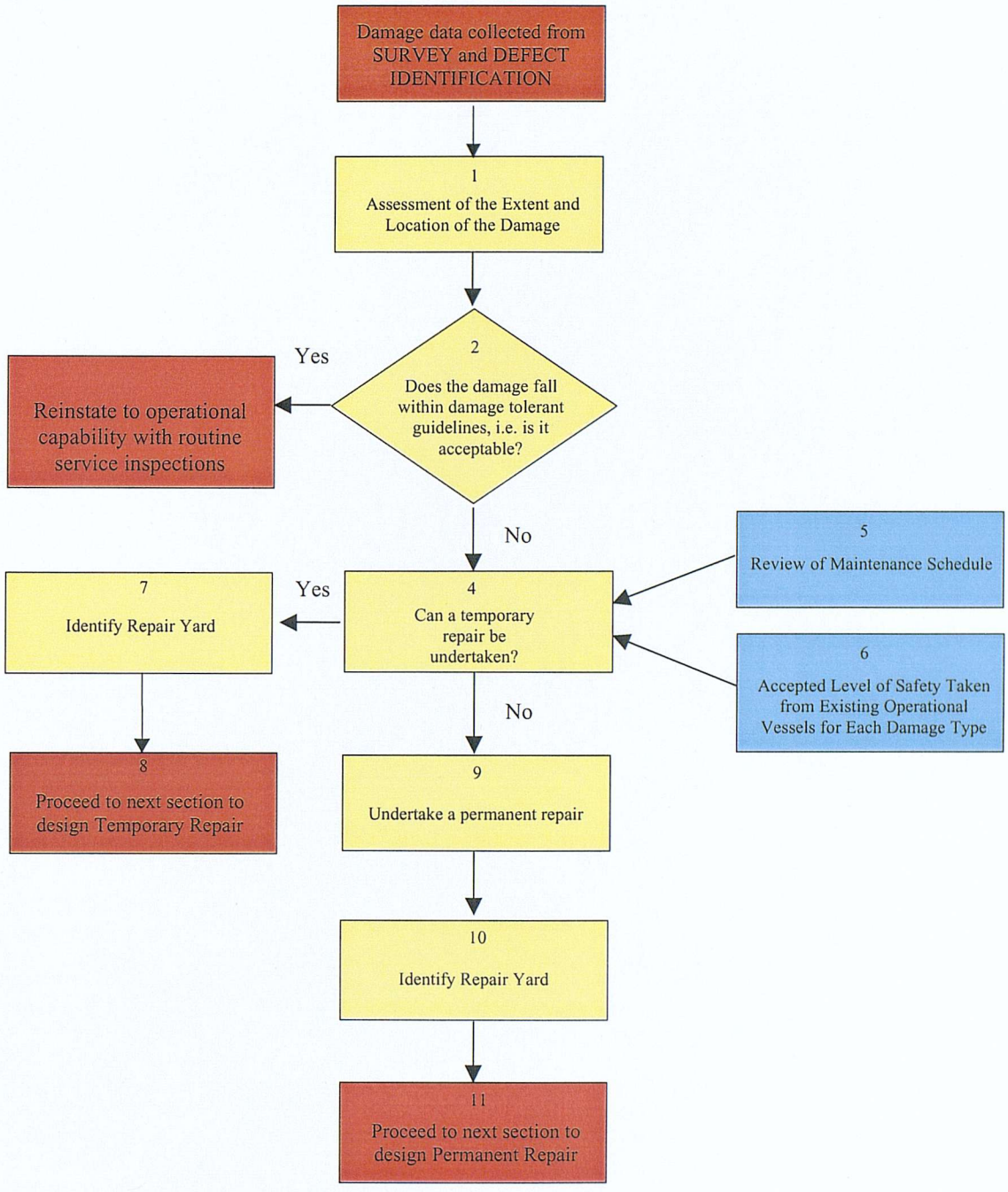

Figure C1.3: Flowchart 2 - Repair Decision

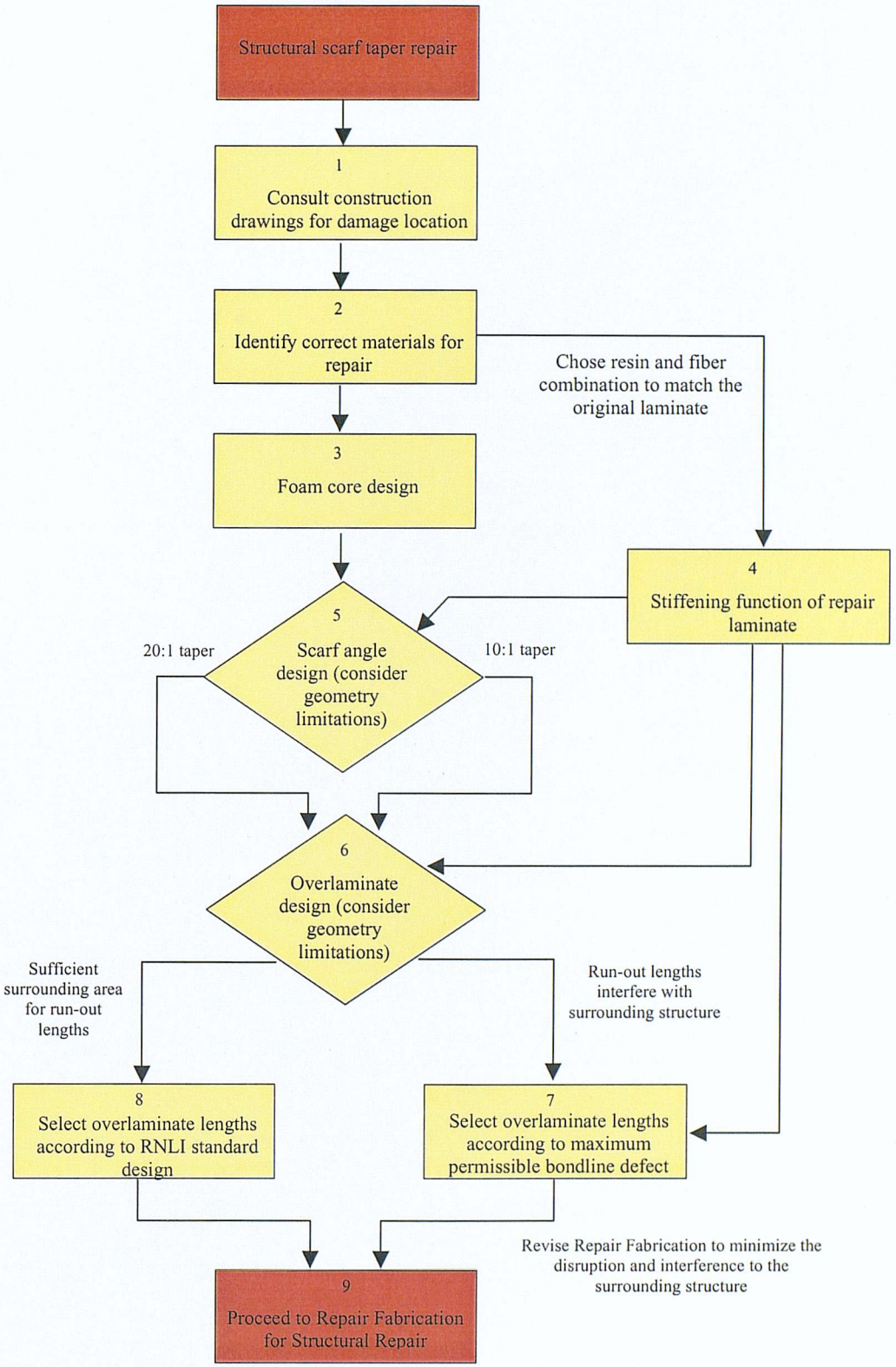

Figure C1.4: Flowchart 3 - Repair Design - Permanent Structural Repair

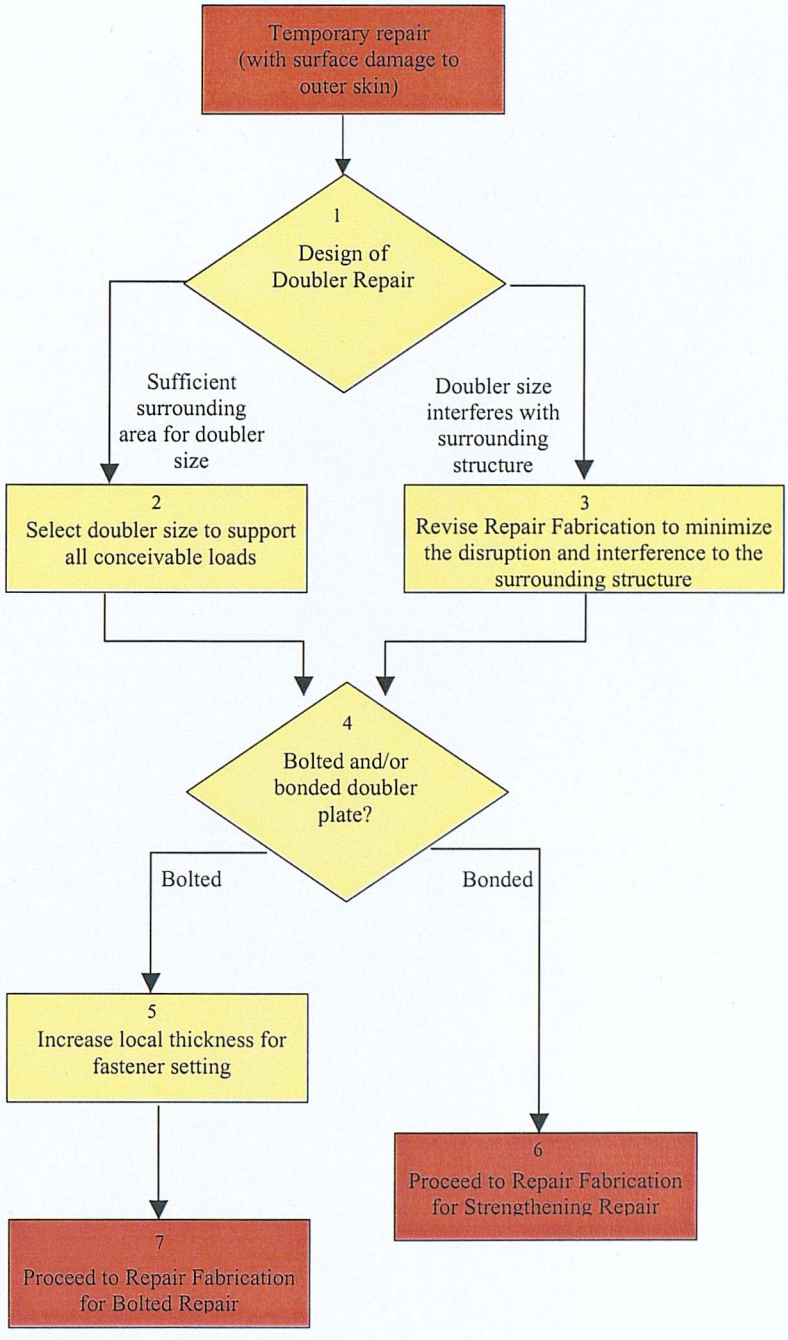

Figure C1.5: Flowchart 4 - Repair Design - Temporary External Double Repair

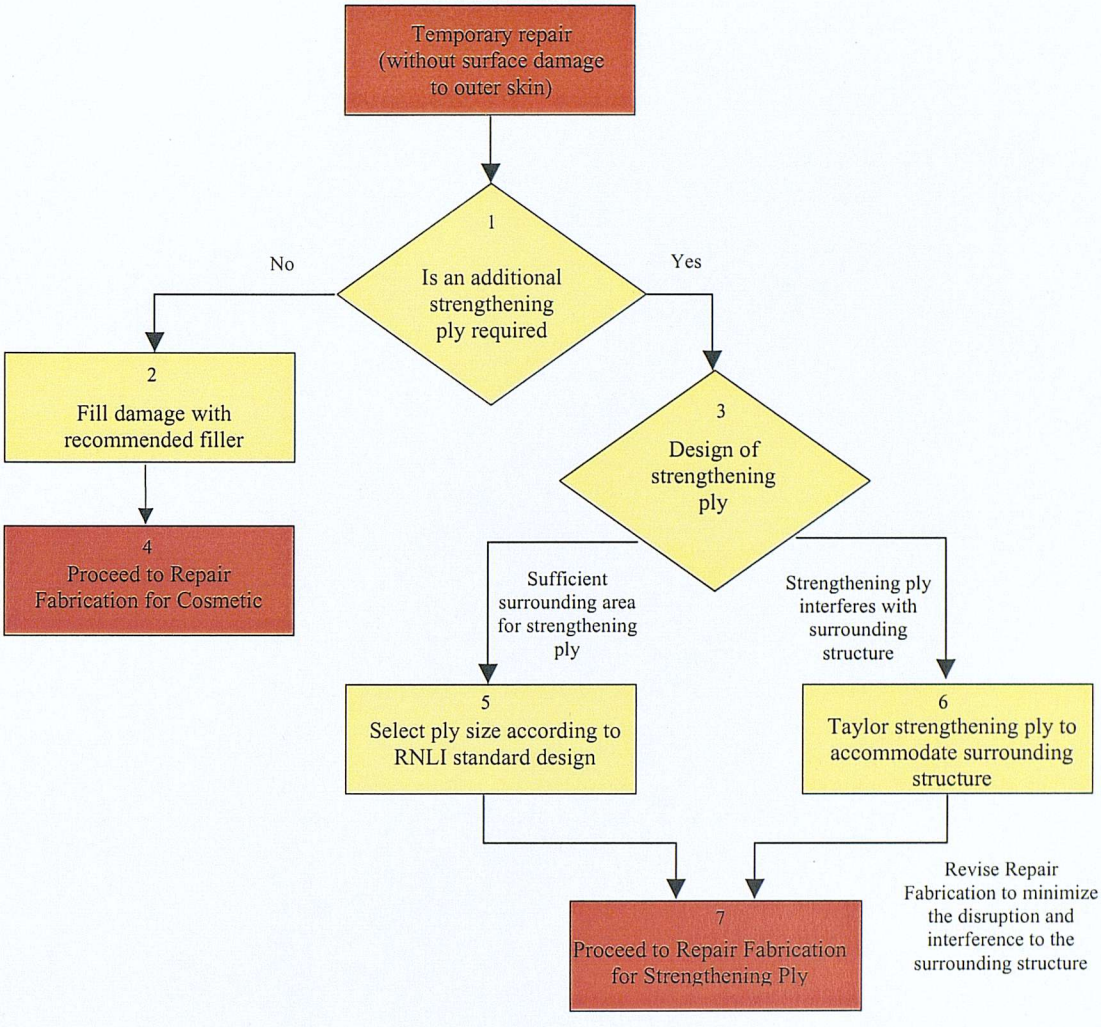

Figure C1.6: Flowchart 5 - Repair Design - Cosmetic Repair to Outer Skin

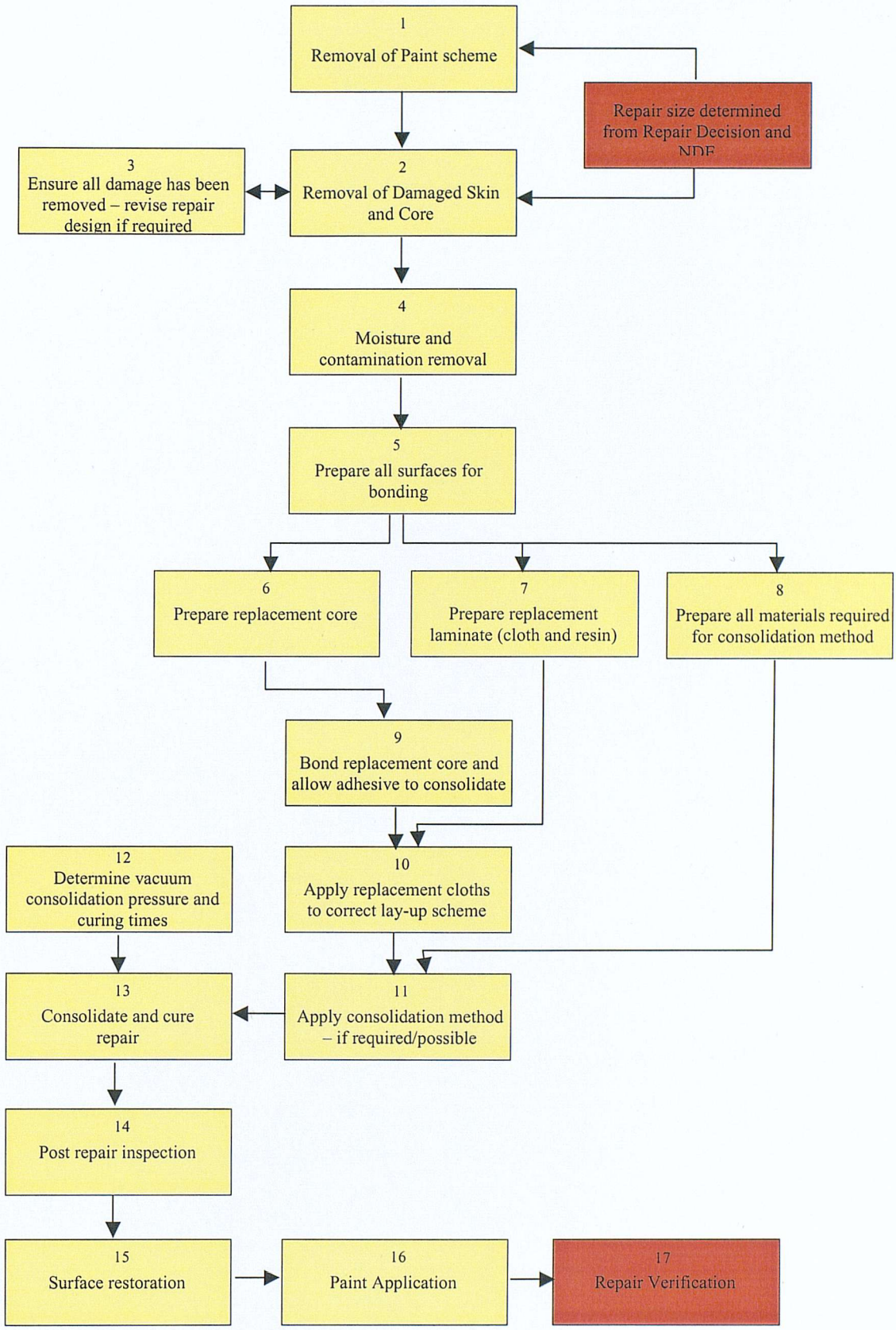

Figure C1.7: Flowchart 6 - Repair Fabrication for Structural Repair

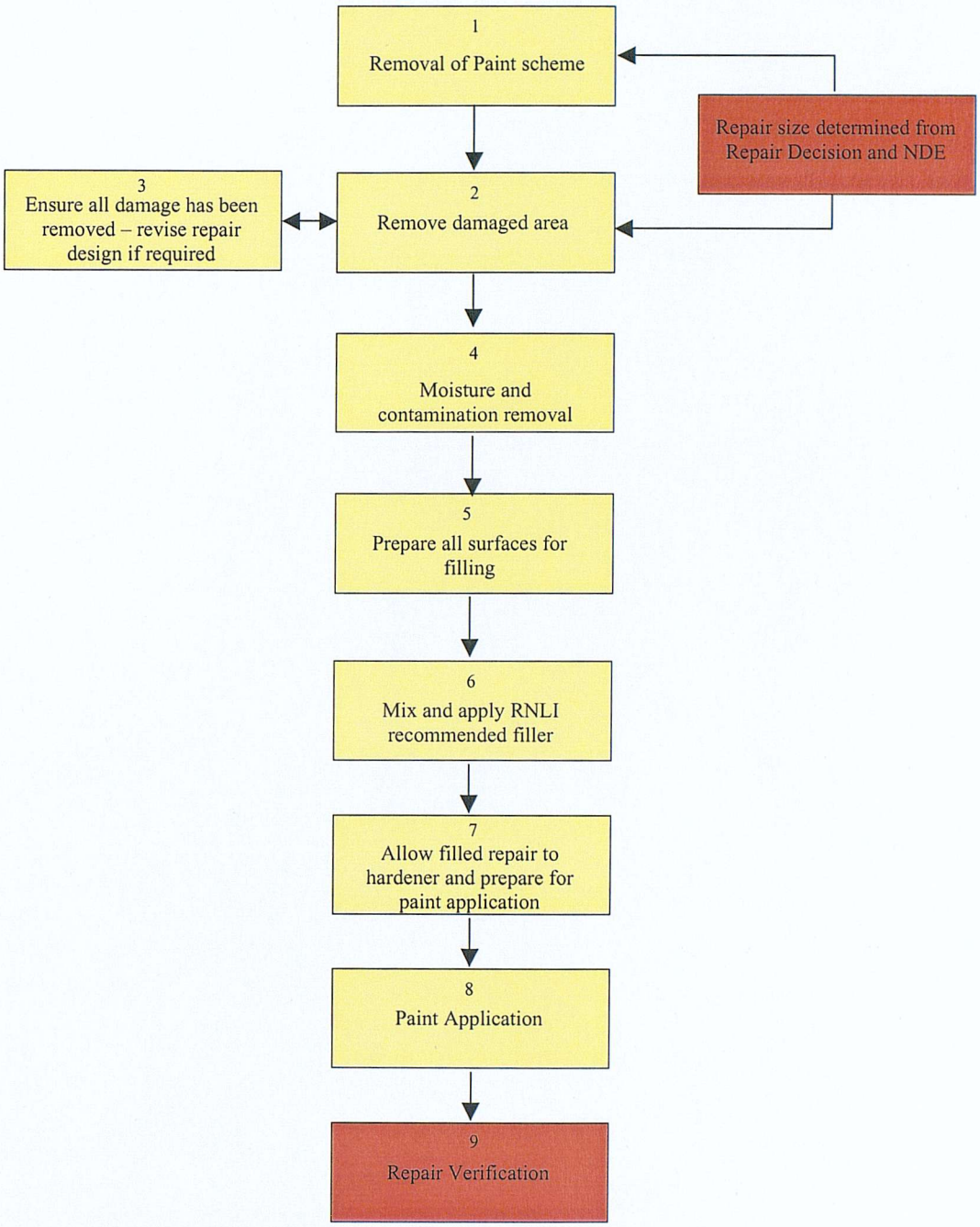

Figure C1.8: Flowchart 7 - Repair Fabrication for Cosmetic Repair

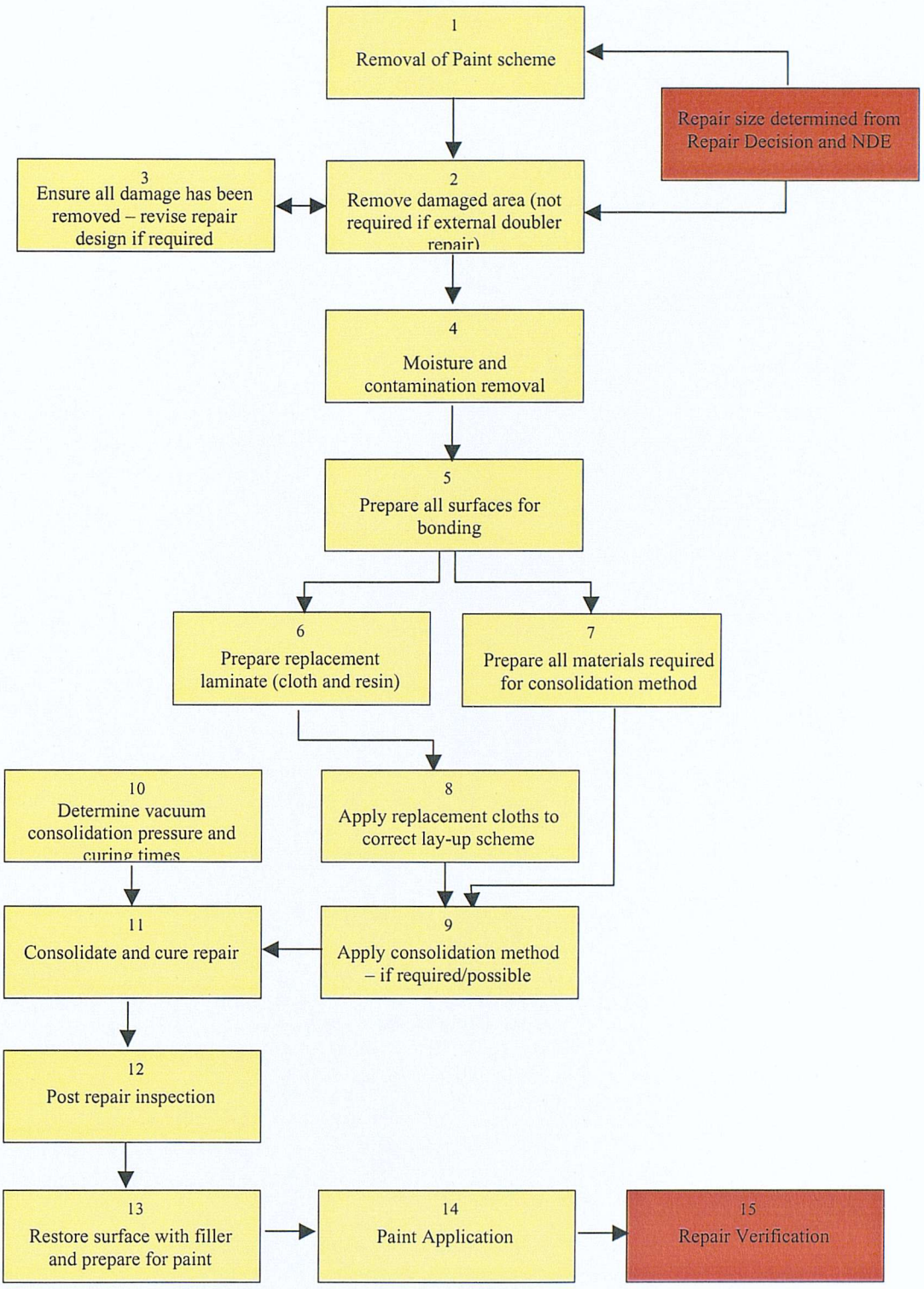

Figure C1.9: Flowchart 8 - Repair Fabrication for Strengthening Ply

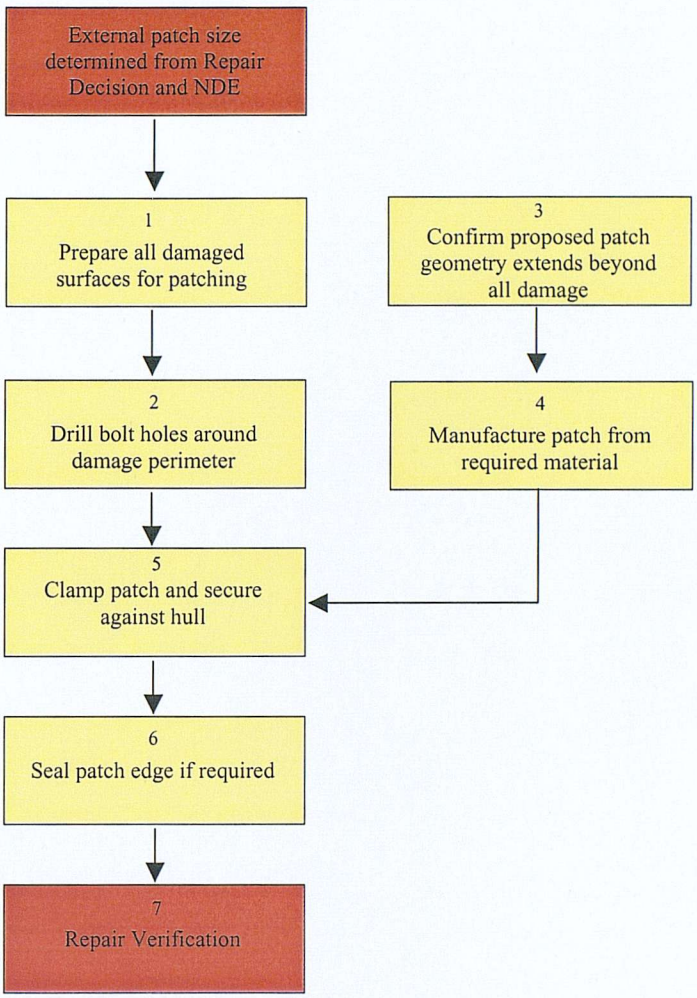

Figure C1.10: Flowchart 9 - Repair Fabrication for Bolted Repair

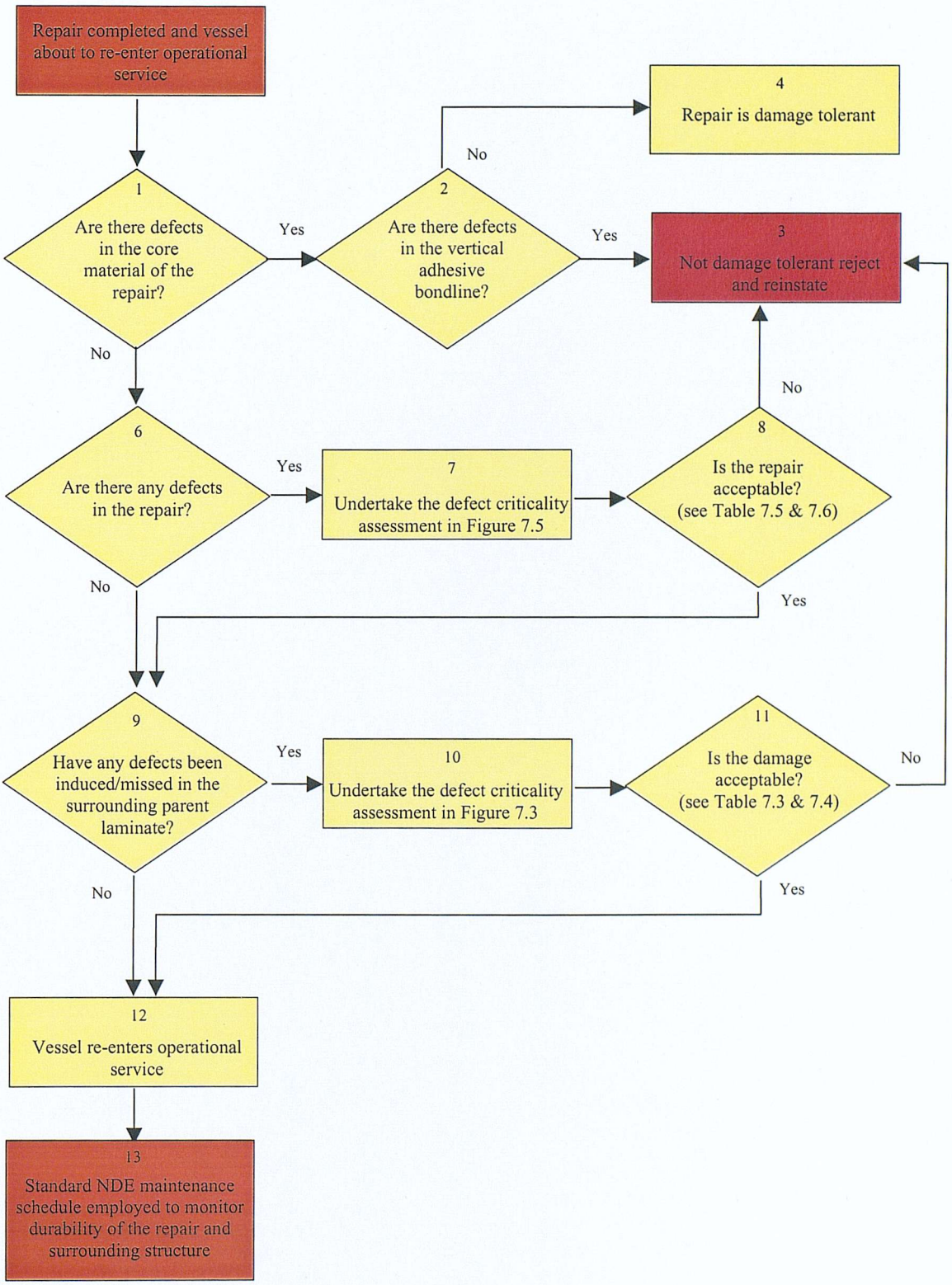

Figure C1.11: Flowchart 10 - Repair Verification and In-service Monitoring

APPENDIX D

D.1 Papers Published

Trask, R.S., Shenoi R.A. and Cripps R.M. 'Design approach for repair adequacy in RNLI polymer composite sandwich structures – an overview', in FRC 2002: 9th International Conference on Fibre Reinforced Composites, Newcastle upon Tyne, England, 26th–28th March 2002, ISBN 0-9540459-2-0.

Trask, R.S. Shenoi, R.A. and Cripps, R.M. 'Repair of sandwich structures used in the hulls of high performance rescue craft', in 6th International Conference on Sandwich Structures, Ft. Lauderdale, Florida, USA, 31st March to 2nd April 2003, CRC Press, London 2003.

D.2 Papers under Preparation

Trask, R.S., Shenoi R.A. and Cripps R.M. 'Repair structural integrity assessment of marine composite sandwich structures' intended for *Trans. RINA*

Trask, R.S., Shenoi R.A. and Cripps R.M. 'Impact and damage tolerance behaviour of repaired composite foam sandwich beams' intended for *J. Sand. Str. Material.*

Trask, R.S., Shenoi R.A. and Cripps R.M.' Residual strength characteristics of repaired, foam cored sandwich beams' intended for *Composites Part A.*